

**A study of the felsic volcanic succession  
south-east of Coronation Hill.  
Palaeovolcanology-Geochemistry-Geochronology  
Record 1992/9**

*A contribution to the BMR Kakadu Conservation Zone Project*

*1987-1992*

*A National Geoscience Mapping Accord Project*

**E A Jagodzinski**



\* R 9 2 0 0 9 0 1 \*

## **DEPARTMENT OF PRIMARY INDUSTRIES AND ENERGY**

Minister for Resources: Hon. Michael Lee

Secretary: Greg Taylor

## **AUSTRALIAN GEOLOGICAL SURVEY ORGANISATION**

Executive Director: Harvey Jacka

© Commonwealth of Australia

**ISSN: 1039-0073**

**ISBN: 0 642 19626 5**

This work is copyright. Apart from any fair dealings for the purposes of study, research, criticism or review, as permitted under the Copyright Act, no part may be reproduced by any process without written permission. Copyright is the responsibility of the Executive Director, Australian Geological Survey Organisation. Inquiries should be directed to the **Principal Information Officer, Australian Geological Survey Organisation, GPO Box 378, Canberra City, ACT, 2601.**

# CONTENTS

PAGE NUMBER

## ABSTRACT

### 1: INTRODUCTION

1.1 Local Geology.....	2
1.2 Revised Stratigraphic Nomenclature.....	4

### 2: GEOCHRONOLOGY

2.1 Introduction.....	10
2.2 Geology of the Gimbat Ignimbrite Member.....	10
2.3 Sample Selection.....	11
2.4 Ion Microprobe Analyses.....	12
2.4.1 Analytical Techniques.....	12
2.4.2 Intrusive quartz-feldspar porphyry: 89123002.....	14
2.4.3 Intrusive quartz-feldspar porphyry: 89123123.....	16
2.4.4 Ignimbrite: 89123138.....	18
2.4.5 Quartz-rich sandstone: 88126005.....	22
2.5 Interpretation of Results.....	22
2.6 Implications for The SHRIMP U-Pb dating technique.....	24
2.7 Stratigraphic implications of results.....	24

### 3: CORONATION SANDSTONE..... 26

3.1 Arkosic Sandstone.....	27
3.2 Basalts.....	28

### 4: GIMBAT IGNIMBRITE MEMBER

4.1 Welded Ignimbrites.....	43
4.2 Massive Volcanic Lithic-boulder Conglomerate.....	48
4.3 Non-welded Ignimbrite.....	50
- <i>Crystal-rich Volcanic Sandstone Facies</i> .....	54
4.4 Massive-Laminated-Cross bedded Sandstones and Conglomerates.....	56
4.5 Massive to flow-folded Aphyric Lava.....	61

### 5: BIG SUNDAY FORMATION

5.1 Crystal-rich Arenite Facies.....	64
5.1.1 Stratigraphy.....	64
5.1.2 General Lithology.....	64
5.1.3 Texture.....	67
5.1.4 Petrology.....	68
5.1.5 Mode of Emplacement.....	70
5.1.6 Origin of the Crystal-rich Arenites.....	71
- <i>crystal-enrichment processes</i> .....	75
- <i>epiclastic reworking</i> .....	79
- <i>volcanic enrichment processes</i> .....	80
- <i>contemporaneous flow transformation or post-eruptive slumping?</i> .....	81
5.1.7 Discussion.....	82
5.1.8 Conclusions.....	85

5.2	Tuffaceous Sediments.....	86
5.2.1	Tuffaceous Siltstone Facies.....	86
5.2.2	Interbedded Sandstone-Tuffaceous Siltstone Facies.....	86
5.2.3	Interpretation.....	96
CHAPTER 6: INTRUSIVE UNITS		
6.1	Flow-folded Rhyolite Facies.....	91
6.2	Quartz-Feldspar Porphyries.....	91
6.3	Felsic Sills and Dykes.....	92
6.4	Malone Creek Granite.....	92
6.5	Syenite Porphyry.....	92
6.6	Sparsely Porphyritic Dacite.....	95
6.7	Dolerite Dykes and Intrusive Bodies.....	95
CHAPTER 7: GEOCHEMISTRY AND MAGMA PETROGENESIS		
7.1	Major Rock Types.....	98
7.1.1	Gimbat Ignimbrite Member.....	98
7.1.2	Malone Creek Granite.....	98
7.1.3	Plum Tree Creek Volcanics and Grace Creek Granite.....	99
7.2	Sampling and Analytical Methods.....	99
7.3	Classification.....	100
7.4	Geochemistry of the Gimbat Ignimbrite Member.....	100
7.4.1	Geochemistry of unit IC <sub>1</sub> and implications for magma chamber dynamics.....	110
7.5	Comparison with the Malone Creek Granite.....	112
7.6	Origin of the Malone Creek Granite.....	113
7.7	Comparison with other granites.....	114
7.8	Rb-Sr and Sm-Nd isotopic data.....	117
7.9	Origin of the Gimbat Ignimbrite Member.....	117
CHAPTER 8: PALAEOVOLCANOLOGY AND PALAEOENVIRONMENT		
8.1	Palaeoenvironment of the Gimbat Ignimbrite Member and Big Sunday Formation.....	124
8.2	Palaeogeography.....	124
8.2.1	Proximity to vent.....	126
8.2.2	Interpretation as an intracaldera setting.....	130
8.2.3	Interpretation as a proximal shield setting.....	130
	- <i>a proximal shield model</i> .....	134
8.2.4	Conclusions.....	134
9:	IMPLICATIONS FOR MINERALISATION.....	136
REFERENCES.....		137
ACKNOWLEDGEMENTS.....		147
APPENDIX A	Point Count Data	
APPENDIX B	Geochemical Data	
APPENDIX C	XRD Data	
APPENDIX D	Contractor's Report; Professor R.A.F. Cas	
APPENDIX E	Electron Microprobe Data	

## ABSTRACT

The volcanics which outcrop around the southern margin of the Malone Creek Granite southeast of Coronation Hill are mapped as part of the Pul Pul Rhyolite of the El Sherana Group. The lithology of the volcanic succession in the area of study is quite different to that of the type section of Pul Pul Rhyolite in the South Alligator Valley. A new stratigraphic member is therefore proposed and named the Gimbat Ignimbrite Member. It may correlate with rhyolite lavas at the type section of the Pul Pul Rhyolite, but evidence is inconclusive.

Detailed geochronological work has shown that the sequence is at least 30 Ma younger than the age currently accepted for the El Sherana Group. Stratigraphic implications of these new data are discussed.

The Gimbat Ignimbrite Member comprises mainly quartz-feldspar-lithic-bearing ignimbrites deposited subaerially and forming a sequence ~ 830 m thick. This sequence also contains small volumes of massive to flow-banded, aphyric to sparsely porphyritic rhyolite lavas. The top 200 m of ignimbrite hosts lenses of interbedded volcanics sandstones and conglomerates deposited in erosional gullies during breaks between ignimbrite-forming eruptions.

The Big Sunday Formation (El Sherana Group) unconformably overlies the Gimbat Ignimbrite Member and can be divided into two units. The basal unit consists of thick, laterally extensive crystal-rich arenites, interpreted to be subaqueously deposited pyroclastic debris flows. These are considered to have erupted subaerially as pyroclastic flows, then transformed in transit into water-supported mass flows (debris flows) when they entered a deep water basin. The basal unit is conformably overlain by tuffaceous siltstone and interbedded turbiditic sandstones deposited in a deep water basin (lake).

The Gimbat Ignimbrite Member is intruded by several acidic and mafic bodies including the Malone Creek Granite, quartz-feldspar porphyries, sparsely porphyritic dacites, syenite porphyries, felsic sills and dykes and dolerite bodies and dykes.

The spatial relationship between the Malone Creek Granite and the Gimbat Ignimbrite Member is suggestive of a resurgent caldera complex, but geochemical evidence suggests they are unrelated. Geochemical evidence also suggests the Gimbat Ignimbrite Member is unrelated to the other felsic suite which outcrops locally: the Plum Tree Creek Volcanics of the Edith River Group, and comagmatic Grace Creek Granite.

Detailed analysis of the facies suggests that the Gimbat Ignimbrite Member is a proximal facies association deposited near vent, but there is not enough evidence preserved to determine whether the ignimbrites are an intracaldera succession, or a proximal outflow sequence. The latter interpretation is favoured in the absence of convincing evidence for an intracaldera setting.

It is concluded that there is unlikely to be any mineralisation, particularly of the U and Au-Pt-Pd type found at Coronation Hill in the South Alligator Valley, associated with the Gimbat Ignimbrite Member.

# 1. INTRODUCTION

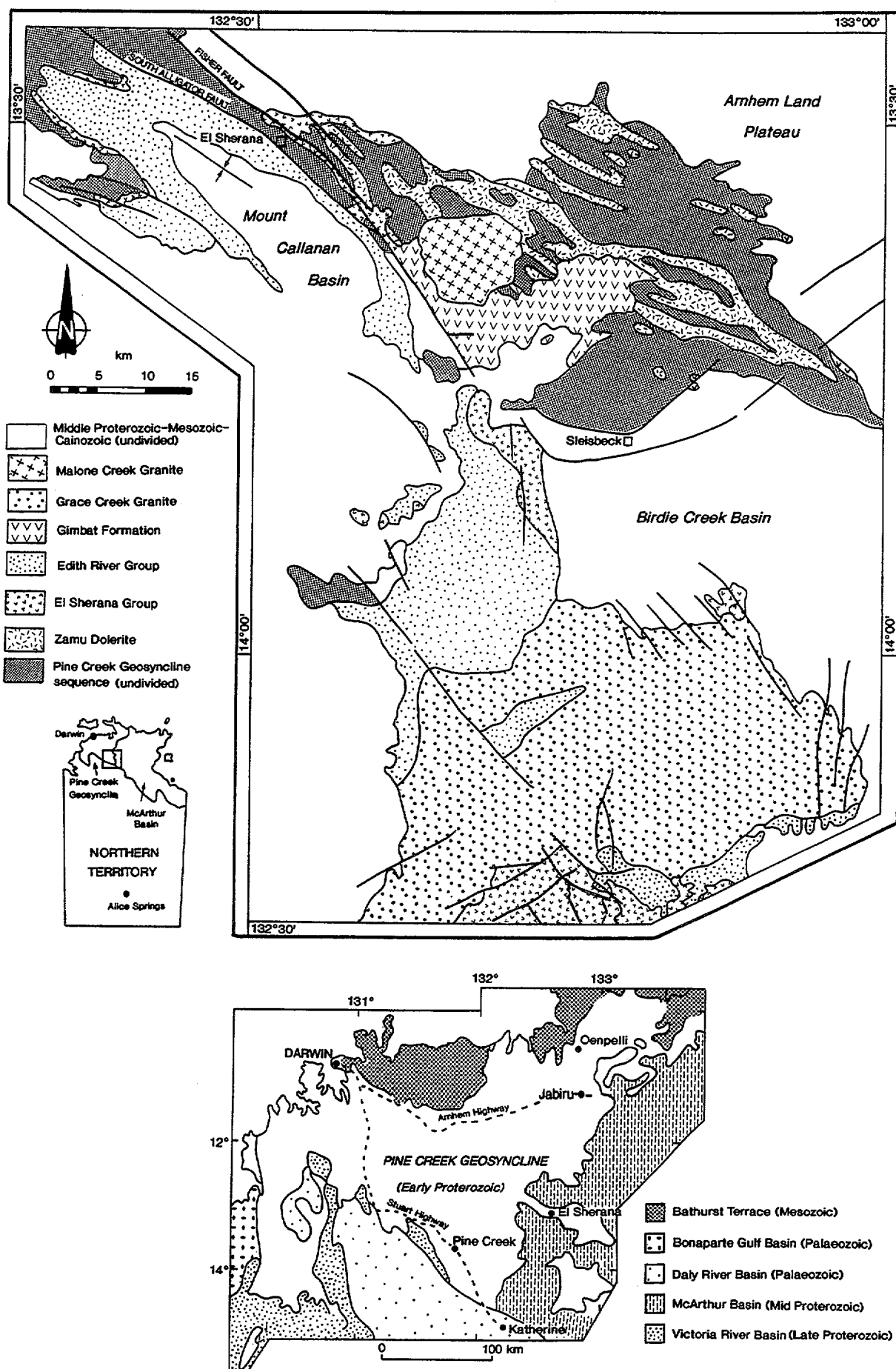


Figure 1.1: Local Geology of the area.

### 1. INTRODUCTION

This report represents a study of the felsic volcanic sequence and related sediments which outcrop at the headwaters of the South Alligator and Katherine River systems ~ 10 km southeast of Coronation Hill, in the Katherine-El Sherana area, Northern Territory. Prior to this study, these units were mapped as part of the Pul Pul Rhyolite of the late Early Proterozoic El Sherana Group (Needham & Stuart-Smith, 1985a; 1985b; Stuart-Smith et al, 1988). This study finds there is no conclusive evidence that the volcanic sequence correlates with the type section of the Pul Pul Rhyolite in the South Alligator Valley. The volcanics are lithologically different to the volcanics of the Pul Pul Rhyolite type section, being comprised mainly of ignimbrite rather than rhyolite lava. A new stratigraphic member within the Pul Pul Rhyolite, named the Gimbat Ignimbrite Member, is therefore proposed.

Detailed geochronological work carried out in the course of the present study has shown that volcanic units within the sequence are ~ 40 Ma younger than the currently accepted age of the El Sherana Group. A detailed geochronological study of the Gimbat Ignimbrite Member is included in this report, and the implications for the regional stratigraphy and problems which may arise using SHRIMP (Sensitive High Resolution Ion Microprobe) U-Pb dating techniques are discussed.

The report documents and interprets the volcanic facies within the Gimbat Ignimbrite Member, determines facies associations and reconstructs the palaeovolcanological history and depositional environments of the Gimbat Ignimbrite Member and overlying Big Sunday Formation. Finally the geochemistry and isotope geology of the sequence are discussed in terms of tectonic models of Proterozoic lithospheric evolution.

#### 1.1 LOCAL GEOLOGY

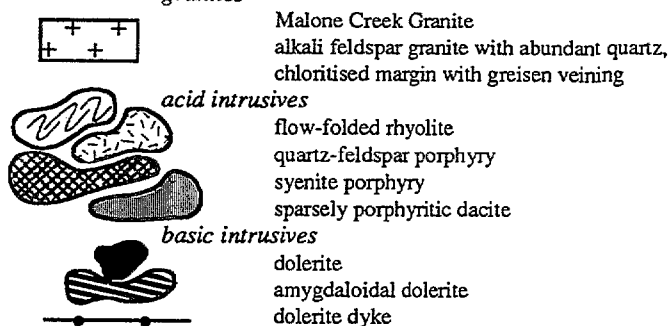
The Gimbat Ignimbrite Member and overlying Big Sunday Formation outcrop in the Stow region (Stuart-Smith et al. 1988) which lies in the southeastern part of the Pine Creek Inlier, an Early Proterozoic terrain of northern Australia. The regional geology and stratigraphy of the Pine Creek Inlier is described by Walpole et al. (1968), Needham et al. (1980, 1988) and Needham and Stuart-Smith (1985a).

The Gimbat Ignimbrite Member outcrops around the southern margin of the Malone Creek Granite (Fig. 1.1; 1.2; 1.3) to the southwest of the South Alligator Valley. The basement to the Gimbat Ignimbrite Member consists of the Coronation Sandstone (El Sherana Group), Burrell Creek Formation, and Zamu Dolerite. The Burrell Creek Formation is the uppermost unit of the Pine Creek Geosyncline Sequence, and consists of deep water turbiditic sediments: metamorphosed greywackes, schists, phyllites and phyllitic siltstone, interpreted to be deep water fine-grained sediments with coarser-grained turbiditic intervals (Stuart-Smith et al. 1984). The Zamu Dolerite intrudes the Burrell Creek Formation as thick sills. Both lithologies occur as lithic fragments in various ignimbrite and epiclastic units of the Gimbat Ignimbrite Member, suggesting the eruptive centre truncates these basement units. The Gimbat Ignimbrite Member unconformably overlies basalts and minor arkosic sandstones and conglomerates of the Coronation Sandstone, El Sherana Group.

The Gimbat Ignimbrite Member is unconformably overlain by the Big Sunday Formation. Both are truncated by a major fault system (the Palette Fault system) to the southwest, which isolates them from the stratigraphy of the El Sherana Group and Edith River Group west of the fault.

Figure 1.2 Legend

**Intrusive Rocks**



dl

**Big Sunday Formation**

tuffaceous siltstones and interbedded turbiditic sandstones



crystal-rich sandstone; closed framework mass flow unit formed as pyroclastic flows enter water,  
disintegrate and transform into water-supported mass flows

! ! ! ! denotes diffusely bounded pods of ignimbrite in the crystal-rich sandstones

**Gimbat Ignimbrite Member**



massive to flow banded, pink to brick red coloured aphyric rhyolite lava



sandstones and conglomerates deposited in fluvial channels. Locally planar and cross  
laminated. The fluvial channels contain several other recognisable units, and are mapped out in detail  
in Figure 1.3.

\* *Ignimbrites*

BC boulder conglomerate. Boulders of dolerite, quartz-feldspar porphyry, sandstone and crenulated  
metamorphic basement up to 2m in diameter, in a fine-grained silicic matrix interpreted to be of  
pyroclastic origin.

I<sub>NON</sub> non-welded ignimbrite

I<sub>E</sub> eutaxitic ignimbrite. Local sorting (grading) of pumice and lithic fragments

I<sub>E</sub> (3) crystal and fiamme poor ignimbrite

I<sub>E</sub> (2) pumice concentration zone

I<sub>E</sub> (1) lithic concentration zone

I<sub>D</sub> ignimbrite containing metamorphic basement clasts

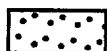
I<sub>C</sub> columnar jointed, densely welded ignimbrite

I<sub>B</sub> ignimbrite containing layered rhyolite clasts

I<sub>A</sub> ignimbrite containing quartz-feldspar porphyry clasts

I<sub>UNDIFF</sub> undifferentiated ignimbrite. Detailed mapping could not be carried out in this area due  
to lack of fresh outcrop. Ignimbrites contain dolerite, quartz-feldspar porphyry and  
basement fragments and are locally densely welded and columnar jointed

**Coronation Sandstone**



Pbc<sub>s</sub> arkosic sandstone, medium to coarse grained, mature, well sorted  
denotes coarser pebble horizons



Pbc<sub>b3</sub> fine grained basalt with vertical flow folding



Pbc<sub>b2</sub> fine grained basalt with resorbed quartz phenocrysts

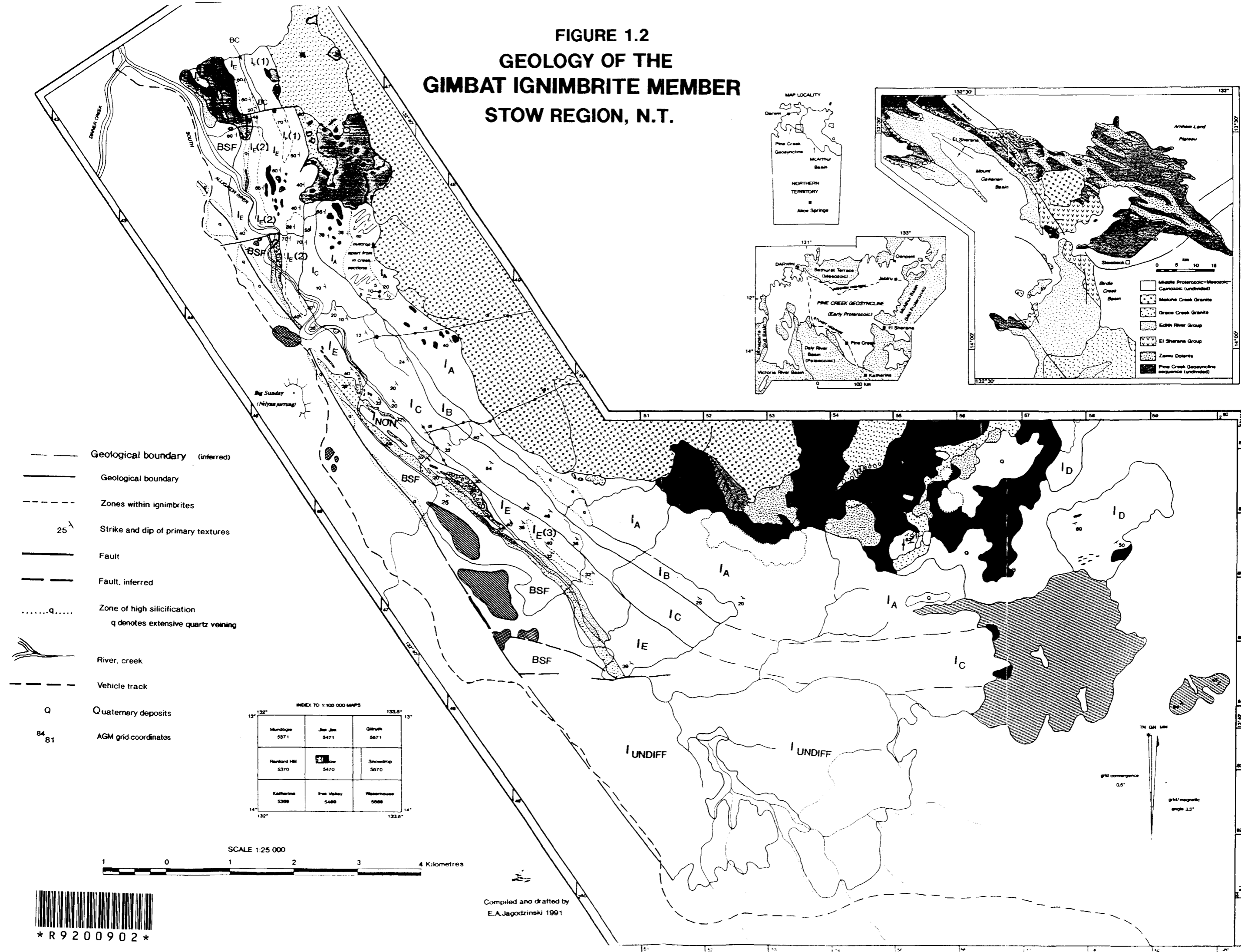


Pbc<sub>b1</sub> amygdaloidal basalt

\* N.B. The Gimbat Ignimbrite Member has a first order subdivision into facies, which may be stratigraphically  
repeated. Facies are further subdivided into units on the basis of stratigraphic position, lithology and/or types  
of lithic clasts they contain. Some units are then further subdivided into lithic or pumice concentration zones

denotes lithology (eg I = ignimbrite) ——— I<sub>E</sub> (3) ——— denotes zone within unit  
denotes unit of facies

**FIGURE 1.2**  
**GEOLOGY OF THE**  
**GIMBAT IGNIMBRITE MEMBER**  
**STOW REGION, N.T.**



### 1.2 REVISED STRATIGRAPHIC NOMENCLATURE

The volcanic succession outcropping approximately 10 km southeast of Coronation Hill, and to the east of the Palette Fault was assigned to the Pul Pul Rhyolite of the El Sherana Group by Needham & Stuart-Smith (1985a;b). Authors who carried out earlier regional mapping of the area in the 1960's had mapped this volcanic sequence as undivided Edith River Volcanics, with the Coronation Sandstone and Pul Pul Rhyolite forming members within the Edith River Volcanics, which were confined geographically to the South Alligator Valley further to the northwest (Fig. 1.4). That is, on a lithological basis, they did not recognise the three-fold subdivision of the El Sherana Group (Scinto Breccia; Coronation Sandstone; Pul Pul Rhyolite) south of Pul Pul Hill in the South Alligator Valley (Stewart 1965; Walpole et al 1968).

Needham & Stuart-Smith (1985a;b) elevated the Coronation Sandstone and Pul Pul Rhyolite to formation status, placed them within the newly defined El Sherana Group, and extended them into the undivided volcanic sequence to the southeast (Fig. 1.4). Their scheme divides the stratigraphy into units which represent different depositional environments, and therefore each formation contains a variety of lithologies. The Coronation Sandstone contains sediments deposited in a braided river system, with minor felsic and mafic volcanics (Friedmann 1992). The Pul Pul Rhyolite represents a major period of felsic volcanic activity within the El Sherana Group, and the overlying Big Sunday Formation contains sediments deposited in a lacustrine environment.

In agreement with Stewart (1965), this report finds there is no lithological basis for correlation between the Pul Pul Rhyolite in the South Alligator Valley and the volcanic succession to the southeast. The type section of the Pul Pul Rhyolite consists mainly of a rhyolitic, porphyritic lava, which is locally underlain by ignimbrite in the El Sherana-Monolith area, whereas the volcanics to the southeast comprise a thick (~830m) pile of ignimbrites with associated volcanoclastic sediments (Fig. 1.5). In addition, the volcanics in the South Alligator Valley have a maximum thickness of ~ 230 at Monolith and thin to the southeast towards Coronation Hill (Fig. 1.5), suggesting they may have a separate volcanic centre. It is therefore proposed that the thick ignimbrite sequence southeast of Coronation Hill be termed the Gimbat Ignimbrite Member, in order to distinguish it from the lavas and minor ignimbrite in the type area (Fig. 1.4).

The Gimbat Ignimbrite Member may correlate with volcanics of the type section, as it is also overlies the Coronation Sandstone, but evidence is inconclusive, because outcrop between the two areas is discontinuous, there are no marker horizons as the two areas are lithologically distinct, there are no age data available for the Pul Pul Rhyolite in the South Alligator Valley and geochemical comparisons can not be made, as the Pul Pul Rhyolite has undergone alteration related to mineralisation in the South Alligator Valley. It is an equally viable possibility that the Gimbat Ignimbrite Member overlies the type volcanics of the Pul Pul Rhyolite. They thin towards the Gimbat Ignimbrite Member and may pinch out altogether in this area. The nature of the contact between the Coronation Sandstone and Gimbat Ignimbrite Member can not be discerned, but appears to be unconformable, as the ignimbrites infill a palaeotopography formed on Coronation Sandstone.

Placing the volcanics in a separate stratigraphic member within the Pul Pul Rhyolite recognises the lithological distinction between the two areas, while allowing for the possibility of stratigraphic correlation between them. It also maintains the stratigraphic scheme of Needham & Stuart-Smith (1985b), in which the Pul Pul Rhyolite represents the main period of felsic volcanic activity within the El Sherana Group. Appendix C contains a formal definition of the new stratigraphic unit.



Figure 1.3 Legend

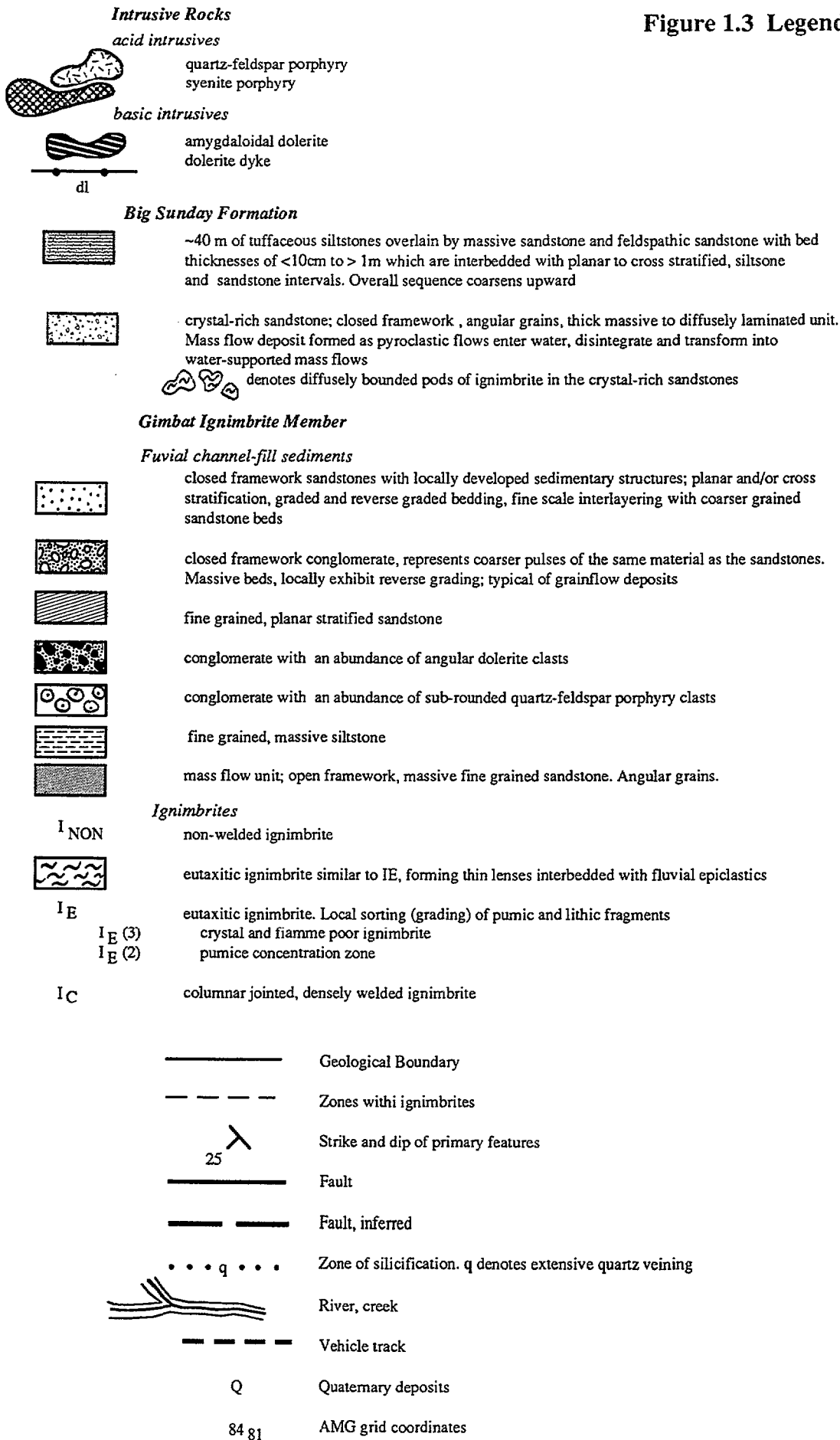


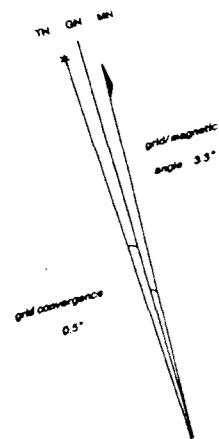
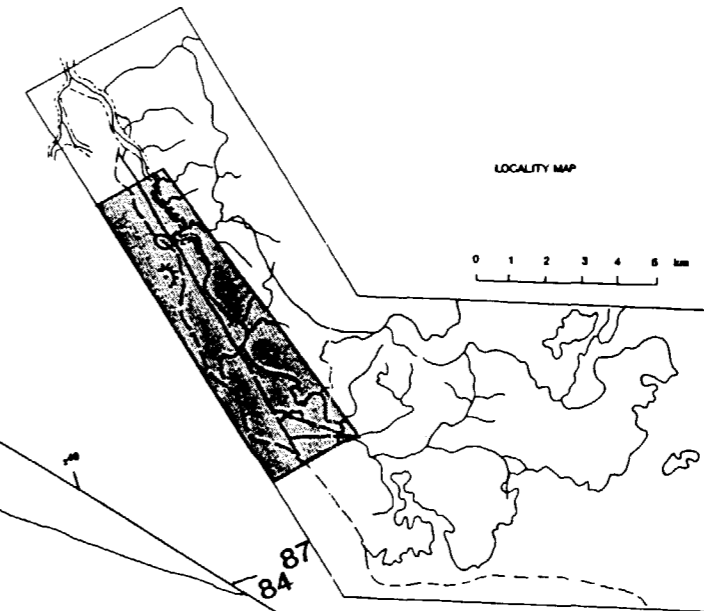
**FIGURE 1.3**  
**EPICLASTIC DEPOSITS OF THE**  
**GIMBAT IGIMBRITE MEMBER**  
**STOW REGION, N.T.**

0 0.5 1.0 1.5 2.0 kilometres

Scale 1:10 000

LOCALITY MAP

0 1 2 3 4 5 km



crystal-rich arenites

pods of ignimbrite

fluvial channel

GR 47 6886

fluvial channel

GR 477 862

GR 480 801 - 480 808

10m vertical scale

planar stratification  
 cross stratification  
 diffuse stratification

coarser pulses in ignimbrite result from ash winnowing in the fluidised head of a pyroclastic flow  
 black, glassy rhyolite  
 basal shear

Gimbat Ignimbrite Member

GR 47 8082 - 47 8079

Big Sunday Formation

GR 47 8676 - 47 8672

Big Sunday Formation

Gimbat Ignimbrite Member

intraclasts

felsic sills and dykes

GR 480 863 - 480 861



\* R 9 2 0 0 9 0 4 \*

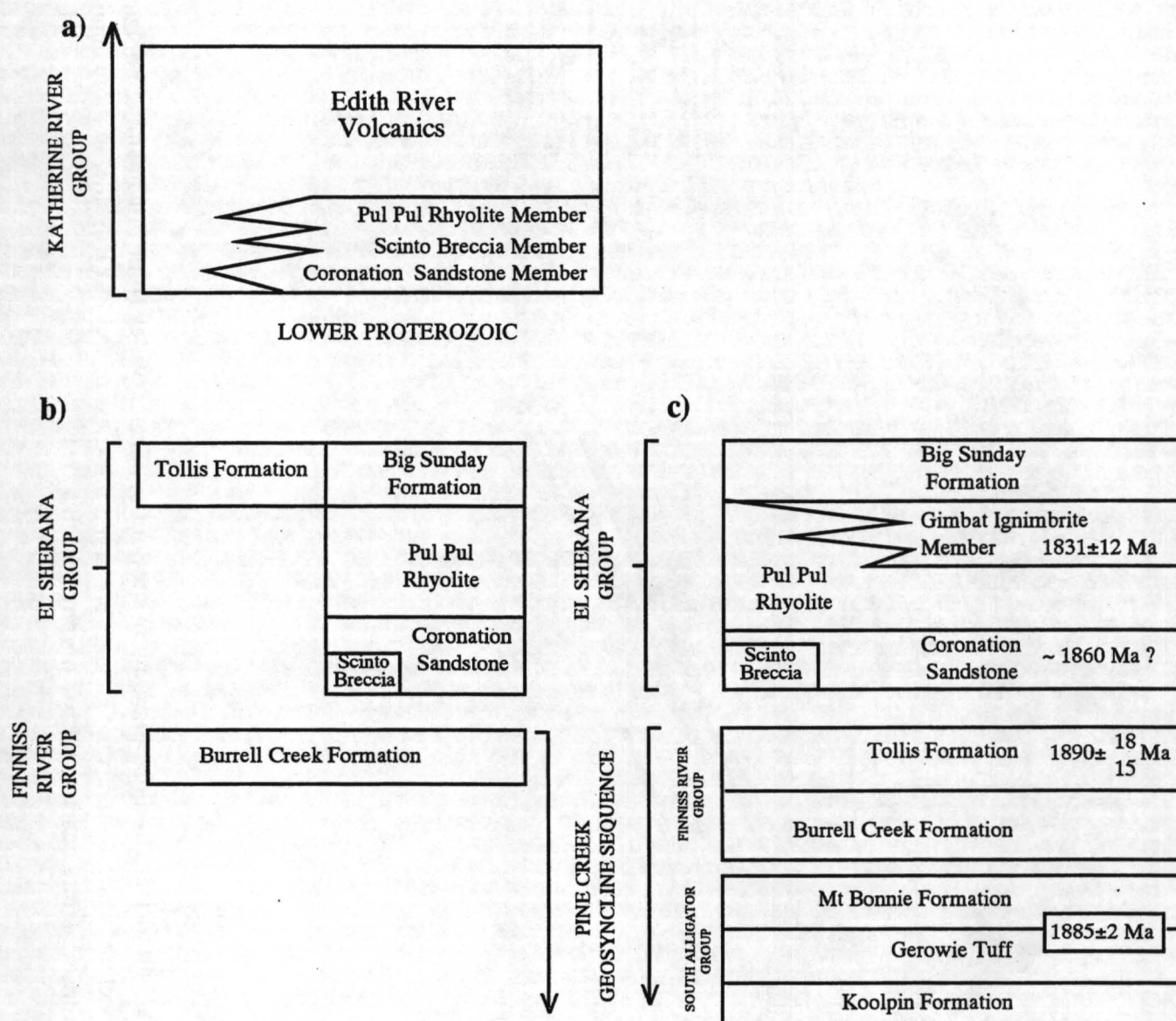


**Figure 1.4:** Revision of the stratigraphy in the Katherine-El Sherana area, and review of previous schemes. (a) Walpole et al (1968). (b) Needham & Stuart-Smith (1985). (c) Proposed stratigraphy, this report (Tollis Formation based on mapping of K.Hein).



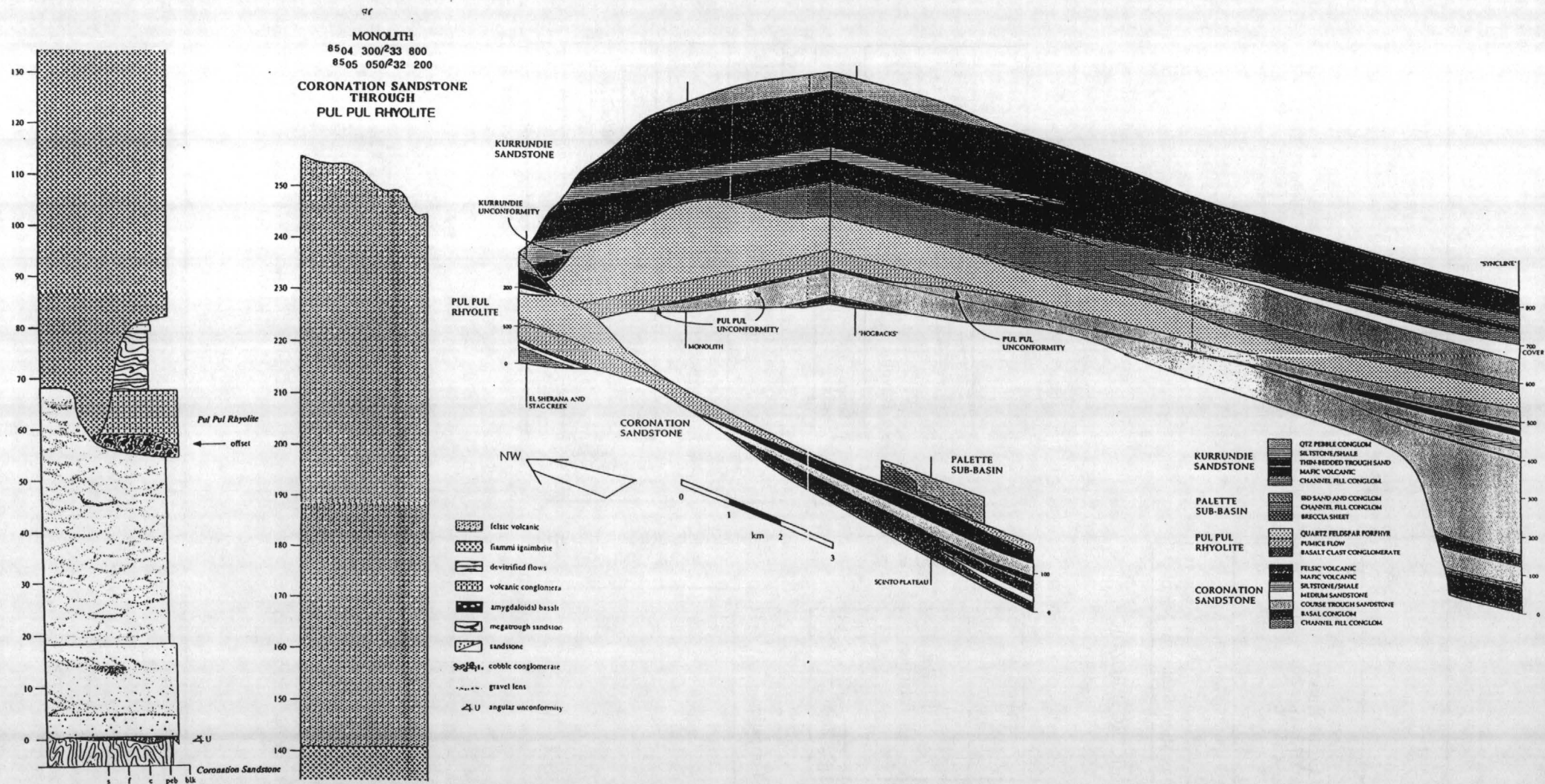
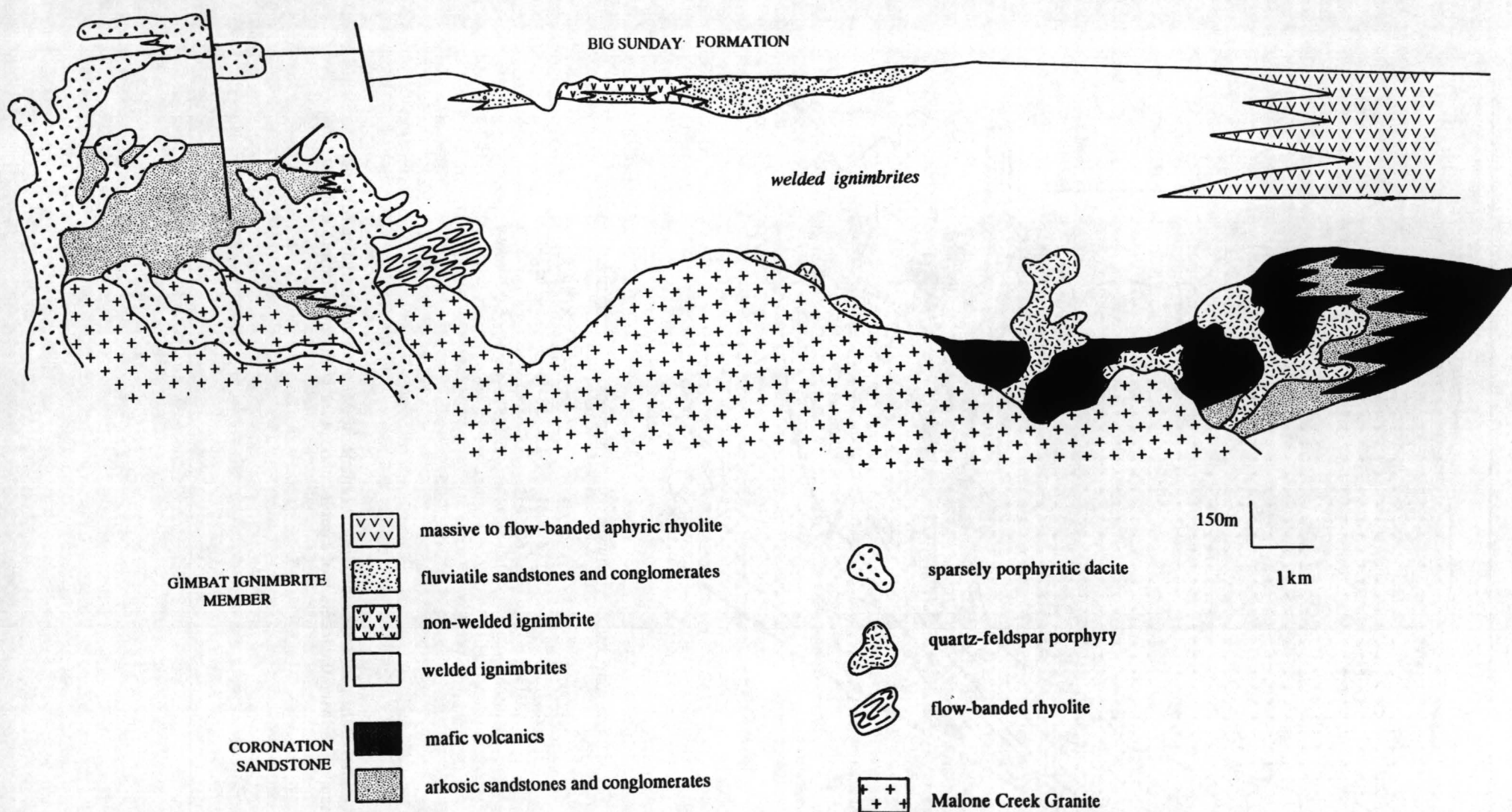


Figure 1.5a: Fence Diagram of the El Sherana/Edith River Group stratigraphy in the South Alligator Valley from Friedmann & Grotzinger 1991. The inset shows the monolith section, which contains the greatest preserved thickness of Pul Pul Rhyolite, in more detail. Note the Pul Pul Rhyolite comprises mainly quartz-feldspar porphyry in this area.



**Figure 1.5b:** Facies of the Pul Pul Rhyolite in the study area. Note the higher proportion of welded ignimbrites and the absence of thick porphyritic lavas compared with the Pul Pul Rhyolite in the South Alligator Valley

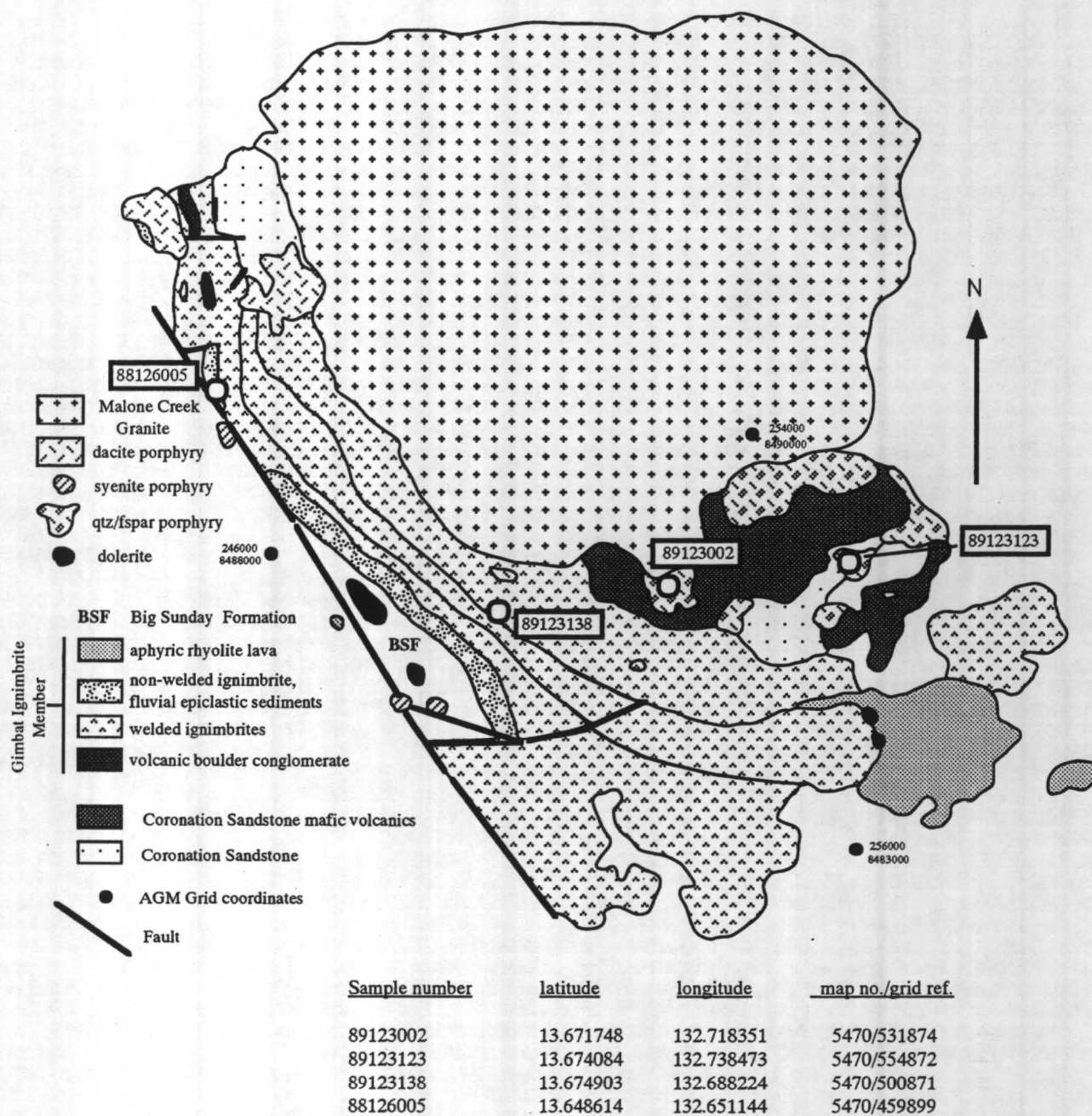


Figure 2.1: Simplified map of the geology of the Gimbat Ignimbrite Member and intrusive Malone Creek Granite, showing the location of samples chosen for U-Pb ion microprobe dating.

## 2. GEOCHRONOLOGY

### 2.1 INTRODUCTION

SHRIMP zircon geochronology was carried out on the volcanic and sub-volcanic association of the Gimbat Ignimbrite Member with the initial aim of constraining the age of the El Sherana Group. Only indirect age constraints were available prior to this study. Based on previously available geochronological data, the age of the El Sherana Group was considered to be between  $1885 \pm 2$  Ma (U-Pb ion probe age determination of tuff horizons in the underlying Gerowie Tuff and Mount Bonnie Formation; Needham et al, 1988) and 1870-1860 Ma (conventional U-Pb data for the overlying Edith River Group and co-magmatic Grace Creek Granite; Needham et al, 1988). Ion microprobe U-Pb data from an andesitic tuff from the Tollis Formation, considered to be part of the El Sherana Group (a correlative of the Big Sunday Formation, overlying the Pul Pul Rhyolite), regress to give an age of  $1890 \pm_{15}^{18}$  Ma (Page & Williams, 1988). Preliminary ion microprobe results for a felsic volcanic sampled from the pit of the El Sherana uranium mine suggest the age of the Coronation Sandstone is approximately 1860 Ma (unpublished data; R.W. Page pers. comm.). Based on these data, the age of the El Sherana Group was considered to be between 1870 and 1860 Ma.

The isotopic data resulting from this study yielded unexpected results, which suggest the rocks studied are considerably younger than the currently accepted age for the El Sherana Group. The results have important stratigraphic implications which are discussed in Section 2.7, and also have implications for SHRIMP ion microprobe dating techniques, emphasizing the importance of applying available geological and petrographic information, when interpreting geochronological data.

### 2.2 GEOLOGY OF THE GIMBAT IGNIMBRITE MEMBER

Subdivision of members of the Gimbat Ignimbrite Member into facies, facies analysis and facies relationships are outlined in detail in Sections 4-9, but brief lithological descriptions and a summary of stratigraphic relationships are given here to outline the geological context of the samples chosen for dating.

The geology of the Gimbat Ignimbrite Member and sample localities and a map are presented in Fig. 2.1. The felsic volcanic sequence of the Gimbat Ignimbrite Member is dominated by quartz-feldspar-bearing rhyolitic ignimbrites, with minor rhyolite lavas, which form a succession approximately 830 m thick. The ignimbrites are variably welded with a well defined eutaxitic texture defined by attenuated pumice clasts (fiamme), and local development of columnar jointing. As well as crystals and pumice, the ignimbrites contain abundant lithic fragments, a common feature of pyroclastic flow deposits. Lithic fragments derived from the country rock are incorporated into ignimbrites during the explosive eruption (vent flaring and widening), or as the highly erosive pyroclastic flow travels across the land surface. Dolerite is the most common lithic clast in the ignimbrites; others include quartz-feldspar porphyry, vein quartz, quartz sandstone, plutonic quartz and metasedimentary basement clasts. Both the composition and the size of lithic clasts are variable throughout the sequence.

The ignimbrites divide into 6 mappable units based on stratigraphic position, degree of welding and dominant lithic clast components. Most of the ignimbrites are 'normal' layer 2b ignimbrites (Sparks et al, 1973) deposited from the main body of the pyroclastic flow. They contain discontinuous lithic concentration zones which probably mark the lithic-rich bases of individual flow units. These lithic concentration zones contain moderate concentrations of lithic clasts (~ 20%) up to 20 cm in diameter, in an open framework configuration.



The top 150 m of the ignimbrite sequence is not welded and hosts conglomerate and volcanic sandstone lenses which are interpreted to represent incised fluvial gullies formed during periods of quiescence between volcanic eruptions. Their grain and lithic compositions suggest a mixed basement and contemporaneous pyroclastic source. The ignimbrites and fluvial sediments are overlain by lacustrine sediments of the Big Sunday Formation, and by flow-banded rhyolites to the south east.


The ignimbrite pile is intruded by rhyolitic quartz-feldspar porphyries, felsic sills and dykes, syenite porphyries, sparsely porphyritic dacites, dolerites, and by the Malone Creek Granite to the north. The quartz-feldspar porphyries and sparsely porphyritic felsic sills and dykes are similar in composition to the ignimbrites, as discussed in Section 7. They intrude as numerous small bodies, some no larger than 2-4 m<sup>2</sup> in outcrop size, and the largest covering an area of 750 x 500 m. The ignimbrites also contain lithic clasts of quartz-feldspar porphyry. This suggests the magma had partly chilled subsurface before the remainder vesiculated and erupted to form the ignimbrites, which incorporated chilled porphyry clasts at depth. Later, remaining magma intruded the ignimbrite beds and solidified to form small intrusive domes. This intimate field and chemical association infers that the ignimbrites and subvolcanic quartz-feldspar porphyries together comprise a coherent magmatic association.

### 2.3 SAMPLE SELECTION

U-Pb dates were obtained on four samples, two of which are quartz-feldspar porphyries, chosen for dating on the assumption that the quartz-feldspar porphyries and ignimbrites are comagmatic. Quartz-feldspar porphyries were dated in preference to ignimbrites, because the ignimbrites are likely to contain a mixed population of magmatic zircons and xenocrystic zircons derived from the country rock during eruption and deposition. Ignimbrites are the product of explosive volcanic activity, which often causes fragmentation of country rock, vent flaring and widening during eruption, so that large volumes of country rock are incorporated into the erupting magma as xenoliths and xenocrysts. In addition, the flow-front or head of a pyroclastic flow is highly erosive, so that xenoliths are incorporated into flow as it travels over the land surface. Thus in terms of implications for dating, the nature of an ignimbrite is very similar to that of a sediment. It may contain numerous different zircon populations, obtained from several different source rocks, making it difficult to discern the crystallisation age of the sample.

Samples 89123002 and 89123123 are intrusive quartz-feldspar porphyries, and their ages provide a minimum constraint on the age of the ignimbrite sequence. Sample 89123138 is the only ignimbrite sample dated, obtained from ignimbrite unit I<sub>B</sub>, which contains abundant clasts of layered rhyolite (5-20 cm), and local concentrations of large dolerite clasts (10-20 cm). These samples are compared with data obtained for a sediment from one of the fluvial channels which incise the top of the ignimbrite pile (88126005). Fig. 2.2 is a schematic cross section showing the relative stratigraphic positions of the samples dated.

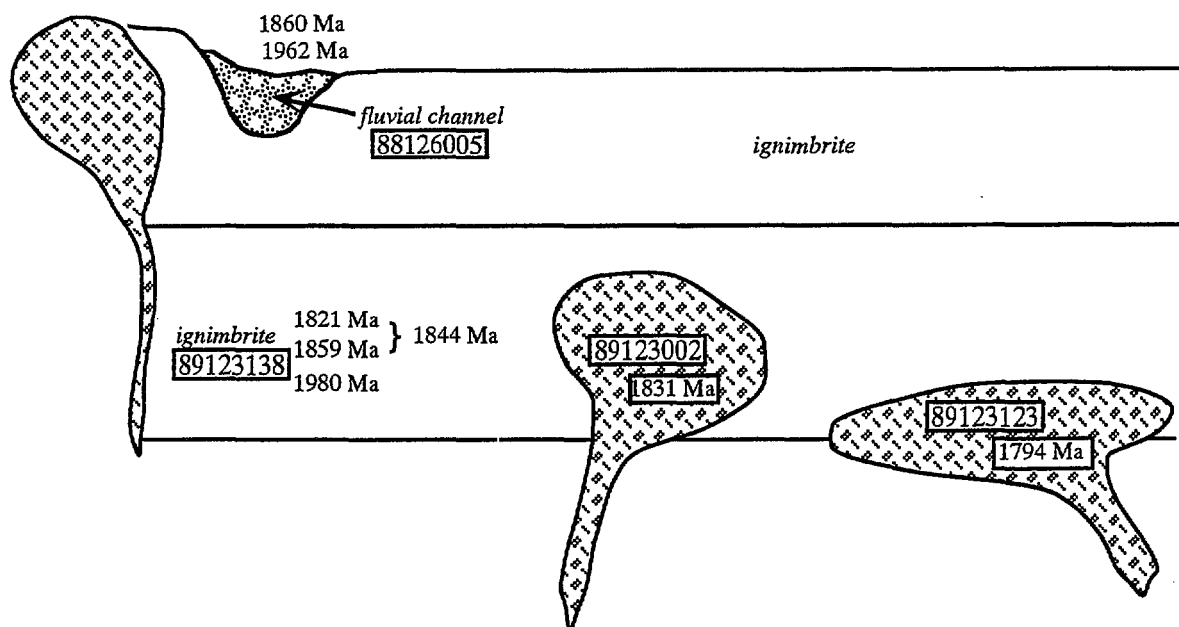


**Figure 2.2:** Schematic diagram of relative ages and stratigraphic position of samples dated during this study.  denotes quartz-feldspar porphyry.

## 2.4 ION MICROPROBE ANALYSES

### 2.4.1 Analytical techniques

The techniques for the U-Th-Pb analysis of zircons using SHRIMP follow those described by Compston et al (1984) and Williams & Claesson (1987). Zircons were mounted in epoxy, polished to expose their centres, and either carbon or gold coated. U-Th-Pb isotopic compositions were measured on areas of zircon 25-40  $\mu\text{m}$  in diameter, by focussing a 10 kV primary beam of negative oxygen ions onto the sectioned crystal, then extracting the positive sputtered secondary ions emitted normally to the surface. These were accelerated to 11 kV and transferred to a double focussing mass spectrometer operated at a mass resolution of 6500 to eliminate significant interferences. Isotopic ratios were measured using an electron multiplier. Each analysis is the mean of seven scans through the mass stations of interest.

Pb/U ratios of unknown zircons were determined by normalising to laboratory standard zircons, SL3 or SL13, for which radiogenic  $^{206}\text{Pb}/^{238}\text{U}$  is taken to be 0.0928, equivalent to an age of 572 Ma. Reproducibility of the Pb/U ratio of the standard was better than  $\pm 2.5\%$  for all samples, and this uncertainty is included in the quoted analytical errors. Uncertainties in the analyses listed in the data tables are listed as  $1\sigma$ , and uncertainties in ages as 95% confidence limits ( $2\sigma$ ). Ages are calculated using the constants recommended by the IUGS Subcommittee on Geochronology (Steiger and Jager 1977).

**Table 2.1:** Ion microprobe analytical data for a quartz-feldspar porphyry, intruding the Gimbat Ignimbrite member of the Pul Pul Rhyolite: Sample 89123002.

Grain-spot	U ppm	Th/U	$^{206}\text{Pb}/^{204}\text{Pb}$	$^{208}\text{Pb}/^{206}\text{Pb}$	$^{206}\text{Pb}/^{238}\text{U} \pm 1\sigma$	$^{207}\text{Pb}/^{235}\text{U} \pm 1\sigma$	$^{207}\text{Pb}/^{206}\text{Pb} \pm 1\sigma$	Age (Ma)
1.1	151	0.63	18997	0.1833	$0.3229 \pm 92$	$5.015 \pm 155$	$0.1126 \pm 10$	$1842 \pm 16$
2.1	268	0.46	21195	0.1289	$0.3275 \pm 93$	$5.110 \pm 151$	$0.1132 \pm 6$	$1851 \pm 10$
3.1	192	0.59	18232	0.1697	$0.3120 \pm 88$	$4.819 \pm 145$	$0.1120 \pm 8$	$1832 \pm 13$
4.1	212	0.66	9355	0.1808	$0.3207 \pm 91$	$4.947 \pm 155$	$0.1119 \pm 11$	$1830 \pm 18$
5.1	95	0.89	16464	0.2589	$0.3401 \pm 33$	$5.251 \pm 140$	$0.1120 \pm 26$	$1832 \pm 43$
6.1	205	0.55	1317	0.1429	$0.3040 \pm 82$	$4.556 \pm 158$	$0.1087 \pm 20$	$1777 \pm 34$
7.1	154	0.96	974	0.2736	$0.3181 \pm 86$	$4.831 \pm 173$	$0.1101 \pm 22$	$1802 \pm 38$
8.1	307	0.62	4168	0.1709	$0.3342 \pm 89$	$5.099 \pm 151$	$0.1107 \pm 11$	$1810 \pm 18$
9.1	333	0.77	833	0.2111	$0.3187 \pm 85$	$4.838 \pm 156$	$0.1101 \pm 17$	$1801 \pm 28$
10.1	118	0.65	429	0.2040	$0.3193 \pm 88$	$4.868 \pm 243$	$0.1106 \pm 42$	$1809 \pm 71$
11.1	156	0.65	345	0.1793	$0.3211 \pm 87$	$4.747 \pm 225$	$0.1072 \pm 38$	$1753 \pm 66$
12.1	185	0.62	1837	0.1746	$0.3087 \pm 83$	$4.707 \pm 146$	$0.1106 \pm 14$	$1809 \pm 23$
13.1	191	0.60	3091	0.1704	$0.3235 \pm 87$	$5.012 \pm 150$	$0.1124 \pm 11$	$1838 \pm 18$
14.1	67	0.98	782	0.2404	$0.3366 \pm 96$	$4.830 \pm 294$	$0.1041 \pm 52$	$1698 \pm 96$

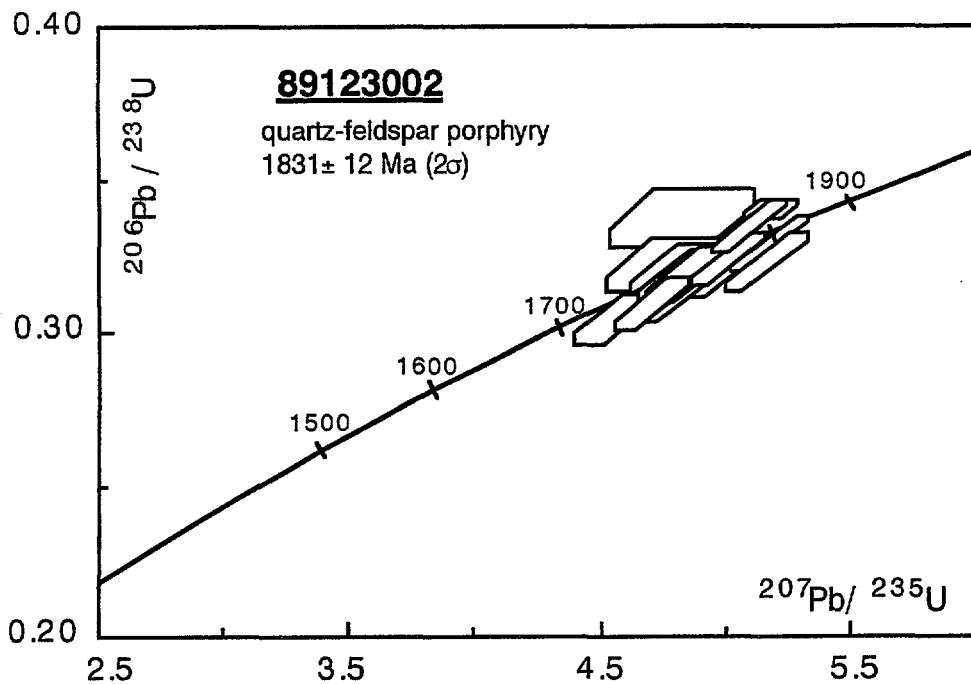


**Figure 2.3:** Concordia diagram showing zircon analyses from 89123002, an intrusive quartz-feldspar porphyry near the base of the Gimbat Ignimbrite Member.

The data have been corrected for common Pb by reference to the abundance of  $^{204}\text{Pb}$ . All data have corrected by assuming that the common Pb is the composition of average crustal Pb the same age as the zircons (using the model of Cumming and Richards 1975).

#### 2.4.2 Intrusive quartz-feldspar porphyry: 89123002

The zircons from sample 89123002 are generally stubby euhedral to subhedral prisms with aspect ratios between 1:1 and 3:1, and well preserved crystal terminations. Most are internally clear, colourless, and contain few solid and fluid inclusions. and some exhibit well developed euhedral zoning. None exhibit structurally discordant cores. The morphology is consistent with a magmatic origin for the zircons.

The zircons have moderately low U contents (< 330 ppm) and Th/U (0.4 - 1.0), within the normal igneous zircon range (Table 2.1). Initial Pb contents are very low. All 14 analyses are concordant and have the same  $^{207}\text{Pb}^*/^{206}\text{Pb}^*$  within error. The weighted mean  $^{207}\text{Pb}^*/^{206}\text{Pb}^*$  age is 1831 ± 12 Ma (Fig. 2.3).

**Table 2.2:** Ion microprobe analytical data for a quartz-feldspar porphyry, intruding the Gimbat Ignimbrite member of the Pul Pul Rhyolite: Sample 89123123.

Grain-spot	U ppm	Th/U	$^{206}\text{Pb}/^{204}\text{Pb}$	$^{208}\text{Pb}/^{206}\text{Pb}$	$^{206}\text{Pb}/^{238}\text{U} \pm 1\sigma$	$^{207}\text{Pb}/^{235}\text{U} \pm 1\sigma$	$^{207}\text{Pb}/^{206}\text{Pb} \pm 1\sigma$	Age (Ma)
1.1	154	0.69	2371	0.1883	$0.3234 \pm 53$	$4.795 \pm 112$	$.10755 \pm 157$	$1758 \pm 27$
2.1	152	1.01	3520	0.2794	$0.3165 \pm 52$	$4.778 \pm 114$	$.10949 \pm 166$	$1791 \pm 28$
3.1	113	0.70	2545	0.1900	$0.3217 \pm 54$	$4.864 \pm 125$	$.10966 \pm 192$	$1794 \pm 32$
4.1	103	0.81	4373	0.2295	$0.3162 \pm 54$	$4.860 \pm 135$	$.11145 \pm 224$	$1823 \pm 37$
5.1	190	0.66	3964	0.1864	$0.3172 \pm 52$	$4.795 \pm 106$	$.10965 \pm 143$	$1794 \pm 24$
6.1	106	0.83	3263	0.2352	$0.3324 \pm 56$	$4.976 \pm 133$	$.10857 \pm 203$	$1776 \pm 34$
7.1	140	0.71	2239	0.1953	$0.3217 \pm 53$	$4.776 \pm 121$	$.10766 \pm 184$	$1760 \pm 32$
8.1	189	0.39	4113	0.1067	$0.3180 \pm 52$	$4.822 \pm 115$	$.11000 \pm 168$	$1799 \pm 28$
9.1	214	0.54	4761	0.1520	$0.3194 \pm 52$	$4.827 \pm 106$	$.10960 \pm 140$	$1793 \pm 24$
10.1	284	0.59	5257	0.1671	$0.3244 \pm 52$	$4.915 \pm 94$	$.10989 \pm 93$	$1798 \pm 16$
11.1	38	0.36	1749	0.0940	$0.4370 \pm 85$	$9.347 \pm 317$	$.15512 \pm 395$	$2403 \pm 44$
12.1	189	0.60	184	0.3138	$0.2286 \pm 38$	$3.474 \pm 164$	$.11023 \pm 462$	$1803 \pm 78$
13.1	240	0.58	5043	0.1623	$0.3172 \pm 52$	$4.797 \pm 102$	$.10969 \pm 130$	$1794 \pm 22$
14.1	210	0.75	8028	0.1941	$0.3113 \pm 51$	$4.769 \pm 96$	$.11111 \pm 111$	$1818 \pm 18$
15.1	121	0.68	925	0.1981	$0.3190 \pm 54$	$5.057 \pm 159$	$.11497 \pm 281$	$1879 \pm 45$
16.1	77	0.92	1353	0.2451	$0.3216 \pm 56$	$4.593 \pm 164$	$.10359 \pm 301$	$1689 \pm 55$

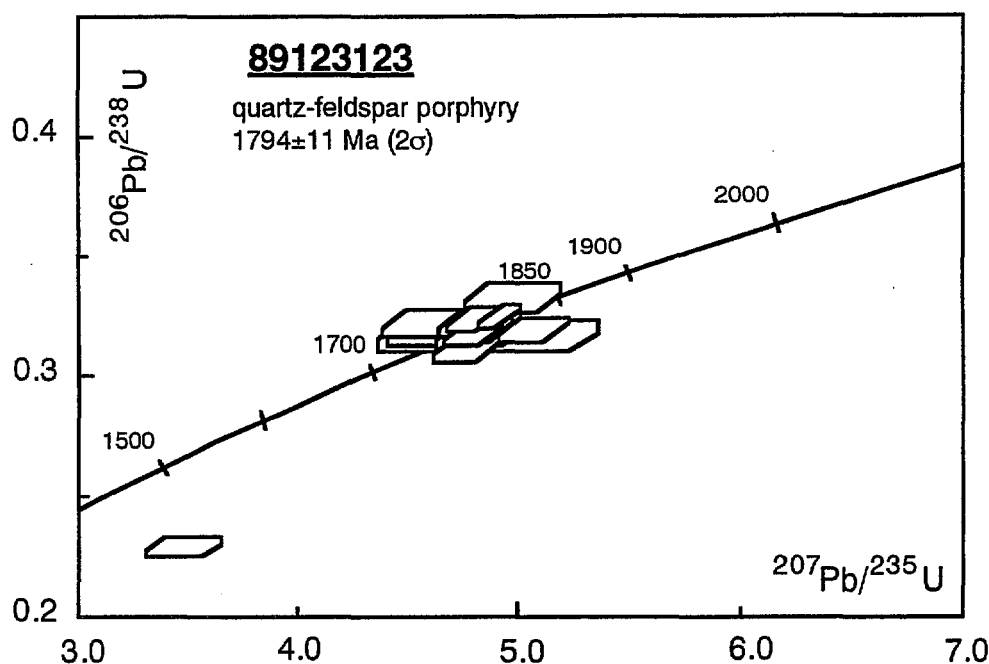


**Figure 2.4:** Concordia diagram showing zircon analyses from 89123123, an intrusive quartz-feldspar porphyry near the base of the Gimbat Ignimbrite Member.

### 2.4.3 Intrusive quartz-feldspar porphyry: 89123123

The zircons from sample 89123123 have a similar appearance to those of sample 89123002. They are consistent with a magmatic origin, internally clear, colourless, with well-developed zoning in some crystals. Most are stubby subhedral crystals, but many are euhedral and prismatic in form, with low aspect ratios between 1:1 and 2:1. Rare grains contain structurally discordant cores and a few grains are rounded with pitted surfaces caused by mechanical abrasion.

The zircons have moderately low U contents (< 300 ppm) and Th/U ratios between 0.4 - 1.0. Initial Pb contents are very low (Table 2.2). On a Concordia plot 15 of the 16 analyses have the same  $^{207}\text{Pb}^*/^{206}\text{Pb}^*$  within error and yield a weighted mean age of 1794±11 Ma (Fig. 2.4). Most of these analyses plot on or near Concordia. Some are marginally reverse discordant, and one analysis is approximately 20% discordant. Grain 11.1 is probably a xenocryst and was not included in the pooling of the data. It has a different morphology to the bulk of the zircon population, being rounded with an abraded surface, has a lower U content and a  $^{207}\text{Pb}/^{206}\text{Pb}$  age of 2403±44 Ma.

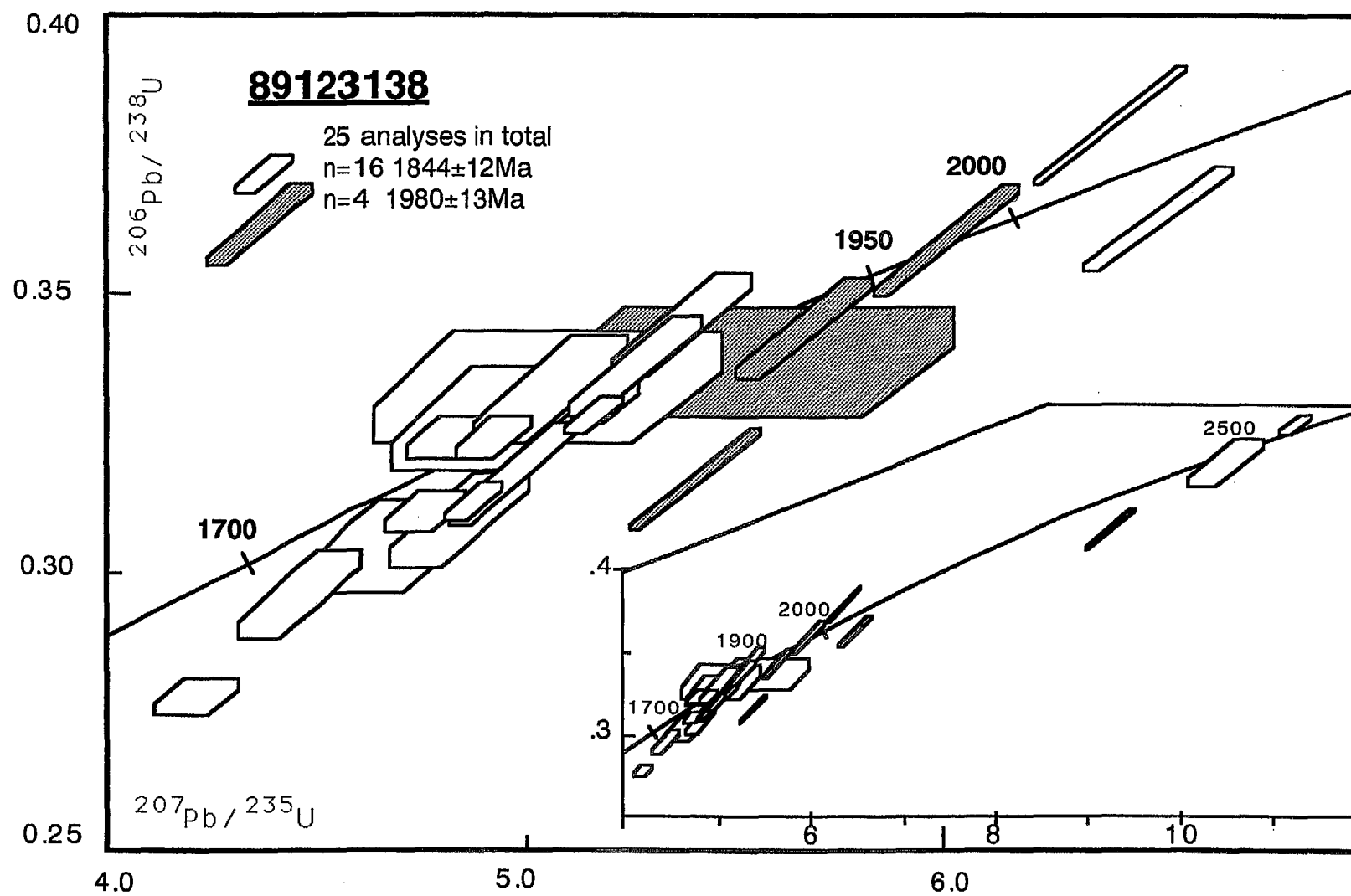


**Figure 2.5:** Concordia diagram showing zircon analyses from 89123138, an ignimbrite (unit IB) of the Gimbat Ignimbrite Member. Inset shows data for all samples.

#### 2.4.4 Ignimbrite: 89123138

The zircon population of sample 89123138 exhibits a wide diversity of zircon morphologies compared with zircons of the quartz-feldspar porphyries. Many are clear, euhedral, prismatic zircons with internal growth zoning common, and are interpreted as being of magmatic origin. These crystals have moderate aspect ratios from 1.1 to 3.1. Some grains are fragmented, which is consistent with explosive volcanism. Equally many are interpreted as xenocrysts. They are equant in form, with rounded terminations and sometimes have abraded or pitted surfaces. These are considered to be of detrital origin and probably derived from the country rock (metasedimentary basement rocks) and incorporated into the ignimbrite during pyroclastic eruption.

U contents generally span between 30 and 300 ppm but are over 500 ppm for two grains, and over 1000 ppm for another two (Table 2.3). There is a wide range in  $^{207}\text{Pb}^*/^{206}\text{Pb}^*$  implying some inheritance in the zircon population. On a Concordia diagram, several age populations were identified (Fig. 2.5). Three grains have a  $^{207}\text{Pb}/^{206}\text{Pb}$  age of  $\sim 2500$  Ma. Four are pooled to give an age of  $1980 \pm 16$  Ma. The remaining 16 analyses regress to give a  $^{207}\text{Pb}^*/^{206}\text{Pb}^*$  age of  $1844 \pm 12$  Ma. A weighted histogram of the  $^{207}\text{Pb}^*/^{206}\text{Pb}^*$  ages of this population, shows that the spread of ages exceeds that due to analytical uncertainty and suggests there may be two age groupings within this single population, which cannot be statistically resolved (Fig. 2.6). These populations regress to give  $^{207}\text{Pb}^*/^{206}\text{Pb}^*$  ages of  $1821 \pm 18$  Ma (based on 10 samples) and  $1859 \pm 14$  Ma (based on 6 grains).

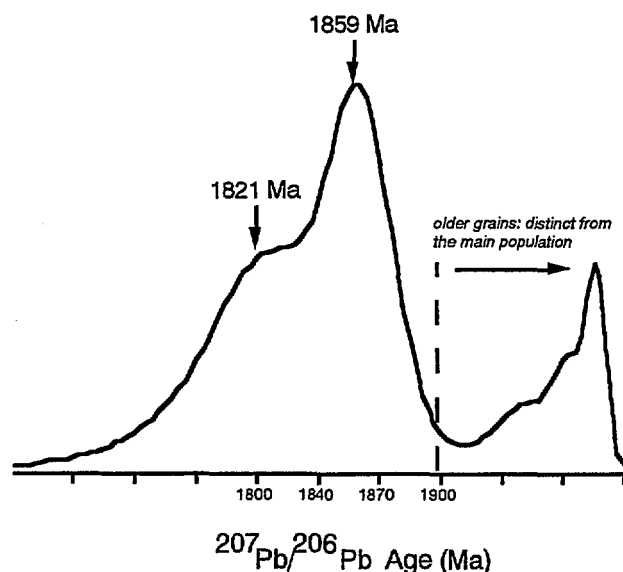


**Figure 2.6:** Histogram (Gaussian summation) of the  $^{207}\text{Pb}^*/^{206}\text{Pb}^*$  ages of data for 8912.3138, showing the bimodal distribution of ages in the main zircon population.

**Table 2.3:** Ion microprobe analytical data for a felsic volcanic (ignimbrite) in the Gimbat Ignimbrite Member of the Pul Pul Rhyolite: Sample 89123138.

Grain-spot	U ppm	Th/U	$^{206}\text{Pb}/^{204}\text{Pb}$	$^{208}\text{Pb}/^{206}\text{Pb}$	$^{206}\text{Pb}/^{238}\text{U} \pm 1\sigma$	$^{207}\text{Pb}/^{235}\text{U} \pm 1\sigma$	$^{207}\text{Pb}/^{206}\text{Pb} \pm 1\sigma$	Age (Ma)
1	156	0.45	14273	0.1291	0.3280 $\pm$ 35	5.162 $\pm$ 71	0.1141 $\pm$ 37	1866 $\pm$ 13
2	69	1.18	9024	0.3352	0.3241 $\pm$ 38	4.920 $\pm$ 90	0.1101 $\pm$ 95	1801 $\pm$ 23
3	75	0.97	2862	0.2621	0.3107 $\pm$ 36	4.755 $\pm$ 95	0.1110 $\pm$ 40	1815 $\pm$ 27
4	59	1.17	3516	0.3221	0.3240 $\pm$ 40	4.847 $\pm$ 133	0.1085 $\pm$ 10	1775 $\pm$ 43
5	57	1.38	5049	0.3700	0.2779 $\pm$ 34	4.214 $\pm$ 99	0.1100 $\pm$ 14	1799 $\pm$ 35
6	101	0.67	6292	0.1829	0.4885 $\pm$ 57	11.295 $\pm$ 160	0.1677 $\pm$ 11	2535 $\pm$ 12
7	164	0.51	3816	0.1325	0.3302 $\pm$ 36	5.189 $\pm$ 82	0.1140 $\pm$ 21	1864 $\pm$ 18
8	122	1.04	42644	0.2980	0.3125 $\pm$ 34	4.872 $\pm$ 68	0.1131 $\pm$ 19	1849 $\pm$ 14
9	302	0.65	15067	0.1846	0.3596 $\pm$ 102	6.006 $\pm$ 176	0.1211 $\pm$ 7	1973 $\pm$ 9
10	592	0.20	87951	0.0575	0.3167 $\pm$ 89	5.406 $\pm$ 155	0.1238 $\pm$ 8	2012 $\pm$ 6
11	31	1.10	2132	0.2935	0.4651 $\pm$ 142	10.540 $\pm$ 408	0.1644 $\pm$ 14	2501 $\pm$ 35
12	1046	0.25	4242	0.0712	0.4251 $\pm$ 119	9.275 $\pm$ 264	0.1583 $\pm$ 16	2437 $\pm$ 4
13	1187	0.03	6578	0.0085	0.3804 $\pm$ 107	6.399 $\pm$ 182	0.1220 $\pm$ 25	1986 $\pm$ 5
14	49	0.84	5163	0.2313	0.3330 $\pm$ 102	5.050 $\pm$ 417	0.1100 $\pm$ 21	1799 $\pm$ 139
15	70	1.73	2577	0.5008	0.3327 $\pm$ 97	5.058 $\pm$ 185	0.1103 $\pm$ 12	1804 $\pm$ 35
16	138	0.64	57604	0.1898	0.3175 $\pm$ 90	4.968 $\pm$ 153	0.1135 $\pm$ 12	1856 $\pm$ 15
17	295	1.64	318	0.3715	0.3046 $\pm$ 82	4.678 $\pm$ 213	0.1114 $\pm$ 8	1822 $\pm$ 62
18	87	0.67	144	0.2185	0.3377 $\pm$ 100	5.532 $\pm$ 491	0.1188 $\pm$ 6	1938 $\pm$ 151
19	70	0.92	1128	0.2565	0.3273 $\pm$ 93	4.913 $\pm$ 240	0.1089 $\pm$ 4	1780 $\pm$ 68
20	511	0.28	8299	0.0736	0.3438 $\pm$ 92	5.661 $\pm$ 164	0.1194 $\pm$ 33	1948 $\pm$ 15
21	253	0.55	2951	0.1477	0.3443 $\pm$ 92	5.372 $\pm$ 165	0.1131 $\pm$ 4	1851 $\pm$ 22
22	279	1.00	11550	0.2749	0.3368 $\pm$ 91	5.262 $\pm$ 156	0.1133 $\pm$ 3	1853 $\pm$ 18
23	158	0.74	2082	0.2204	0.3094 $\pm$ 84	4.836 $\pm$ 169	0.1133 $\pm$ 80	1854 $\pm$ 34
24	346	1.10	1581	0.2759	0.2961 $\pm$ 79	4.458 $\pm$ 149	0.1092 $\pm$ 21	1786 $\pm$ 31
25	531	0.29	9473	0.0793	0.3635 $\pm$ 97	6.515 $\pm$ 180	0.1300 $\pm$ 10	2098 $\pm$ 9

**Table 2.4:** Ion microprobe analytical data for a fluvial epiclastic sediment in the Gimbat Ignimbrite Member of the Pul Pul Rhyolite: Sample 88126005.

Grain-spot	U ppm	Th/U	$^{206}\text{Pb}/^{204}\text{Pb}$	f <sub>206%</sub> a)	$^{208}\text{Pb}/^{206}\text{Pb}$	$^{206}\text{Pb}/^{238}\text{U} \pm 1\sigma$	$^{207}\text{Pb}/^{235}\text{U} \pm 1\sigma$	$^{207}\text{Pb}/^{206}\text{Pb} \pm 1\sigma$	Age (Ma)
1-1	247	0.43	1074	1.43	0.1081	0.3307±49	5.338±118	0.1171±17	1912±27
2-1	120	1.28	6193	0.25	0.3551	0.3167±87	4.873±156	0.1116±15	1825±25
3-1	382	0.26	12587	0.12	0.0704	0.3398±50	5.384±92	0.1149±8	1879±13
4-1	220	0.18	7205	0.21	0.0499	0.3568±54	5.923±105	0.1204±9	1962±14
5-1	1097	0.09	35714	0.04	0.0249	0.3388±48	5.346±80	0.1144±4	1871±6
5-2	1259	0.09	12183	0.13	0.0241	0.3580±96	5.680±155	0.1151±3	1881±5
6-1	139	0.43	7411	0.21	0.1169	0.3172±87	4.953±155	0.1132±14	1852±22
7-1	175	0.31	3720	0.41	0.0799	0.3252±88	4.920±153	0.1097±13	1795±22
8-1	288	0.34	8986	0.17	0.0934	0.3260±88	5.108±146	0.1136±7	1858±12
9-1	138	0.88	1066	1.44	0.2396	0.3305±91	5.203±192	0.1142±24	1867±39
10-1	109	0.67	975	1.58	0.1683	0.2861±79	4.244±169	0.1076±27	1759±48
11-1	227	0.53	11669	0.13	0.1469	0.3299±89	5.204±151	0.1144±9	1870±14
12-1	740	0.10	11453	0.13	0.0301	0.3630±97	6.035±166	0.1206±5	1965±7
13-1	443	0.83	3063	0.50	0.2383	0.3661±98	6.085±174	0.1205±8	1964±12
14-1	223	0.25	8041	0.19	0.0648	0.3509±95	5.661±165	0.1170±9	1911±15
15-1	88	0.87	2657	0.58	0.2325	0.3182±88	4.753±173	0.1084±22	1772±38
15-2	182	1.35	1875	0.82	0.2928	0.2791±76	4.196±146	0.1090±20	1783±34
16-1	64	0.56	27809	0.05	0.1572	0.4564±128	10.402±326	0.1653±18	2510±18
17-1	158	0.66	1018	1.51	0.1317	0.2814±77	4.379±158	0.1129±23	1846±38
18-1	154	1.26	1132	1.36	0.2045	0.2785±76	4.109±154	0.1070±24	1749±42
19-1	415	0.45	22257	0.07	0.1240	0.3938±106	7.010±195	0.1291±6	2086±7
20-1	83	0.65	7387	0.19	0.1676	0.5126±144	12.107±374	0.1713±17	2570±16
21-1	242	0.56	7092	0.22	0.1594	0.3440±93	5.407±156	0.1140±8	1864±14
22-1	134	0.62	7355	0.21	0.1716	0.3274±89	5.133±158	0.1137±13	1860±20
23-1	68	0.65	2496	0.57	0.1590	0.4770±135	10.619±348	0.1615±22	2471±23
24-1	78	0.53	1121	1.37	0.1324	0.3658±102	5.709±214	0.1132±25	1851±40
25-1	81	1.25	1350	1.14	0.2955	0.3579±100	5.279±224	0.1070±31	1749±53
26-1	292	0.16	4714	0.33	0.0341	0.3601±97	5.885±170	0.1185±9	1934±13
27-1	159	0.62	3660	0.42	0.1765	0.3511±96	5.515±172	0.1139±14	1863±22
28-1	191	1.00	5710	0.27	0.2790	0.3540±96	5.859±171	0.1200±10	1957±14
29-1	188	0.35	4078	0.38	0.0921	0.3281±89	5.077±156	0.1122±13	1836±21
30-1	213	0.72	39777	0.04	0.1990	0.3965±108	7.410±214	0.1355±10	2171±12
31-1	1214	0.55	12760	0.12	0.1554	0.3289±47	5.174±77	0.1141±4	1865±6
31-2	1749	0.50	22257	0.07	0.1392	0.3415±91	5.351±145	0.1136±3	1858±4
32-1	511	0.12	906	1.70	0.0519	0.3489±50	5.829±109	0.1212±12	1973±18
33-1	572	0.06	21213	0.07	0.0171	0.3433±49	5.709±89	0.1206±5	1965±8

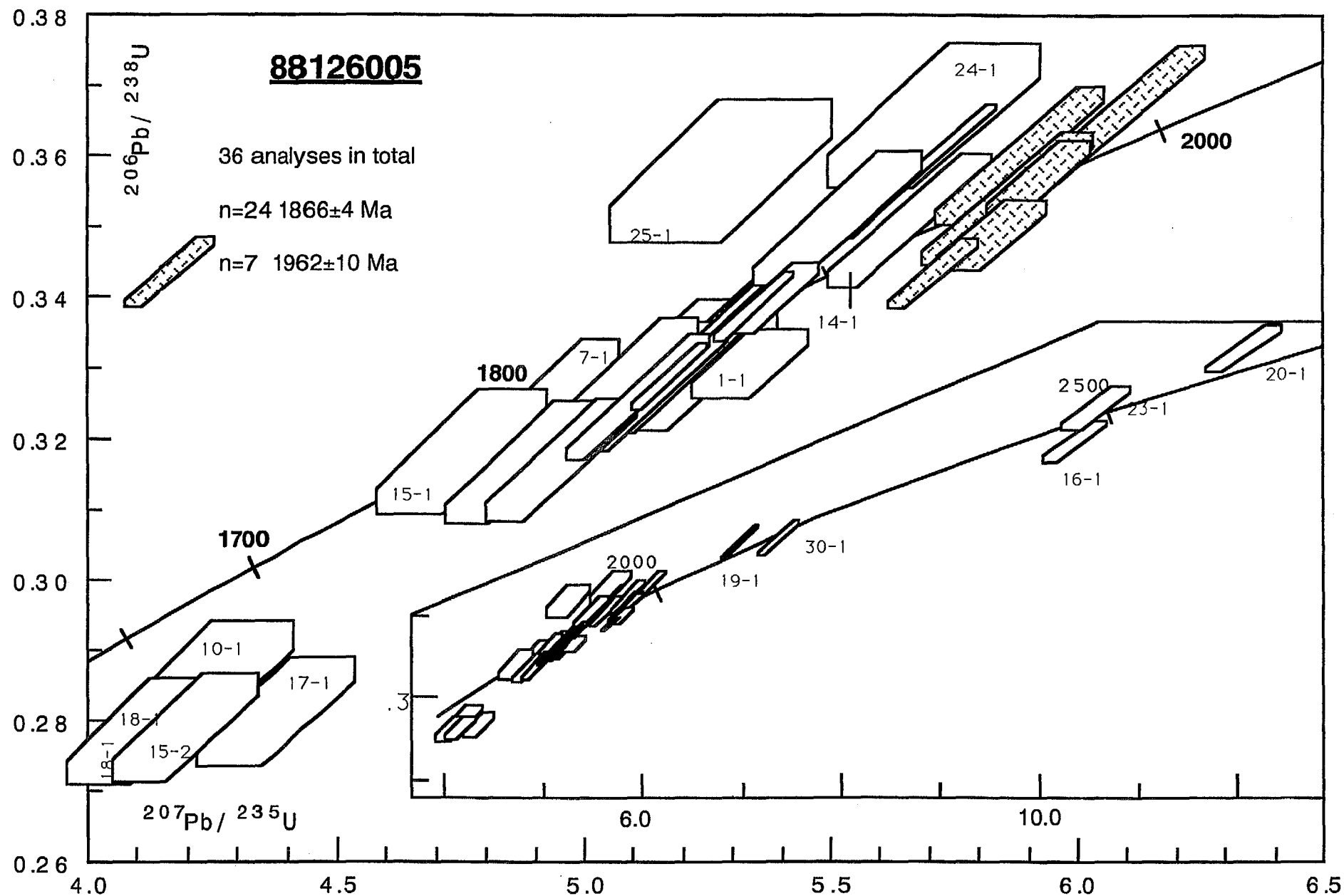


**Figure 2.7:** Concordia diagram for zircons from 88126005, a quartz-rich sandstone obtained from a fluvial channel incising ignimbrites of the Gimbat Ignimbrite Member. Inset shows all data for the sample.

### 2.4.5 Quartz-rich sandstone: 88126005

The zircon population of sample 88126005 is dominated by clear, subhedral, prismatic zircons, probably originally of magmatic origin, with internal growth zoning common. These crystals have moderate aspect ratios from 1.1 to 3.1. Most grains have rounded terminations, consistent with some degree of sedimentary reworking of the zircon population. Other grains are equant in form, with rounded terminations and sometimes have abraded or pitted surfaces, and are interpreted to be derived from metasedimentary basement rocks.

U contents generally span between 60 and 750 ppm but two grains contain between 1000 - 2000 ppm, (Table 2.4). 36 analyses were carried out on 33 grains, and on a Concordia diagram, several age populations were identified (Fig. 2.7). Three grains have a  $^{207}\text{Pb}^*/^{206}\text{Pb}^*$  age of  $\sim 2500$  Ma. Two grains have a  $^{207}\text{Pb}^*/^{206}\text{Pb}^*$  age of  $\sim 2100$  Ma. Seven are pooled to give an age of  $1962 \pm 10$  Ma. These grains are obviously xenocrysts and correspond with xenocryst populations identified in ignimbrite sample 89123138, suggesting similar source rocks for both samples. The remaining 24 analyses pool to give a  $^{207}\text{Pb}^*/^{206}\text{Pb}^*$  age of  $1866 \pm 4$  Ma.

## 2.5 INTERPRETATION OF RESULTS

One of the quartz-feldspar porphyries yielded a  $^{207}\text{Pb}^*/^{206}\text{Pb}^*$  age of  $1831 \pm 12$  Ma. The other was considerably younger ( $1794 \pm 11$  Ma). The ignimbrite sample has a  $^{207}\text{Pb}^*/^{206}\text{Pb}^*$  age 13 Ma older than the 1831 Ma quartz-feldspar porphyry ( $1844 \pm 12$  Ma), and also contains several xenocrystic populations,  $\sim 2500$ , 2100 and 1980 Ma in age. The fluvial sediment also contains these xenocryst populations, and the remainder of the samples pool to give an age of  $1866 \pm 4$  Ma.

Given that the zircon populations of the quartz-feldspar porphyry samples are interpreted to be of magmatic origin based on morphology, their single concordant age populations and Th/U ratios  $< 1$ , their  $^{207}\text{Pb}^*/^{206}\text{Pb}^*$  ages are interpreted to be the crystallisation age of each sample. The intrusive porphyry 89123002, provides a minimum age constraint on the ignimbrites.

Taken at face value, the data suggest the ignimbrites extruded at  $\sim 1844$  Ma, and were intruded by quartz-feldspar porphyry  $\sim 10$  Ma later and again  $\sim 50$  Ma later.

However an alternative interpretation, consistent with geochemical and stratigraphic evidence that the two lithologies are co-magmatic, should also be considered. It is possible that the older  $^{207}\text{Pb}^*/^{206}\text{Pb}^*$  age of  $1844 \pm 12$  Ma obtained for ignimbrite 89123138, reflects inheritance in the crystal population which cannot be statistically resolved from the magmatic zircon population (assumed to be 1831 Ma). Markedly older, early Proterozoic basement-derived grains,  $\sim 1980$  Ma and  $\sim 2500$  Ma old are recognised in the zircon population, and it is quite plausible that a third xenocrystic population only slightly older than the magmatic zircons also exists in the sample, imprinting an inherited component on to the U/Pb systematics. A weighted histogram of the  $^{207}\text{Pb}^*/^{206}\text{Pb}^*$  ages of the main zircon population, shows that the spread of ages exceeds that due to analytical uncertainty and that there is a bimodal distribution of ages (Fig. 2.6). The data can be resolved into two age populations, one of  $1859 \pm 14$  Ma, based on the regression of 6 grains. The remaining 10 grains regress to give a  $^{207}\text{Pb}^*/^{206}\text{Pb}^*$  age of  $1820 \pm 18$  Ma. The older zircon population is similar in age to one of the zircon populations in the quartz-rich sandstone ( $1866 \pm 4$  Ma.), suggesting that both lithologies contain zircons derived from a source rock of this age. The younger population approximates within analytical error, the expected crystallisation age of the ignimbrites, of  $1831 \pm 12$  Ma. It is slightly

younger, but this reflects analytical uncertainty in the data. Zircons comprising the younger age population have very low U contents (largely < 100 ppm) so that errors on individual analyses are high, and the regressed age of  $1820 \pm 18$  Ma is subsequently poorly defined. It is likely that further analysis of the zircon population would resolve more concisely the two age populations.

This second interpretation of the ignimbrite data, is more consistent with geochemical and stratigraphic evidence that the quartz-feldspar porphyries are comagmatic with the ignimbrites, and therefore the preferred age of the Gimbat Ignimbrite Member is  $1831 \pm 12$  Ma. The flaw in the argument is that the  $^{207}\text{Pb}^*/^{206}\text{Pb}^*$  ages (crystallisation ages) of the quartz-feldspar porphyry samples suggest that there is more than one generation of quartz-feldspar porphyry intruding the ignimbrite pile. While some porphyries crystallised at  $1831 \pm 12$  Ma. Others must have intruded at a much later time, representing a separate and unrelated phase of magmatic activity.

There is however, petrographic and isotopic evidence to suggest that the  $1794 \pm 11$  Ma porphyry (89123123) is unrelated to the ignimbrite-forming magmatic event. Firstly, this porphyry contains a higher percentage of phenocrysts (60% crystals) than other quartz-feldspar porphyries outcropping in the region (20-30 % crystals). Secondly, the initial  $\epsilon_{\text{Nd}}$  ratio for 89123123 is significantly lower than those for the ignimbrites of the Gimbat Ignimbrite Member (-1.4 c.f. -3.1-4.9; Section 7). The difference in initial  $\epsilon_{\text{Nd}}$  ratios suggests this quartz-feldspar porphyry body was derived independently of the ignimbrites, from a different crustal source at a different time. Thus the age of  $1794 \pm 11$  Ma is interpreted to date a much later magmatic event, unrelated to extrusion of the ignimbrites. Unpublished ion microprobe data on a syenite porphyry intrusion collected from the local area (sample 88126005) give a preliminary result of  $\sim 1800$  Ma (unpublished data; R.W. Page pers. comm.), also suggesting a significant thermal event occurred at this later time.

Several age populations are recognised in the quartz-rich sandstone, sample 88126005. The main age population has a  $^{207}\text{Pb}^*/^{206}\text{Pb}^*$  age of  $1866 \pm 4$  Ma. The absence of a strong zircon population that is 1831 Ma in age suggests that this sandstone was sourced externally, rather than being derived from local reworking of the subjacent ignimbrites. This is consistent with point-counting data, which shows that the sandstone contains grains largely derived from older metasedimentary basement, dolerite and sandstone (Appendix B). A weighted histogram of the  $^{207}\text{Pb}^*/^{206}\text{Pb}^*$  ages of the 88126005 zircon population, shows a small parasitic peak to the left of the main peak (Fig. 2.8). This may suggest there are a few 1831 Ma zircons in the population, indicating some sedimentary input from the underlying volcanic pile.

The  $\sim 1960$  Ma age population observed in samples 88126005 and 89123138 is not observed in any of the outcropping units of the Pine Creek Inlier (unpublished ion microprobe data), suggesting the zircons are derived from a source that does not currently have surface expression. The existence of zircons of this age may infer a significant thermal event in the lower crust at  $\sim 1960$  Ma. Needham *et al.* (1988) noted that the Koolpin Formation of the lower South Alligator Group, was characteristic of sediments deposited during a thermal subsidence phase following a period of normal major extension and normal faulting. Felsic volcanics which were extruded during the upper parts of the South Alligator Group and overlie the Koolpin Formation are dated at around  $1885 \pm 2$  Ma. Theoretically, the thermal pulse which triggered the rift-sag package could be predicted to be some 50 to 70 Ma older than the thermal subsidence phase, inferring that a major lower crustal thermal anomaly would be predicted in the Pine Creek Inlier at  $\sim 1950$  Ma.

### 2.6 IMPLICATIONS FOR THE SHRIMP U-PB DATING TECHNIQUE

These results have significant implications for U/Pb dating techniques. The SHRIMP ion microprobe has continually proven to be a superior tool for dating rocks which have multi-stage histories, because it measures small areas ( $< 30 \mu$ ) within single crystals, allowing composite zircon populations to be resolved into different age groups. In contrast isotopic compositions obtained by conventional mass-spectrometric techniques often represent mixtures of several zircon populations which exist within a single sample. Although the ion microprobe dating method does much to eliminate this problem, results obtained in this study (sample 89123138) imply that where two zircon populations are close in age, they may merge to form a single statistical population, possibly with a bimodal distribution of ages, which cannot be resolved into its two age components. When problems like this occur, careful consideration of available geological and petrographic information is required in order to make a meaningful interpretation of the data. For example, taken on its own merit, the data for sample 89123138 yields a  $^{207}\text{Pb}^*/^{206}\text{Pb}^*$  age of  $1844 \pm 12$  Ma, which would be taken as the crystallisation age of the ignimbrite sequence. However, data obtained from the associated quartz-feldspar porphyries suggesting magma crystallisation occurred at  $1831 \pm 12$  Ma, combined with a statistically incoherent zircon population in the ignimbrites, suggest a case can be made for the ignimbrites being  $1831 \pm 12$  Ma in age.

The results also emphasize that care must be taken in choosing samples for dating. Where the aim is to obtain a crystallisation age for a succession of volcanic rocks or a volcano-plutonic complex, coherent units such as lavas or intrusive rocks should be chosen for dating where possible. These lithologies are unlikely to be greatly contaminated by country rock during eruption and deposition. In contrast, ignimbrites are the product of violent and explosive volcanic activity and large volumes of country-rock will usually be assimilated into the pyroclastic flow during eruption and deposition. As this is the case, one encounters the same problems in obtaining a meaningful crystallisation from clastic volcanic rocks, as from sedimentary rocks. They both may contain numerous different zircon populations, obtained from several different source rocks, so that extreme caution must be applied when determining the crystallisation age of the sample.

The problems faced when dating ignimbrites are less likely to arise with dating air-fall tuffs, although these are also the product of pyroclastic eruption. Tuffs may also contain accessory lithic fragments derived from the walls of the vent, but as their eruption is less violent than ignimbrite-forming eruptions, the volume of accessory lithic clasts and crystals will be less. Air-fall tuffs will also lack the accidental lithic component present in most ignimbrites, which derived from erosion of the ground surface over which the pyroclastic flow travels.

### 2.7 STRATIGRAPHIC IMPLICATIONS OF RESULTS

The  $1831 \pm 12$  Ma (or  $1844 \pm 12$  Ma) age obtained for the Gimbat Ignimbrite Member is incompatible with published data which suggest the age of the El Sherana Group is approximately  $1890 \pm_{15}^{18}$  Ma, based on ion microprobe U-Pb data from an andesitic tuff from the Tollis Formation (Page & Williams, 1988). The age is also incompatible with the currently accepted conventional U-Pb age of the Edith River Group, of between 1870 and 1860 Ma (unpublished data, quoted in Needham et al, 1988; Page & Williams, 1988). The validity of these earlier dates and their interpretation in terms of stratigraphy, are therefore reconsidered.

	8912-3208*	11†	5†	4a†	31b†
<b>Quartz</b>	<b>251</b>	<b>295</b>	<b>262</b>	<b>305</b>	<b>267</b>
<b>Feldspar total</b>	<b>128</b>	<b>3</b>	<b>2</b>	<b>2</b>	<b>1</b>
plag	0	1	0	0	0
Kspar	112*	2	2	2	1
perthite	16	0	0	0	0
<b>Lithics total</b>	<b>131</b>	<b>7</b>	<b>3</b>	<b>19</b>	<b>27</b>
Qp	46/69/15	4	2	10	20
Ls	1	1	0	0	1
Lv	0	2	1	9	6
<b>no. of grains</b>	<b>510</b>	<b>305</b>	<b>267</b>	<b>326</b>	<b>295</b>

† values from South Alligator Valley (Friedmann, 1990)

\* arkosic sandstone from study area

Qp = polycrystalline quartz, where values are subdivided (e.g. 46/69/15) denotes metamorphosed fragments/plutonic quartz and granitic fragments/ chert respectively

Ls = sandstone fragments

Lv = volcanic fragments

- K-feldspar + plagioclase: plagioclase could only be recognised when twinning present. Electron microprobe analysis suggests most grains are K-feldspar

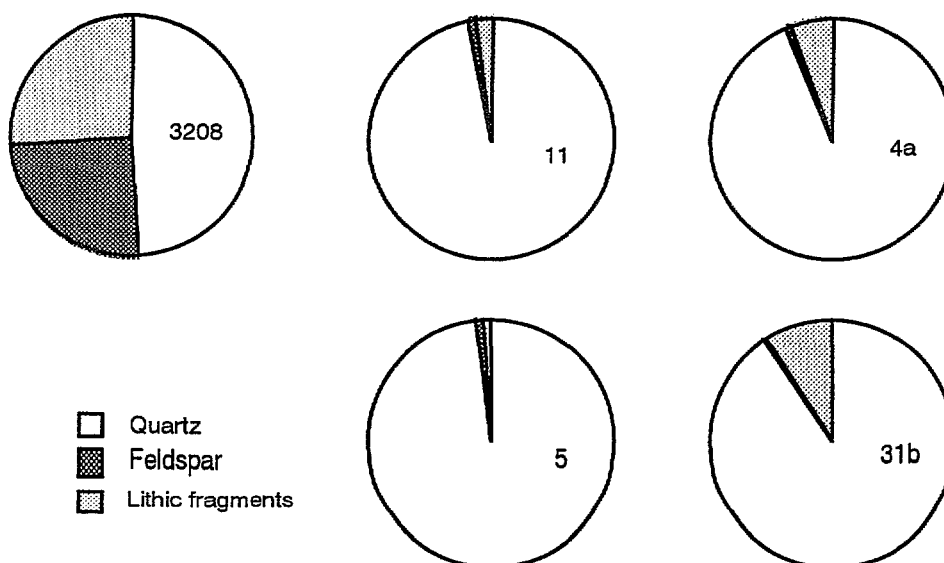


**Figure 3.1:** Comparison of modal analyses of the Coronation Sandstone in the South Alligator Valley (Friedmann & Grotzinger, 1991) and in the study area.

In the first case, the large conflict in ages between the Gimbat Ignimbrite Member ( $1831 \pm 12$  Ma) and the overlying Tollis Formation ( $1890 \pm_{15}^{18}$  Ma) needs to be resolved. Needham & Stuart-Smith (1985) first suggested a correlation between the Tollis Formation and Big Sunday Formation, and placed the Tollis Formation in the El Sherana Group (Fig. 1.4). It had previously been mapped as Burrell Creek Formation, and contains the same lithologies present in the Burrell Creek Formation. Needham & Stuart-Smith (1985) separated it from the Burrell Creek Formation on the basis of different fold styles observed in the Edith Falls Basin. It must be noted however, that the authors never provide a geological basis for its correlation with the Big Sunday Formation, in this, or subsequent publications.

Recently, K.Hein from the University of Tasmania mapped in detail an area north of the Edith River in the vicinity of Mt Todd, and has formed a strong case for placing the Tollis Formation at the top of the Burrell Creek Formation, and belonging to that formation (K.Hein, pers comm). Her conclusions are in accord with observations made by J.Friedmann & J.Grotzinger (sedimentologists contracted to the BMR Kakadu Conservation Zone Project), who suggested the Tollis Formation was part of the basement sequence (Pine Creek Geosyncline Sequence), and does not, based on lithology and style of deformation, correlate with the less deformed Big Sunday Formation (Friedmann, pers comm).

This report therefore concludes that the discrepancy in ages between the Gimbat Ignimbrite Member (representing the El Sherana Group) and Tollis Formation occurs because the Tollis Formation has been incorrectly correlated with the Big Sunday Formation. Based on the work of K.Hein, it is suggested that it be placed at the top of the Burrell Creek Formation (Fig.1.4). This suggestion is consistent with age data available for basement lithologies. The  $1890 \pm_{15}^{18}$  Ma age of the Tollis Formation agrees strongly with the best estimate for the stratigraphic age of the South Alligator Group which underlies the Burrell Creek Formation, of  $1885 \pm 2$  Ma (Needham et al, 1988).

The remaining problem with accepting the  $1831 \pm 12$  Ma age for the Gimbat Ignimbrite Member is its inconsistency with the currently accepted conventional U-Pb age of the overlying Edith River Group (of between 1870 and 1860 Ma). In this case, the data available for the Edith River Group is likely to be suspect, as they form a poorly defined discordant line. These data should be discounted in the light of the new evidence presented in this report, and it is possible that when the samples are reanalysed using SHRIMP, a younger age for the Edith River Group will be obtained.

### 3. CORONATION SANDSTONE

The Coronation Sandstone of the El Sherana Group is a thick sequence of sedimentary and volcanic rocks which is faulted against and unconformably overlies older Early Proterozoic rocks (Stuart-Smith et al, 1988). It has a large-scale lensoidal geometry, and laps up against and locally drapes over northwest-trending ridges of older rocks, apparently being confined in a valley palaeotopography (Stuart-Smith et al, 1988; Friedmann & Grotzinger, 1991). The unit is irregularly distributed and is mostly confined to the valley of the South Alligator River between El Sherana and Coronation Hill. It also outcrops as lenses beneath the Gimbat Ignimbrite Member around the southern margin of the Malone Creek Granite, and as small outliers farther to the east and north (Stuart-Smith et al, 1988). The unit is typically < 100 m in thickness, but reaches thicknesses of over 600 m (Friedmann & Grotzinger, 1991). Facies of the Coronation Sandstone in the South Alligator Valley are described in detail by Friedmann & Grotzinger, (1991). They consist predominantly of coarse to very coarse-grained, pebbly, trough-cross

bedded sandstone underlain by basal conglomerates and minor sandstone, which are interpreted to be deposited by braided river systems. In this area, the sandstone ranges in composition from quartz to lithic sandstone, with a minor feldspar and detrital mica component. Lithic fragments are mostly polycrystalline quartz and chert, with uncommon volcanic, sedimentary, and metasedimentary fragments. Feldspars are typically completely altered or replaced by clay minerals.

In the South Alligator Valley, volcanic rocks occur but are volumetrically minor and consist of two units, one felsic and one mafic in composition. The felsic volcanic is a 4 to 6.5 m thick rhyolite containing quartz and potassium feldspar phenocrysts, and lacking macroscopic evidence of fiamme. The mafic lava is a basalt up to 40 m thick, containing amygdules of chert or calcite, which occurs near the top of the section.

Where the Coronation Sandstone outcrops beneath the Gimbat Ignimbrite Member around the margin of the Malone Creek Granite (Fig. 1.2), it comprises a rather different association of facies than is documented in the South Alligator Valley. Sandstone lenses are a minor constituent and arkosic in composition rather than quartz-rich, and mafic volcanics are predominant.

#### 3.1 ARKOSIC SANDSTONE

*Description* The sandstone is a massive, medium-grained (.05-1 mm) arkose containing grains of quartz (50%), fresh feldspars (25%) and lithic fragments (25%; including metamorphosed basement fragments, plutonic and granite fragments and rare chert and sandstone fragments). It is texturally immature with poorly sorted, angular to rounded grains. Rounding of quartz grains is not caused by abrasion of the grains during sedimentary transportation. The quartz is volcanic in origin, and the rounding is a resorption feature of volcanic origin. The framework grains have an interstitial matrix of sericite and chlorite which probably consisted of fine-grained silty material and possibly some phyllosilicate-rich lithics which were compressed during compaction. The original matrix has been replaced during diagenesis and regional metamorphism.

A coarser-grained, planar to cross laminated, poorly sorted pebbly sandstone of similar composition, outcrops locally at the base of the massive sandstone. This pebbly sandstone is the only facies with sedimentary structures present which indicate a tractional mode of deposition.

The nature of the contact between units of the Pul Pul Rhyolite and the arkosic sandstone was not determined. At the northwestern exposure of the Coronation Sandstone the contact is complicated by faulting and by the intrusion of a sparsely porphyritic magma at the contact. In the southeastern area, outcrop is sparse and discontinuous and the contact is not exposed.

*Interpretation* The framework population is consistent with a mixed volcanic, granitic and metasedimentary basement provenance. Volcanic quartz and feldspars with resorption features may have been derived from a contemporaneous volcanic source, such as the rhyolites present in the Coronation Sandstone in the South Alligator Valley. Metamorphic lithic fragments, chert and rare detrital muscovite are likely to be derived from the underlying metasediments of the Pine Creek Geosyncline sequence. In addition, composite quartz grains, perthite grains and granitic fragments indicate a plutonic component to the population.

The rock is texturally immature. Angular feldspars which are fresh or partly altered to clay minerals, indicate very short exposure to weathering and other surface processes, prior to final deposition.

Fig. 3.1 compares modal analyses of the arkosic sandstone with typical samples of the Coronation Sandstone in the South Alligator Valley. The sandstone in the study area is more arkosic in composition, with a greater lithic component than the quartz arenites in the South Alligator Valley. The high percentage of feldspar in the sandstones of this region suggests they are locally sourced by the Burrell Creek Formation, an older Early Proterozoic unit which forms a basement to the Coronation Sandstone in this area, which comprises mainly fine to coarse grained meta-feldspathic greywacke (Stuart-Smith et al, 1988). In contrast quartzites of the Mundogie Sandstone and Masson Formation probably source the Coronation Sandstone in the South Alligator Valley.

#### 3.2 BASALTS

The mafic volcanics are amygdaloidal basalts which account for most of the Coronation Sandstone in the study area. They can be subdivided into two facies based on textural differences. Both facies have the same mineralogy and geochemical composition. Tabular, oscillatory zoned plagioclase, clinopyroxene and large relict olivine phenocrysts pseudomorphed by chlorite (+opaques+minor epidote) or quartz (+ opaques; Fig. 3.2a) form the phenocryst phases. Plagioclase is andesine in composition, and the clinopyroxene is augite (Fig.3.3). Both facies have large amygdules infilled with chalcedony and a secondary mineral assemblage (Fig. 3.2b).

The first facies contains phenocrysts of plagioclase up to 1 mm in diameter, clinopyroxene up to 0.6 mm in diameter and large euhedral to subhedral olivine pseudomorphs. The groundmass is composed of euhedral plagioclase laths which locally form subtrachytic textures, and clinopyroxene which forms a subophitic texture with the plagioclase laths (Fig.3.2c).

This unit is probably a thin valley-fill lava flow. Subtrachytic textures indicating some flow movement during cooling, and the presence of infilled vesicles suggests the basalt is a lava flow rather than an intrusive body. The development of subophitic textures, and the absence of crystal fragmentation, pyroclasts or any other features suggesting explosive eruption, indicates the basalts extruded as coherent lavas.

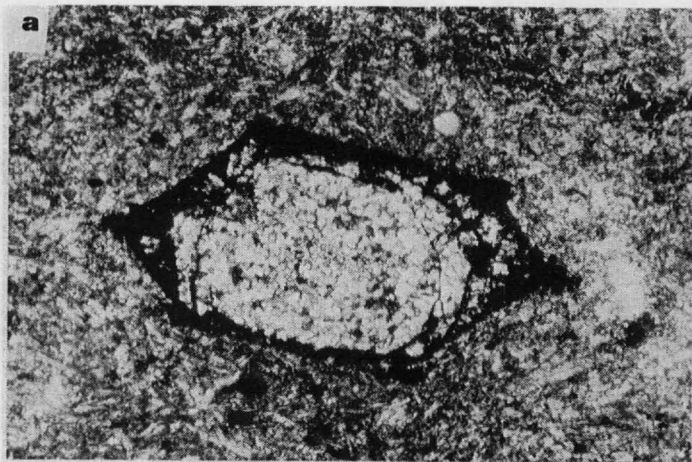
The second facies is finer-grained, with tabular plagioclase and clinopyroxene phenocrysts occurring as glomerophytic aggregates (Fig. 3.2d). The groundmass is a microcrystalline aggregate of clinopyroxene, plagioclase and opaques (magnetite and titanomagnetite).

The finer-grained basalts outcrop as thin, elongate bodies which exhibit vertical flow folding (Fig. 3.2e). Flow folding is rare in basalts, as their rheology or viscosity is usually too low, which suggests the fine-grained basalts may have cooled in a conduit, rather than extruding as lavas. They may be feeder dykes to the surrounding extrusive lavas.

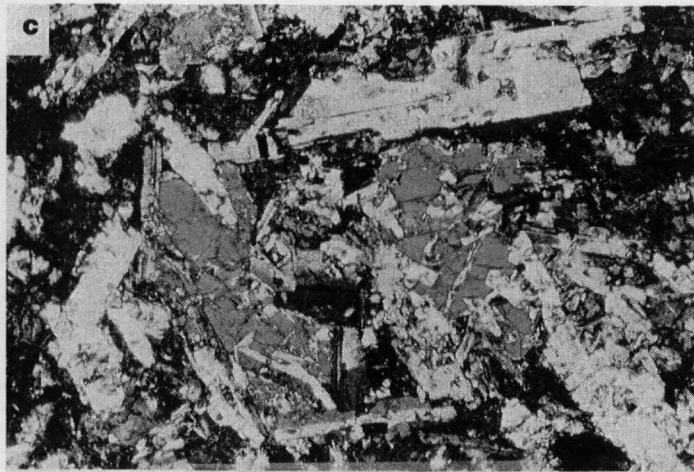
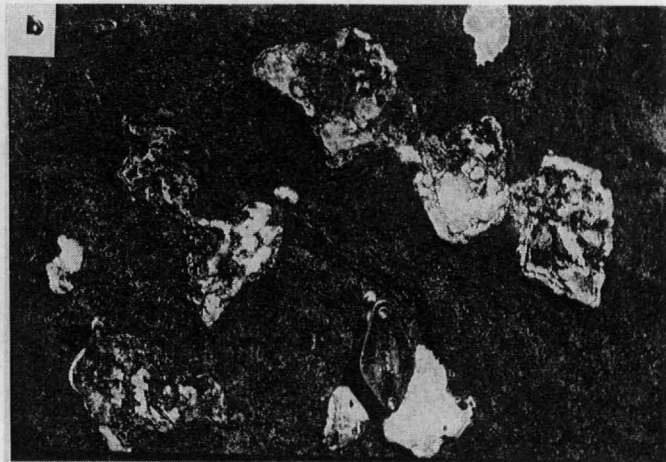
The finer-grained basalts also contain abundant quartz which looks like vein quartz infilling small amygdules in hand specimen (Fig. 3.2f), but in thin section is seen to be volcanic quartz which is embayed and rimmed by a corona of actinolite (reaction rim), indicating resorption by the basaltic melt (Fig. 3.2g). These quartz grains co-exist with olivine pseudomorphs in some samples. The basalts which contain resorbed quartz crystals are locally intruded by a siliceous rock with a fine-grained granophyric texture with finer grained cherty patches (Fig. 3.2h). The margins of the acidic and basic domains are highly irregular and in thin section small blobs of the silicic material have broken off and are included in the basalt. These features all indicate that magma mixing has occurred. This is supported by the chemistry of the basalts, which have

**Figure 3.2**

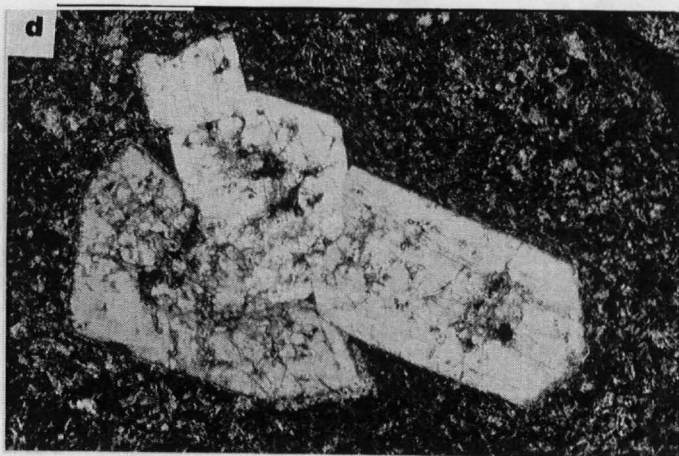
- (a) Olivine phenocryst Pseudomorphed by quartz and opaques (sample 89123018)
- (b) Silica-filled amygdules in basalt (GR 540873)
- (c) Photomicrograph showing subophitic textures in clinopyroxene and plagioclase (sample 89123001)
- (d) Glomeroporphyritic aggregate of clinopyroxene in a fine-grained basaltic (cpx-plag-opaques) groundmass (sample 89123019)
- (e) Vertical flow-folding in elongate pipe-like body of fine-grained basalt (GR 520875)
- (f) Quartz xenocrysts in elongate pipe-like body of fine-grained basalt (GR 521876)
- (g) Photomicrograph of quartz xenocryst in fine-grained basaltic groundmass showing resorption features and a reaction corona of amphibole (sample 89123019)
- (h) Magma mixing of melts of acidic (light grey) and basaltic composition. Note the quartz xenocrysts in the basaltic material, and the irregular contact between the two domains (GR 525870).



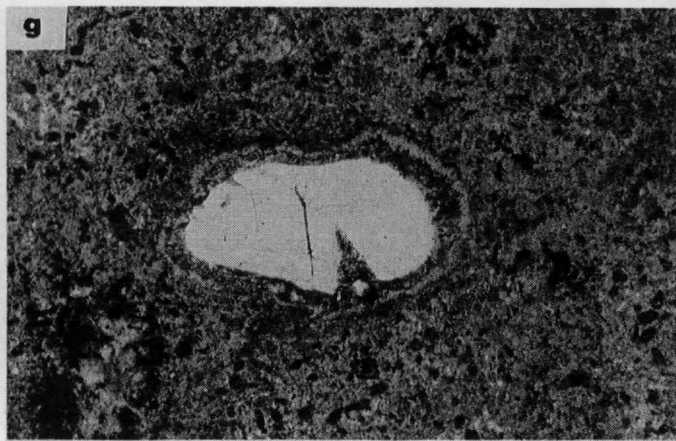
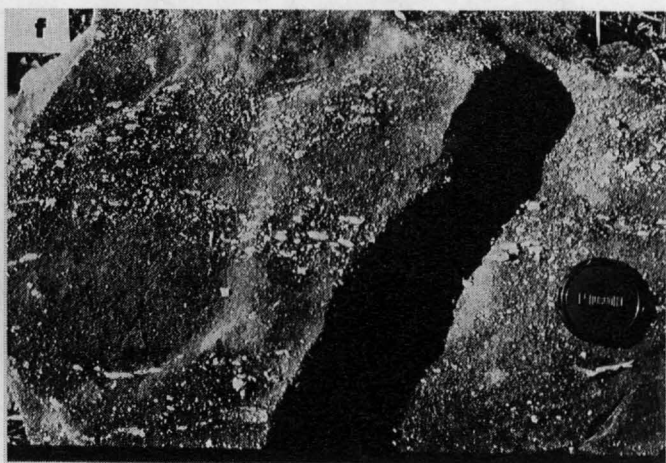
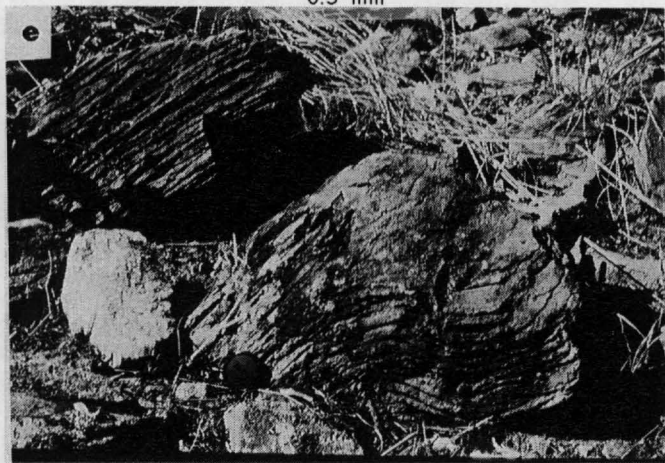
0.5 mm



0.5 mm



0.5 mm



0.5 mm



**Table 3.1:** Whole-rock analyses of representative samples from the Coronation Sandstone basalts and intrusive dolerites from the study area.

	<i>basalts</i>			<i>basalts showing evidence of mixing with a rhyolitic fluid</i>				<i>dolerite</i>	
Sample #	3001	3004	3117	<u>3009</u>	<u>3014</u>	<u>3018</u>	<u>3017a</u>	3057	3105
SiO <sub>2</sub>	49.44	56.46	54.35	62.15	61.38	61.86	55.45	46.55	51.2
TiO <sub>2</sub>	1.32	1.41	1.46	0.50	0.68	0.62	0.71	1.77	1.49
Al <sub>2</sub> O <sub>3</sub>	14.85	14.68	15.06	13.21	14.46	14.16	16.60	14.63	13.30
Fe <sub>2</sub> O <sub>3</sub>	11.90	10.66	10.81	6.21	6.14	6.49	7.65	15.17	11.89
MgO	7.21	3.01	3.41	4.51	3.84	3.59	5.27	7.76	3.33
CaO	6.52	4.71	3.86	3.63	5.17	5.10	5.49	5.66	6.03
Na <sub>2</sub> O	2.42	2.78	2.84	2.64	2.77	2.75	2.91	2.21	3.97
K <sub>2</sub> O	2.44	3.13	4.18	4.63	4.11	3.96	2.23	1.71	1.38
P <sub>2</sub> O <sub>5</sub>	0.42	0.84	0.88	0.28	0.36	0.30	0.32	0.51	0.21
L.O.I.	0.38	2.46	0.40	0.57	0.43	0.41	0.37	0.34	0.26
<b>Total</b>	100.08	100.17	100.13	100.01	100.18	100.15	99.94	99.71	100.21
qtz	-	11.2	6.00	13.4	12.6	14.0	7.5	-	3.3
or	14.5	18.5	24.8	27.4	24.3	23.5	13.2	10.2	8.2
ab	20.5	23.5	24.0	22.3	23.4	23.3	24.6	18.7	33.6
an	22.4	18.4	13.9	10.6	14.9	14.6	25.5	24.9	14.4
di	6.2	.2	-	5.2	7.3	7.6	-	.2	12.0
hy	21.1	17.7	18.8	15.3	12.2	11.9	20.9	26.4	13.9
ol	4.2	-	-	-	-	-	-	5.7	-
mt	3.5	3.1	3.2	1.8	1.8	1.9	2.2	4.4	3.5
il	2.5	2.7	2.8	.96	1.3	1.2	1.4	3.4	2.8
ap	1.0	2.0	2.1	.68	.86	.72	.76	1.2	.5
mg	60.0	41.1	43.9	64.2	60.8	57.9	63.0	55.9	41.0
Ba	1363	2086	1575	2291	1499	1382	917	786	392
Li	40	32	27	21	12	11	32	37	19
Rb	110	88	168	210	142	134	99	110	45
Sr	256	355	281	320	430	409	405	284	93
Pb	19	28	17	58	41	33	24	17	18
Th	3	16	17	47	30	31	34	4	9
U	2	5	4	11	7	8	8	1	2
Zr	137	246	255	198	220	206	238	190	341

much higher  $\text{SiO}_2$  and lower  $\text{Fe}_2\text{O}_3$  values than the uncontaminated lavas (Table 3.1). Pb, Th and U are also notably higher in the contaminated basalts, and they contain more normative quartz, magnetite and orthoclase.

The basalts have been affected by lower greenschist facies regional metamorphism and by contact metamorphism near the margin of the Malone Creek Granite. The amygdules contain a secondary mineral assemblage of chlorite-prehnite-pumpellyite-calcite $\pm$ epidote, which is consistent with the regional metamorphic grade of lower greenschist facies. This assemblage also overprints the groundmass of the basalts. Plagioclase is altered to clay minerals or is sericitised and albitised. Where affected by contact metamorphism, the mafic minerals are replaced by a green amphibole (actinolite), which overprints the regional metamorphic assemblage.

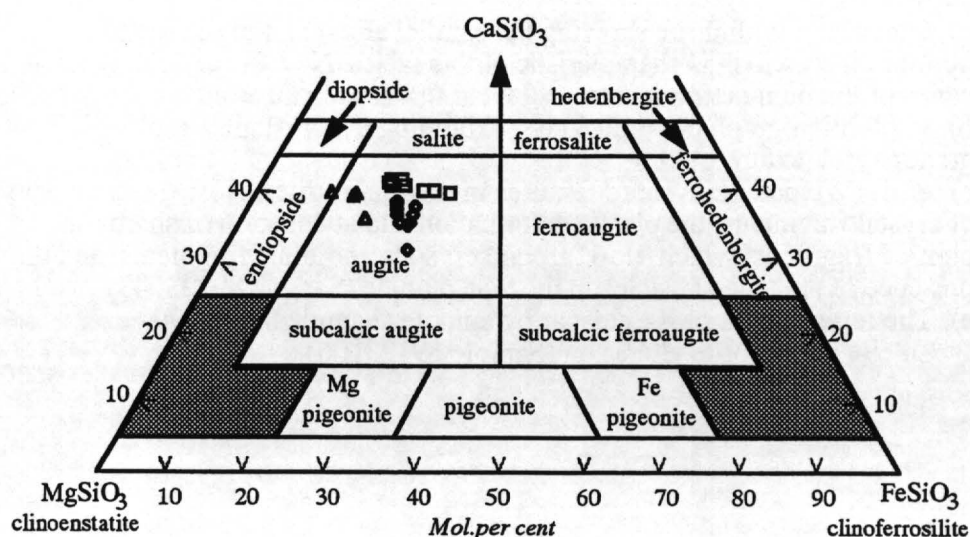


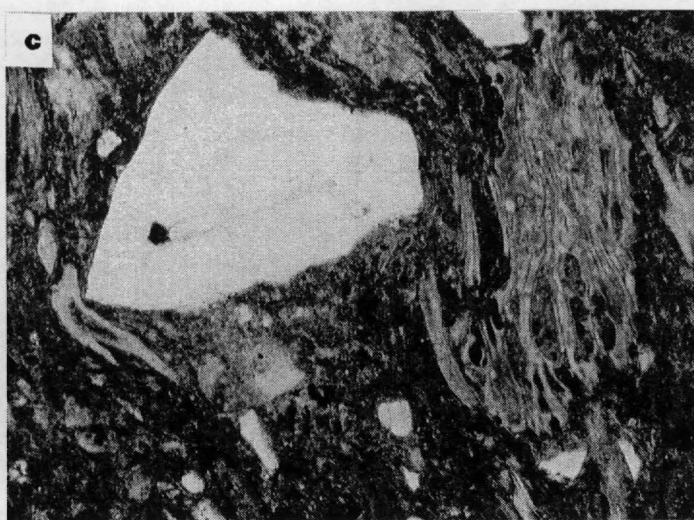
**Figure 3.3:** Plot of clinopyroxene compositions in basalts of the Coronation Sandstone. Data obtained from electron microprobe.

**Figure 4.1:**

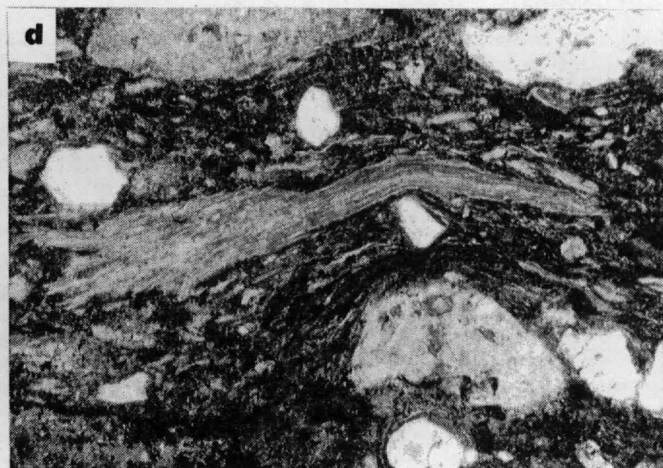
- a) Outcrop of ignimbrite showing the parallel alignment of flattened pumice clasts which is characteristic of this facies. Note the extremely ragged edges of the pumice fragments
- b) Photomicrograph of pumice clast exhibiting a recrystallised spherulitic to granophyric texture
- c) & d) Welded glass shard textures in the ignimbrites. Note the angularity of crystal fragments, the plastic deformation and attenuation of shards and pumice fragments which 'flow' around crystals and lithic fragments, and the presence of stretched vesicles in the tube pumice (Sample 89123043)
- e) The replacement of K-feldspar by epidote (Sample 89123099)
- f) Calcite and fluorite alteration (Sample 89123106)



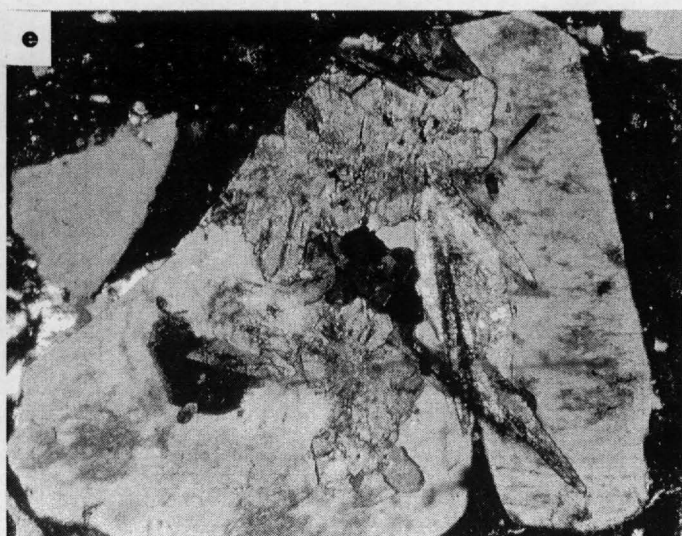
0.25 mm



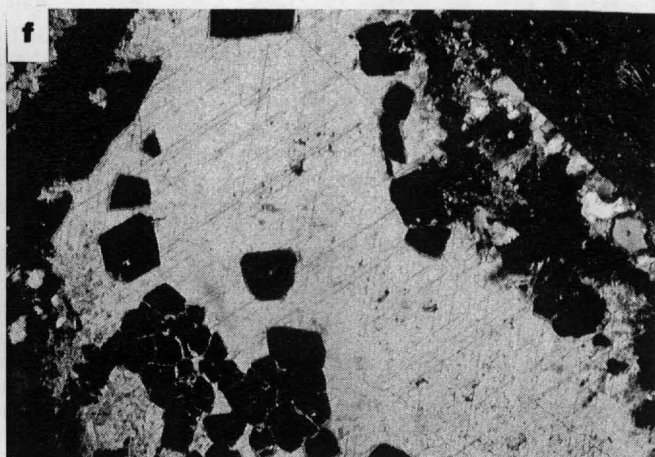
0.5 mm



0.5 mm



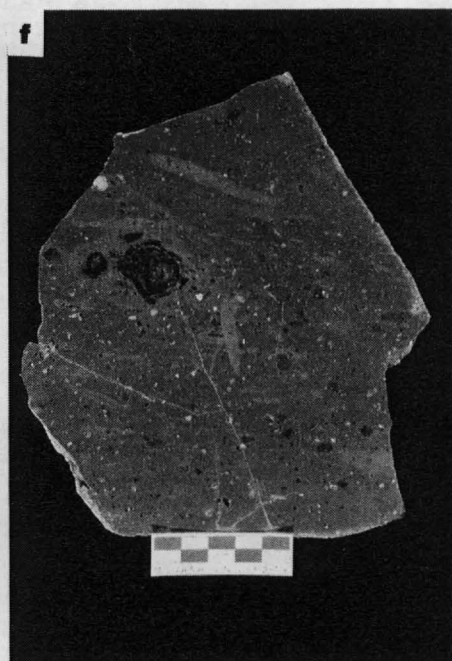
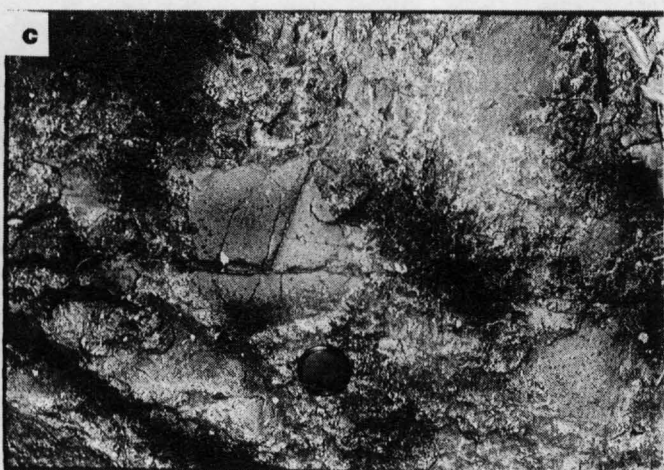
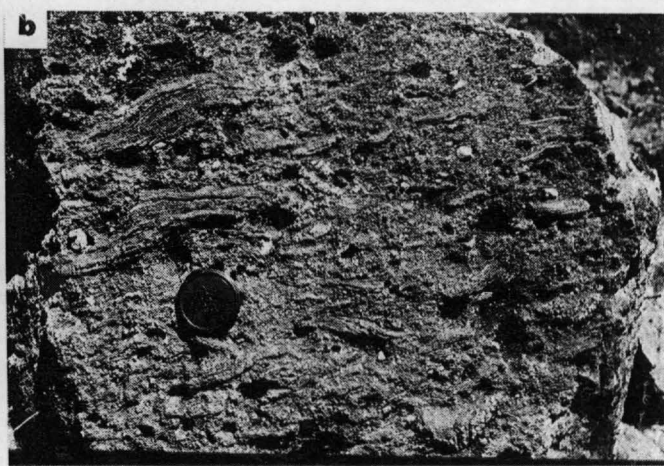
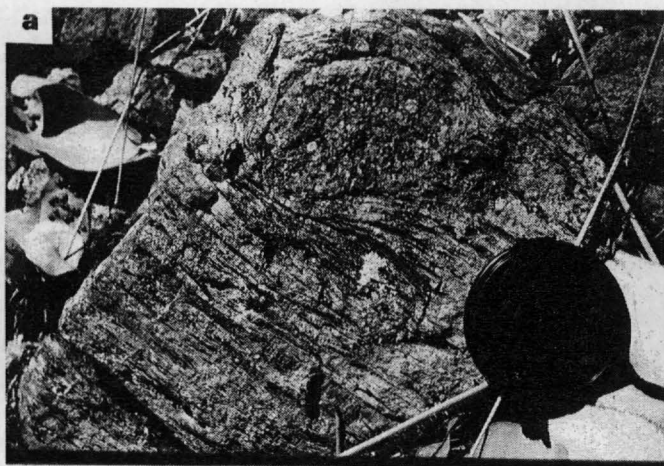
0.5 mm



1.5 mm

**Figure 4.2:**

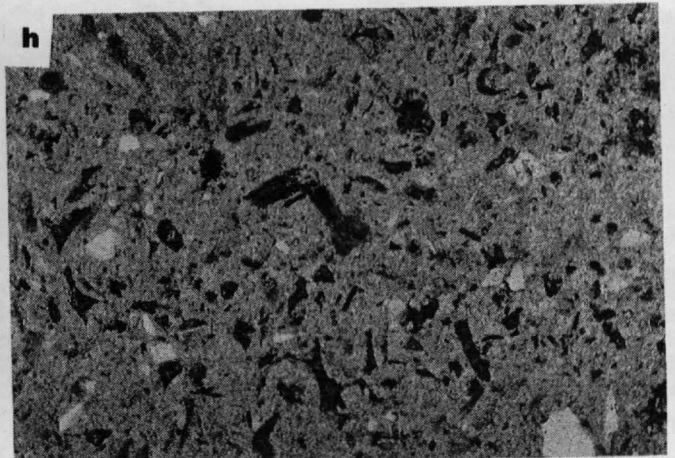
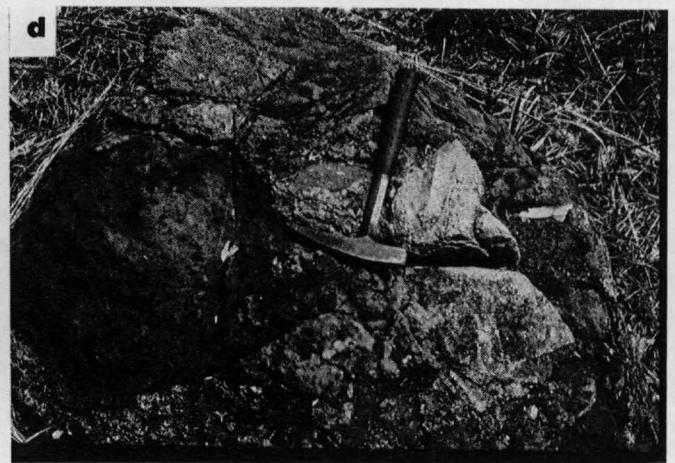
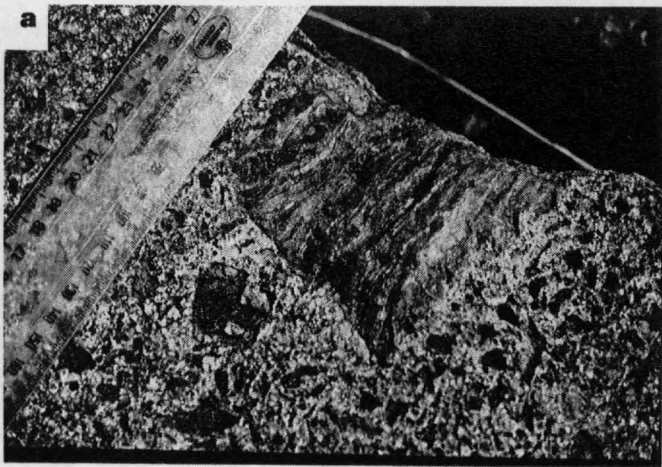
- a) Clast of quartz-feldspar porphyry in ignimbrite unit I<sub>A</sub>, with the lenticular red pumice clasts typical of the facies. The eutaxitic fabric deforms around the clast
- b) Cognate xenoliths of layered rhyolite showing a compaction alignment, unit I<sub>B</sub>
- c) Local concentration of angular dolerite clasts in unit I<sub>B</sub>
- d) Profile of well developed columnar jointing which is characteristic of ignimbrite unit I<sub>C</sub>
- e) Plan view of the columnar jointing in Fig. 4.1d
- f) Handspecimen of the densely welded ignimbrite unit I<sub>C</sub> showing the compaction of small, pink-coloured fiamme typical of the facies, and the presence of rare, small lithic fragments
- g) Photomicrograph of the densely welded ignimbrite unit I<sub>C</sub> showing the extreme plastic deformation and compaction of shards and pumice clasts, wrapping around a euhedral K-feldspar crystal



1.5 mm

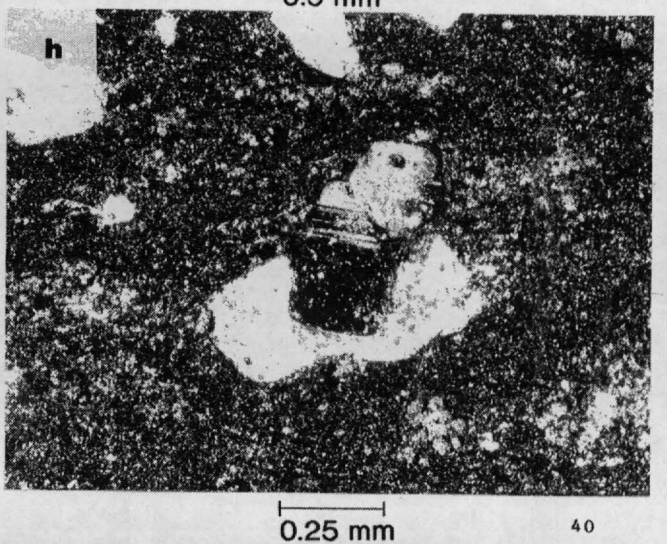
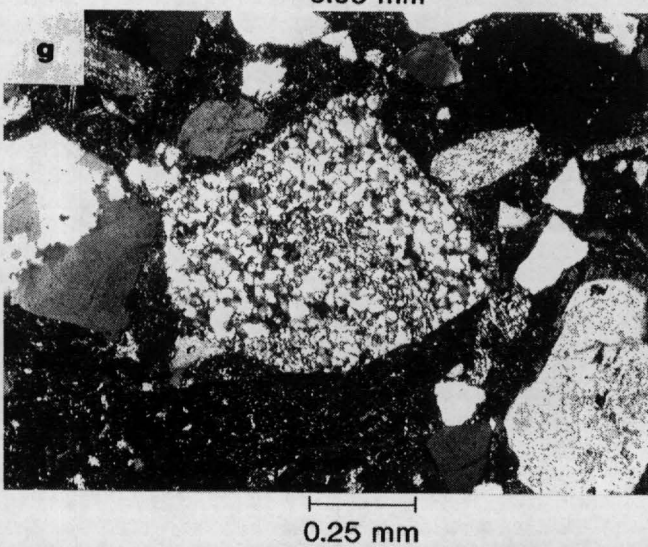
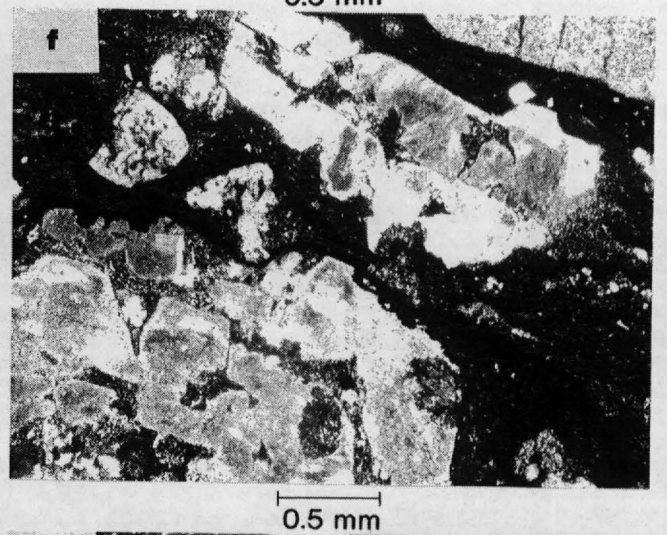
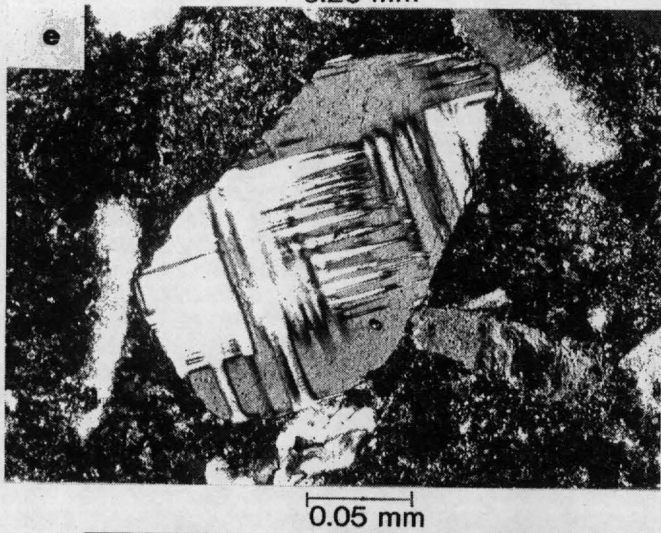
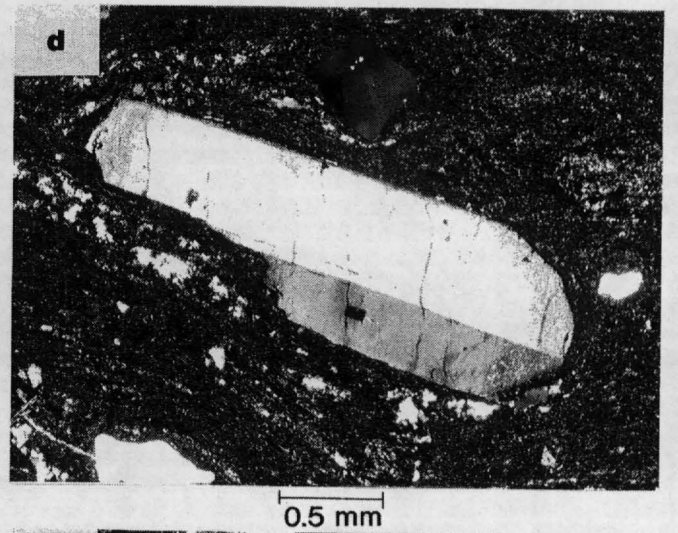
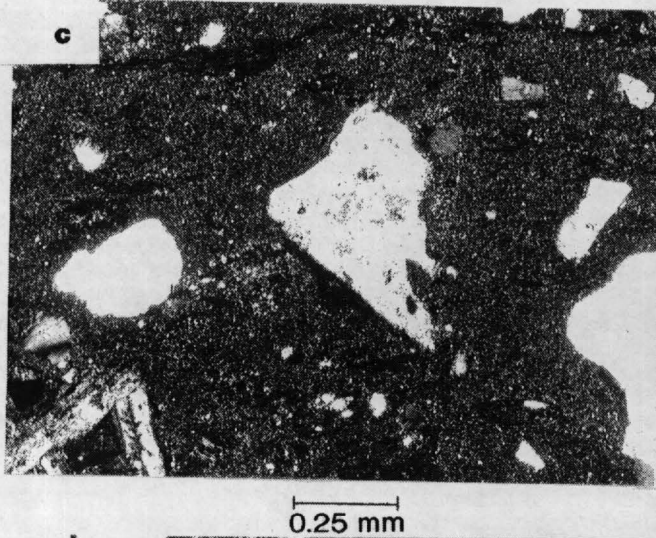
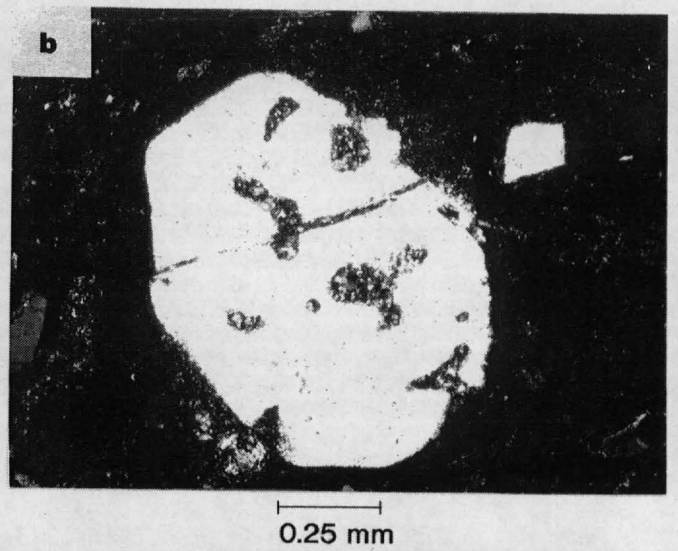
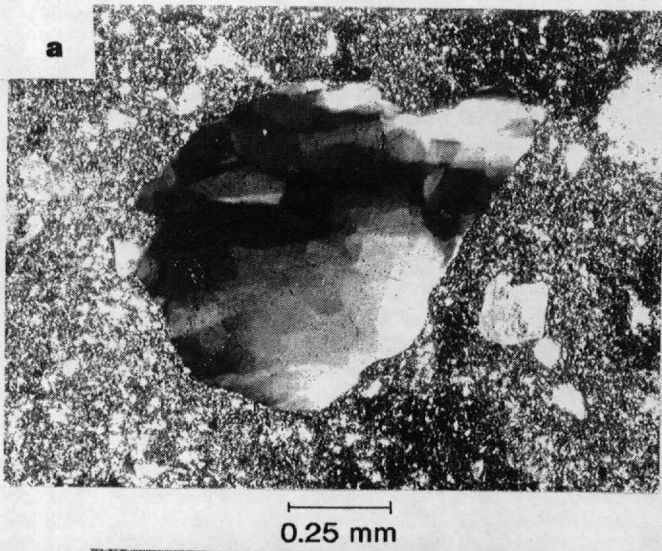
**Figure 4.3:**

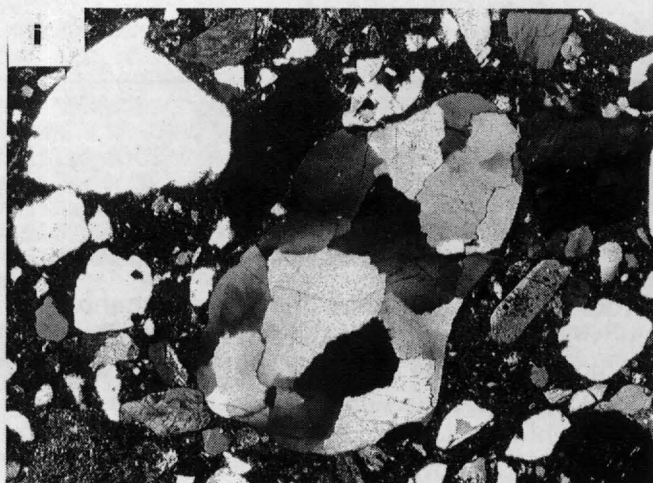
- a) Basement clast of metamorphosed sediment (Burrell Creek Formation) in ignimbrite unit I<sub>D</sub> from the southeastern part of the area
- b) A lithic concentration zone in ignimbrite unit I<sub>E</sub>, containing many dolerite fragments (Dinner Creek area)
- c) A pumice concentration zone in ignimbrite unit I<sub>E</sub> showing a high concentration of pumice clasts, and an absence of lithic clasts compared with the rest of the unit (Dinner Creek area)
- d) & e) Lithic boulders in the volcanic boulder conglomerate facies include dolerite, crenulated metamorphic basement fragments, quartz-feldspar porphyry and sandstone
- f) A 2m diameter rounded dolerite boulder in the volcanic boulder conglomerate facies
- g) The volcanic matrix to the volcanic boulder conglomerate facies consists of angular lithic fragments in an aphanitic (red) siliceous matrix
- h) Photomicrograph of the non-welded ignimbrite showing the preservation of undeformed chloritised shards in the groundmass



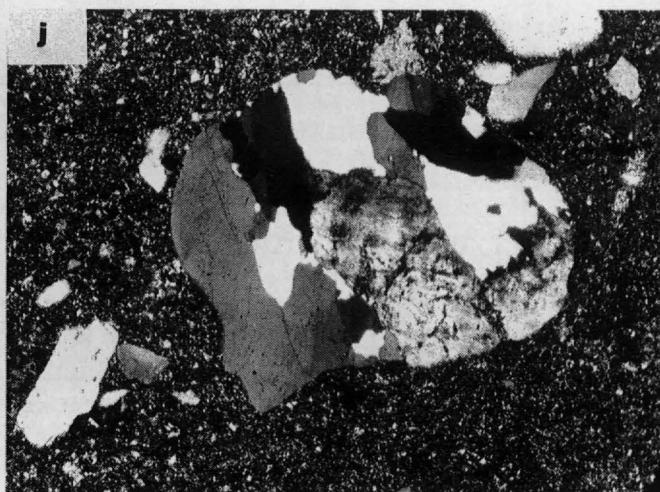
**Figure 4.4:** Pyroclasts/grains which comprise the ignimbrites and fluvial epiclastic sediments of the Gimbat Ignimbrite Member and the overlying crystal-rich arenites of the Big Sunday Formation

- a) basement-derived monocrystalline quartz exhibiting strong undulose extinction
- b) resorbed volcanic quartz
- c) fragmented, angular feldspar crystal
- d) euhedral (and broken) feldspar
- e) perthitic feldspar
- f) resorbed feldspar crystals
- g) chert
- h) composite feldspar aggregates (glomerophytic clusters)
- i) composite quartz grain of plutonic origin
- j) granite fragment consisting of composite quartz and feldspar
- k) strained metamorphosed basement clast (mylonite)
- l) metamorphosed basement clast (gneiss)
- m) sandstone
- n) dolerite
- o) welded ignimbrite clast (occurs in the non-welded ignimbrite)
- p) quartz-feldspar porphyry clast





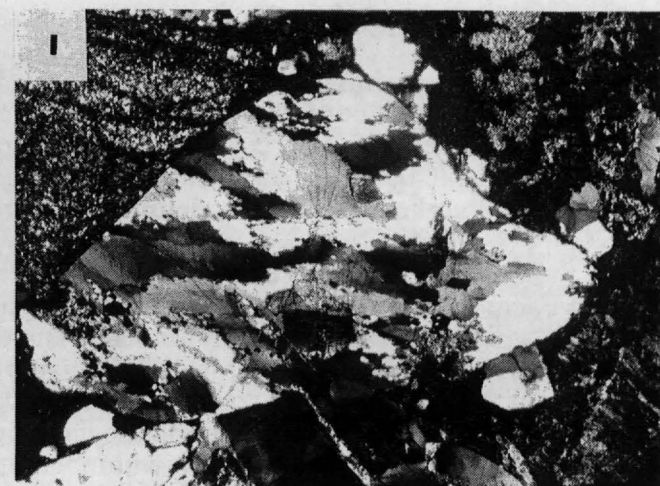
0.5 mm



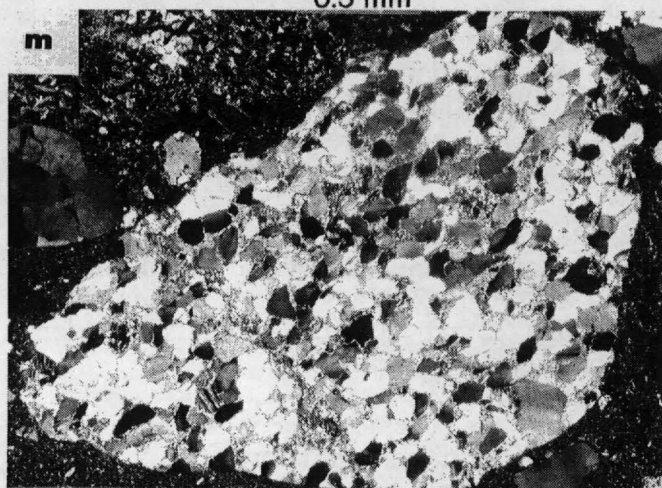
0.25 mm



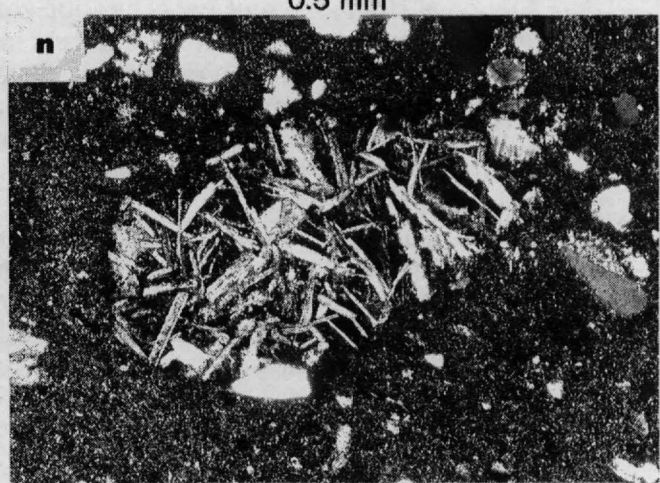
0.5 mm



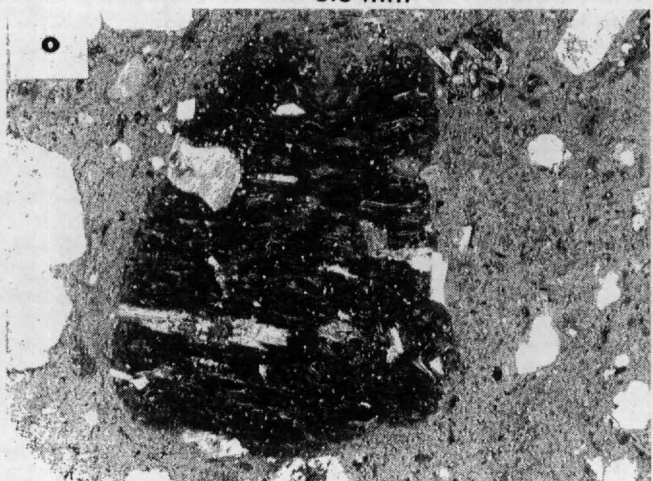
0.5 mm



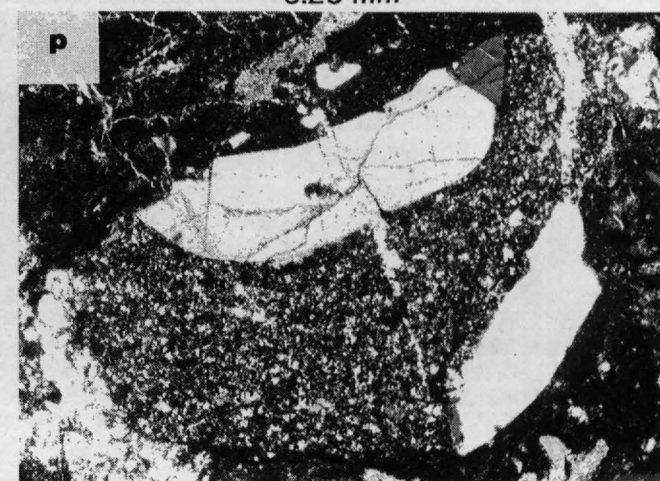
0.5 mm



0.25 mm



0.5 mm



0.25 mm

## 4. GIMBAT IGNIMBRITE MEMBER

### 4.1 WELDED IGNIMBRITES

*Description:* Volumetrically, welded ignimbrites encompass most of the Gimbat Ignimbrite Member. The distribution of the sub-facies depositional units within the ignimbrite pile are illustrated in Figs 1.2; 1.3. The ignimbrites cover most of the area and form tabular units which have consistent thicknesses along strike lengths up to 12 km. Individual units range from 60 to 400 m in thickness. Four units outcrop as a conformable sequence ~ 830 m thick with strikes trending around the margin of the Malone Creek Granite and dipping ~ 30° away from the granite margin. A fifth unit forms two isolated outcrops separated by quaternary sands in the east of the area. One smaller lensoidal unit only 10 m thick and 1.5 km long, is interlayered with fluvial epiclastic units in the southeast.

The ignimbrites consist of crystal, lithic and pumice fragments which have an open framework configuration in a fine-grained matrix. They are internally massive with a homogeneous matrix, although the size and proportion of lithic and pumice fragments is variable between and within different units. Columnar jointing is locally developed in several ignimbrite units, and is a definitive feature of one unit (Unit I<sub>C</sub>; Table 4.1; Fig. 4.2e).

The ignimbrites are characterised by lenticular pumice clasts which average between 0.5-20 cm in length, with maximum dimensions of 300x40cm in local pumice concentration zones (Fig. 4.1a). The clasts are flattened and display a parallel to subparallel alignment, defining a planar foliation or outcrop scale eutaxitic texture. There is reverse size grading of pumice clasts within some units, and the clasts have variable degrees of attenuation. A simple compaction factor obtained by measuring the length:width ratio of the fiamme at several localities yielded similar results between and within units, ranging from 5.4 to 9.7. Units in the northwest near Dinner Creek generally displayed higher degrees of attenuation (7.5-9.7) with a value of 21.9 obtained from a pumice concentration zone containing large pumice clasts. Reverse grading of pumice clasts is uncommon but occurs in the Dinner Creek area. The pumice are usually a red to red-brown colour, but one unit is characterised by smaller fiamme which are pink in colour on both the fresh and weathered surface (Unit I<sub>C</sub>; Table 4.1; Fig. 4.2f). In this section the pumice clasts may have a spherulitic texture (Fig. 4.1b), or are altered to granular aggregates of quartz, iron-stained feldspar, chlorite, epidote, calcite and sericite in varying proportions.

Six sub-facies were distinguished based on lithic and crystal content, types of lithic fragments, degree of welding and stratigraphic position. Descriptions of these sub-facies and their characteristic features are outlined in Table 4.1, and Fig. 1.2 shows their distribution. The distinguishing features of each unit are illustrated in Figs 4.2 and 4.3a;b;c. Despite the variation between units a general description for welded ignimbrites can be applied.

Phenocrysts of quartz, alkali feldspar and plagioclase (and accessory zircon and magnetite) constitute 10 to 20% of the rock. Quartz is monocrystalline and undeformed, and forms euhedral crystals exhibiting embayments and resorbed margins, or angular crystal fragments (Fig. 4.1c). Feldspar crystals are euhedral to fragmented. They are mainly K-feldspar with smaller crystals of plagioclase (albite) distinguished by the presence of multiple twinning.

Quartz and feldspar are present in a ratio of 1.5:1 to 2:1 for most units. Some units contain more feldspar than quartz (unit I<sub>E</sub> locally, northeast of the fault near Dinner Creek, and units I<sub>B</sub>, I<sub>C</sub>). Phenocrysts have an average grainsize of 0.2 mm and can occur up to 4 mm in diameter or length.

**Table 4.1:** Sub-facies of the Welded Ignimbrites.

Unit Name	Distribution & Geometry	Description / Distinguishing Features	Genetic Classification
I <sub>A</sub> Quartz-feldspar porphyry-bearing ignimbrite	Lowest stratigraphic unit. 290m	Contains abundant quartz-feldspar porphyry clasts 2-8 cm, and large dolerite clasts. Concentration of lithics locally as high as 40%. Large attenuated red pumice clasts 5-10cm.	Layer 2b ignimbrite
I <sub>B</sub> Layered rhyolite-bearing ignimbrite	Overlies I <sub>A</sub> with local unconformity. Conformably underlies and passes gradationally into I <sub>C</sub> . 60-96m	Contains abundant clasts of layered rhyolite (5-20cm) with random orientation at the base of the unit, becoming more aligned toward the top, and exhibiting normal grading. Local concentrations of large dolerite clasts 5-20cm. Fiamme absent.	Layer 2b lithic concentration zone
I <sub>C</sub> Densely welded, columnar jointed ignimbrite	Conformably overlies I <sub>B</sub> . ~ 220m	Characterised by well developed columnar jointing and compaction layering, a low proportion of phenocrysts (13%) with more feldspar than quartz, rare, small dolerite lithics (.5-2mm up to 5cm), and small pink fiamme (≤1cm up to 5-10cm). Highly attenuated, plastically deformed tube pumice and shards preserved in thin section.	Layer 2b ignimbrite
I <sub>D</sub> Basement fragment-bearing ignimbrite	2 outcrops on the southeastern sandplains. Isolated from the remainder of the ignimbrite succession. Extent of the facies obscured by younger sandplains	Contains large clasts of basement schists and metapelites (Burrell Creek Formation) up to 15cm, quartz-feldspar porphyry and dolerite clasts, large attenuated red pumice clasts. Secondary calcite and fluorite	Layer 2b ignimbrite
I <sub>E</sub> Lithic-quartz feldspar-ignimbrite	Overlies I <sub>C</sub> ; broadly conformable but locally unconformable. Facies top has high relief (erosional). Variable thickness from 60-420m Thinnest in the central area and thickest in the northwest. One thin lensoidal unit 10m x 1.5 km interlayers with epiclastic channel facies.	Euhedral to fragmented crystals of quartz, feldspar. Dolerite clasts up to 10cm. Abundant attenuated red pumice clasts up to 300x40 cm. Variable lithic and pumice content. Locally developed columnar jointing and locally preserved vitriclastic textures with plastically deformed shards and tube pumice.	Layer 2b ignimbrite
I <sub>E</sub> (1) Lithic-rich ignimbrite	Outcrops within I <sub>E</sub> in the northwest near Dinner Creek. Contacts with I <sub>E</sub> are gradational.	High concentration of large subangular dolerite clasts (10-30cm). Pumice rare. Vitriclastic textures preserved	Layer 2b lithic concentration zone
I <sub>E</sub> (2) Pumice-rich ignimbrite	Outcrops within I <sub>E</sub> in the northwest near Dinner Creek, with a gradational contact.	Large highly attenuated red fiamme (up to 300x40 cm) exhibiting reverse grading. Small lithics (<5cm); mainly dolerite. Feldspar > quartz.	Layer 2b pumice concentration zone
I <sub>E</sub> (3) Crystal and pumice-poor ignimbrite	Lenticular outcrop within I <sub>E</sub> ~ 3km southeast of Big Sunday.	Similar in composition and mineralogy to I <sub>E</sub> but contains few fiamme or crystals.	Layer 2b ignimbrite

\* Figures 4.2 and 4.3a;b;c illustrate the distinguishing features of each facies.



\* R 9 2 0 0 9 0 8 \*

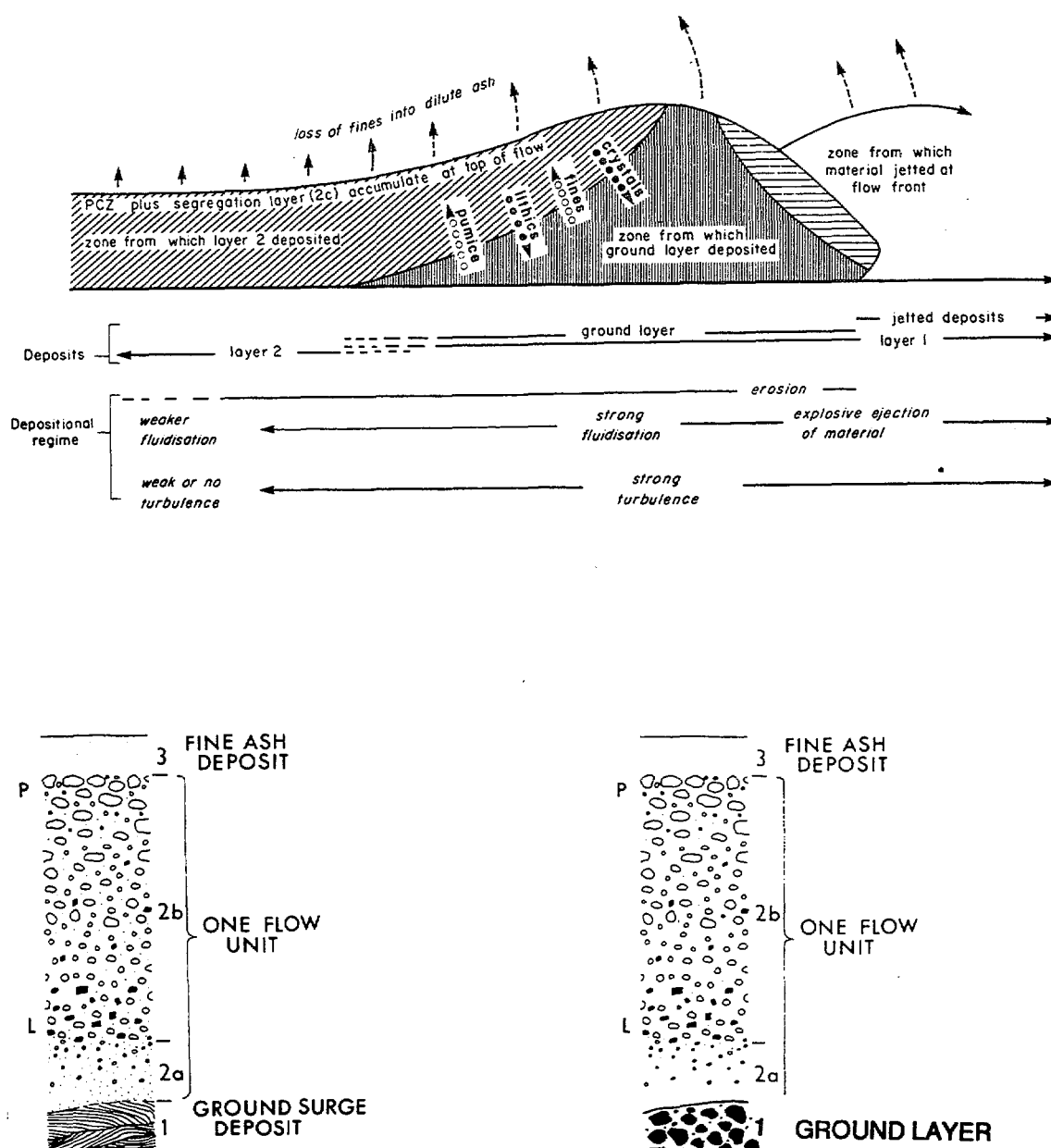


**Figure 4.5:** a) Dynamic model summarising processes which generate the different layers deposited by a rapidly moving pyroclastic flow (Wilson, 1985) b) Schematic sections through one flow of an ignimbrite showing layers 2a and 2b, with overlying fine- ash deposit (layer 3). Layer 1 is either a ground surge deposit (LHS) or a ground layer deposited from the head of a pyroclastic flow (RHS).

Lithic fragments constitute 5 to 20% of the rock. In order of predominance they include dolerite, quartz-feldspar porphyry, granitic fragments and gneissic granite, metamorphosed siltstones and basement schists and gneisses, chert and sandstone. They range in shape from angular to rounded, and in diameter from 0.5 - 5 cm up to 5 - 20 cm. The size and proportion of lithic fragments is variable throughout the facies (5-20%), with some notable lithic concentration zones. These contain a higher proportion (30-40%) of the larger sized fragments (those between 5-20 cm in diameter). There is no systematic decrease or increase in the size of lithic fragments either vertically or laterally. Fig. 4.4 illustrates the types of crystals and lithic clasts that occur in the welded ignimbrites, and in the overlying fluvial sandstones and conglomerates (Section 4.4).

The groundmass is a devitrified volcanic glass, usually red coloured and aphyric, and locally recrystallised to a spherulitic or fine-grained granophyric texture. Relict fibrous tube pumice textures and plastically deformed shards and pumice shreds are locally preserved (Figs 4.1c;d; 4.2g).

Chlorite and hematite are common, and epidote is also present in places, generally replacing fiamme and large feldspar grains, along with chlorite (Fig. 4.1e). In the eastern-most part of the area, calcite and fluorite are common secondary minerals (Fig. 4.1f).

*Interpretation:* This facies has all the features of layer 2b deposits of subaerially erupted welded ignimbrites, and their various lithic concentration zones. The presence of angular crystal fragments, pumice and shards, and abundant lithic fragments indicates fragmentation by pyroclastic processes. The thick, massive, open framework characteristics of the facies indicate deposition processes by mass-flow with yield strength. The development of columnar jointing, the mesoscopic eutaxitic texture, and microscopic welded vitriclastic textures and devitrification features such as spherulites are evidence for a hot state of emplacement. Welding in ignimbrites is a good indication of a subaerial environment of deposition, although welded ignimbrites have been described in shallow marine successions (e.g. Howells et al, 1973; 1985; Francis & Howells, 1973; Lowman & Bloxam, 1981). Given the local setting of the ignimbrites, and the fact that a thick ignimbrite sequence (~ 830 m) was deposited with no evidence of subaqueous reworking between deposition of separate mass-flow units, the environment of deposition is interpreted to be subaerial.

Pyroclastic flow deposits are usually composed of a number of flow units. Each flow unit is usually regarded as the deposit of a single pyroclastic flow, and several or many pyroclastic flows may be generated during the course of a single eruption (Sparks et al, 1973; Sparks, 1976). The individual pyroclastic flow units may be stacked on top of each other, and indistinguishable unless separated by other pyroclastic layers (fall or surge deposits) or reworked epiclastic deposits. Thus it is impossible to tell how many flow units comprise the ignimbrite succession of the Gimbat Ignimbrite Member. The subfacies distinguished based on lithological criteria may represent separate flow units and may each comprise several flow units.

Individual flow units may also be separated out by identifying the different layers and facies within a pyroclastic flow, particularly those which form at the base of a flow unit. A pyroclastic flow will assume a certain form when moving, which can be divided into a head, a body and a tail region (Fig. 4.5; Wilson, 1985). These three regimes have different fluidisation states, which result in the development of separate layers and facies within a pyroclastic flow deposit. Sparks et al (1973) first proposed a layering scheme for pyroclastic flow units (Fig. 4.5). Layer 1 deposits represent either the deposit of a pyroclastic surge moving in advance of a pyroclastic flow, or deposits from the highly inflated and fluidised flow head (fines-depleted ground layer). Not all pyroclastic flow deposits contain layer 1 deposits. The pyroclastic flow may not

#### 4. GIMBAT IGIMBRITE MEMBER

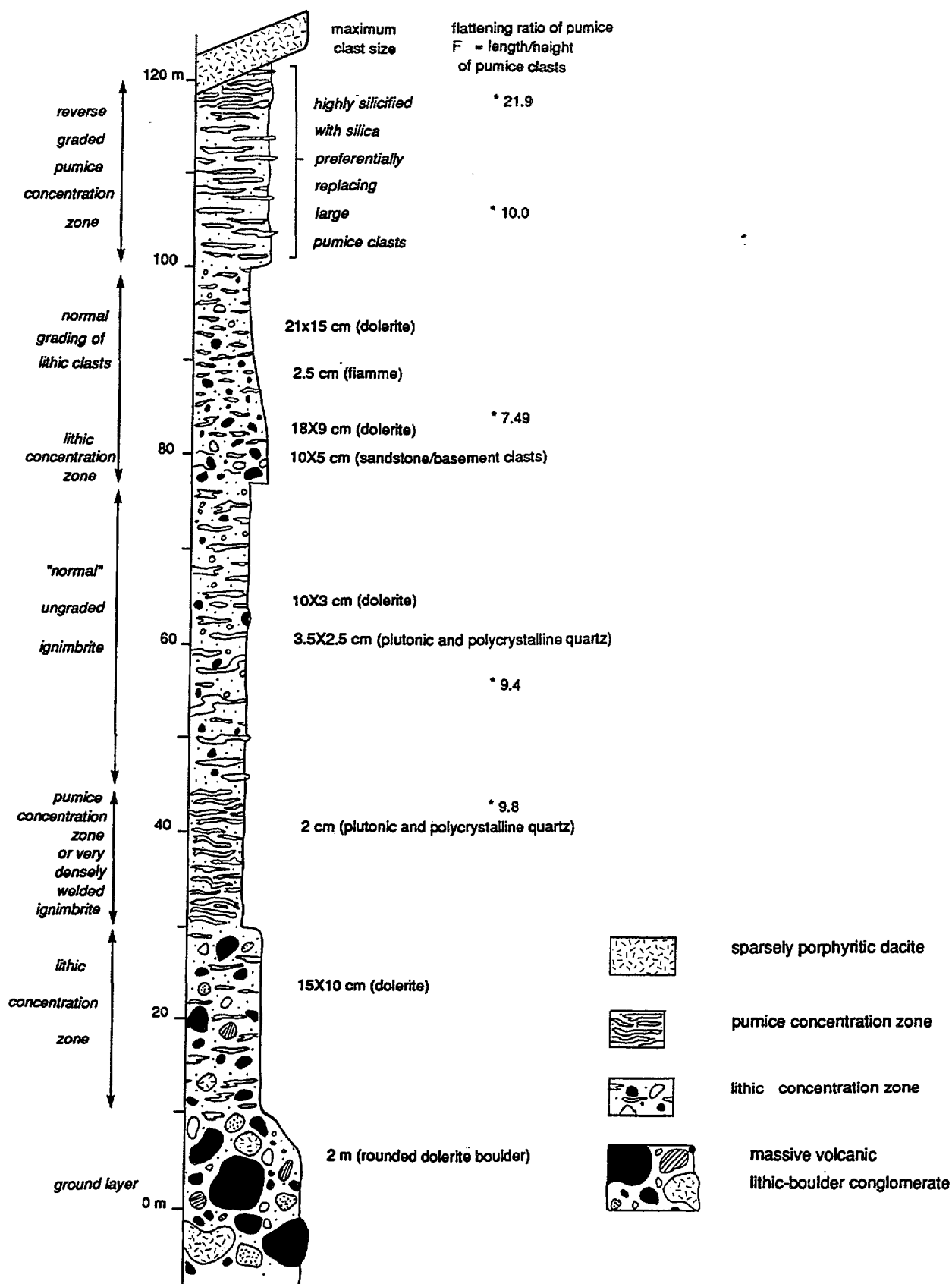


Figure 4.6: Measured section through welded ignimbrite (Unit Ig) in the Dinner Creek area, showing the vertical variation in pumice and lithic content, and degree of compaction which can occur within ignimbrite units.  
(G.R.)

be preceded by a surge, and only fast-moving pyroclastic flows (e.g. Taupo Ignimbrite) ingest enough air at the flow-front to develop highly inflated, turbulent heads from which a prominent, fines-depleted ground layer can be deposited (Walker et al, 1980; Walker et al, 1981; Walker, 1985). Layer 2 is deposited by the body of the pyroclastic flow, and layer 3 is the deposit of the overriding ash cloud.

Layer 2 may have a fine-grained basal layer (layer 2a) which varies in thickness from a few cm to 1 m, which may have faint stratification. Layer 2a results from a shearing effect at the boundary layer between the moving pyroclastic flow and the ground surface (Sparks, 1976). The basal layer lacks the larger pumice and lithic clasts, and any clasts within the layer show a reverse grading.

The main portion of an ignimbrite flow unit (layer 2b) may show 'coarse-tail grading' of the larger clasts. This is a gravity- or buoyancy-induced grading which affects the coarser fraction of the pyroclasts due to their high settling velocities, while the finer fractions, or matrix of the flow unit, remains homogeneous. It results in the development of well-defined lithic concentration zones at the base of layer 2b, and if the flow unit is poorly expanded, reverse grading of pumice clasts, with pumice concentration zones at the top of the layer (Fig. 4.5).

The ignimbrite subfacies may be interpreted in terms of this layering scheme. Units I<sub>A</sub>, I<sub>C</sub> and I<sub>D</sub> have a regular distribution of lithic and pumice clasts and are thus interpreted to be ungraded layer 2b ignimbrites. Unit I<sub>B</sub> contains a high proportion of lithic clasts (~ 30 - 40%), Pumice clasts are conspicuously absent, and the unit grades locally into the overlying unit I<sub>C</sub>. It is therefore interpreted to be a layer 2b lithic concentration zone forming part of the same flow unit as unit I<sub>C</sub>. Unit I<sub>E</sub> is non-graded over most of the flow area, but to the northwest near Dinner Creek, lithic and pumice concentration zones were identified, and a measured section through this area (Fig. 4.6) shows the vertical variation within the unit. Although it was not possible to map out the internal variation along strike, the presence of lithic and pumice concentration zones implies unit I<sub>E</sub> comprises several flow units.

#### 4.2 MASSIVE VOLCANIC LITHIC-BOULDER CONGLOMERATE

*Description:* 35 m of volcanic conglomerate underlie ignimbrite Unit I<sub>E</sub> and locally a 2b lithic-concentration zone of unit I<sub>E</sub> to the north of an ENE-trending fault near Dinner Creek (Fig. 1.2). The facies forms a prominent ridge with a continuous strike length of 800 m and is conformable with the strike trends of the adjacent ignimbrites. The facies appears to be truncated by the ENE-trending fault and although the overlying lithic-rich ignimbrite reappears on the southern side of the fault, the massive, volcanic boulder conglomerate does not underlie it. The lithic-boulder conglomerate is in sharp contact with the underlying and overlying ignimbrite and the contact with the overlying lithic concentration zone is sharp to locally gradational.

The conglomerate is internally massive and clast supported and poorly sorted, with clasts ranging in size from fine sand to boulders up to 2 m in diameter, with a small amount of interstitial matrix. The boulders are heterolithic, with rounded dolerite (the most abundant clast type), subangular to rounded quartz-feldspar porphyry and sandstone, and angular meta-siltstone and crenulated metamorphic basement clasts (Figs 4.3 d;e;f;g). The dolerite boulders are the largest (2 m maximum diameter), quartz-feldspar porphyries average 30x15 cm, with a maximum diameter of 1 m, and sandstone and basement clasts are up to 20 cm in diameter. The matrix consists of fine siliceous material with a recrystallised granophyric to cherty texture, supporting smaller angular crystal fragments (quartz, K-feldspar and minor plagioclase) and smaller lithic clasts in an open framework structure. The smaller clasts (up to 5 cm) are predominantly subangular to angular dolerite fragments, and also include angular plutonic

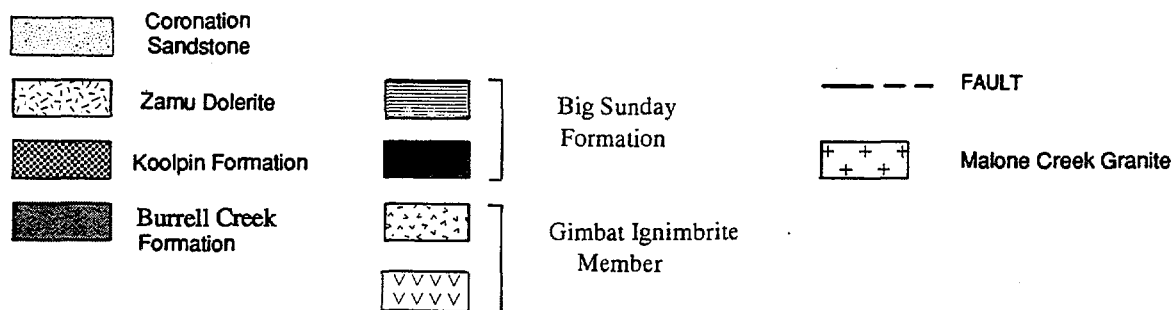
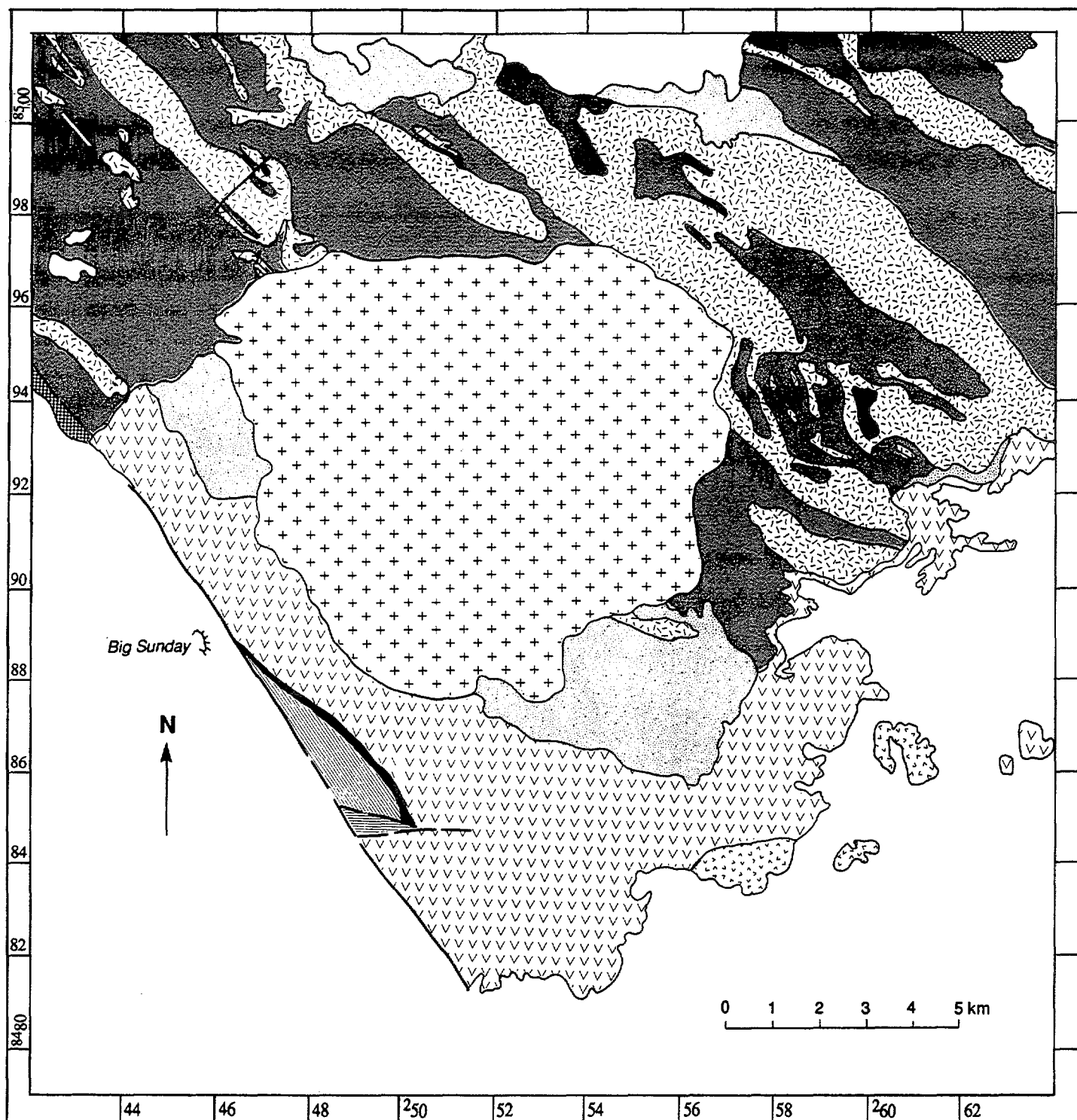


Figure 4.7: Geology of the area of study, showing the distribution of Burrell Creek Formation, Zamu Dolerite and Coronation Sandstone, which comprise the basement to the Gimbat Ignimbrite Member (adapted from Stow 1:100 000 Map Sheet).

quartz. Some fragmental material in the matrix appears to be relict pumice, and the groundmass contains chloritised, flattened shards. The matrix has the same composition and texture as the overlying ignimbrites, and is interpreted to be a devitrified volcanic glass.

*Interpretation:* The facies is interpreted to be a co-ignimbrite breccia, based on the features described above (internally massive, clast-supported, small amount of ignimbrite matrix; ie fines depleted), and its close association with other ignimbrite facies, especially the gradational contact with the overlying layer 2b lithic-concentration zone. The absence of tractional structures in the facies and more importantly, the ignimbritic nature of the matrix rule out a fluvial origin for the facies, although the rounded lithic boulders are suggestive of reworking by epiclastic processes.

The co-ignimbrite breccia could be either a ground layer, or a lag fall breccia or a lag breccia. The larger lithic fragments in this facies were most likely loose, weathered boulders on the ground surface, captured by the erosive head of a pyroclastic flow, indicating the co-ignimbrite breccia is a ground layer. Lag breccias in contrast, would contain coarse accessory lithic fragments derived from near-surface flaring of the volcanic vent, which drop out of the 'deflation zone' of a collapsing eruption column (Walker, 1985; Eichelberger & Koch, 1979). These lithic fragments would be angular to subangular in shape, rather than rounded.

This ground layer and the overlying graded ignimbrite (I<sub>E</sub>), with its basal lithic concentration zone and reverse grading of pumice fragments are interpreted to be the constituents of a single pyroclastic flow. The pyroclastic flow must have travelled at high velocity, developing a large, fluidised head, given the thickness of the ground layer and the size of the accidental boulders it contains. Only fast-moving pyroclastic flows (e.g. Taupo Ignimbrite) ingest enough air at the flow-front to develop highly inflated, turbulent heads from which a prominent, fines-depleted ground layer can be deposited (Walker et al, 1980; Walker et al, 1981; Walker, 1985). Flows with larger heads are more erosive, and the size of accidental lithic fragments is a good indicator of the degree of erosion which has occurred at the flow head.

The development of a ground layer does not necessarily indicate the flow was proximal to vent. A pyroclastic flow can segregate to form a well-developed head within a few kilometres of the vent (Druitt & Sparks, 1982; Suzuki-Kamata & Kamata, 1990), which is capable of transporting metre-sized boulders up to 10 km and 10 - 30 cm lithic clasts ~ 30 km from the source, and the resultant ground layer can extend to nearly the distal limits of the ignimbrite (Walker et al, 1981; Suzuki-Kamata & Kamata, 1990). However, the ground layer systematically decreases in lithic content and grainsize with distance from vent (Walker, 1983). Based on this fact, the facies is interpreted to be within close proximity to vent. It is markedly thick, containing accessory lithic clasts 20-30 cm in diameter, and would have thinned out considerably in the distal regions of the flow. All lithologies identified in the lithic component of the ground layer, and in the surrounding ignimbrites, are exposed in outcrop to the north and west of the facies, and probably underlie the ignimbrite succession (Fig. 4.7), also suggesting the volcanic vent was situated locally.

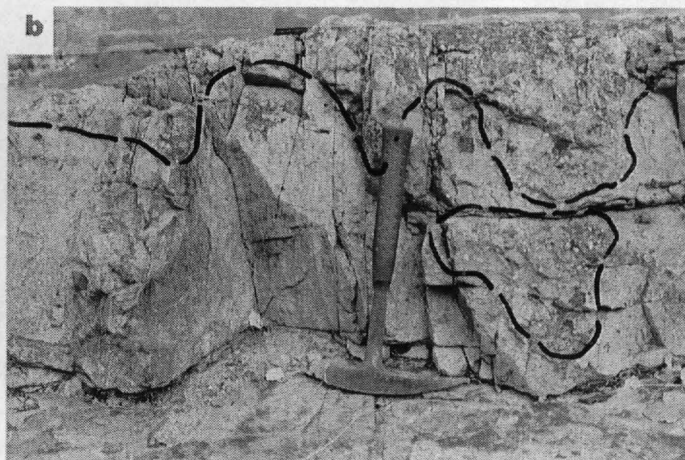
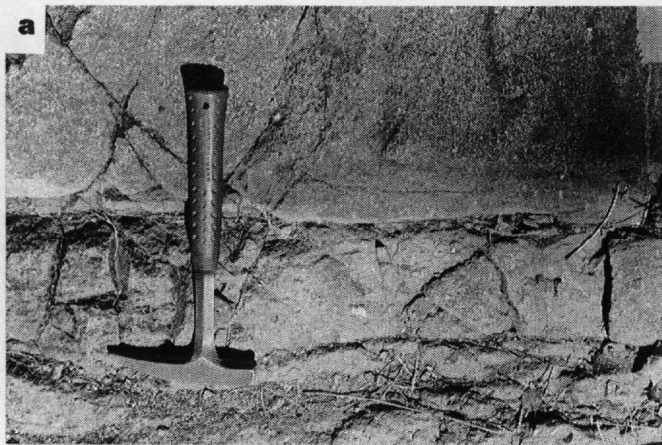
#### 4.3 NON-WELDED IGNIMBRITE

*Description.* This facies conformably overlies unit I<sub>E</sub> at the top of the welded ignimbrite sequence, in the central to southeastern part of the study area (Fig. 1.2; 1.3). It forms one unit extending 3.5 km along strike, with an average thickness of 60 m. The top of the facies is highly eroded.

The facies is a massive, open framework breccia with poorly sorted euhedral to angular or fragmented crystals and lithic fragments in an aphanitic siliceous matrix. The facies contains no

**Figure 4.8:**

- a)** Fine-grained laminated layer at the base of the non-welded ignimbrite, overlying the contact with welded ignimbrite; creek section (GR479880-476878)
- b)** Irregular, coarser-grained pebbly stringers (crystal-rich volcanic sandstone facies) interlayer with the main body of the non-welded ignimbrite. The trace outlines the highly irregular contact, the presence of load casts and load balls of pebbly material dropping into the underlying, finer-grained material
- c)** Interbedded sandstone and conglomerate. The layers are internally massive and the conglomerate layers contain well-rounded quartz cobbles
- d)** Close-up of the contact between coarse sandstone and conglomerate layers. Both layers are internally massive
- e)** An epiclastic unit characterised by the abundance of sub-angular to rounded quartz-feldspar porphyry clasts in a fine grained, black matrix. The unit also contains smaller, angular dolerite clasts
- f)** An epiclastic unit characterised by the abundance of angular dolerite clasts in a quartz-rich matrix
- g)** Hand specimen of the aphyric rhyolite lava showing its brick red colour and total lack of phenocrysts
- h)** Photomicrograph of aphyric rhyolite lava showing the development of spherulitic textures and the absence of phenocrysts



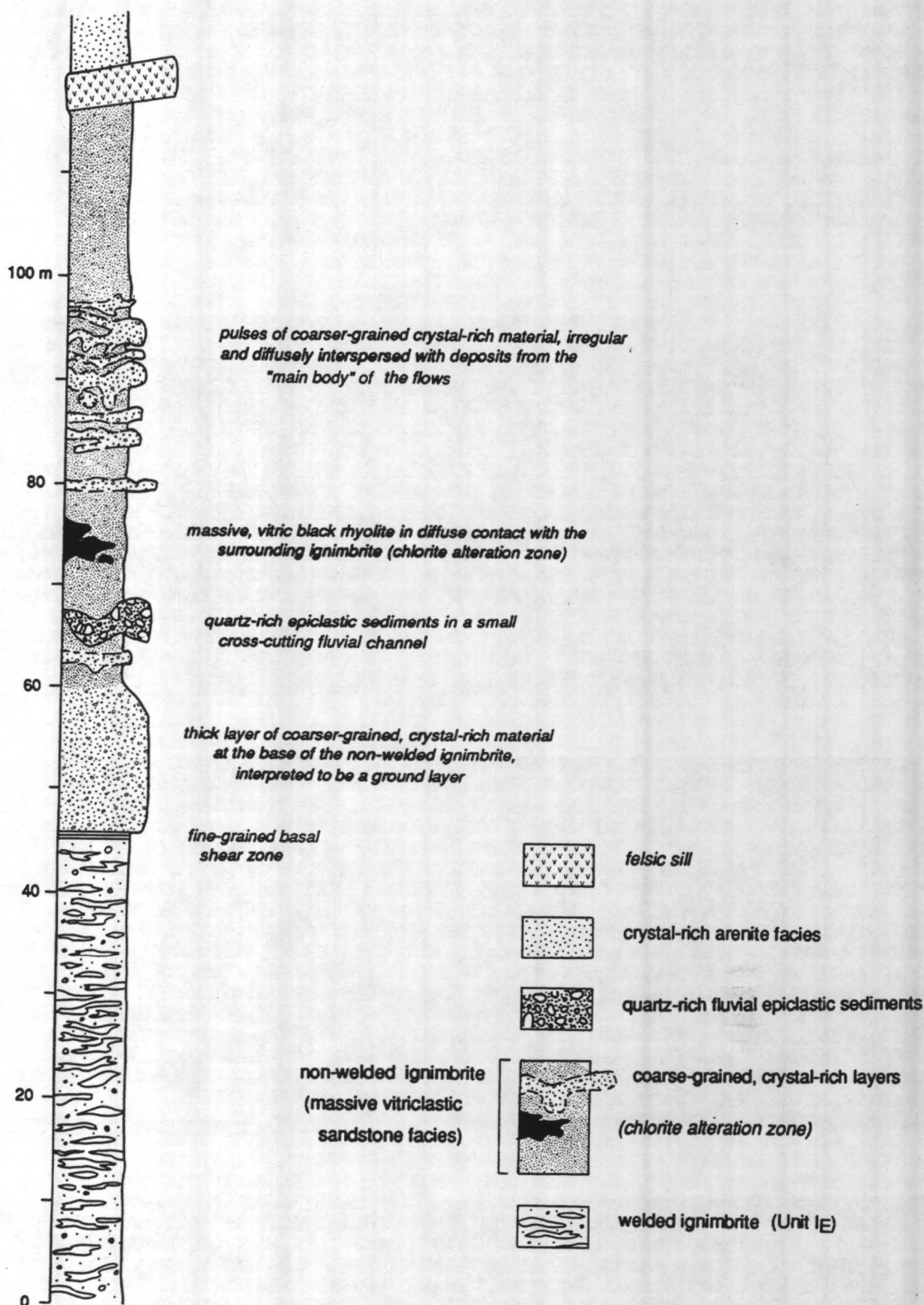


Figure 4.9: Measured section through the massive, vitriclastic sandstone facies, Ignimbrite Creek. (G.R. 479 880 - 476 878)

large lenticular pumice fragments and there is no evidence of welding, in contrast to the underlying ignimbrite units. Relict tube pumice fragments and chloritised cusped shards without evidence of being flattened and welded are visible in thin section (Fig. 4.3h).

The facies is geochemically and mineralogically identical to the underlying ignimbrite. It contains ~ 15% fragmented to euhedral crystals of quartz, K-feldspar, minor plagioclase and accessory zircon and opaques. The facies contains between 3 to 17% lithic fragments with a maximum diameter of 3 cm. Lithic fragments include dolerite and 'milky' quartz visible in hand specimen. In thin section, the 'milky' quartz is identified as plutonic, metasedimentary or sandstone fragments.

At one creek, tributary to the South Alligator Valley (GR 478879), a fine-grained crystal-rich basal layer, 10 cm thick with fine stratification and lacking lithic clasts, separates the unit from the underlying ignimbrite (Fig. 4.8a).

#### *Crystal-rich Volcanic Sandstone Facies*

At this same creek (GR 478879), the non-welded ignimbrite is irregularly interbedded with closed-framework, coarser-grained sandstones (Crystal-rich Volcanic Sandstone Facies). This facies could not be identified in the bouldery outcrops of the ridges surrounding the creek section, but is assumed to be present throughout the non-welded ignimbrites.

In the creek bed, the fine-grained crystal-rich basal layer of the non-welded ignimbrite is overlain by 15 m of crystal-rich volcanic sandstone (Fig. 4.9) which has a lower matrix component. It exhibits a reverse grading and has a higher concentration of crystals and lithics at the base (55%) than at the top (39%). The crystal-rich volcanic sandstone is conformably overlain by more non-welded ignimbrite.

Upsection, irregular stringers of coarser-grained, crystal-rich sandstone ~ 20-100 cm thick cross-cut the non-welded ignimbrite over a 25 m interval (Fig. 4.9). These crystal-rich stringers are extremely irregular, do not form definite layers, and cannot be traced laterally. Crystal and lithic concentrations are as high as 67-74% and form a tightly packed framework with little interstitial matrix. Crystals are angular to fragmented and have the same mineralogy as those in the non-welded ignimbrite. Lithic fragments are large (2 mm - 1.5 cm) and rounded and include welded ignimbrite, presumably derived from the underlying ignimbrites. Upsection, the coarser layers show a progressive enrichment of lithic relative to crystal fragments (Fig. 4.10).

Load casts occur at the base of the pebbly material, and balls of the pebbly material have dropped into the underlying non-welded ignimbrite (Fig. 4.8 b), suggesting these were unconsolidated at the time the crystal-rich stringers were deposited. The coarse layers are overlain by non-welded ignimbrite and the contact is sharp to gradational, with some large lithic fragments incorporated into the base of the overlying non-welded ignimbrite.

*Interpretation.* The fragmental morphology of the crystal component, the angularity of lithic fragments and the presence of undeformed pumice fragments and chloritised cusped shards in the matrix of this facies, suggest fragmentation by pyroclastic processes. The massive poorly sorted open framework nature of the facies indicates emplacement by mass flow processes with yield strength. In the absence of welded textures, the facies could be interpreted to be a pyroclastic or juvenile secondary mass-flow (debris flow) deposit. Given that the facies overlies a thick succession of welded ignimbrites and is identical to these ignimbrites except for the absence of fiamme, deposition by pyroclastic flow is concluded and the facies is interpreted to be a non-welded ignimbrite.



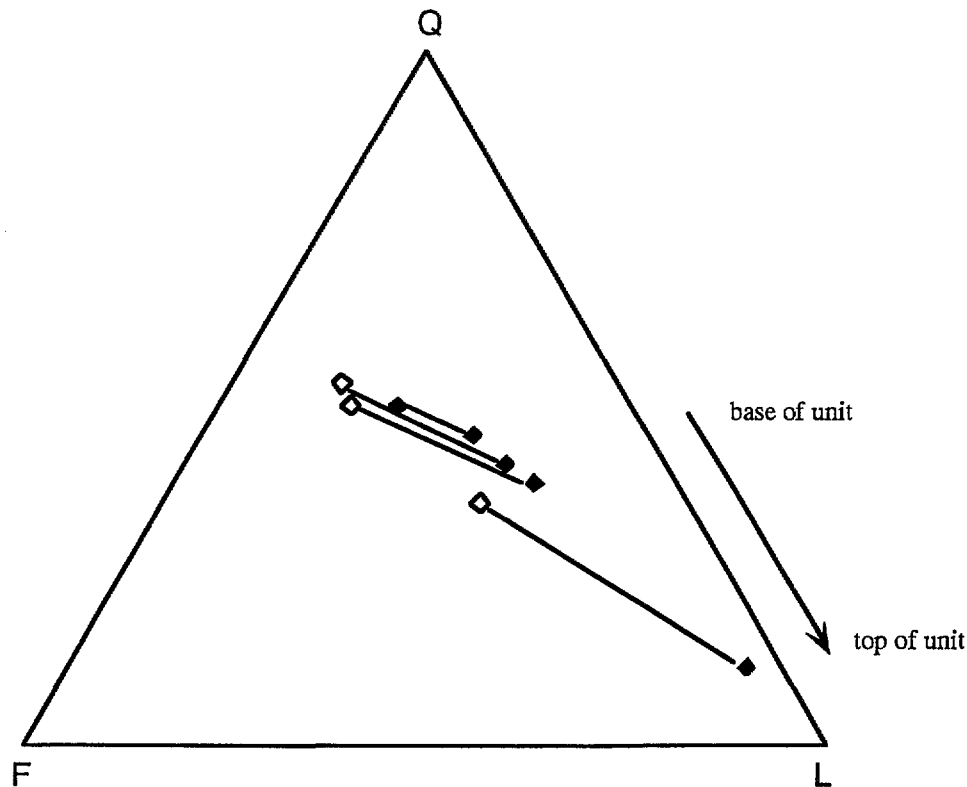


**Figure 4.10:** Modal analysis plot for the  $\diamond$  non-welded ignimbrites and  $\blacklozenge$  crystal/lithic concentration zones within the facies. Tie lines link the main body of the flow with the underlying crystal/lithic-rich ground layer, and show that upsection, each ground layer becomes progressively more lithic-rich.

The fine-grained basal layer is interpreted as a ground layer or layer 2a deposit (Sparks et al, 1973) formed due to a shearing effect at the boundary-layer between the moving pyroclastic flow and the ground surface (Sparks, 1976).

The coarser-grained crystal-rich layers in the non-welded ignimbrite have the same mineralogy, but are enriched in crystals and lithic clasts. They may represent the deposits from the head of the pyroclastic flow. The head is the most fluidised part of a pyroclastic flow, into which large quantities of air can be ingested (Wilson, 1980). Strong fluidisation and turbulence in the flow head promote elutriation of fines which stream into the main body of the flow. This results in the head deposits being fines depleted and enriched in crystals and lithics. The presence of some large lithic fragments near the base of the non-welded ignimbrites immediately above the coarser layers suggests that there is some exchange of material between the flow head and the overriding body of the flow.

Repetition of the head deposits upsection may represent either pulses of material in a single flow perhaps corresponding to pulses in the eruption rate, or the deposition of several flow

units or flow lobes of the one flow in quick succession. The progressive increase in the lithic component in each head deposit indicates vent flaring occurred, so that progressively more accessory lithic material was incorporated into the pyroclastic flow during the course of the eruption.

#### 4.4 MASSIVE-LAMINATED-CROSS BEDDED SANDSTONES AND CONGLOMERATES

*Description:* The top 200 m of the ignimbrites hosts dominantly massive to planar laminated and cross bedded quartz-rich sandstones and conglomerates. The facies occurs as lensoidal units which are not laterally continuous, and lens out over strike lengths up to 1.8 km. The outcrop pattern shows the sandstone and conglomerate beds are highly erosive into the underlying non-welded ignimbrite (Fig. 1.3). Smaller lenses also occur interstratified with the welded ignimbrites near the top of the ignimbrite succession (Fig. 1.3). The facies is thicker and more extensive to the southeast, and individual units are interbedded with thin layers (5-10 m) of welded ignimbrite (Fig. 1.3).

The lenses have a range of thicknesses up to 20 m. Sandstones and conglomerates form thick interbedded units with individual beds up to 15-40 cm thick (Fig. 4.8 c), and thinly interbedded fine- and coarse-grained sandstone are common over a scale of tens of centimetres (Fig. 4.8 d). The interbeds are internally massive. Conglomerates and medium to coarse-grained sandstones form open framework massive units. Cross bedding and planar laminations are present in the medium-grained to finer-grained units. Some lenses have upward fining cycles, from pebble conglomerate to fine-grained sandstone which vary from being massive to diffusely planar stratified to cross-bedded in texture (Fig. 4.11).

The sandstones range from fine to coarse in grain size and grains are angular to rounded in shape and poorly to well sorted. Many of the units are massive with an open-framework structure. Those which exhibit tractional structures have less matrix and a closed-framework organisation. The proportion of matrix varies from 50-60% in the massive units to 25-40% in those exhibiting tractional features. The textural maturity thus varies from immature to submature.

The facies is composed of lithic to arkosic sandstones, pebbly-sandstones and conglomerates. The constituent grains include quartz, K-feldspar, minor plagioclase, minor opaques and zircon and an abundance of lithic fragments.

Quartz is the main constituent and there are several varieties, both monocrystalline and polycrystalline. The quartz is mainly volcanic quartz, monocrystalline and clear with minor embayments and straight extinction, and is angular to sub-angular, indicating minimal abrasion. Slightly larger, sub-rounded to rounded monocrystalline quartz grains exhibit strong undulose extinction and have a dusty appearance, with abundant vacuole trails. This quartz is probably basement derived (from metasediments of the Pine Creek Geosyncline Sequence) or of plutonic origin. Sub-rounded to rounded polycrystalline quartz is either plutonic in origin, or those exhibiting a higher degree of strain, sutured internal grain boundaries and irregular internal grain size are derived from basement metasediments. Chert is a minor constituent. The degree of rounding indicates the basement-derived polycrystalline and monocrystalline quartz grains are more reworked than the volcanic quartz. Feldspars are mainly K-feldspar with minor plagioclase, and grains are angular to euhedral in shape, indicating it is probably volcanically derived and has undergone only minor reworking.

The lithic component is dominated by polycrystalline quartz originating from plutonic sources, or the metasedimentary basement. Basement fragments include highly deformed gneisses and mylonites. Dolerite, sandstone, siltstone, chert, devitrified or fine-grained volcanic fragments

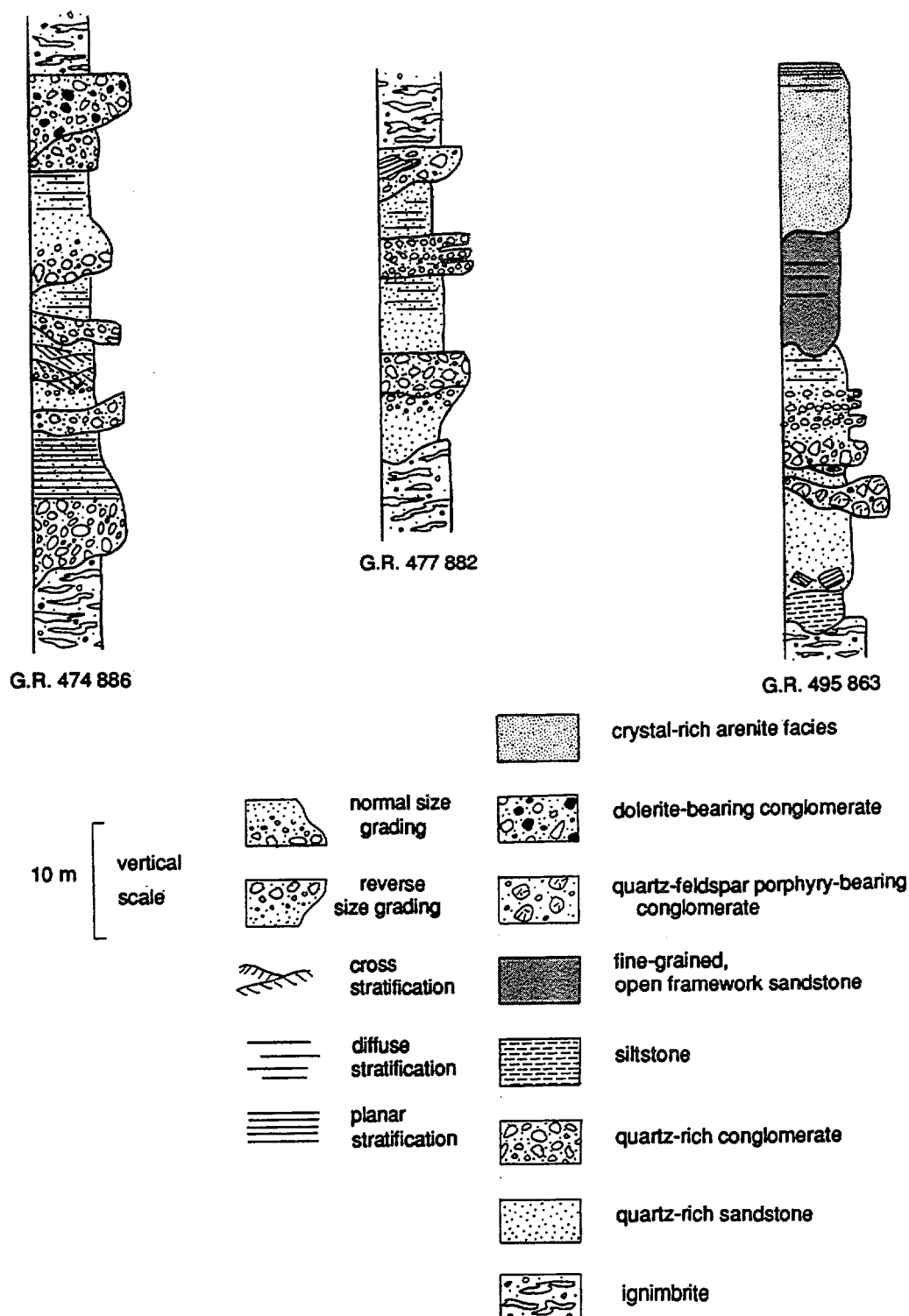


Figure 4.11 Measured sections through several channels infilled with epiclastic material, showing bedding features, grading and relationships between individual units typical of the facies.

and quartz-feldspar porphyry fragments are widespread throughout the facies but occur in minor proportions.

Compared with the underlying ignimbrites, the sandstones and conglomerates have a lower feldspar content (Fig. 4.12), and basement- or plutonic-derived undulose quartz is more abundant, although volcanic quartz is still the most abundant type. Lithic grains are mainly granite clasts or metasedimentary basement clasts, whereas in the ignimbrites, dolerite is the main lithic component (Fig. 4.13).

The matrix component of the sandstones and conglomerates consists of very fine-grained siliceous material, which may be derived from the vitriclastic ash-component of the underlying ignimbrites.

Two conglomerate lenses within this facies have unusual compositions compared with the normal quartz-rich sediments of the facies. Each has a distinctive coarse-lithic component. The first forms a lens surrounded by medium-grained quartz-rich massive to planar laminated sandstones and contains large, rounded quartz-feldspar porphyry cobbles (Fig. 4.8e). The second underlies an interbedded sandstone and conglomerate facies (Fig. 1.3) and contains an abundance of angular dolerite fragments in a finer-grained siliceous matrix (Fig. 4.8f). In each case, the sediment must have been sourced from an area locally enriched in the lithology of the dominant clast-type. Table 4.2 summarises the different units within this facies.

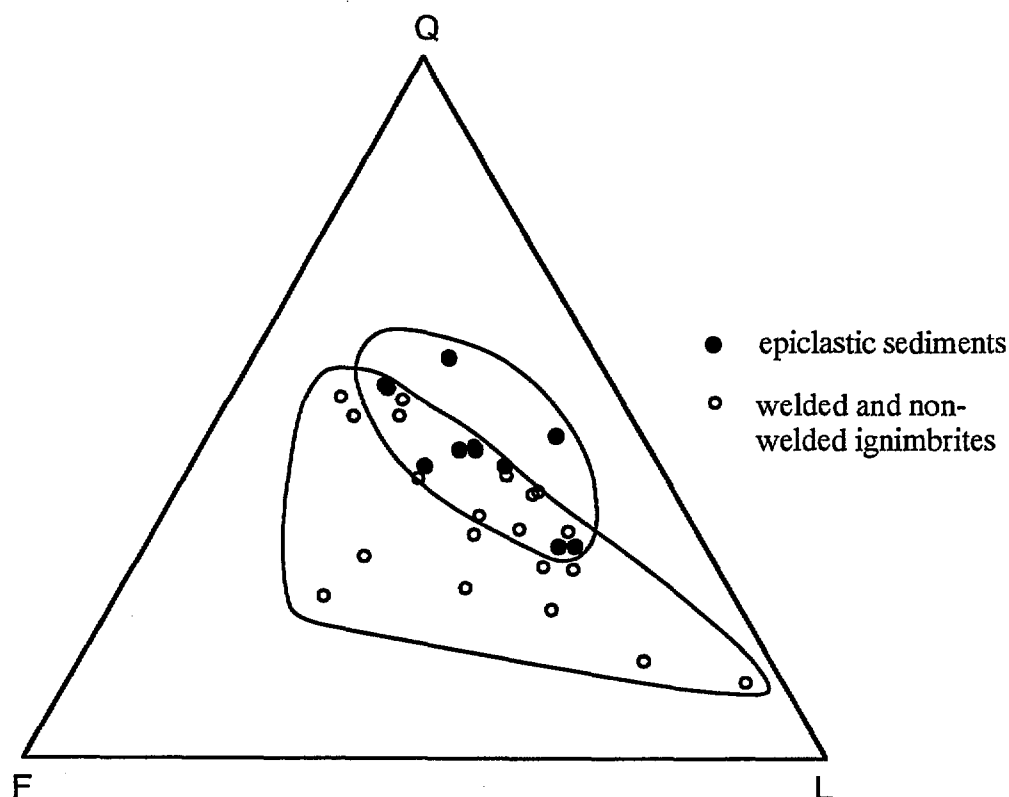


**Figure 4.12:** Q-F-L plot of representative modal analyses comparing the massive--laminated-cross bedded sandstones and conglomerates with the underlying welded and non-welded ignimbrites. Note that the epiclastic sediments contain a higher proportion of quartz.

### *Interpretation*

Most of the sandstones and conglomerates comprising this facies are medium to coarse-grained non-graded massive deposits in which larger grains are supported by a mud or silt-sized matrix. This indicates rapid deposition by viscous mass flow, such as mud flow or debris flow with a high sediment load.

The matrix-poor sandstone beds which exhibit tractional structures were deposited by cohesionless, inertial processes. Upward fining sequences and the preservation of lower flow regime structures such as planar and cross beds reflect a gradual reduction in energy conditions and diminishing current velocities during deposition.

The restricted geography, lensoidal geometry and highly erosive nature of the units suggest small channel-form environments, for which a fluvial origin is most likely. The channels are interpreted to represent local sediment-filled erosional gullies developed between ignimbrite eruptions. Volcanic terrains contain thick accumulations of unconsolidated debris which are unstable and highly erodible, promoting the development of deeply-incised canyons and gullies

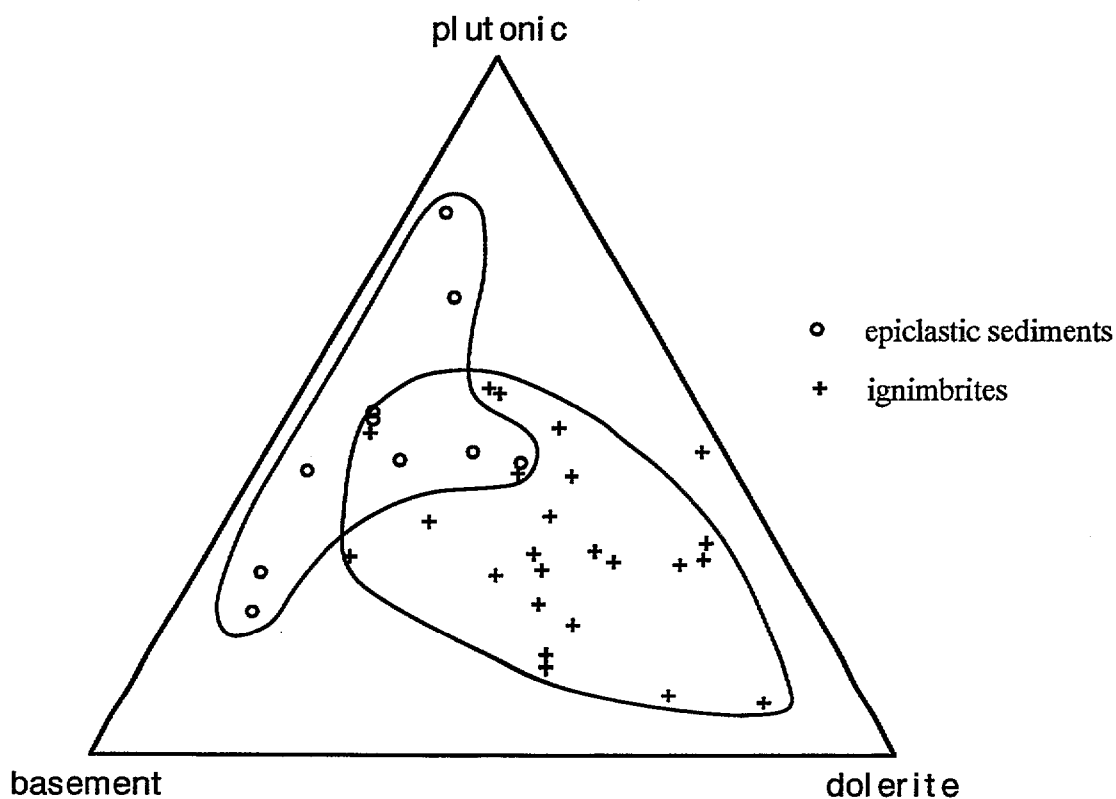


**Figure 4.13:** Modal analysis data comparing the composition of the dominant lithic components in the massive--laminated-cross bedded sandstones and conglomerates and the underlying welded and non-welded ignimbrites. The ignimbrites have a higher proportion of dolerite clasts.

Table 4.2 Units of the Massive-Laminated-Cross bedded Sandstone and Conglomerate Facies.

Unit Name	Distribution & Geometry	Description / Distinguishing Features
E1 Quartz-rich massive-laminated-cross-bedded sandstone	Comprises most of the channel-fill epiclastic sequences and forms large lenses throughout the area.	Contains angular volcanic quartz and feldspar, and rounded basement-derived quartz and lithic fragments (mainly polycrystalline quartz). Grains have a predominantly open framework configuration with 50-60% matrix and units are internally massive. Locally units display upward fining and tractional structures such as planar to cross laminations are developed. In this case the grains have a closed-framework configuration with less interstitial matrix (25-40%). Matrix is composed of fine-grained siliceous material.
E2 Massive quartz-rich conglomerate	Forms thin interbeds with quartz-rich sandstones and outcrops locally as thicker lenses of coarse-grained material.	Comprised of the same material as the sandstones but is coarser-grained. Internally massive with variable proportions of matrix and packing of the larger grains. Open to closed framework.
E3 Fine-grained planar-laminated siltstone	Overlies quartz-rich sandstones and conglomerates at several localities, forming 150-700m lenses.	Comprised of the same material as the sandstones but much finer grained. Massive to plane-laminated. Clays absent, so immature sediment.
E4 Dolerite-rich conglomerate	200m lens underlying an interbedded sandstone-conglomerate facies in a channel to the north of Big Sunday	Contains large angular to subangular dolerite clasts which have a lensoidal shape (5x2cm) in a matrix of quartz grains (1-3mm). Closed framework.
E5 Quartz-feldspar porphyry-rich conglomerate	Thin, 200 m lens in quartz-rich sandstones in the Buffalo Creek area.	Contains large subrounded clasts of quartz-feldspar porphyry (up to 6cm) and dolerite clasts (2cm) in a black, fine-grained to aphanitic matrix. Open framework.
E6 Very fine-grained, open framework sandstone	Thin lens extending for 1.5 km overlying quartz-rich sandstones in the Buffalo Creek area.	Appears massive, glassy and aphanitic in hand specimen. Fine grained (0.1-0.2 mm) angular crystals and lithics occur in a finer grained matrix. Open framework. Mass flow unit; deposition by debris flow.

\* See Figures 4.8 c;d;e;f illustrate for illustrations of these facies.

and rapid rates of sedimentation. This is consistent with the mass flow processes prevalent during sedimentation of the epiclastic deposits. The absence of grading within most of the massive units indicates high sediment loads which is consistent with the abundant supply of loose volcanic detritus. Welded ignimbrites and lavas are less susceptible to erosion and have a good preservation potential which explains why most of the epiclastic channels have developed in the non-welded ignimbrite at the top of the succession.

It is possible that the open-framework sandstones and conglomerates represent short-lived reworking of the ash-pile during major rainstorms, during which large amounts of sediment was dumped into erosional gullies by debris flow. The closed framework sandstones may then represent later reworking of this detritus within the fluvial gullies, over long periods of time.

The mineral and lithic assemblage of the epiclastic deposits indicates they have a mixed basement and contemporaneous pyroclastic source, and that the proportion of basement-derived to volcanic-derived detritus varies between individual beds. Volcanic detritus includes volcanic quartz and feldspar, and some dolerite, metasedimentary and granitic lithic fragments, which form the xenolith population in the ignimbrites. This material is almost certainly derived from the subjacent ignimbrites, as suggested by the significant erosional incision of these ignimbrites. Volcanic quartz and feldspar have angular to euhedral grain shapes indicate minimal reworking of volcanically derived detritus.

An additional source area enriched in metasedimentary basement and granitic fragments is required to explain a higher proportion of these lithologies relative to dolerite in some of the epiclastic deposits than is observed for the xenolithic population of the ignimbrites (Fig. 4.13). The epiclastic deposits also contain a higher proportion of sub-rounded to rounded, high-strained quartz grains. This suggests a provenance area consisting of greenschist to amphibolite grade metasediments of the Pine Creek Geosyncline Sequence. The basement-derived grains are generally more rounded than the volcanic components indicating greater reworking, and probably derivation from a more distal source region.

Conglomerate lenses with an abundance of dolerite or quartz-feldspar porphyry cobbles must be derived from very local sources, enriched in these respective lithologies.

The palaeogeographical implication of the petrologic data is that the Pine Creek Geosyncline Sequence metasediments were exposed to form a palaeohigh at the time of deposition of the fluvial epiclastic deposits. The occurrence of unmetamorphosed sandstone lithic clasts in the facies suggests that sediments of the Coronation Sandstone were also outcropping at this time. Ignimbrite deposits are largely topographically controlled, filling valleys and depressions and flattening out the pre-existing topography, but basement ridge tops must have remained partly exposed following ignimbrite deposition, forming a source region to the epiclastic deposits.

#### 4.5 MASSIVE TO FLOW FOLDED APHYRIC LAVA

*Description.* In the southeast of the area, the ignimbrite succession is overlain by a coherent, non-vesicular rhyolite lava (Fig. 1.2) which forms an elongate dome-shaped body. The lava outcrops over a strike length of 4 km but isolated outcrops occur in the sandplains further east, suggesting the extent of the facies is much greater; perhaps as much as 8 km. The margins of the rhyolite are flow-folded and sparsely porphyritic, with up to 5% euhedral phenocrysts of quartz, alkali feldspar and plagioclase up to 2 mm in diameter, and minor opaques. Quartz crystals are embayed, with resorbed edges. The orientation of the flow-folding is variable, so the attitude of bedding could not be determined. The core of the rhyolite body is massive and

aphyric forming a resistant ridge rising above the surrounding plains. In hand specimen it has a brick-red, granular appearance (Fig. 4.8g). The groundmass of the rhyolite is devitrified to form abundant micro-spherulites of radiating clusters of alkali feldspar fibres ~ 0.5 mm in diameter (Fig. 4.8h). Where flow-banding is preserved, there is differential development of micro-spherulitic textures in the different layers.

*Interpretation.* The lava contains less than 5% crystals and the core of the lava flow is aphyric which suggests it extruded near liquidus temperature. The large size of the phenocrysts implies they crystallised within the magma chamber prior to eruption rather than during flowage and cooling of the lava body. In the latter case, microlites are more likely to form. Flow-banding at the margins suggests the lava moved by laminar flow, in which case the aphyric core may represent an internally rigid 'plug' within a laminar flow.

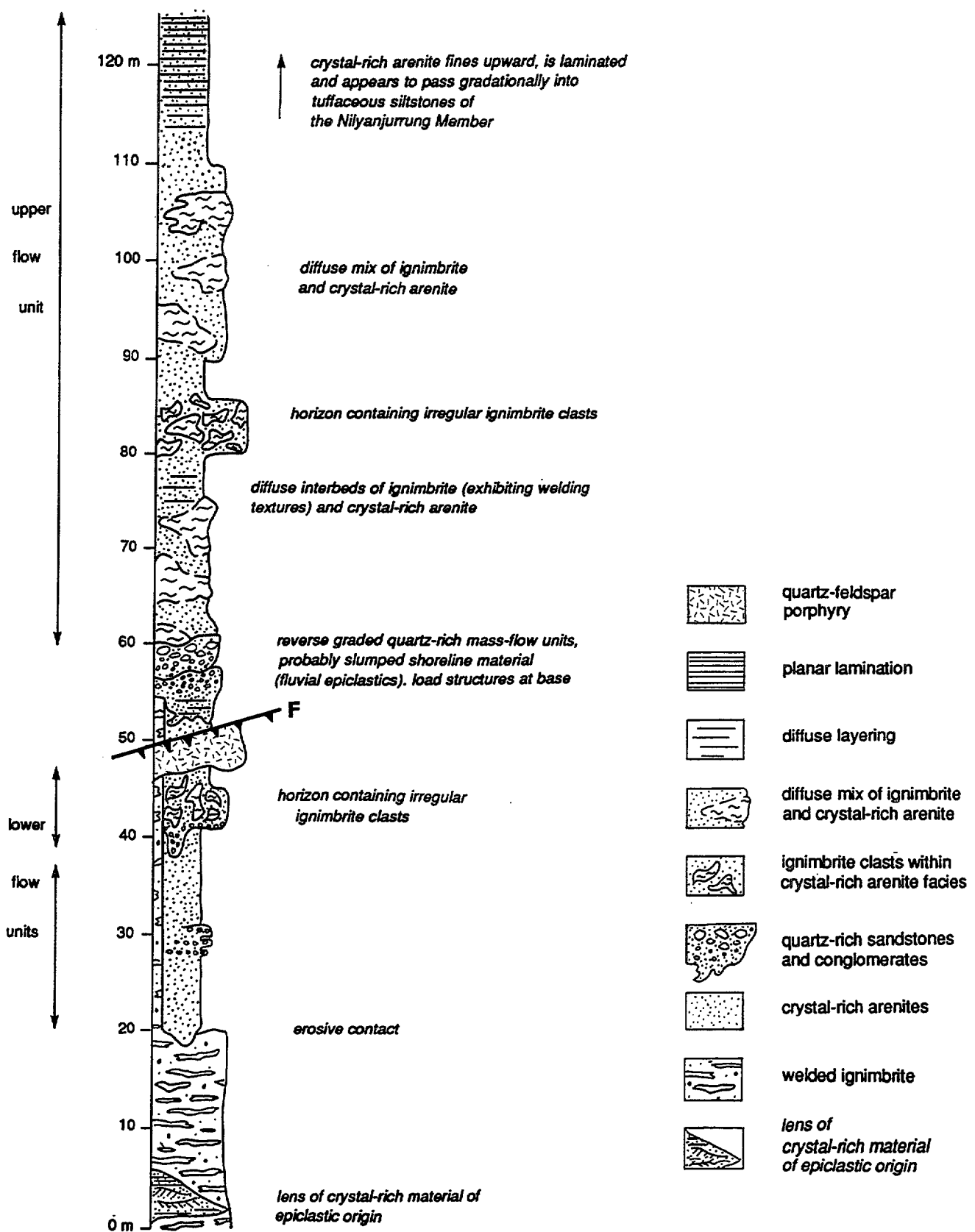


Figure 5.1 Measured section through the thickest exposure of the crystal-rich arenite facies, South Alligator River section.  
(G.R. 468 891 - 466 886)

## 5. BIG SUNDAY FORMATION

The Big Sunday Formation of the El Sherana Group unconformably overlies the subaerial welded ignimbrites and fluvial epiclastic sediments of the Gimbat Ignimbrite Member. Its base consists of thick, massive crystal-lithic rich volcanic arenites. These are conformably overlain by a subaqueously deposited turbiditic sequence, comprised of tuffaceous siltstones and interbedded sandstones (Fig. 1.3).

### 5.1 CRYSTAL-RICH ARENITE FACIES

#### 5.1.1 Stratigraphy

The massive crystal-lithic rich volcanic arenites at the base of the Big Sunday Formation form a laterally extensive horizon with a sheet-like geometry at the top of the Gimbat Ignimbrite Member, but are best exposed in an across strike section along the South Alligator River (GR 468 891-466 886, Stow Region 1:100 000 Geological Sheet). Here a thicker accumulation of the facies overlies and fills a buttress unconformity against a vertical wall of ignimbrite, suggesting a palaeovalley or canyon infill (Fig. 1.3; 5.1). The relief on this unconformity suggests the palaeovalley was approximately 30 m deep (Fig. 5.1). The basal contact of the arenite is erosional into welded ignimbrite with ~ 1m of relief, indicating the ignimbrites had solidified prior to deposition of the crystal-rich arenite. The contact of the facies with the overlying tuffaceous sediments is not exposed, but in the South Alligator River section the crystal-rich arenite fines upward and appears to grade into the overlying tuffaceous siltstones, suggesting their relationship is conformable.

#### 5.1.2 General Lithology

The crystal-rich arenites form depositional units which are tens of metres thick. For the purpose of the following discussion the facies is subdivided into three units. The palaeovalley fill consists of at least two sedimentation units (designated the 'lower' and 'upper' units) each ~ 50 m thick, which are separated by thinner, quartz-rich mass flow units (Fig. 5.1). The third unit is the laterally extensive horizon at the base of the tuffaceous siltstones, ~ 30m thick, which may be the lateral or outflow equivalent of the upper palaeovalley unit or may be a third, overlying sedimentation unit (Fig. 1.3).

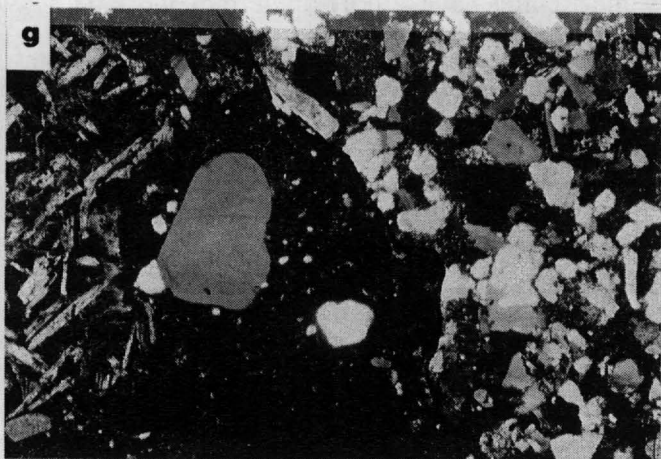
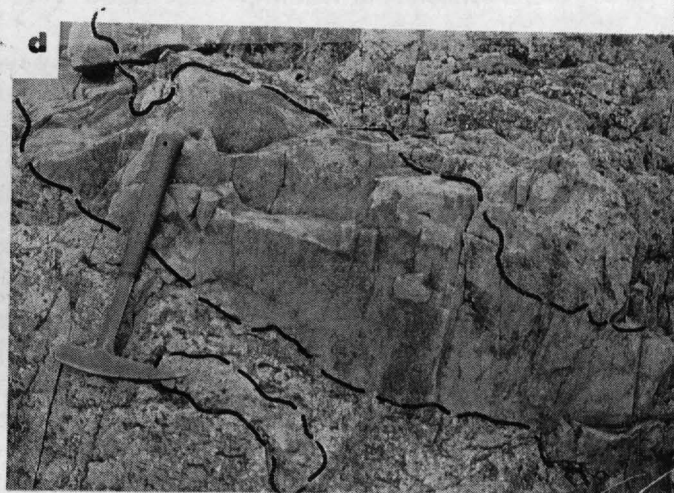
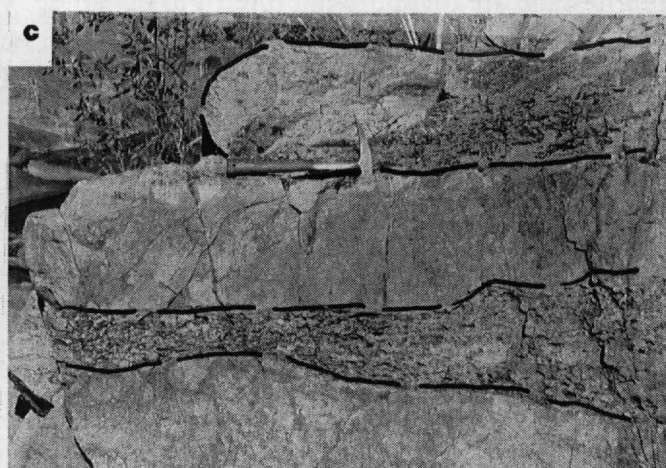
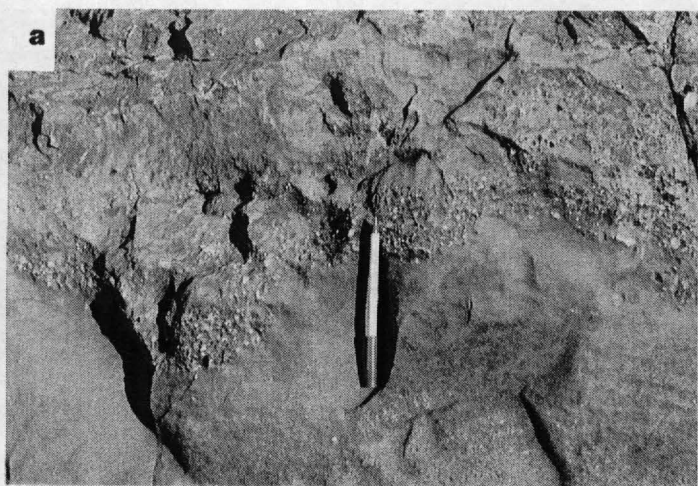
The crystal-rich arenites are massive in texture and lack continuous size grading. Normal grading (the upward decrease in grainsize of the whole crystal population) is confined to the upper levels of thick sedimentation units, and only occurs in the upper unit in the palaeovalley and locally at the top of the laterally extensive horizon. Where normal grading occurs, it is accompanied by diffuse to planar lamination. Coarse-tail grading occurs in the lower palaeovalley unit, which has a coarser-grained horizon that also contains large irregular-shaped ignimbrite clasts (see below; Fig. 5.2a). This horizon passes abruptly upsection into arenite of regular grainsize. This coarser-grained horizon marks the base of an amalgamated sedimentation unit.

Planar lamination, cross-bedding or other structures indicating tractional deposition are conspicuously absent from the facies. The massive units are uninterrupted apart from rare zones of diffuse lamination. The upper unit in the palaeovalley exhibits normal grading and diffuse to planar lamination of its upper level.

The lower unit in the palaeovalley has a fine-grained, inversely graded basal layer a few centimetres thick. Fine laminations in this layer are defined by a few finer-grained (average grainsize 0.1 mm) ash-rich layers. The contact between the basal layer and the main body of the

**Figure 5.2:**

- a) Coarse-tail grading during mass-flow deposition of crystal-rich arenites resulted in the formation of a lithic and coarse-crystal rich later at the base of one mass-flow unit in the South Alligator River section (GR 468891-466886). The coarse layer is overlain by a horizon bearing irregular-shaped ignimbrite clasts
- b) Irregular 'wispy'-shaped intraclasts of ignimbrite in a matrix of crystal-rich arenite. The clasts have a distinctly different texture to the host arenites, containing large lithic-clasts in an aphanitic groundmass, indicating this is not an alteration feature. The clasts exhibit eutaxitic textures
- c) d) e) & f) A horizon in the crystal-rich arenite facies in the South Alligator River section, which consists of a diffuse mix of ignimbrite and crystal-rich arenite. Note the eutaxitic texture in the ignimbrite patches, and the extremely irregular boundaries between the two facies
- g) Photomicrograph of the crystal-rich arenite facies taken at the contact between an ignimbrite clast and the crystal-rich matrix, showing the obvious textural difference between the two facies
- h) Photomicrograph of an ignimbrite clast in the crystal-rich arenite facies, showing the attenuation of relict shards/pumice shreds which is indicative of welding in the ignimbrite



1.5 mm

0.3 mm

unit is gradational. The base of the upper palaeovalley unit is sharp and erosional into the ignimbrites which form the canyon walls. Load structures occur where the base of the unit is in contact with the quartz-rich mass-flow arenites, suggesting these sediments were unconsolidated when the crystal-rich sandstone was deposited.

In the palaeovalley area, the facies displays some very unusual features. There are two horizons which contain red-coloured clasts that are extremely irregular and wispy in shape (Figs 5.1: 5.2b). At first these appear to be irregular patches of alteration, but in thin section the clasts have a very different texture to the host crystal-rich arenite (Fig. 5.2 g:h). They contain angular crystals and lithic fragments which have an open framework configuration, in an aphanitic siliceous matrix. This contrasts with the closed framework, crystal-rich nature of the enclosing arenite. The groundmass contains relict vitriclastic textures which include flattened chloritised shards and pumice shreds (Fig. 5.2h). The clasts exhibit textural and compositional features similar to the underlying welded ignimbrites and are therefore interpreted to be large ignimbrite fragments. Macroscopically the ignimbrite clasts show evidence of welding, with fiamme flattened to form eutaxitic textures. Microscopically welding textures are poorly preserved due to metamorphic overprinting of the groundmass, but the flattened pumice shreds suggest plastic deformation and welding. The extremely irregular and wispy shape of the clasts, and their uniformity of composition indicates they are intraclasts, rather than extraneous lithic clasts incorporated into the unit during transportation and deposition. If these were clasts derived from the erosion of a pre-existing ignimbrite, they would be more regular in shape and show signs of reworking and abrasion, and would be more compositionally diverse.

The upper unit contains horizons which are a diffuse mix of crystal-rich arenite and what appears to be welded ignimbrite with a eutaxitic texture, or crystal-rich arenite containing pumice clasts aligned to form a pseudo-eutaxitic texture (Figs. 5.2c:d:e:f). The boundaries between the two facies are extremely irregular and gradational. The relative proportion of arenite to ignimbrite at any given stratigraphic level is variable. This diffuse mix of ignimbrite and crystal-rich arenite also contains irregular lenses of quartz-rich coarse pebbly arenite, of similar composition to the quartz-rich mass flow arenites which underlie this unit.

### 5.1.3 Texture

In general, the grain population has a closed framework organisation. A matrix component consisting of very fine-grained siliceous material and small ( $< .05\mu$ ) crystals fills the intergranular spaces. It is likely the matrix was originally glassy ash, as suggested by the rare presence of spherulitic textures. Lithic fragments, especially dolerite are sometimes deformed to infill interstitial gaps, forming a pseudomatrix. The matrix is commonly overprinted by secondary minerals of metamorphic origin such as calcite, chlorite, epidote and sericite. Commonly the matrix component ranges between 22% and 35%. The original matrix component may have been higher, but intergranular spaces have been further reduced by pressure solution at grain boundaries forming siliceous overgrowths on the grains. The original matrix component was probably slightly greater, but no more than about 40%, given the closed framework aspect of the rock. The basal layer of the lower unit in the palaeovalley has a finer-grained crystal population and higher matrix content of 50%. The ignimbrite clasts within the crystal-rich facies have an open framework structure, with 72% groundmass. Where a diffuse mix of ignimbrite and crystal-rich arenite occurs, the arenites have a more open framework with a groundmass component ranging between 40% and 60%. This is a lower grain/matrix ratio than is typically observed in the crystal-rich arenite. The matrix is also typically fresher, lacking a strong metamorphic overprint, and commonly exhibits a spherulitic texture. The intermixed ignimbrite domains have a groundmass component of about 60% at their margins, and the margins are gradational.

The crystal-rich arenites are texturally immature to submature. They range from being well to poorly sorted. The horizons containing large ignimbrite intraclasts are poorly sorted due to the presence of these cobble- to boulder-sized clasts. The arenite matrix itself is relatively well-sorted. Sorting is also poor where the arenites are diffusely mixed with welded ignimbrite, due to the higher component of volcanic ash. Generally however, the arenites form a closed framework aggregate, and sorting is fairly good with an average grainsize of 0.2mm. Crystal fragments are angular to euhedral and generally show no effects of abrasion. Quartz and less commonly K-feldspar are sometimes embayed and have a rounded form which has a volcanic rather than sedimentary origin, and is attributable to magmatic resorption. Some lithic fragments (mainly plutonic grains or metasedimentary basement fragments) may have been rounded by sedimentary processes, but these grains were probably rounded in an earlier sedimentary event rather than during deposition of the thick massive sedimentation units.

### 5.1.4 Petrology

The crystal-rich arenites are composed of sand-sized (average grainsize ~ 0.2mm) crystals and crystal fragments of quartz, K-feldspar and albitised plagioclase, and various types of rock fragments. Vitriclasts are a minor component of the lithic population and shards are absent from the facies. Fig. 4.4 illustrates the types of crystals and lithic clasts which occur in the ignimbrites and fluvial sediments of the Gimbat Ignimbrite Member. The crystal-rich arenites contain the same crystal and lithic clast populations.

Volcanic quartz is the most common framework constituent and constitutes about 50% of the crystal population. The quartz is monocrystalline, occurs as angular crystal fragments or as euhedral crystals sometimes exhibiting resorption features such as embayments and rounded corners. It is free of inclusions and generally exhibits straight extinction, although undulose extinction is observed, occurring under greenschist facies metamorphism. Grainsize is up to 1mm. Quartz and feldspars occur at a ratio of roughly 2:1, with feldspar grains forming 25-30% of the crystal population. K-feldspar is the most common and occurs as well-formed euhedral crystals occasionally with rounded corners due to resorption, and as crystal fragments. Microperthites are common and may have a plutonic source or could be low-grade metamorphic unmixing of original volcanic potassium feldspar. Mild undulose extinction in some quartz grains may also be due to a low-grade metamorphic overprint. The rest of the K-feldspar is either sanidine or orthoclase, both of which can occur as a volcanic phenocryst phase. Some grains exhibit simple twinning. Some grains are albitised and overprinted by clay minerals, giving the grains a dusty appearance, or are overprinted by sericite  $\pm$  calcite. Rare microcline grains probably have a plutonic source. Grainsize is up to 2 mm. Plagioclase is positively identified only where lamellar twinning is present, so its quantity may be underestimated. Electron microprobe analysis of the untwinned feldspars suggests that



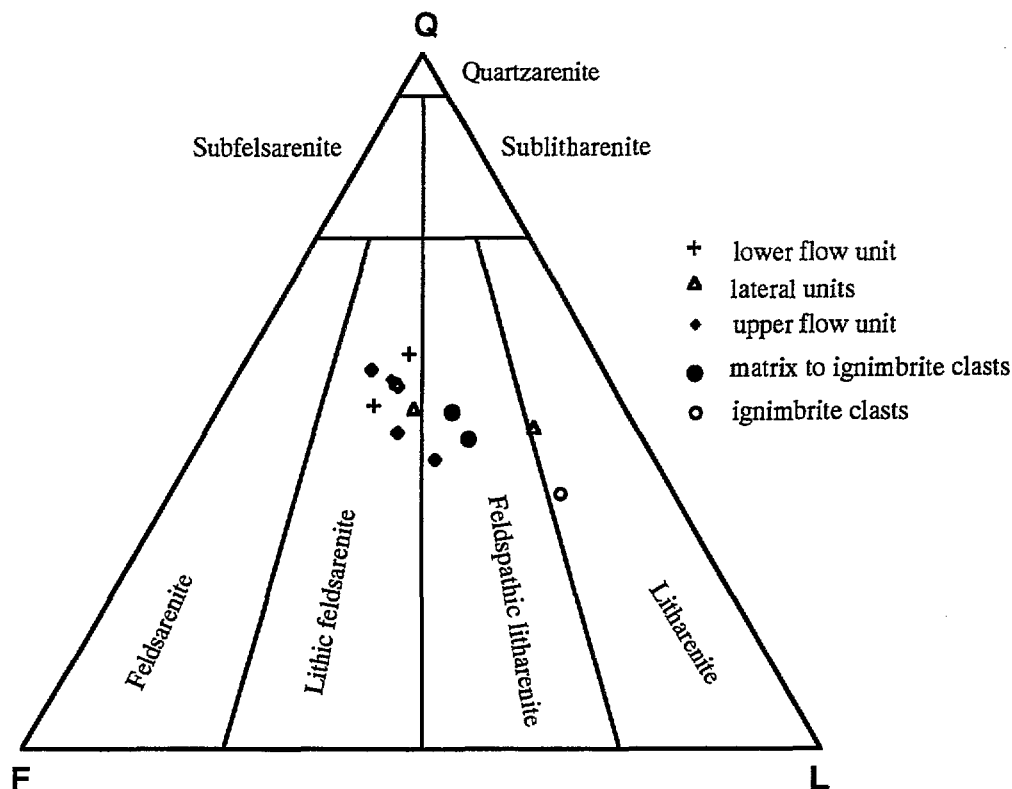


**Figure 5.3:** Classification of the massive crystal-rich arenite facies using modal analysis data (based on Folk, 1980).

plagioclase is a minor component of the crystal-rich facies. Plagioclase grains are smaller than the K-feldspars.

Zircon and opaques are minor components of the crystal population.

Lithic fragments consist predominantly of polycrystalline metamorphic basement fragments, plutonic quartz and granite fragments, dolerite and chert in order of abundance, with rare clastic sedimentary rock fragments and vitriclasts.

The metamorphic basement fragments are polycrystalline quartz aggregates, quartz-feldspar aggregates or quartz-( $\pm$ feldspar)-phyllosilicate aggregates with highly variable grain size, sutured grain boundaries and undulose extinction of individual crystals comprising the aggregates. They are probably phyllite, schist and gneissic fragments derived from the Burrell Creek Formation.

The composite quartz and quartz-feldspar aggregates of plutonic origin differ from the polycrystalline metamorphic fragments in that the internal grains are coarser and more even grained, with straight to mildly undulose extinction of individual crystals and an absence of sutured boundaries. The feldspar in these granite fragments is sometimes microcline or microperthite.

Dolerite fragments consist predominantly of albitised plagioclase laths with interstitial chlorite and opaques, and occasionally larger, tabular K-feldspar crystals. Dolerite clasts are sometimes deformed during compaction of the host arenite to form a pseudomatrix infilling the interstitial spaces between crystals, or breaks down to form plagioclase aggregates. The dolerite is probably of Zamu Dolerite generation, derived from the sills which form part of the basement to the Gimbat Ignimbrite Member and outcrop to the north and west of the succession.

Sedimentary rock fragments are extremely rare and consist of sandstone or finer-grained siltstone clasts. Rare vitriclasts occur locally and are most common in the arenites which are diffusely mixed with welded ignimbrites. The vitriclasts are sand-sized and lack phenocrysts. They are granophyric aggregates of quartz and feldspar with locally spherulitic textures, and are interpreted to be devitrified, aphyric volcanic rock fragments, or volcanic rock fragments consisting entirely of groundmass material. They may be derived from the underlying ignimbrites, from quartz-feldspar porphyries intruding these ignimbrites or from contemporaneous pyroclastic flows.

The crystal-rich arenites plot as lithic felsarenites or felsic litharenites on modal analysis plots (Folk, 1980; Fig. 5.3). They have a clastic assemblage consisting of volcanic quartz + K-feldspar (+ minor plagioclase) + lithics roughly occurring in the proportion of 2:1:1. That is, the crystal-rich arenites contain about 50% quartz, and 25% feldspar and lithics, although there are minor variations from sample to sample. Of the lithic component, metamorphic basement fragments and granitic grains are the most abundant. The welded ignimbrites which locally mix diffusely with the crystal-rich arenites or occur as clasts within the arenites, have the same mineral assemblage as the clastic population of the crystal-rich arenites, suggesting a genetic relationship exists between the two facies.

### 5.1.5 Mode of emplacement

The massive nature of the crystal-rich units and the absence of features indicating tractional current transport, indicates they were emplaced by mass-flows. The massive texture and lack of internal structures and well-developed size grading are diagnostic of deposition from high concentration, poorly-expanded mass flows (Middleton and Hampton, 1976; Lowe, 1982; c.f. Cas, 1979; 1983). The development of tractional features is inhibited by the high sediment concentration and rapid deposition rate, in such flows. These also limit particle freedom so that total size grading is not developed or is only poorly developed (Cas & Wright, 1987). Coarse-tail grading of only the heaviest or coarsest grains, as occurs in the lower unit of the palaeovalley, is a common feature of high concentration turbidity currents (Allen, 1970). The main grain-support mechanism was probably dispersive pressure involving grain interaction and collision, and fluid turbulence may have been a subordinate grain-support mechanism (e.g. Cas, 1979).

A thin (3 cm) planar-laminated, reverse graded layer occurs at the base of the lower flow unit in the palaeovalley. This layer may represent a boundary layer effect, developed due to intense shearing in the basal part of the flow. It is the equivalent to layer 2a deposits in subaerial ignimbrites (Sparks et al., 1973). Internal shearing may also produce diffuse layering, which occurs throughout the massive units (c.f. Cas 1979).

Bedforms are only found at the top of some massive units, where they are represented by horizontal laminae and are accompanied by normal grading into finer-grained crystal and ash sediment. These normal graded sediments are deposited from the more expanded and fluidised flow tops in which turbulent suspension is the main grain support mechanism, allowing freedom of particle movement so that particles can be sorted hydraulically.

The crystal-rich arenite facies rests on top of a significant unconformity which is erosional into subaerially deposited ignimbrites, and is overlain by a relatively deep water turbidite sequence so theoretically, the possible palaeoenvironmental settings could span through subaerial to deep water. However, similar very thick crystal-rich mass flow units have only previously been documented from a clearly established deep water turbidite succession. This is the Merriens Tuff of the Hill End Trough, which is overlain and underlain by thousands of metres of turbidite (Cas, 1979; 1983). The crystal-rich arenite facies is also totally dissimilar to any known subaerial ignimbrite facies. Therefore, because it passes conformably into a turbidite sequence, the interpreted environment of the crystal-rich facies is also deep-water. This would imply there was extremely rapid subsidence or inundation by water between the last phase of erosion associated with the unconformity, and deposition of the crystal-rich arenite facies.

### 5.1.6 Origin of the crystal-rich arenites

Massive crystal-rich deposits tens of metres thick such as those of the crystal-rich arenite facies, are generally interpreted to be the water-transformed equivalents of contemporaneous gas-supported pyroclastic flows, or to be redeposited from thick accumulations of pyroclastic debris (Cas, 1979, 1983). In either case, a penecontemporaneous eruption is required to produce the anomalously large volume of material required to source the thick massive deposits, as they represent mass flux rates which are orders of magnitude greater than those produced by normal surface processes, but consistent with those produced by pyroclastic flow-forming eruptions (Cas & Wright, 1991). In contrast, epiclastic or volcanoclastic turbidites in sedimentary terrains rarely exceed a thickness of several metres (Bouma, 1962; Bailes, 1980). The angularity of the crystals and the abundance of crystal fragments in the crystal-rich facies also suggest the initial mode of fragmentation was by pyroclastic eruption.

The pyroclastic debris in the crystal-rich arenites could have been generated from either a subaerial or subaqueous volcanic source. The stratigraphic position of the facies, at the transition between subaerially deposited volcanics and relatively deep-water basin sediments, suggests either a shallow water site, or a subaerial site, with passage of the pyroclastic flow into a subaqueous regime. If erupted subaqueously, the volcanic centre must have been placed at relatively shallow water depths, as studies by McBirney (1963) indicate that silicic magmas can only vesiculate enough for pyroclastic eruption to occur at depths of 1 km or less. Two lines of evidence suggest that the crystal-rich arenites have an original subaerial origin although their final deposition was subaqueous. The first is the compositional similarity of the pyroclastic debris to the underlying subaerial ignimbrites, suggesting the two facies are of similar origin. The second is compositional evidence of interaction with the underlying fluvial epiclastic deposits, suggesting the facies transgressed the subaerial/subaqueous interface during transportation.

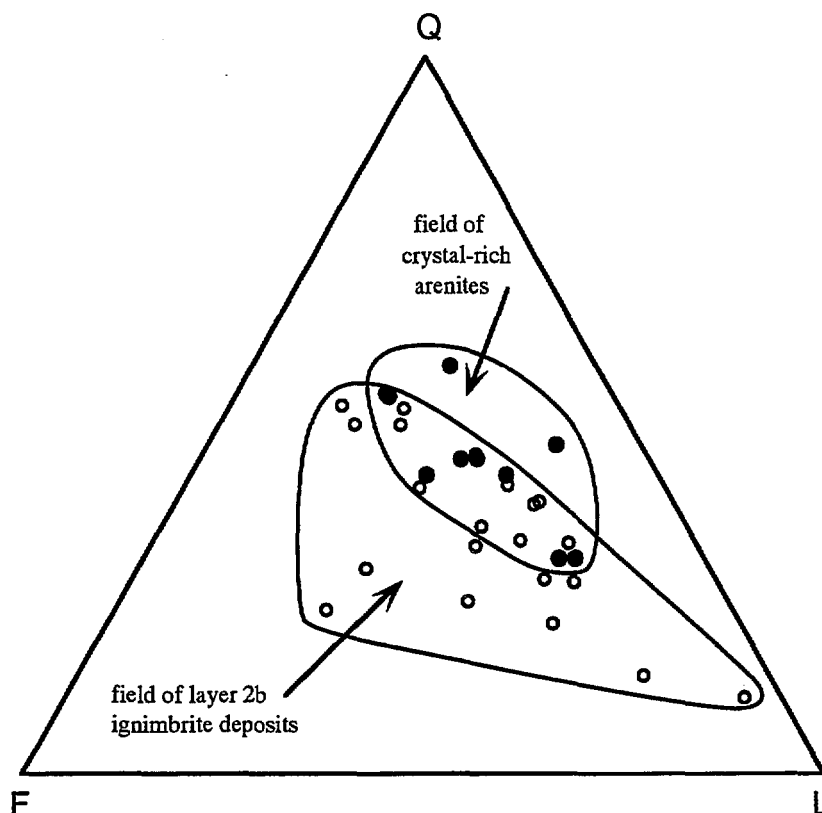


**Figure 5.4:** A comparison of modal analyses of the crystal-rich arenite facies with those of the Gimbat Ignimbrite Member, showing the relative enrichment of quartz in the crystal-rich arenites.

● = crystal - rich arenites    ○ = welded and non-welded ignimbrites

The major mineral and lithic types described in the crystal-rich arenites also occur as phenocrysts and lithics in the underlying subaerial ignimbrites and the irregular ignimbrite clasts contained within the crystal-rich facies. The relative proportion of each mineral and lithic component is similar for each facies so that their fields overlap on a Q-F-L plot (Fig. 5.4). The same lithotypes comprise the lithic population in both facies. The common assemblage in both facies suggests that the crystal-rich arenites were derived from a similar source to the ignimbrites.

There are minor differences in the mineral and lithic assemblages of the two facies. The ignimbrites and ignimbrite clasts contain more dolerite fragments in the lithic assemblage than the crystal-rich arenites (Fig. 5.5). The crystal-rich arenites are slightly richer in quartz (Fig. 5.4). There are several possible explanations for these anomalies:

(1) The eruption that produced the crystal-rich arenites contained a lower percentage of dolerite and a higher percentage of quartz than the other subaerial ignimbrites. This is a possibility because the subaerial ignimbrites show a progressive depletion in dolerite towards the top of the succession. However, the ignimbrite intraclasts within the crystal-rich facies,

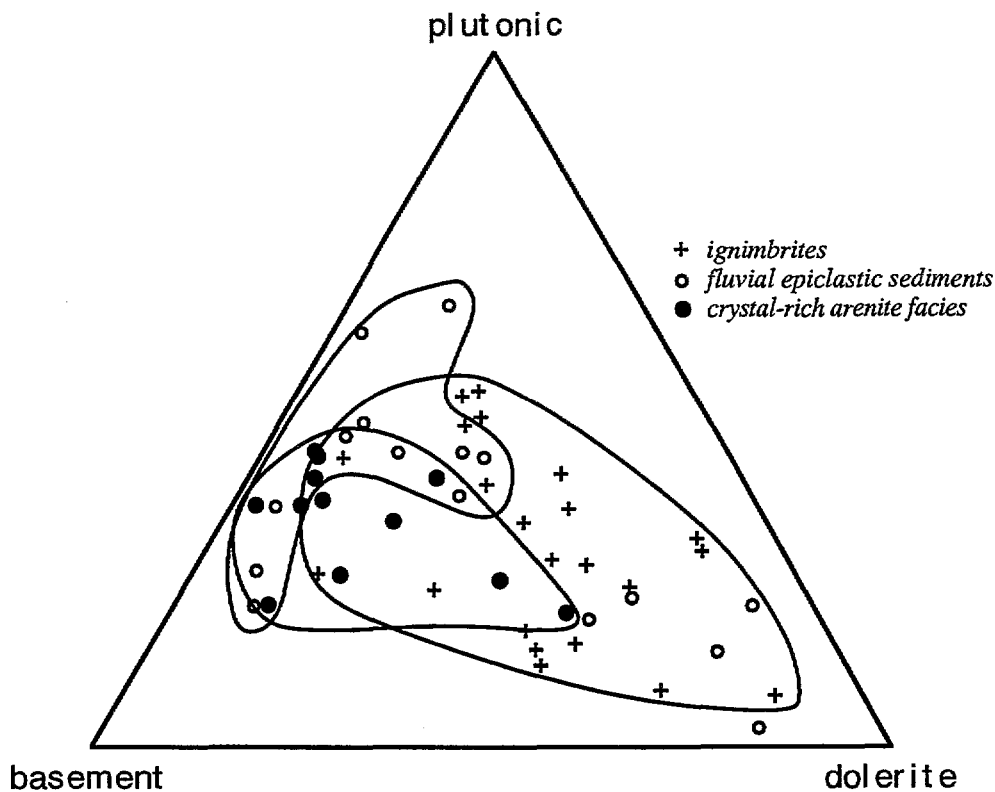


**Figure 5.5:** Modal analysis data for ignimbrites and fluvial epiclastic sediments of the Gimbat Ignimbrite Member, and crystal-rich arenites of the Big Sunday Formation, comparing the composition of the dominant lithic components in the three facies.

which are probably relicts of the original subaerial pyroclastic flow also have a high percentage of dolerite relative to the host arenites.

(2) The lower dolerite count in the crystal-rich arenites could in part be a statistical aberration caused by the problem of point counting inhomogeneous grainsize populations, as occur in the ignimbrites. The lithic fragments are slightly coarser-grained than the crystals and this is particularly the case for the dolerite clasts, which can be 3-4 times larger than the average grainsize of the crystals. These large grains may be over-counted, biasing the statistical analysis in their favour. In contrast, the arenites are more even grained and dolerite clasts have the same grainsize as the crystals and other lithics. However, this statistical problem would only have a minor effect on the modal analyses, and further explanation is required to explain the relative depletion of dolerite in the crystal-rich facies. Visual estimates indicate that the proportion of dolerite grains is indeed lower in the crystal-rich facies, so that certain processes must have acted to remove part of the dolerite component, or to dilute it relative to the other lithic components.

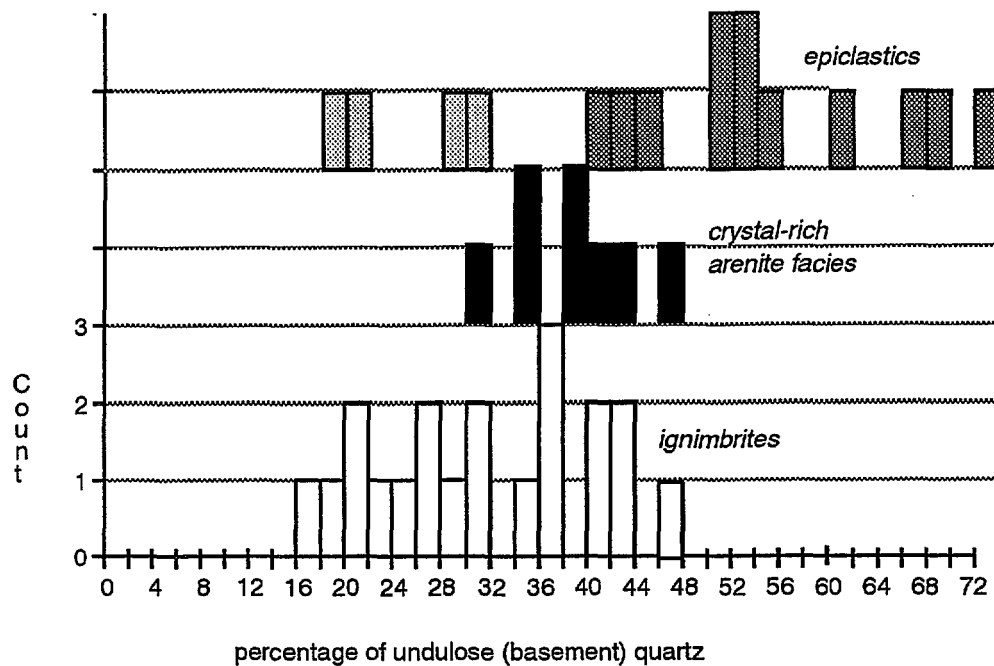


**Figure 5.6:** Histogram showing the percentage of basement-derived quartz (strong undulose extinction, some degree of rounding) for each facies. Note that the crystal-rich arenite values lie between those of the ignimbrites and epiclastics, suggesting detritus was derived from both these facies. Note also the range of values for epiclastic units. Some are small lenses derived entirely from erosion of contemporaneous pyroclastic debris (stipple) whereas the quartz-rich units typical of the facies indicate a mixed basement-pyroclastic source (grey). Also note that some ignimbrites have a high proportion of basement-derived quartz. These are lithic concentration zones; ground layers or units with a high proportion of metasedimentary basement clasts in hand specimen.

(3) It is possible that dolerite was removed from the clastic population by hydraulic sorting processes operating in the sediment mass-flows. The presence of coarse-tail grading in the lower flow unit of the palaeovalley indicates that hydraulic sorting of the more dense, coarser-grained fraction did occur. Although this explains the depletion of dolerite clasts, it does not explain the relative enrichment of quartz in the crystal-rich arenites. The quartz and feldspar crystals and quartz-feldspar bearing lithics have similar densities and would not be segregated during hydraulic sorting.

(4) The fourth possibility is that the subaqueous deposits were contaminated by a sedimentary source of lithics and crystals. A possible source of contamination is the fluvial epiclastic sediments which underlie much of the crystal-rich facies (Fig. 1.3). These epiclastic sediments erode into the underlying non-welded ignimbrite (Fig. 1.3). Their stratigraphic position suggests they were deposited at the shoreline of the basin in which the crystal-rich arenites were deposited. In hand specimen, these units are described as quartz-rich sediments. Modal analyses indicate that many of the fluvial units have a mixed source of contemporaneous pyroclastic detritus, and basement metasediments and that granitic quartz, polycrystalline basement clasts and chert dominate over dolerite grains in the lithic population (Fig. 5.5). Contamination from this source would have the effect of diluting the original dolerite component of the facies. In addition, the fluvial epiclastic sediments are quartz-rich, containing

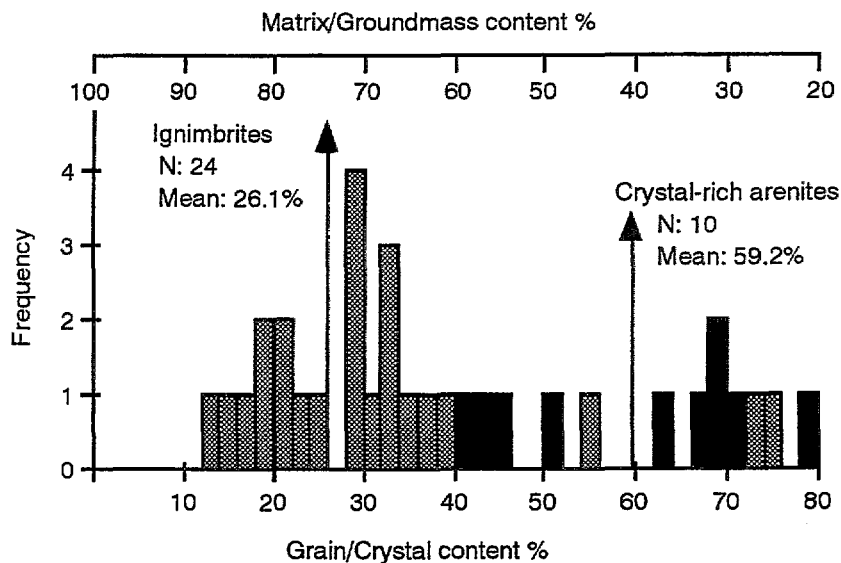


**Figure 5.7:** Comparison of the grain and matrix proportions of the crystal-rich arenites with the phenocryst and groundmass proportions of the ignimbrites.

volcanic quartz grains exhibiting clear extinction, derived from erosion of the surrounding ignimbrites and quartz-grains exhibiting mild to highly undulose extinction with abundant fluid inclusions, derived from volcanic or sedimentary units from the basement provenance. Fig. 5.6 shows that the crystal-rich arenites have more undulose quartz grains than the subaerial ignimbrites, and the source of these grains is likely to be the fluvial epiclastic sediments.

Small, diffusely bound lenses of quartz-rich coarse to pebbly sandstones occur within the crystal-rich arenite succession. The lenses are compositionally equivalent to the fluvial epiclastic sediments underlying much of the crystal-rich facies and their presence supports other compositional evidence that the crystal-rich facies transgressed the shoreline during transportation. These lenses are interpreted to be pieces of shoreline that were ripped up by the erosive flow head and incorporated into the flow as it passed over the shoreline sediments.

#### *Crystal-enrichment processes*

A diagnostic feature of the crystal-rich arenites is that they are depleted in the fines fraction (ash-sized particles) relative to the subaerial ignimbrites, which they are compositionally similar to them (Fig. 5.7). If both facies originated from subaerially erupted pyroclastic flows, this crystal-enrichment must reflect secondary processes which occurred during transportation and final emplacement of the crystal-rich facies, but did not affect the land-deposited ignimbrites. The relative crystal-enrichment of the facies is unlikely to be a primary feature, because only certain subfacies within the ignimbrites such as the ground layers show a comparable depletion in fines to form crystal- and lithic-rich grain aggregates, and these are only a few metres in thickness. Explosive eruption of highly crystallised primary magmas is extremely rare. A study of Cainozoic silicic volcanics (Ewart, 1979) showed that the majority of samples have phenocryst concentrations of less than 40% (Fig. 5.8). Furthermore, if the ignimbrite clasts contained within the facies are remnants of the original gas-supported pyroclastic flow they provide some indication of the original phenocryst concentration in the erupting magma. Both the ignimbrite clasts and the subaerial ignimbrites have low phenocryst

concentrations, ranging between 12 and 40%, compared with the crystal-rich arenites, which have crystal contents between 40 and 80%.

Two possible origins exist for the crystal-enriched mass-flow arenites. Original pyroclastic flow deposits could have been reworked and redeposited by post-eruptive epiclastic processes which separated the ash component from the crystal and lithic fractions. Alternately the facies may represent the contemporaneous transformation of a hot gas-supported pyroclastic flow into a water-supported mass flow upon mixing with an ambient body of water.

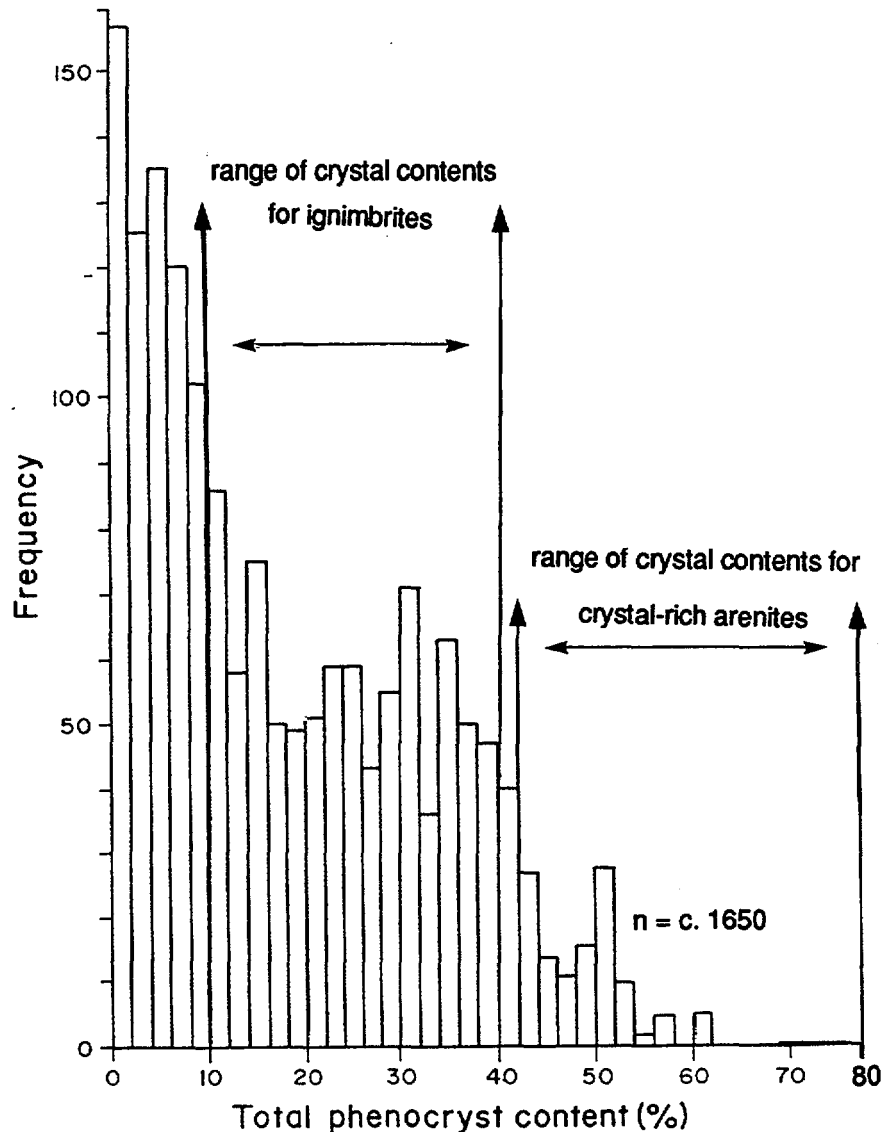


**FIGURE 5.8:** Total crystal contents for some Cainozoic volcanic rocks from the circum-Pacific region (plotted from the data in Ewart, 1979), compared with the crystal contents in the ignimbrites and crystal-rich arenite facies (after Cas, 1983).

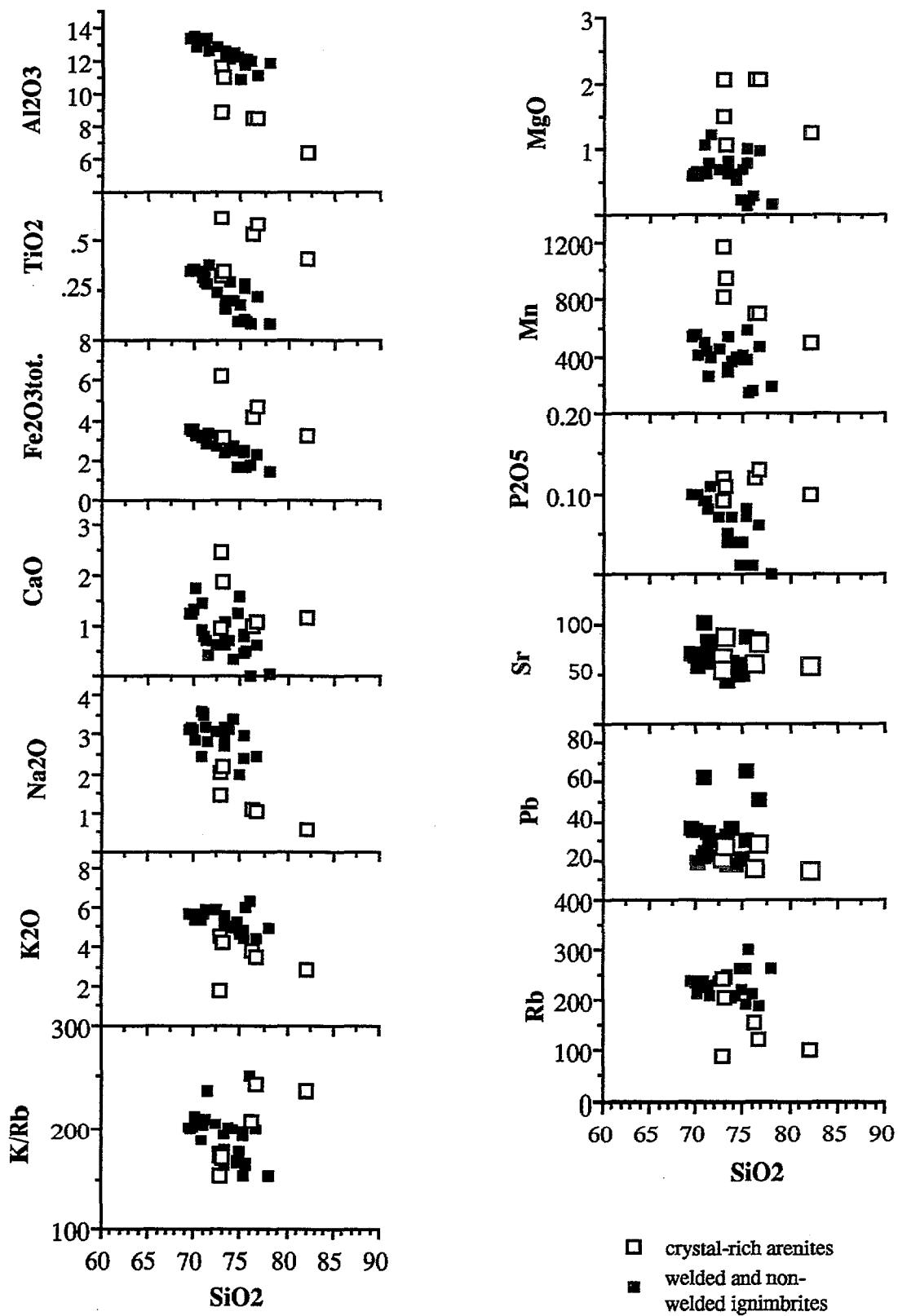


**Figure 5.9:** Geochemical Trends in ignimbrites of the Gimbat Ignimbrite Member, and the overlying crystal-rich arenites of the Big Sunday Formation.

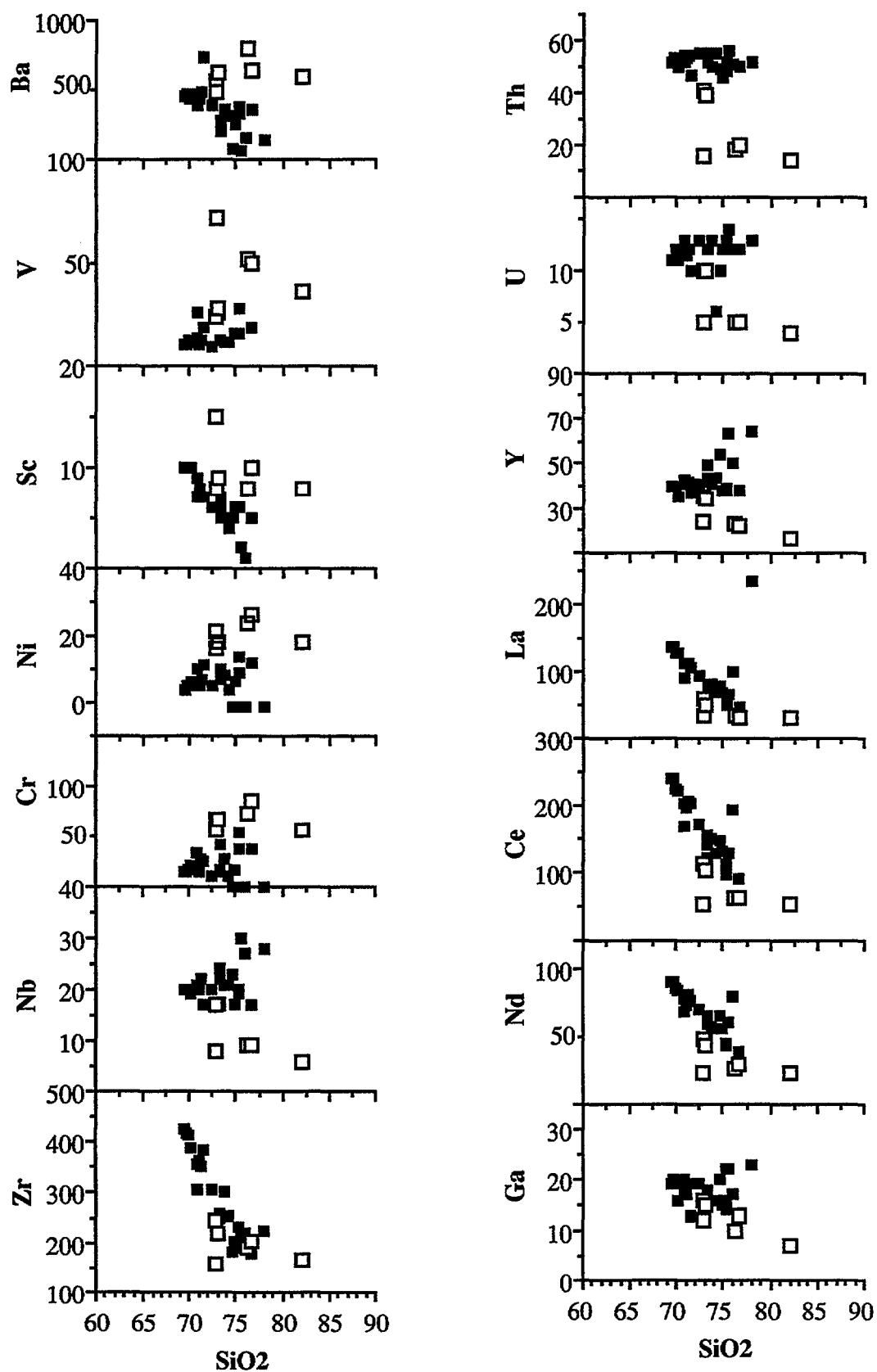


Figure 5.9 continued

*Epiclastic reworking*

Epiclastic reworking of previously deposited pyroclastic debris could mechanically sort and separate the glassy ash from the crystal and lithic fractions. In this case, the mineral grains and crystal fragments are mainly angular and unabraded and there is an absence of tractional features, which does not support a reworked origin for the facies. The feldspars are mainly fresh to slightly cloudy. Analysis of the clay component of the crystal-rich units by X-ray diffractometry showed it to be comprised of chlorite+sericite+calcite (Appendix D), all representing metamorphic alteration of feldspar phenocrysts and feldspars in the matrix. Only one sample contained possible smectite. This indicates that the feldspars had not significantly broken down to clay minerals in the time between eruption and final deposition, suggesting minimal exposure of the pyroclastic debris to surface weathering processes. This is also suggested by the fact that the matrix of the crystal-rich arenites is siliceous and therefore likely to have originally been composed of volcanic ash. If the matrix was originally clay-rich, it would have been altered to sericite during metamorphic alteration.

A short time factor between eruption and emplacement, without intervening exposure to surface processes is also supported by geochemical evidence. Wyborn & Chappell (1983) studied the changes in the chemical composition of Ordovician and Silurian greywackes of the Snowy Mountains region (southeastern Australia) as they progressed through two cycles of chemical weathering, erosion and deposition. With each sedimentary cycle, the amount of feldspar is progressively diminished and the sedimentary rocks trend towards a pure quartz-clay end-member. Geochemically, Ca, Na, Sr and Pb were lost as feldspars were converted to clay minerals because these elements are not admitted into or captured by the lattice structure of the clays. Therefore if volcanoclastic detritus is weathered and reworked, it will be depleted in these elements relative to the source rocks. In contrast the crystal-rich arenites show no sign of depletion in Pb and are enriched in CaO and Sr relative to the subaerial ignimbrites (Fig. 5.9). They do show strong Na<sub>2</sub>O depletion, but this can be explained in terms of ash loss.

Only minor compositional differences occur between the ignimbrites and the crystal-rich arenites. Both have the same bulk composition. The differences can be explained by removal of the vitric fines fraction from the crystal-rich units during deposition. If there has been preferential loss of vitric material from the original subaerial pyroclastic flow, the resulting facies will have a composition enriched in those chemical elements contained in higher proportion by the crystals, and depleted in those contained in higher proportion in the glass (Walker, 1972). In effect the chemical composition will be less evolved than that of the original pyroclastic flow deposits, because removing the glass fraction is analogous to removing the more evolved or fractionated melt component of the original magma. The crystal-rich arenites have a less fractionated trace element pattern than the ignimbrites (Fig. 5.10). They have a lower proportion of K<sub>2</sub>O, Rb, Na<sub>2</sub>O, Zr and LIL elements (REE, U, Th, Nb, Pb). These elements become more enriched in the more fractionated or evolved melt component during crystallisation of a magma. CaO, Sr and Ba will be depleted in the melt component of the magma and will be subsequently enriched in the crystal concentrates, as observed for the crystal-rich arenites (Fig. 5.9). The same holds for MgO, Ni, V, Mn, Sc and Cr, as their concentration in the melt will decrease as crystals form. Increased CaO and P<sub>2</sub>O<sub>5</sub> contents could also be partly explained by the presence of secondary calcite in the matrix of the epiclastic deposits.

The geochemical data suggest that the crystal-rich arenites were not significantly reworked during deposition. Mechanical sorting during deposition or contamination with material from other provenances is not required to explain compositional differences between the ignimbrites and the crystal-rich arenites. Geochemical trends can be explained by loss of vitric material from the original ignimbrite during final deposition.

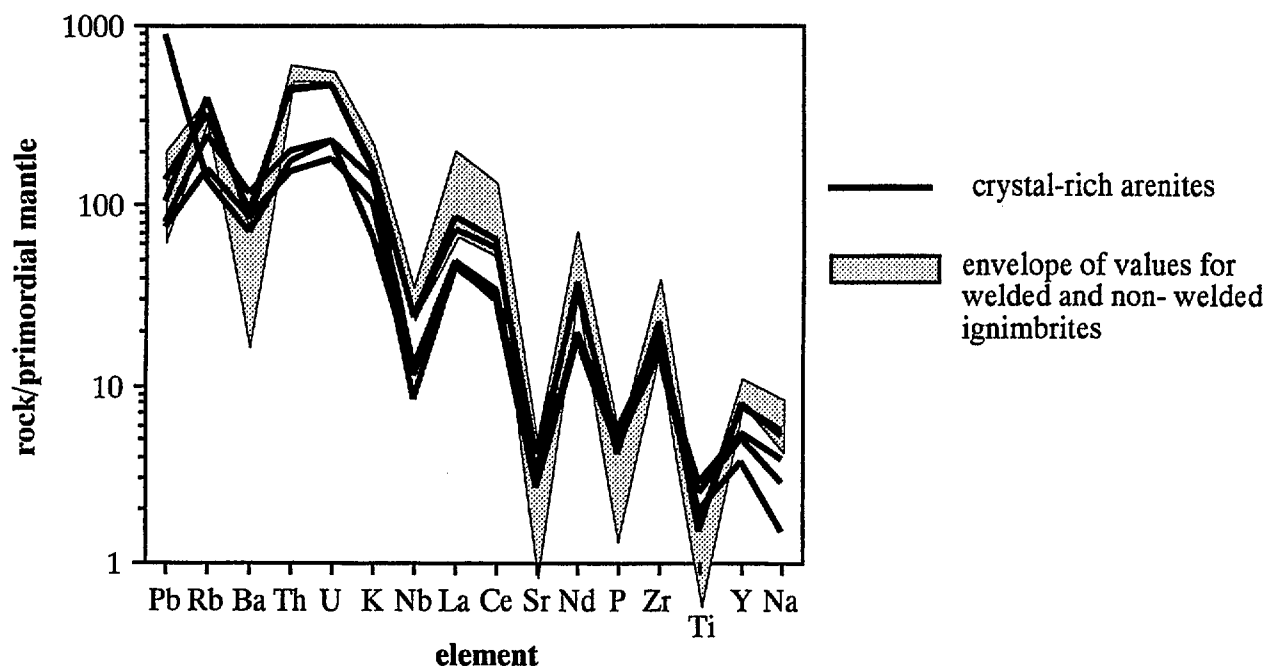


**Figure 5.10:** Extended trace element diagram comparing trace element patterns of the subaerially deposited ignimbrites with the crystal-rich arenite facies. The crystal-rich arenites have a less fractionated pattern, as would be expected with removal of the ash fraction of an ignimbrite.

#### *Volcanic enrichment processes*

All evidence discussed so far is consistent with the crystal-rich arenites originating from subaerial pyroclastic flows entering an ambient body of water. The crystal-rich nature of the deposits suggests that upon reaching the shoreline, the pyroclastic flows did not maintain their integrity, due to interaction with water.

As the vigorous, turbulent flow front comes into contact with cold water, violent phreatic explosions would probably be triggered from the steam generated and trapped beneath the flow. Some authors invoke the Liedenfrost effect to propose models for non-disruptive entry of ash flows into the sea (eg Howells et al 1985), which involves the development of a steam carapace around the advancing flow front, which insulates the pyroclastic flow from interaction with the ambient water. Although this may be effective for effusive, viscous lavas with smooth, non-turbulent boundaries, it is unlikely to prevent mixing of water into a vigorously advancing turbulent flow front. Orton (1988; 1989) proposes that even Welsh Ordovician flows which survived the transition into water relatively intact, experienced some disintegration upon encountering seawater, generating fine-grained phreatomagmatic ash. Thus the occurrence of phreatic explosions at the shoreline is a highly likely outcome of the passage of a hot subaerial pyroclastic flow into water. These secondary eruptions could produce rootless vents at the

shoreline (eg Rotoehu Ash, Walker, 1979; Wright & Coward, 1977) and the fine ash fraction would be removed from the crystal fraction in the secondary eruption columns. Phreatic explosions would also break down the larger pumice clasts, generating fine-grained phreatic ash which would also be carried away in the eruption columns (eg Wright & Mutti, 1981), explaining the absence of pumice clasts in the crystal-rich arenites. In addition, the delicate bubble walls of hot pumice could quench and shatter on contact with external waters.

The second outcome of a hot subaerial pyroclastic flow entering a subaqueous setting is that water would be ingested into the flow front, being driven into the flow by the substantial fluid pressure gradient existing between the gas-particulate system and the denser body of water. As the water mixes with the flow the gas particles comprising the interstitial medium would rapidly cool and collapse and the mechanics of the flow would transform in transit into a cool water-supported debris flow system, with derivative turbidity currents developing in the more expanded flow top. Further removal of ash probably occurred as the pyroclastic debris slumped from the shoreline and was transported to its final setting by the cold state, water-supported mass flows.

### *Contemporaneous flow transformation or post-eruptive slumping?*

Deciding whether thick accumulations of pyroclastic debris represent primary eruptive products or secondary remobilised and redeposited volcanoclastic material presents a problem (Wright & Mutti 1981), especially in ancient volcanic sequences where the pyroclastic debris cannot be correlated with land-based studies. For many examples in the literature, in the absence of evidence for a hot state of emplacement or for primary pyroclastic transport processes (eg Merrions Tuff, Cas 1979, 1983; Dali Ash, Wright & Mutti 1981; Roseau Ash, Carey & Sigurdsson 1980; Sheefrey Tuffs, Stanton 1960), either depositional origin must be considered a possibility. The two scenarios are illustrated in Fig. 5.11 (after Cas & Wright, 1991).

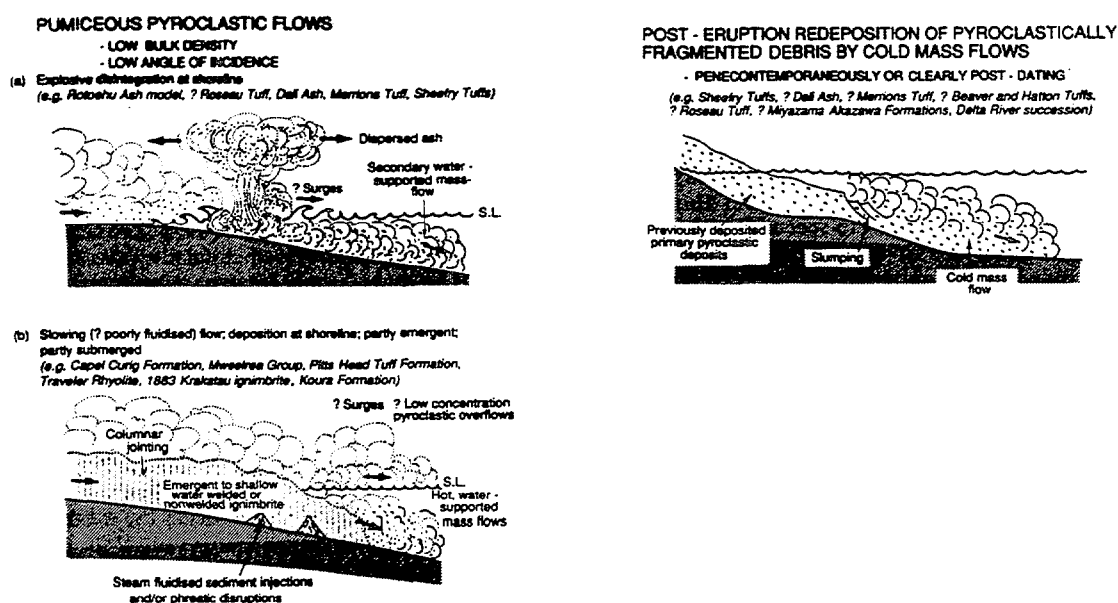


**Figure 5.11:** Various scenarios and outcomes predicted for when a hot subaerial pyroclastic flow transgresses the shoreline and interacts with a cold body of water (from Cas & Wright, 1991).

The model of pyroclastic flows entering water, disintegrating and transforming in transit into water-supported mass-flows is strongly supported by the irregular-shaped ignimbrite clasts and the diffusely bounded pods of ignimbrite which occur randomly throughout the crystal-rich facies. They are interpreted to be relicts of the original pyroclastic flow mass, which survived where ash-winnowing processes were less effective, and their preserved highly irregular shapes argues against post-eruptive reworking of the pyroclastic debris. The alignment of pumice clasts in the diffusely bound pods of ignimbrite may be a eutaxitic texture caused by compaction and welding in the original pyroclastic flow, or it could be a pseudo-eutaxitic texture produced by the alignment of pumice during transport and deposition. Modal analyses of samples taken at the margin between the ignimbrite pods and the crystal-rich facies show that their contact is gradational and at the margins at least, the ignimbrites show some enrichment of crystals relative to the original flow (represented by the irregular ignimbrite clasts, and the subaerial ignimbrites), but not as much crystal-enrichment as the adjacent arenites. This may be representative of the entire facies, or just the margins of the facies, with the centre of the pods being unwinnowed, welded ignimbrites. In either case, the diffusely bounded ignimbrite pods are interpreted to represent patches of the original pyroclastic flow in which removal of ash was less effective than for the remainder of the crystal-rich facies.

### 5.1.7 Discussion

To date, relatively few papers have documented subaqueous pyroclastic flows and their deposits. This is partly because the physical parameters controlling the behaviour of pyroclastic flows upon passage into water and the nature of the resultant deposits are poorly understood. Some authors suggest that pyroclastic flows can maintain their integrity and continue to flow underwater as hot gas-supported pyroclastic flows (eg Sparks et al 1980a,b). Others suggest they will mix with water to generate water-particulate debris flows or with extensive dilution, turbidity currents (eg Carey & Sigurdsson 1980; Wright & Mutti 1981). This section will consider the physical properties of the original subaerial pyroclastic flows at the point where they reached the shoreline, and how these may have affected their behaviour upon passage into water.

The preservation of welding textures in the irregular-shaped ignimbrite intraclasts that occur within the crystal-rich arenite facies, has important implications for the state of the original subaerial pyroclastic flows as they entered the sea. Welding in the clasts, which are believed to be relicts of the original subaerial pyroclastic flow mass, implies that primary welding occurred within the flow while it was still in motion.

Welding occurs when softened, 'sticky' glass fragments within a pyroclastic flow begin to adhere together. Usually it is a secondary, post-depositional feature induced by the increased lithostatic load and the time factor involved during compaction of thick ignimbrite deposits, which act to raise the temperature above the softening point of glass. Also, it is usually only after deflation of the flow that sufficient glass particles are brought close enough, long enough to sinter or weld (Fisher 1989). However, primary welding is plausible if the temperature of emplacement of the pyroclastic flow is above the softening point of glass at minimum load pressure (Chapin and Lowell 1979).

It is envisaged that as the subaerial pyroclastic flow reached the basin shoreline a small plug of sintering or welded tuff had formed somewhere within the flow. Within this plug, the ash flow would have lost its particulate character. The collapse and deformation of the agglutinating shards would result in the elimination of pore space (Smith 1960) and a viscous fluid with a rheology

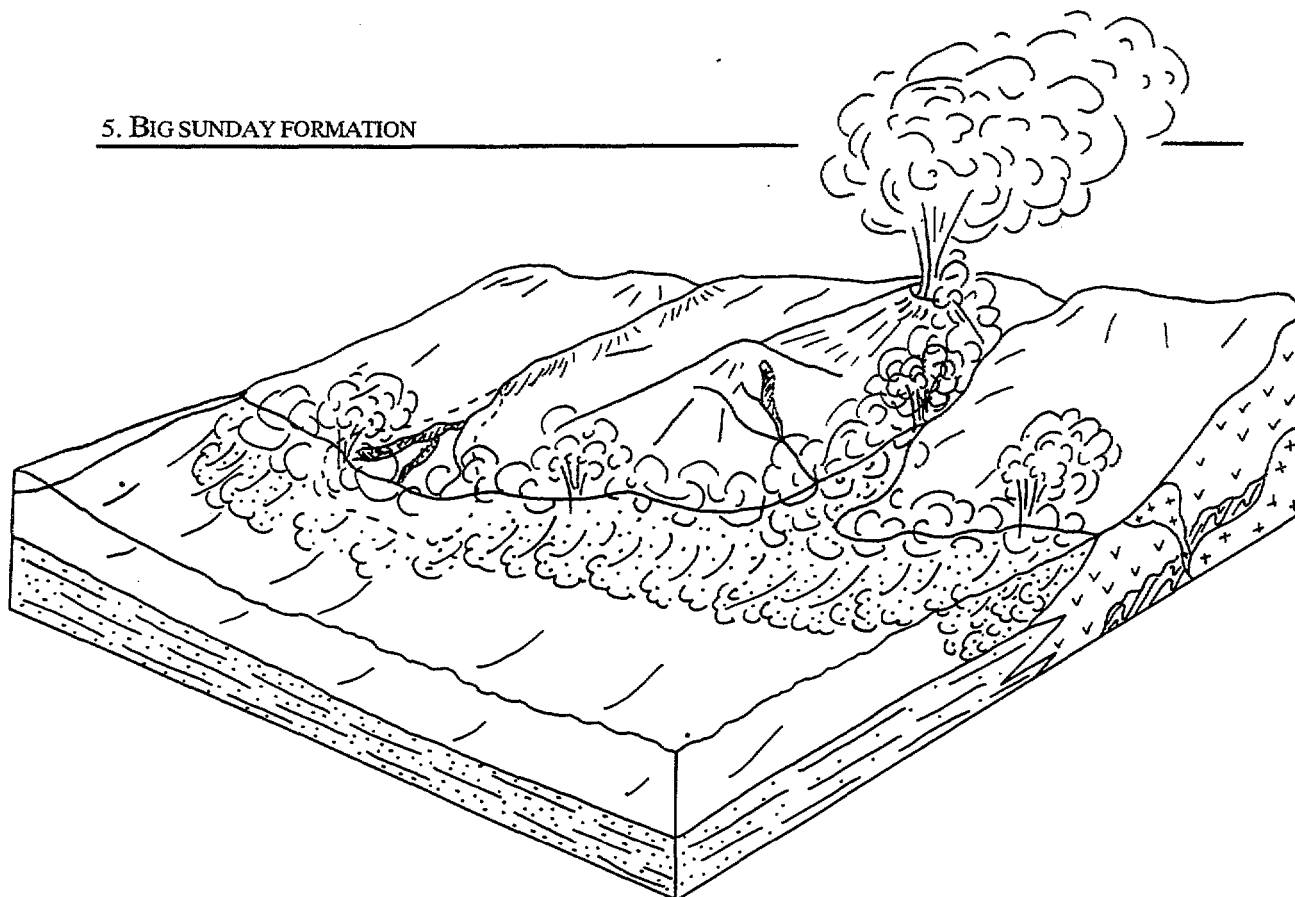


**Figure 5.12:** Schematic block diagram showing eruption and deposition of the crystal-rich arenite facies.

similar to rhyolite lavas would form (eg Schmincke & Swanson 1967). Upon entry into water, the viscous plug would fracture into a series of lithic blocks which would then be incorporated into the water-supported mass flow as intraclasts. Orton (1988) envisaged a similar origin for rotated welded tuff fragments within welded Pitts Head Tuff in Wales. In this case the clasts are blocky and exhibit some degree of rounding thought to be caused by abrasion during final transport and volatile streaming after deposition. This suggests that the welded tuff was essentially solid and underwent brittle fracturing, due to shock waves and steam generated upon entering the Ordovician sea. In contrast, the irregular, wispy shape of the clasts in the crystal-rich arenites of the Big Sunday Formation suggests the rheology of the agglutinated plug was more like that of a viscous fluid than a solid. An analogy would be breaking apart a mass of soft toffee, which is suggestive of a more ductile fracturing behaviour. Another comparison would be semi-solidified mudstone rip-up intraclasts in an intraformational conglomerate.

The significance of primary welding in the original pyroclastic flows is that it implies they were beginning to slow down and 'freeze' thermally as they reached the shoreline, and must have been deflated and poorly fluidised in these final stages of motion.

The crystal-rich facies forms a laterally extensive horizon beneath tuffaceous turbidite sandstones and siltstones, but outside of the palaeovalley area, the crystal-rich arenites do not contain the distinctive relict ignimbrite textures. This suggests that the pyroclastic flows may have been channelled by the palaeovalley and then spread along the shoreline of the basin (Fig. 5.12). Ash winnowing processes may have been more effective along the shoreline where the pyroclastic flow could spread out, exposing a greater surface area to water and thus allowing more efficient interaction with water.

Based on an assessment of the literature on subaqueous pyroclastic flows, Cas & Wright (1991) concluded that when pyroclastic flows enter water they generally undergo explosive disintegration at the shoreline and/or ingest water and transform into water-supported mass flows. They further suggest that for a pyroclastic flow to transgress the shoreline intact, it must be slowing down so that it is deflated and poorly fluidised and virtually depositing its debris as it reaches the shoreline. This indeed appears to be the case for those pyroclastic flows which survive the passage into an aqueous setting relatively intact (eg Ordovician, Wales: Francis & Howells 1973; Howells et al. 1979; Reedman et al 1987; Howells et al 1985; Wright & Coward 1977; Orton 1988; Ordovician, Ireland: Stanton 1960; Dewey 1963; Pudsey 1984; Miocene, Japan: Kano 1990). Even under these conditions phreatic explosions may occur at the shoreline, and evidence suggests that these flows do interact partially with water. They show evidence of disintegration at their distal margins suggesting continuous ingestion of water along flow bases and flow fronts (Orton 1988) and the flow tops are commonly normally graded, fine-grained ashy material (Francis & Howells 1973; Howells et al 1979; Reedman et al 1987; Kano 1990; Cole & DeCelles 1991).

In the case of the crystal-rich arenites, the physical properties of the original subaerial pyroclastic flows appear to be similar to the Welsh Ordovician flows (Garth Tuff; Pitts Head Tuff; Orton 1988), and meet the postulated criteria under which flows may maintain their integrity in the subaqueous environment. In contrast however, these flows disintegrated at the shoreline. The implications are that even poorly-fluidised, relatively dense, slow-moving flows can lose their distinctive character upon entering an ambient body of water, and that other external factors must also determine the ability of a pyroclastic flow to maintain its integrity under water. These other factors may include the angle of entry of the flow into water, the slope of the basin margin, and the eruption rate and volume of the flow, all of which will determine the water depth relative to ignimbrite thickness.

In the cases documented where pyroclastic flows survived the transition into water relatively intact, and maintained sufficient heat to weld, shallow water depths or even significant emergence above water level are inferred and were insufficient to prevent welding. These ignimbrites either blanketed the shelf so that water depths became insignificant, or displaced the water mass causing instant regression of the sea. The deflated thickness of some flow units exceed the water depth so that the shallow marine ignimbrites were partly emergent. In the Koura Formation, Japan, the subaerial pyroclastic flow is considered to have flowed into the shallow water zone and displaced water. Its base clearly rests on water saturated sediment, but most of the facies displays features characteristic of subaerial ignimbrites (Kano 1990). Late Ordovician pyroclastic flows of the Mweelrea Group, Ireland were partly emergent (Stanton 1960; Pudsey 1984), and have deep canyons explained in terms of subaerial erosion into the emergent tops. Water depths were no more than several metres when the ignimbrites were deposited (Pudsey 1984). Shallow marine depositional environments with inferred water depths of < 30m are proposed for the Garth Tuff, Capel Curig Volcanic Formation (Pickerell & Brenchley 1979; Brenchley & Pickerell 1980) and the Pitts Head Tuff Formation (Reedman et al 1987; Cas & Wright 1987) in Wales, and Orton (1989) maintains that the subaqueous correlatives rarely maintain sufficient heat to weld in water depths greater than deflated flow thickness. Both pyroclastic flows disintegrated shortly after traversing the land-water interface.

In each of these situations, the water depth was less than or comparable with deflated flow thickness. In the Welsh examples, the flows survived the transition into the subaqueous environment then rapidly disintegrated as they continued into deeper water (Orton 1989). It appears that water depth relative to deflated flow thickness is a significant factor in determining whether a pyroclastic flow will maintain its integrity upon entering the sea. Perhaps the differences in the resultant subaqueous deposits of the Big Sunday Formation can be attributed to this factor, as the physical parameters of the flow itself appear to be similar to those of

Ordovician flows which survived the transition relatively intact. It is possible that steeper basin slopes and relatively thin pyroclastic flows promoted rapid disintegration of the ignimbrites upon encountering the basin waters.

### 5.1.8 Conclusions

Thick, massive deposits of juvenile pyroclastic debris outcrop between ignimbrites and fluvial epiclastic sediments of the Gimbat Ignimbrite Member and subaqueous tuffaceous sandstone and siltstone turbidites of the Big Sunday Formation. They mark the transition between a dominantly subaerial and subaqueous environment of deposition and are interpreted to be subaqueous pyroclastic debris flow deposits.

Petrographic evidence suggests the facies was derived from pyroclastic flows of subaerial origin which flowed into the basin in which the Big Sunday Formation sediments were deposited. Fluvial and/or shoreline sediments deposited at the shoreline of the basin were incorporated into the flows through mixing processes. At the shoreline vigorous mixing of the hot pyroclastic flows with cold water modified the original flow dynamics considerably, to generate fine-grained phreatic ash and subaqueous debris flows. The fine ash fraction, including fine ash generated by the breakdown of the larger pumice clasts by phreatic explosions, would have been removed in the secondary eruption columns of rootless vents formed at the shoreline (Wright & Coward 1977; Walker 1979).

As water was ingested into the gas-particulate flow system, the flows transformed in transit into water-supported mass flows. Final deposition was by high concentration subaqueous debris flows in which dispersive pressure from grain interaction and collision was the dominant grain-support mechanism and by derivative turbidity currents in the more expanded flow tops.

Relict ignimbrite textures are preserved at several horizons where the crystal-rich facies forms a thicker accumulation, suggesting a palaeovalley infill. Outside of the palaeovalley area, the crystal-rich arenites do not contain the distinctive relict ignimbrite textures. This suggests that ash-winnowing processes may have been more effective where the pyroclastic flows spread out along the shoreline of the basin, exposing more surface area of the pyroclastic flow to cold water and allowing more efficient interaction with water.

Welding textures are observed in the ignimbrite clasts which are believed to represent unaltered intraclasts of the original pyroclastic flow. This suggests the original subaerial pyroclastic flows had begun to weld or agglutinate as they approached the basin shoreline. A viscous plug of semi-solidified welded ignimbrite is believed to have formed in the pyroclastic flow, which fragmented in a ductile manner when the pyroclastic flows entered the water. The irregular-shaped fragments were then incorporated into the final water-supported mass flow as intraclasts.

The flows must have been poorly-fluidised, relatively dense and slow-moving at this stage. Although some pyroclastic flows have survived the passage into water intact under these conditions (eg Capel Curig Volcanic Formation, Pitts Head Tuff, Mweelrea Group, Koura Formation) in this case the subaerial pyroclastic flows lost their distinctive character on entry into the ambient body of water. Other factors such as angle of entry of the flow into water, the eruption rate and volume of the flow must also influence the ability of a pyroclastic flow to maintain its integrity under water. It is postulated that water depth relative to the deflated ignimbrite thickness is a significant factor in determining the behaviour of a pyroclastic flow when it enters the sea, and may be the factor that promoted disintegration of the Gimbat Formation ignimbrites under these circumstances.

### 5.2 TUFFACEOUS SEDIMENTS

A sequence of subaqueously deposited, tuffaceous sedimentary rocks ~ 140 m thick conformably overlies the Crystal-rich Arenite Facies (Fig. 1.3). The main facies of this sedimentary sequence are tuffaceous siltstones and fine to coarse grained, massive to planar and cross laminated greywacke and sandstone.

#### 5.2.1 Tuffaceous Siltstone Facies

The basal 40 m of the section is characterised by thinly bedded planar and cross laminated tuffaceous siltstones (Figs 5.13a:b:c:d), with some thicker massive layers (2-3 cm) of the same grain size. The tuffaceous siltstones are composed entirely of ashy, felsic material (fine-grained quartz and feldspar with no clay component), but do not contain preserved juvenile pyroclasts such as shards and pumice. Upper bedding surfaces are often exposed, forming pavements of exhumed climbing ripples (Fig. 5.13e). Load casts and flame structures occur at the base of the massive layers (Fig. 5.13f), indicating the underlying sediments were unconsolidated prior to their deposition. The stratified tuffaceous siltstones are laterally continuous over a strike length of at least 4.5 km.

#### 5.2.2 Interbedded Sandstone and Tuffaceous Siltstone Facies

In the upper half of the section, the tuffaceous siltstones are interlayered with coarser-grained sandstone intervals (Fig. 5.14). They have a medium grain size, with abundant grains of quartz, K-feldspar and minor plagioclase in a fine-grained siliceous matrix. Quartz consists of clear grains with straight extinction of volcanic origin, and lesser vein quartz, with abundant cross-cutting vacuole trails. Lithic fragments include polycrystalline grains derived from a plutonic source, and minor chert, gneiss and dolerite. Quartz and feldspars occur in subequal proportions, with slightly more quartz in most samples, and using the classification scheme of Folk (1980) the sandstones can be described as feldsarenites. Sandstone beds become coarser-grained upsection, and the coarser-grained sandstones have a higher percentage of quartz and lithic fragments. The proportion of matrix in the sandstones becomes lower upsection, and ranges from 55% to 30%. The rocks are texturally sub-mature, with angular to subrounded grains, and poor to moderate sorting. Some quartz grains have sutured margins, or polycrystalline siliceous overgrowths, indicating some removal of silica and some recrystallisation has occurred. The primary mineralogy is overprinted by a metamorphic assemblage of chlorite + calcite + epidote + sericite.

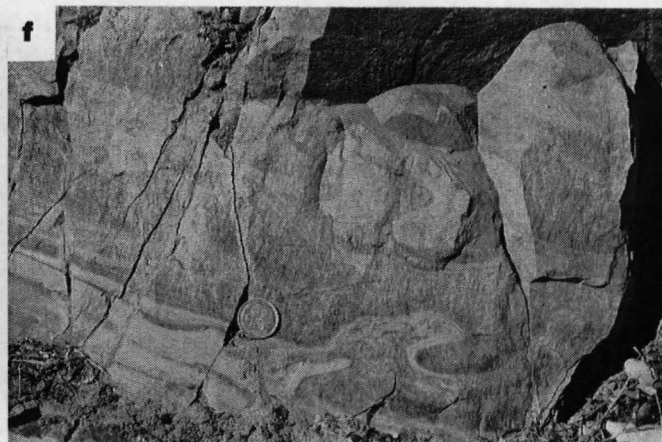
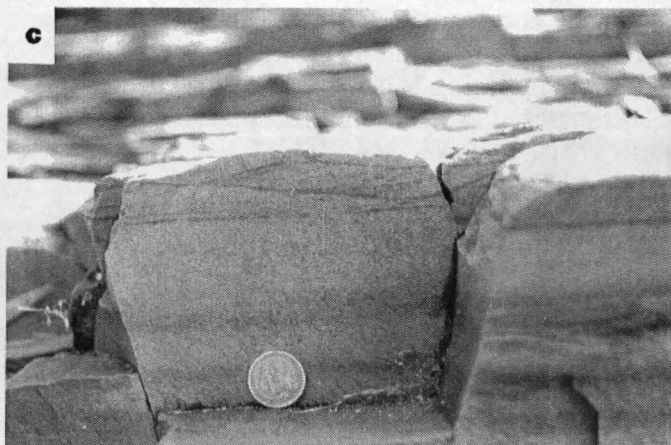
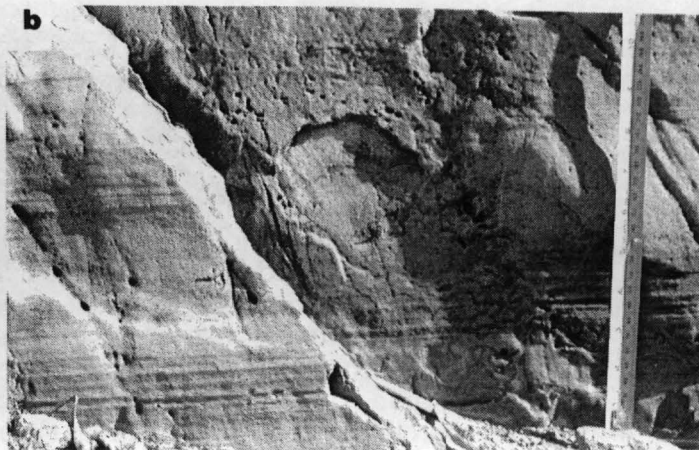
These coarser-grained intervals are identified as turbidites, with definitive features such as graded bedding, sharp bases with flute casts and internal structural divisions consistent with the Bouma sequence (Bouma, 1962). Bed thicknesses increase towards the top of the sequence, from < 10cm to over one metre. Sandstones in the upper stratigraphic horizons have a coarser grain size and a lower percentage of matrix material than those lower in the sequence. Intervals of tuffaceous siltstone are less frequent near the top of the succession. Beds in the middle of the section are dominated by divisions B and C of the Bouma sequence (plane parallel laminae, and ripples and cross laminae respectively). Near the top of the succession more beds begin with Bouma A division and individual sandstone beds amalgamate to form thick sandstone intervals. These beds were emplaced by mass-flow processes involving low sediment concentrations supported by turbulent interstitial fluid (Walker, 1978).

#### 5.2.3 Interpretation

Although the siltstones are composed entirely of volcanically derived, siliceous ashy material a pyroclastic mode of deposition is ruled out by the extreme thickness of the facies and the

**Figure 5.13**

- a) & b) planar laminated tuffaceous siltstones, Big Sunday Formation.
- c) Massive to diffusely stratified sandstone (Bouma division A) passing up into climbing ripple cross laminated sandstone
- d) Massive sandstone (div. A) with planar base grading up into C division cross laminated and D division planar lamination in sandstones
- e) An upper bedding surface exhumed to form a pavement of asymmetrical climbing ripples, showing unilateral current directions
- f) Load cast at the base of a massive sandstone (div. A) bed



presence of cross-stratification and ripple pavements. Planar laminated tuffs of pyroclastic fall deposits are rarely > 10 m thick (Cas & Wright, 1987) and the basal siltstones have an uninterrupted thickness of 40 m. Cross stratification and ripple pavements indicate lateral current transport rather than vertical settling of material.

Tractional sedimentary structures (plane-bed lamination, ripples, cross-stratification) indicate lateral current transport, and the great uninterrupted thickness of the facies indicates a continuous sediment supply process. Palaeocurrent data for these sediments (Friedmann & Grotzinger, 1991) have a unimodal distribution (Fig 5.14) which indicates an environment dominated by unidirectional currents (Reading, 1986). The palaeocurrent readings indicate a flow towards the southeast. Sediment-laden fluvial currents are considered to be the main sediment source for the basal sequence of tuffaceous siltstone. Herringbone-style cross-bedding with accompanying bimodal current distributions are conspicuously absent from the sequence, ruling out a tidal influence on the sediments, as would occur in marine lagoons or marine shoreline sediments or tidal flats (Reading, 1986). Cross-bedding and planar lamination are produced in the upper part of the lower flow regime, and the lower part of the upper flow regime of a flow, respectively. The thicker, massive layers indicate fluctuations in the sediment load of the river. The siltstones are interpreted to have been deposited by the underflow from the mouth of a river draining into a basin (e.g. a lake).

This water-lain sequence of tuffaceous sediments may represent reworking of the underlying ignimbrites or of co-ignimbrite ash falls associated with the underlying subaerial ignimbrites. The thickness of ash-derived sediment is comparable with this interpretation. Crystal concentration studies (Sparks & Walker, 1977) show that ignimbrites lose a substantial amount of vitric dust during eruption and deposition, amounting to an average of at least 35 weight percent of the original juvenile material. This material forms co-ignimbrite ash deposits which have volumes comparable with the ignimbrites (Sparks & Walker, 1977).

Thickening- and coarsening- upward sequences like the one described here, are a typical result of delta or fan progradation (Walker, 1984; Reading, 1986). Thicker, coarser-grained beds, increase in sandstone-siltstone ratio and amalgamated sandstone beds and the progressive increase of proximal turbidites (beginning with the Bouma A division) over distal turbidites (divisions B-D) up section, all indicate deposition under conditions of higher flow regime, reflecting closer proximity to the source, inferred here to be the mouth of a prograding river channel (Walker 1984; Reading 1986). This pattern is consistent with trends identified in prograding deltas .

The interturbidite tuffaceous siltstone corresponds to division E of the Bouma sequence, and represents settling of fines from the tail of the turbidity current or settling of a continuous influx of finer-grained material suspended in the river currents.

Deltaic sequences can form where rivers enter any body of standing water, be it ocean, sea, lake or lagoon. The stratigraphic position of this sequence, between subaerially deposited sandstones and volcanics, its restricted geography and lack of evidence for wave or tidal influences on the deposits suggest the environment was lacustrine. Turbidity currents would have been generated when the inflow of river water was more dense than the lake water, due to increased sediment load. Continuous deposition from sediment-laden currents, as indicated by undisturbed thicknesses of well-developed planar stratification in the tuffaceous siltstones, suggests the inflow of river water had the same density as the body of water into which it flowed (Reading, 1986).

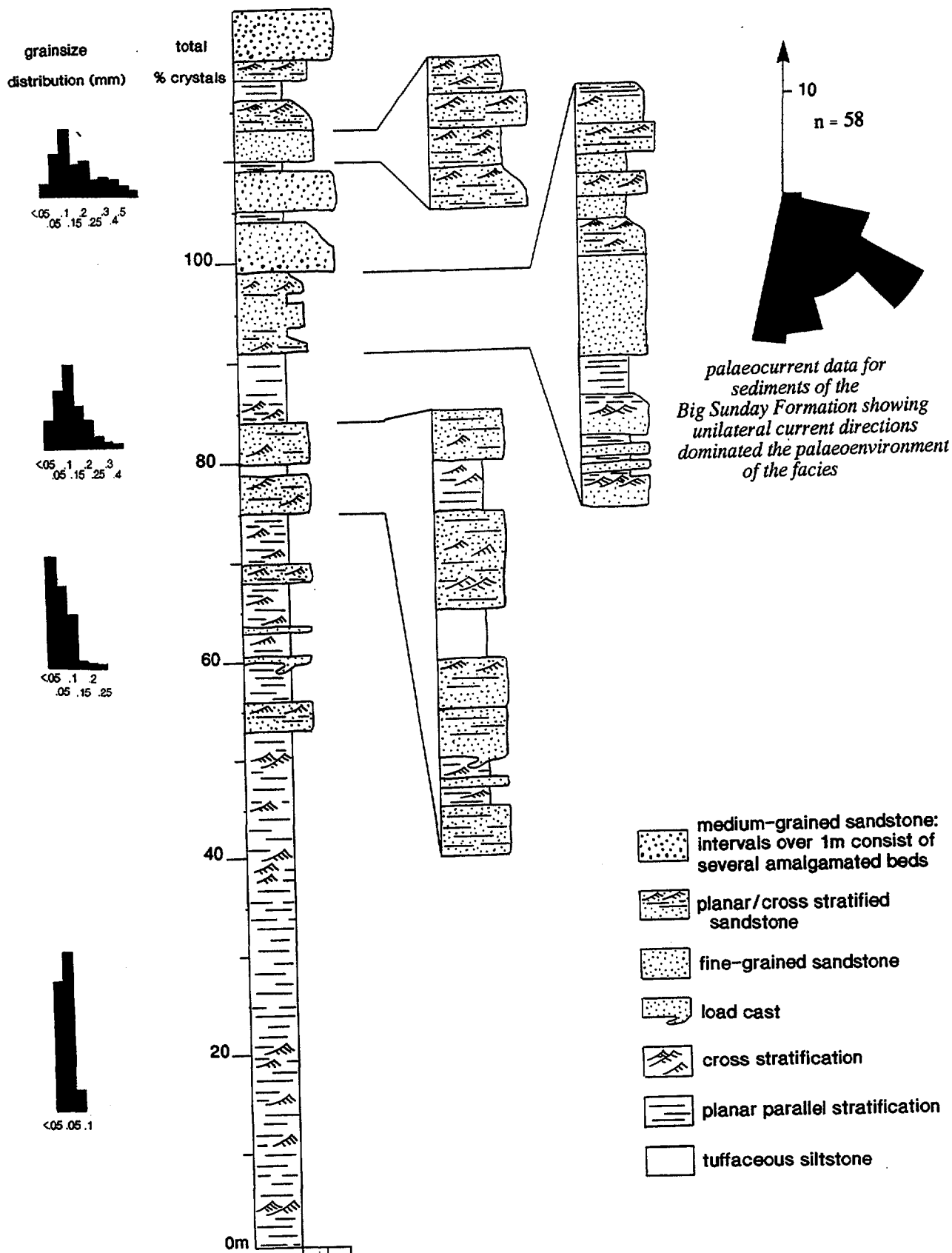


**Figure 5.14:** Measured section through the tuffaceous sediments of the Big Sunday Formation (GR 470875 - 477875). Palaeocurrent data are from Friedmann & Grotzinger (1991).



## 6. INTRUSIVE UNITS

### 6.1 FLOW-FOLDED RHYOLITE FACIES

*Description:* This unit locally occurs at the base of unit IC, and only outcrops in creek sections. The extent of the facies is difficult to determine because the surrounding ridges contain no outcrop and are covered with undefined rubble. The flow-folded rhyolite is geochemically identical to unit IC, the densely welded, columnar jointed ignimbrite. It has a similar low percentage of crystals and small lithic fragments (0.5-4 cm), but contains more quartz than feldspar, whereas unit IC contains a higher percentage of feldspar. The unit exhibits convolute flow-folding (Fig. 6.1a). The flow-bands are the same pink colour as the fiamme in ignimbrite unit IC, in a similar light brown groundmass.

*Interpretation:* Flow-banding usually occurs with extrusion or intrusion of viscous, coherent lavas. An alternative interpretation would be that the flow banding resulted from rheomorphism, the post-depositional secondary flowage of welded tuff. This is consistent with the unit being at the base of a densely welded ignimbrite of similar composition, as it may have flowed under the weight of the overlying material. The pink bands may be stretched pumice clasts. There is no evidence of fragmentation in this unit however, and the outcrop pattern of the facies cross-cuts the regional strike of the ignimbrite sequence, suggesting it intrudes the ignimbrites. The geochemical similarity of the unit to the ignimbrites suggests the facies is comagmatic with the ignimbrites.

### 6.2 QUARTZ-FELDSPAR PORPHYRY

*Description.* The ignimbrites of the Pul Pul Rhyolite are intruded by small quartz-feldspar porphyry stocks, some no larger than 2-4 m<sup>2</sup> in outcrop size with the largest covering an area ~ 750x500 m (Fig. 6.1b). They intrude mainly around the margin of the Malone Creek Granite and at the base of the ignimbrite pile, but small bodies are found throughout the sequence, especially near the Palette Fault. In most cases, their contact relationship with the ignimbrites is difficult to discern, but one cliff exposure along the South Alligator River shows a large porphyry body that is clearly intrusive, with an irregular contact, containing inclusions of the country rock near its margins and cross cutting veins of porphyry emanating from the main body.

The quartz-feldspar porphyries are homogeneous, moderately to highly porphyritic rhyolites (>75% SiO<sub>2</sub>). Most bodies have 25-30% crystals, but some are more porphyritic with crystal concentrations of 50-55%. Phenocrysts consist of euhedral quartz and feldspar (0.25-0.5 mm up to 5 mm) in roughly equal proportions with the percentage of feldspar slightly higher than quartz, and minor fine-grained opaques (magnetite). Glomerophyric aggregates of quartz and feldspar are very common. They occur in a crystalline groundmass of fine-grained siliceous material and slightly coarser recrystallised quartz-feldspar aggregates. Rare devitrification textures such as spherulites are preserved. The quartz is monocrystalline with straight extinction, it contains fluid inclusion trails, and has rounded corners and embayments indicating resorption. K-feldspar is the most abundant feldspar, with minor plagioclase crystals. Feldspar is fresh to slightly altered to sericite, minor chlorite and clay minerals, giving the altered crystals a dusty appearance. This alteration also affects the groundmass of some samples.

*Interpretation:* The quartz-feldspar porphyries were emplaced as coherent masses as indicated by the preservation of glomerophyric crystal aggregates, which would not have survived explosive volcanism. Cross-cutting field relationships with the ignimbrites suggest

that several of the bodies were intrusive into the ignimbrite pile. Others may have breached the surface to form lava domes, so that the facies may be locally extrusive as well as intrusive. The presence of quartz-feldspar porphyry clasts in the ignimbrites suggests that similar porphyries were cogenetic with the ignimbrites. Some of the magma may have crystallised as stocks at depth and were then incorporated into the ignimbrite-forming eruption as accidental lithics. The remainder of the magma may have risen during eruption of the ignimbrites and been emplaced shortly after their deposition. A cogenetic association between the quartz-feldspar porphyries and the ignimbrites is supported by geochemical and geochronological evidence (Sections 2 & 7). They are geochemically very similar to the aphyric rhyolite lava and small felsic sills and dykes which intrude the ignimbrites and the Big Sunday Formation (see below), suggesting all these facies are genetically related.

### 6.3 FELSIC SILLS AND DYKES

The sedimentary rocks of the Big Sunday Formation are intruded by numerous small felsic sills and dykes (Fig. 6.1c) of rhyolitic composition. At two localities, felsic dykes also intrude ignimbrites of the Pul Pul Rhyolite, and are flow-banded and distinctly cross-cut the fabric of the ignimbrites at a low angle. Where fresh, they are light pink in colour and are sparsely porphyritic, with 2-5% euhedral phenocrysts, 0.5 - 1mm in diameter, of resorbed and embayed quartz with rounded edges and twinned plagioclase and K-feldspar also exhibiting resorption features. Feldspars sometimes form glomerophyric clusters. The groundmass has a fine- to medium-grained granophyric texture of quartz and feldspar intergrowths and exhibits some alteration to clay, even in the freshest samples.

### 6.4 MALONE CREEK GRANITE

The Malone Creek Granite is an almost circular pluton about 10 km in diameter. The ignimbrite sequence trends around the south to south-west margins of the pluton (Fig. 1.2). The granite clearly intrudes the Lower Proterozoic siltstones of the Burrell Creek Formation (Fig. 6.1 d) and the Zamu Dolerite (Bryan, 1962), with contact metamorphic effects extending 200m from the granite margin (Stuart-Smith et al 1988). Coronation Sandstone basalts underlying the ignimbrites also show signs of contact metamorphism, with local development of biotite and amphibole overprinting the regional metamorphic assemblage, and sandstones having a recrystallised texture. No contact metamorphic effects have been observed in the ignimbrites, but the granite margin cross cuts their fabric, inferring an intrusive relationship. The granite is rimmed by a fine-grained green coloured rock which consists predominantly of fine-grained biotite crystals, which may be a contact aureole. This unit is approximately 10 m thick.

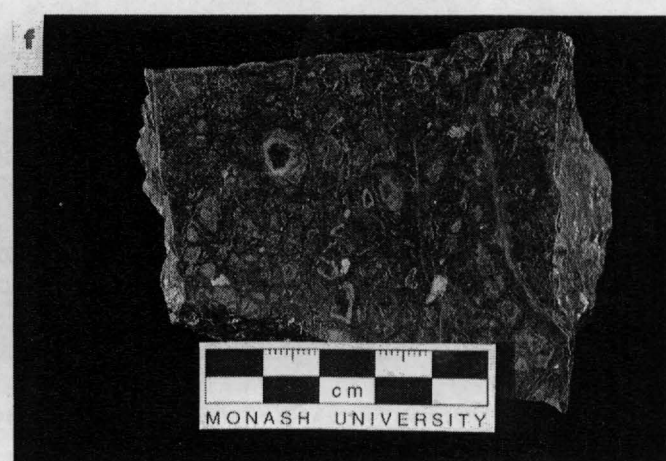
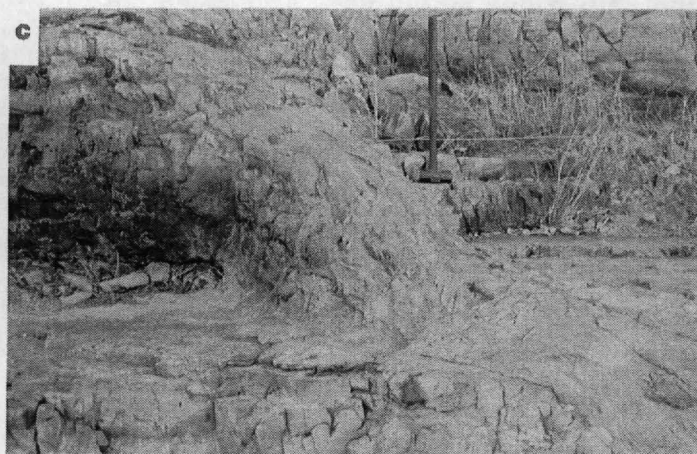
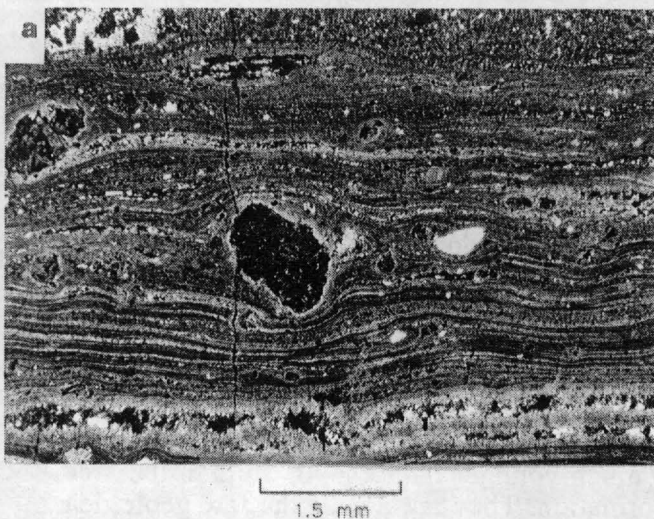
The granite is a quartz-rich alkali feldspar variety. The major constituents are quartz, kaolinised and sericitised microperthite and biotite, with accessory fluorite, allanite, zircon and sphene. Graphic intergrowths of quartz and alkali feldspar are common. The pluton has been mapped as three broadly concentric gradational zones (Stuart-Smith et al, 1988) based mainly on textural criteria rather than mineralogical or geochemical. It has a porphyritic centre, a fine to coarse even-grained middle zone and a fine, even-grained rim with widespread quartz veins and greisens (Stuart-Smith et al 1988).

### 6.5 SYENITE PORPHYRY

Syenite porphyries intrude as dykes and stocks up to 500 m in diameter, mainly along or near the main Palette Fault and quartz-rich splays branching from this fault. The intrusions are massive and red in colour and are characterised by large tabular K-feldspar phenocrysts. In thin section they consist of large, unorientated phenocrysts of K-feldspar and minor plagioclase in a groundmass of fine-grained granophyric intergrowths of quartz and K-feldspar, and minor

**Figure 6.1:**

- a) Flow-folded rhyolite facies
- b) Small quartz-feldspar porphyry body intruding ignimbrite
- c) Felsic dyke intruding the tuffaceous siltstone of the Nilyanjurrung Member
- d) Intrusive contact of the Malone Creek Granite showing the granite clearly cross-cutting the fabric of the Burrell Creek Formation, and containing clasts of Burrell Creek Formation
- e) Sparsely porphyritic dacite: the fine network of veinlets are silica-filled fractures. Hematite and chlorite alteration emanates from the fracture system
- f) Sparsely porphyritic dacite near Palette Fault. Shows siliceous alteration giving the rock a nodular appearance
- g) A vein of rhyolite cross-cutting dolerite which intrudes the ignimbrites (net-veining)
- h) A late-stage dolerite dyke cross-cutting ignimbrite (left)



chlorite, epidote and carbonate. Most primary ferromagnesian minerals have been altered to chlorite, but some primary biotite remains. All feldspars contain a dusting of hematite. The syenites are mineralogically distinctive as they contain no visible quartz in the phenocryst assemblage. All quartz occurs interstitially as a final crystallisation phase.

The syenites also have a very distinctive chemistry which differs from other felsic igneous rocks in the region (Fig. 6.2). They have ~ 63% SiO<sub>2</sub>, have less evolved trace element patterns than the other acidic units in which Rb and Ba are unfractionated, and are characterised by high Zr values (up to 700 ppm), Ce (up to 400 ppm), and Ba (up to 1947 ppm).

On geological evidence the porphyries are much younger than known units in the area, intruding units as young as the Big Sunday Formation. They are one of the few geological units in the area to the southeast of Coronation Hill which do not have a metamorphic overprint. Their close spatial association with the Palette Fault system suggests their intrusion may be linked with this faulting event. Preliminary ion-microprobe results suggest the syenite porphyry intruded at ~ 1800 Ma.

#### 6.6 SPARSELY PORPHYRITIC DACITE

Near Dinner Creek in the northwest of the study area, sparsely porphyritic dacite (63-66% SiO<sub>2</sub>) intrudes ignimbrites and underlying sandstone as two large stocks and several small boulder-sized outcrops (Fig. 1.2). The larger bodies discordantly cross-cut the volcanic stratigraphy. The dacite bodies are coherent, frequently preserve flow banding and are locally autobrecciated at the margins. They are sparsely porphyritic, with 3% phenocrysts of quartz, plagioclase and K-feldspar up to 1 mm in diameter. There is a higher percentage of feldspar than quartz and feldspars are clay to sericite ( $\pm$  epidote) altered. Plagioclase is albitised. The groundmass is largely aphyric with quartz and feldspar microlites. It is hematized and iron-stained, and red in colour, and has a high iron content (5% Fe<sub>2</sub>O<sub>3</sub><sub>tot</sub>) compared with other acid intrusives in the area (1-3% Fe<sub>2</sub>O<sub>3</sub>).

The dacites are highly altered and silicified and laced with a network of quartz veinlets and fractures with hematite and chlorite alteration (Fig. 6.1e). In outcrop, the fine fracture network is marked by resistant quartz ridges, or a red alteration staining emanating from the fractures. Along a splay of the main Palette Fault, the alteration emanating from these tiny fractures and veinlets forms a nodular pattern of small circles, and the rock is light grey in colour (Fig. 6.1f). The chemistry of the dacites is consistent however, regardless of the different types of alteration, and resembles the chemistry of the coarser-grained syenite porphyries (Fig. 6.2). The sparsely porphyritic dacite also has a close spatial association with faults cross-cutting the ignimbrite sequence, suggesting it may also be related to the main faulting event in the area, intruding at the same time as the syenite porphyries.

#### 6.7 DOLERITE DYKES AND INTRUSIVE BODIES

Boulder-sized outcrops of dolerite intrude the ignimbrites. Where fresh they contain plagioclase laths up to 2mm in diameter forming spherulitic clusters or penetrating larger augite crystals to form a subophitic texture. Prehnite and chlorite form interstitially to the plagioclase and augite, and the plagioclase is altered to sericite. Opaques are abundant. Where altered, the plagioclase is albitised and primary ferromagnesian minerals alter to chlorite, epidote and opaques (magnetite). Some of the dolerite outcrops are intruded by a network of veins of quartz and acid volcanic material of similar composition to the adjacent ignimbrites (Fig. 6.1g). The dolerite intruded by these veins appears as closely spaced angular to rounded inclusions.

## 6. INTRUSIVE UNITS

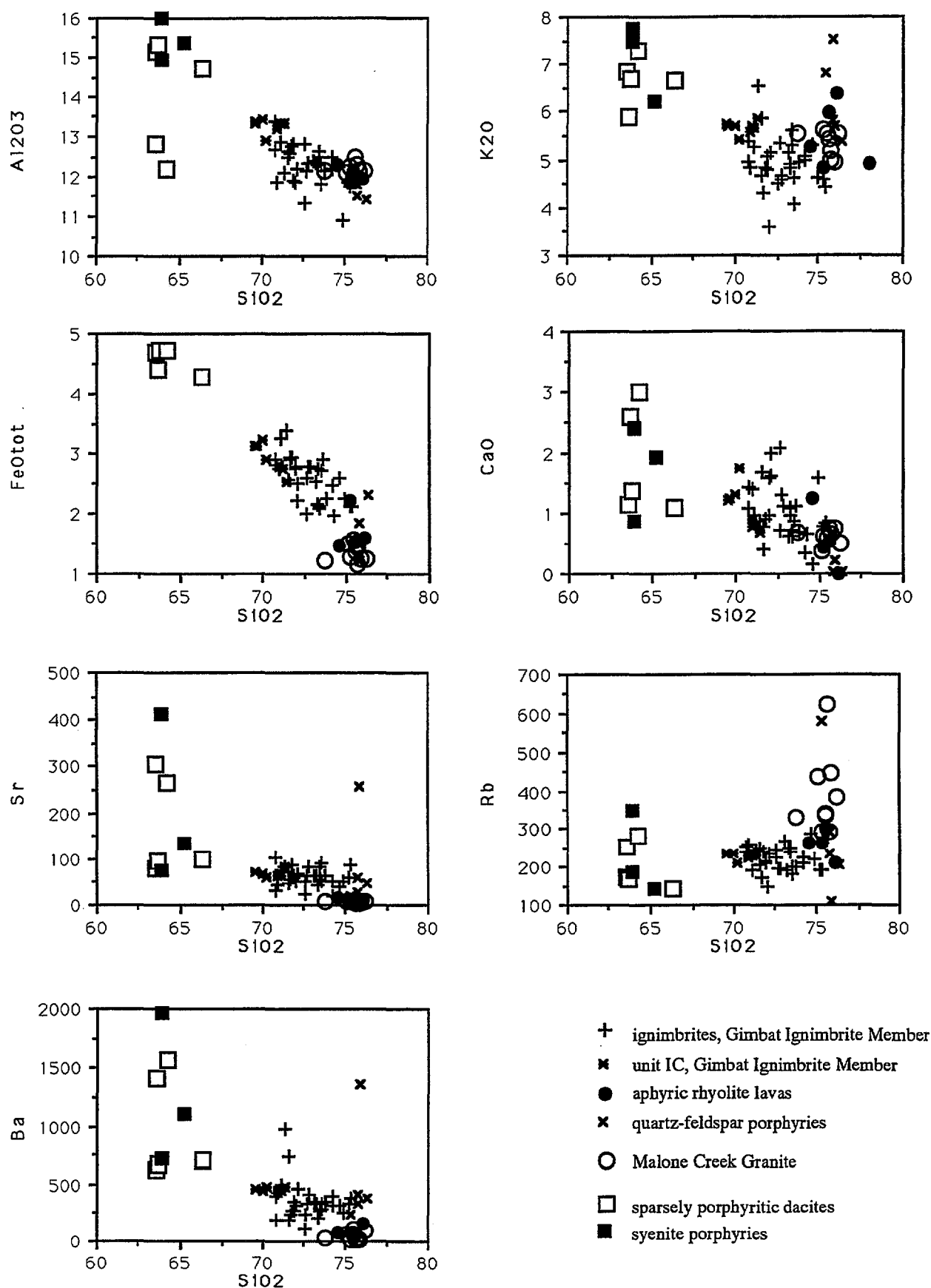


**Figure 6.2:** Select geochemical plots showing the similar chemistries of the sparsely porphyritic dacites and syenite porphyries, and how their chemistry contrasts with the felsic volcanics of the Gimbat Ignimbrite Member.



These features are similar to those described for net-vein complexes, which result from the co-mingling of felsic and mafic magmas in relatively high-level intrusions (e.g. Blake et al 1965; Walker & Skelhorn 1966; Blake 1966; Yoder, 1973; Wiebe 1980; Taylor et al 1980). The mafic magma comes into contact with felsic magma or intrudes pre-existing granite which is then partially melted and remobilised. The basalt magma (900-1300°C) chills against the felsic melt (750-950°C; Sparks et al 1977) and solidifies, preventing mixing of the two liquids. The adjacent felsic melt becomes superheated and in turn intrudes the solidified mafic rock as a network of thin veins (Blake 1981). As the mafic magma cools, it may form pillows in the felsic liquid, explaining the rounded shape of the dolerite inclusions.

Although net-veining has been described for intrusive magmas, similar principles may apply when mafic dykes intrude a thick pile of extrusive rhyolitic volcanics, such as the ignimbrites of the Pul Pul Rhyolite.

A prominent intrusion of dolerite about 1 km long and 30 m wide, intrudes the subaqueous sedimentary rocks of the Big Sunday Formation. It is composed of sericitised and albitised plagioclase, augite, chlorite and minor calcite, with a sub-ophitic texture, and contains large amygdules infilled with chalcedony, calcite and chlorite in places.

Swarms of east-northeast-trending vertical dolerite dykes (Fig. 6.1h) intrude the ignimbrites and intrusive units of the Pul Pul Rhyolite, including the Malone Creek Granite. These dykes are regional features, also intruding Lower Proterozoic sediments and filling major joints in the Plum Tree Creek Volcanics, Grace Creek Granite, Cullen Granite, Birdie Creek Volcanics and lower members of the Kombolgie Formation (Stewart 1965; Stuart-Smith et al 1988). Stuart-Smith et al (1988) suggest they correlate with a dyke dated at 1370 Ma (Page et al., 1980), which transgresses the Ranger orebody. The dykes have ophitic textures and are composed of andesine, augite, chlorite and magnetite. They are variably metamorphosed to form an albite-sericite-chlorite-epidote assemblage.

### 7. GEOCHEMISTRY AND MAGMA PETROGENESIS

In this section the different geochemical suites of the Gimbat Ignimbrite Member and other granites and volcanics outcropping locally are defined and classified. The relationship between different geochemical suites is considered based on their petrographic, geochemical and isotopic characteristics. The data are used to constrain the possible origins of the magmas represented by these suites and the tectonic setting in which they formed is considered.

#### 7.1 MAJOR ROCK TYPES

##### 7.1.1 Gimbat Ignimbrite Member

Felsic volcanic rocks of rhyolitic composition dominate the igneous rocks of the Gimbat Ignimbrite Member, and they are fragmental and of pyroclastic origin. Ignimbrites, with well preserved eutaxitic textures and variable degrees of welding are the most common felsic volcanic rock, with subordinate volcanic breccias containing angular lithic fragments (mainly dolerite) up to 20 cm in diameter and volcanic conglomerates containing rounded lithic boulders up to 2m in diameter. Fragmental rocks of epiclastic origin are also preserved in the section, as fluvial channel-fill sequences, and a laterally extensive, thick mass-flow unit at the top of the succession, believed to be derived from pyroclastic flows entering water, disintegrating and transforming into water supported mass flows.

In thin section, pyroclasts constitute up to 30% of the ignimbrites and range from 0.1 to 0.6 mm in size, with a greater span of grainsize up to 4.0 mm in the coarser grained ignimbrites. The pyroclasts have phenocryst, lithic and juvenile components. Quartz is the most common phenocryst, with sodic plagioclase, microcline and potassic feldspar less common. The lithic component constitutes ~ 25% of the pyroclasts and includes metasedimentary basement clasts (gneiss and schist fragments), dolerite, plutonic quartz, quartzite, chert and quartz grains exhibiting undulose extinction. The volcanic matrix is composed largely of a very fine siliceous matrix devitrified and recrystallised to a cherty texture.

Grains constitute up to 80% of the epiclastic sediments and have a greater range in grainsize than the ignimbrites. They have the same composition as the ignimbrite pyroclasts, but the channel-fill sediments have a higher percentage of lithic fragments, indicating a mixed basement and contemporaneous pyroclastic source. The geochemistry of the epiclastic deposits is discussed in Section 5.1.6.

##### 7.1.2 Malone Creek Granite

The Gimbat Ignimbrite Member is intruded by the Malone Creek Granite, an almost circular pluton about 10 km in diameter. The granite is a fine to coarse even-grained to porphyritic (especially near the margins), quartz-rich alkali feldspar granite, containing phenocrysts of quartz and K-feldspar up to 1 cm across, 1% biotite, 5% kaolinised and sericitised plagioclase and microperthite, and minor allanite, zircon and sphene, in a fine groundmass of predominantly graphically intergrown quartz and K-feldspar. It commonly contains accessory fluorite, epidote and carbonate, and these phases are abundant in the outer margins of the pluton.

### 7.1.3 Plum Tree Creek Volcanics and Grace Creek Granite

The Plum Tree Creek Volcanics of the Edith River Group, and their intrusive equivalent, the Grace Creek Granite, outcrop ~ 15 km south of the Gimbat Ignimbrite Member. The Plum Tree Creek Volcanics are interpreted to be rhyodacitic ignimbrites (Stewart, 1965; Needham & Stuart-Smith 1985 a;b). They are crystal-rich (30-50% crystals) with phenocrysts of microcline and andesine (up to 1 cm in length), and minor quartz and pseudomorphs of chlorite after hornblende or biotite. They contain rare mafic xenoliths. The groundmass consists of microcrystalline quartz, kaolinised feldspar, chlorite and trace zircon, apatite, sphene and biotite. The quartz sometimes forms as small laths in the groundmass, and rarely occurs in phenocrystic proportions.

These units contrast mineralogically with ignimbrites of the Gimbat Ignimbrite Member, in which quartz is the main phenocryst phase. In the Plum Tree Creek Volcanics and Grace Creek Granite, the main phenocryst phase is plagioclase, and quartz is largely confined to the groundmass.

The Plum Tree Creek Volcanics are intruded by the Grace Creek Granite, a medium-grained, porphyritic granite, mineralogically and geochemically similar to the volcanics, but with a fine-grained graphic groundmass. Quartz is more common in the phenocryst phase than in the volcanics. Contacts between the granite and volcanics are gradational and ill-defined. The granite is probably a subvolcanic intrusion, comagmatic with the Plum Tree Creek Volcanics (Needham & Stuart-Smith, 1985a:b).

### 7.2 SAMPLING AND ANALYTICAL METHODS

Approximately 100 samples representative of each of the igneous and some epiclastic rock units were collected from the study area for chemical analysis. Major and trace elements were analysed in the Bureau of Mineral Resource's laboratories. All major elements and most trace elements were analysed by X-ray fluorescence, using Li-borate glass discs and pressed powder pellets respectively (Norrish & Chappell 1977). Li, Be, Co, and Ag were determined by atomic absorption spectrophotometry and FeO concentrations were determined by titration. Rare earth elements (REE) analyses for 12 samples were obtained using the spark source mass spectrometer at the Research School Of Earth Sciences, Australian National University (RSES, ANU) after the methods and techniques described in Taylor & Gorton (1977). Chondrite normalising values are from Taylor & McLennan (1981).

Nd and Sr isotopic determinations, and Sm isotope dilution analyses were carried out using a Finnigan MAT 261 multicollector mass spectrometer at RSES, ANU, operated in static mode. Rb was analyzed using a Nuclide single collector mass spectrometer. Powdered rock samples and mineral separates were dissolved in teflon-lined bombs at 200°C, using HF and HNO<sub>3</sub>; 6N HCl was used to dissolve carbonates and to leach sulphates. After conversion to 1N HCl solutions, Rb, Sr and the REE were separated using cation exchange columns, and Sm and Nd were subsequently isolated using HDEHP columns. Sr isotopic ratios were fractionation corrected to  $^{86}\text{Sr}/^{88}\text{Sr} = 0.1194$ , and normalised to a value of  $^{87}\text{Sr}/^{86}\text{Sr} = 0.70800$ . Nd isotopic ratios were corrected for fractionation by normalising to  $^{146}\text{Nd}/^{144}\text{Nd} = 0.72190$ , and are reported relative to  $^{143}\text{Nd}/^{144}\text{Nd} = 0.512642$ .

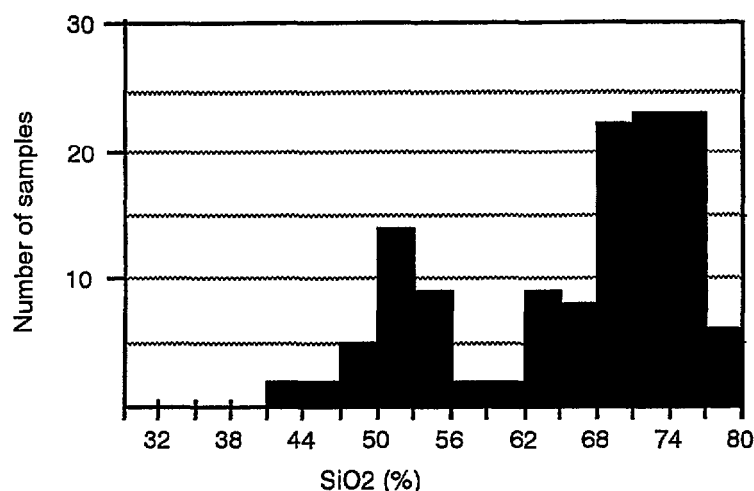


**Figure 7.1 :** Frequency distribution histogram of SiO<sub>2</sub> wt. % for samples collected from the study area. Suites represented are the Gimbat Ignimbrite Member and associated intrusives, Malone Creek Granite, Grace Creek Granite, Plum Tree Creek Volcanics, Coronation Sandstone and Zamu Dolerite.

### 7.3 CLASSIFICATION

Silica values for igneous rocks which outcrop in the region of the study area have a well-defined bimodal distribution (Figure 7.1). Igneous rocks of intermediate composition are rare, not only in the study area, but in the Pine Creek Inlier as a whole (Wyborn, 1988).

Geochemically, all felsic igneous suites considered in this study classify as granites or adamellites, or the volcanic equivalents, rhyolite and rhyodacite (Fig. 7.2). Samples are metaluminous to mildly peraluminous, with an ASI ratio ( $\text{Al}_2\text{O}_3/\text{Na}_2\text{O}+\text{K}_2\text{O}+\text{CaO}$ ) of  $< 1.1$  (Fig. 7.3) and less than 1% normative corundum (Appendix A). These features define the rocks as I-type or 'infracrystal', derived from sources that have never undergone surficial weathering, based on the criteria of Chappell & White (1984).

### 7.4 GEOCHEMISTRY OF THE GIMBAT IGNIMBRITE MEMBER

The geochemical data for the Gimbat Ignimbrite Member form relatively smooth, continuous trends on Harker variation diagrams (Fig. 7.4), which range in composition from 69 - 75% SiO<sub>2</sub>. Although there is a significant amount of scatter of data points, general trends are still apparent. Scatter is due to alteration which particularly affects the alkali elements. Metamorphism is unlikely to have affected chemical trends. It has been shown to be largely isochemical in similar Proterozoic rocks of the Mt Isa Inlier (Wilson, 1978; Wyborn & Page, 1983). Some of the scatter is likely to be due to the elutriation of ash during eruption and deposition of the ignimbrites, and contamination by lithic clasts, especially the abundant dolerite fragments which would imprint a mafic signature on the silicic parent magma.

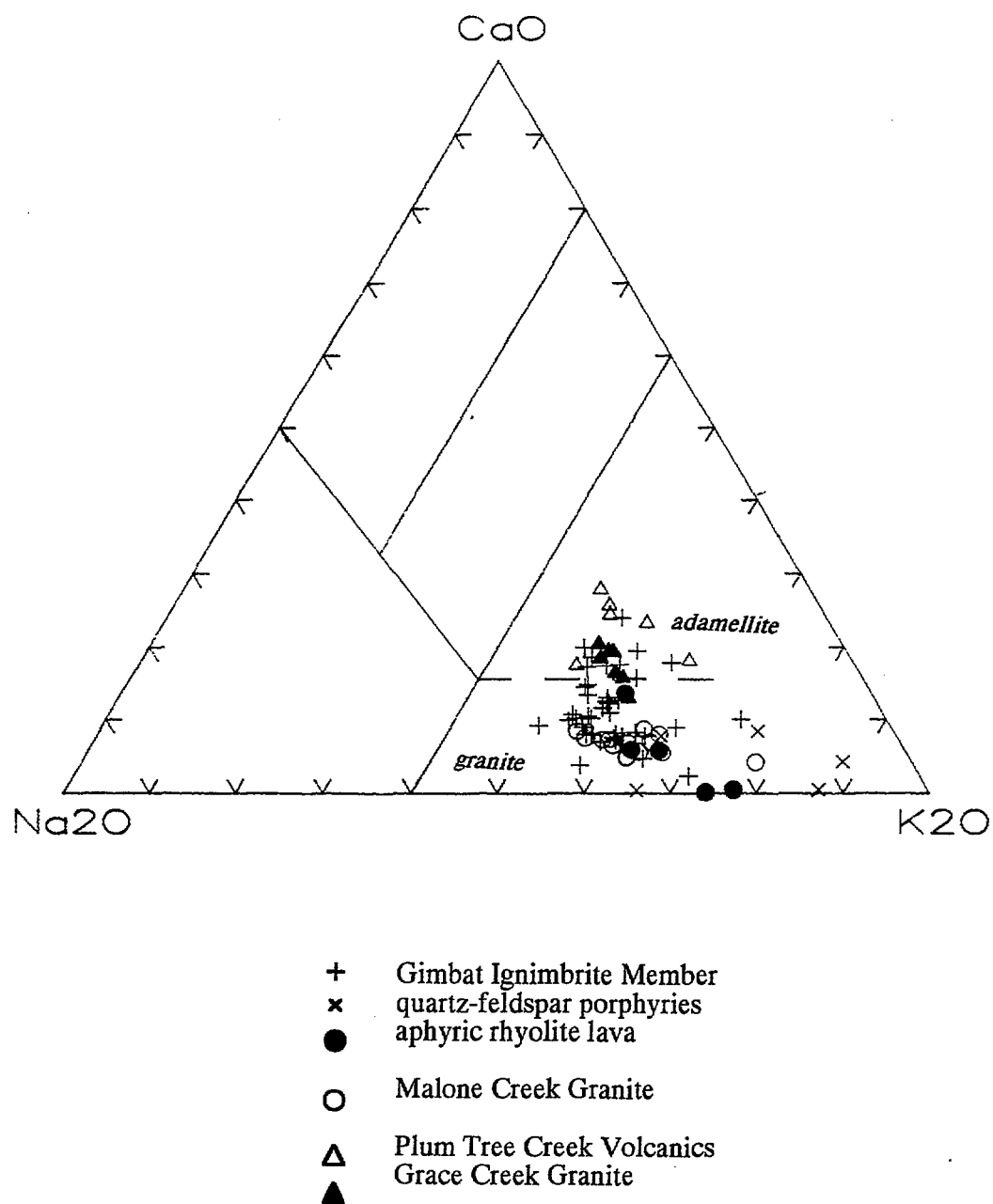


Figure 7.2: Classification of felsic volcanics in the area of study (after White, pers. comm. 1988)

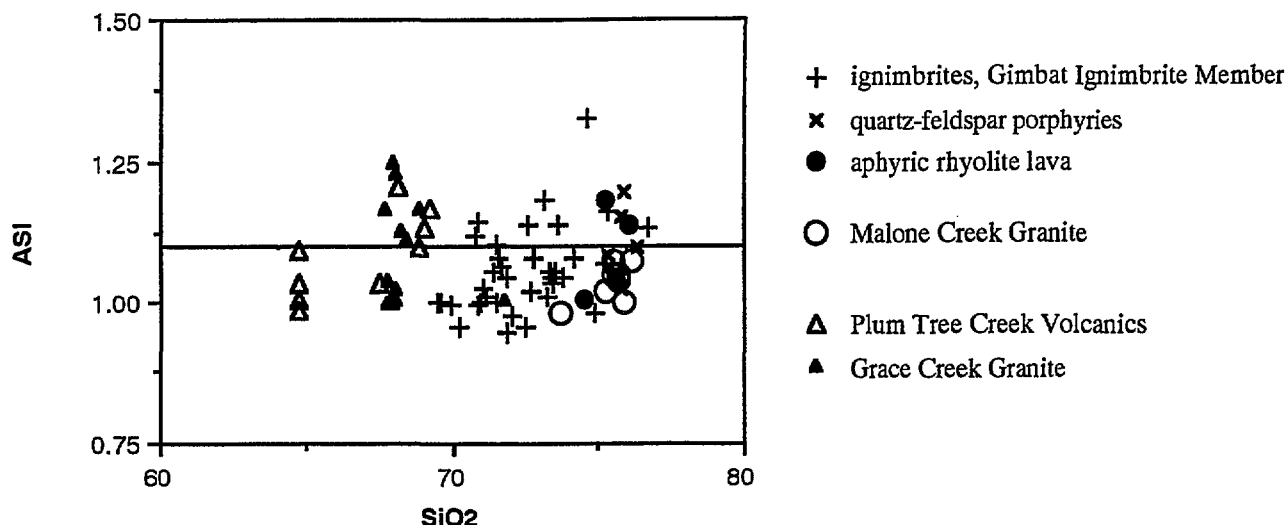


Figure 7.3: ASI ratios for felsic volcanics.

The range of  $\text{SiO}_2$  and chemical variation in the ignimbrite suite is largely controlled by magmatic differentiation and perhaps to some extent by secondary processes during eruption and deposition (such as ash-winnowing). The dominant role of magmatic differentiation is supported by petrographic evidence. The ignimbrites which have  $< 70\%$   $\text{SiO}_2$  (unit IC: densely-welded ignimbrite) are petrographically distinct, with a higher proportion of feldspar phenocrysts than the other ignimbrite samples. The comagmatic quartz-feldspar porphyries plot at the high silica end of the trends, and the remainder of the ignimbrites range between these two end-members, suggesting the span of  $\text{SiO}_2$  values is a primary feature. The ignimbrite suite shows depletion in  $\text{Al}_2\text{O}_3$ ,  $\text{TiO}_2$ ,  $\text{Fe}_2\text{O}_{3\text{tot}}$ ,  $\text{MgO}$ ,  $\text{CaO}$ ,  $\text{P}_2\text{O}_5$  and Sc with increasing  $\text{SiO}_2$ , while  $\text{K}_2\text{O}$ ,  $\text{Na}_2\text{O}$  and most trace elements have constant values over the range of  $\text{SiO}_2$  (Fig. 7.4).  $\text{Ga}/\text{Al}$  decreases with increasing  $\text{SiO}_2$  (Fig. 7.5). The ignimbrites and co-genetic quartz-feldspar porphyries are light rare earth element (LREE) enriched, have strongly depleted Eu anomalies and flat HREE patterns (Fig. 7.6).

Chemically, the aphyric massive to flow-banded rhyolite lava that overlies the Gimbat Ignimbrite Member in the southeast has a highly evolved composition and plots as a high silica end-member to the ignimbrites. The enrichment of incompatible elements, flat REE pattern and the extreme negative Eu anomaly of the lava attests to its highly evolved or fractionated character (Fig. 7.6).

The observed chemical variations are consistent with melt evolution controlled by the removal of plagioclase, K-feldspar, quartz, apatite and zircon. The depletion of trace elements such as Ba and Sr, and the progressive increase in magnitude of the Eu anomaly suggests melt evolution is largely controlled by the removal of feldspar crystals. In addition, minor phase differentiation is required to deplete  $\text{CaO}$ ,  $\text{P}_2\text{O}_5$ , Zr and the LREE in the melt. The decreasing  $\text{Ga}/\text{Al}$  ratio observed with increasing  $\text{SiO}_2$  is unusual, because Ga is expected to concentrate in later formed minerals, as it has a larger ionic radius (0.62Å) than Al (0.57Å; Goodman, 1972). Wyborn (1983) documented a similar situation in the Boggy Plain supersuite, and found that

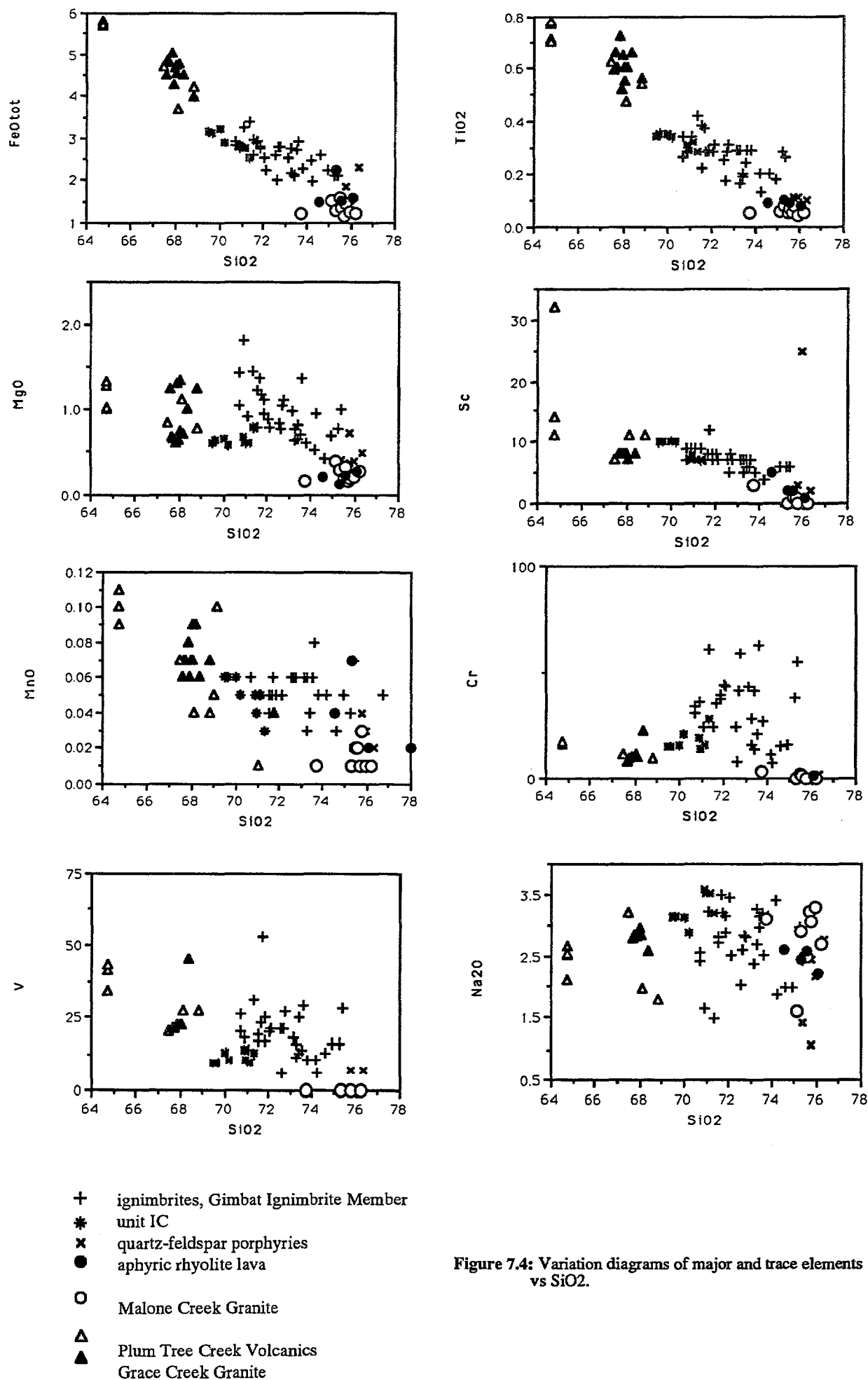


Figure 7.4: Variation diagrams of major and trace elements vs SiO<sub>2</sub>.

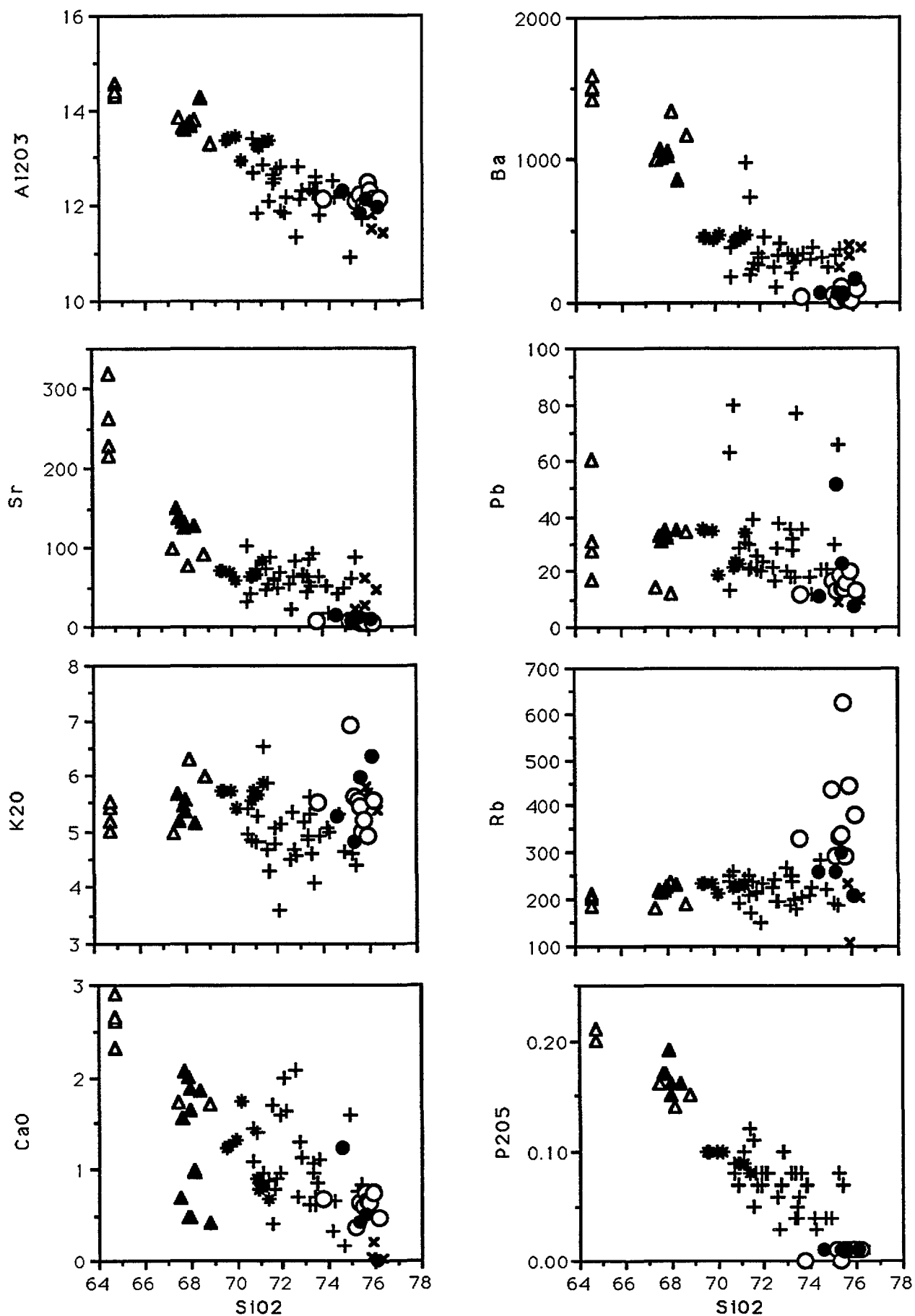


Figure 7.4 continued

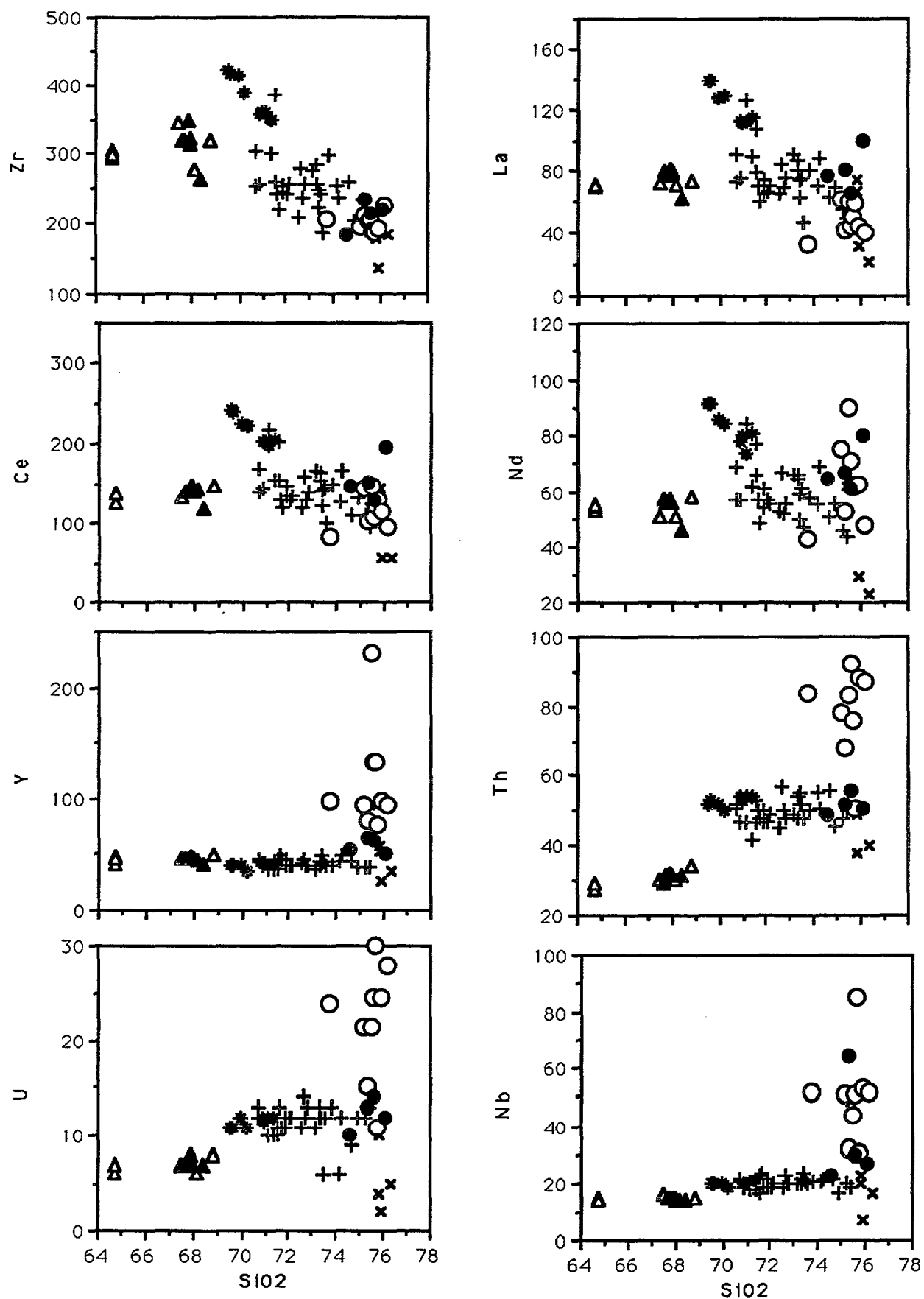


Figure 7.4 continued

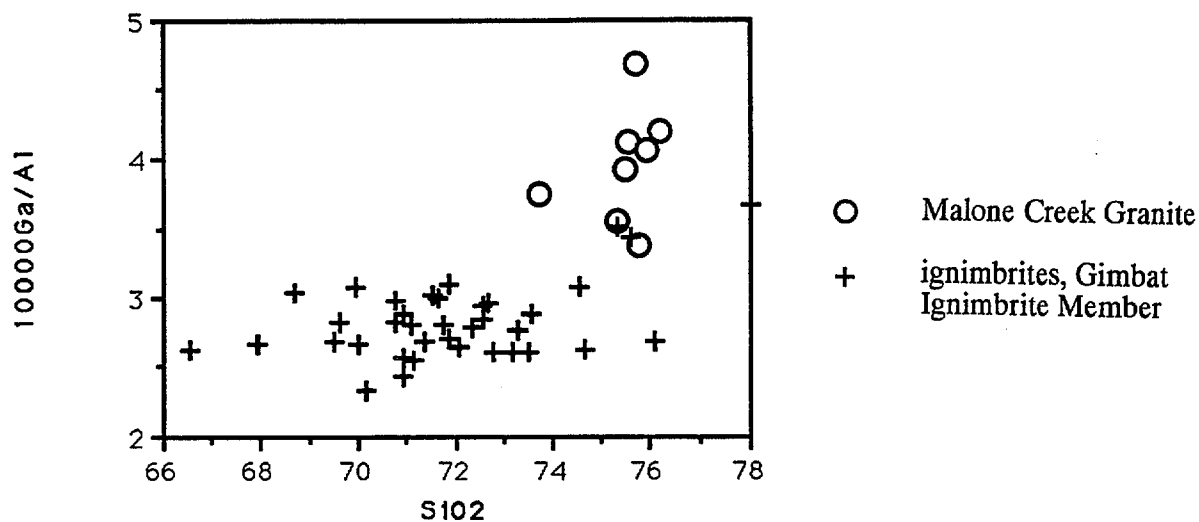
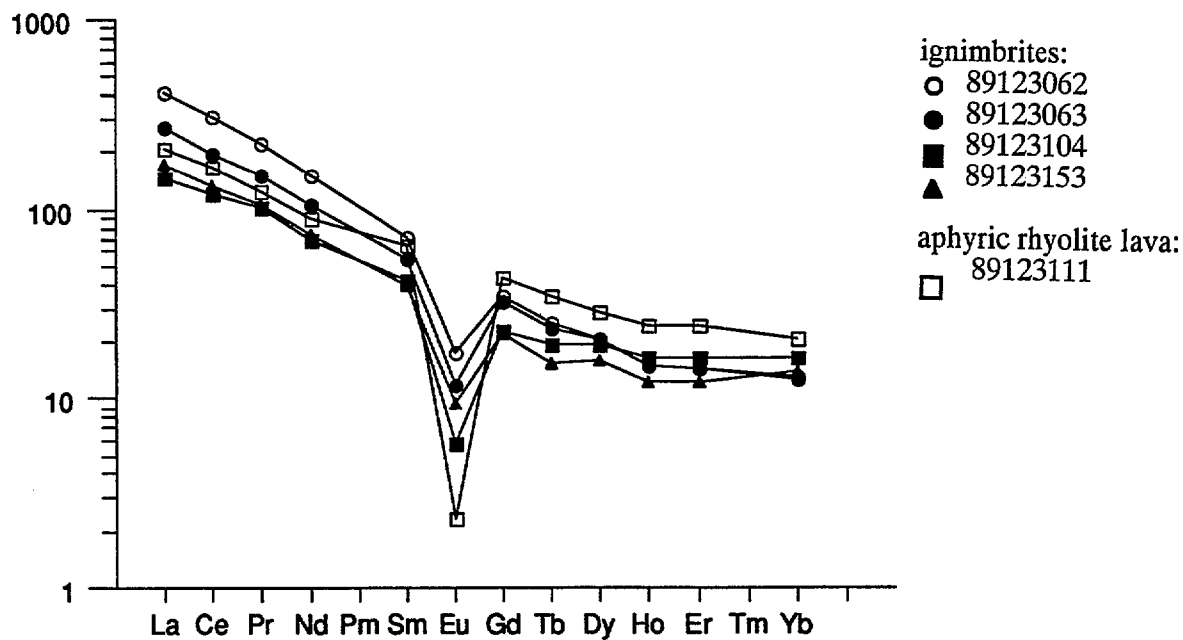
Figure 7.5: Ga/Al vs SiO<sub>2</sub>

Figure 7.6: REE data for select samples of the Gimbat Ignimbrite Member

although Ga did increase in later formed minerals, the Ga/Al ratio decreased from amphibole to biotite to plagioclase to K-feldspar. Thus the decreasing trend is due to the progressive removal of plagioclase and perhaps biotite or amphibole from the melt.

The lithic fragments were removed from 12 samples, and plotting these hand-picked samples tightened the trends and reduced the amount of scatter. The hand-picked samples have higher SiO<sub>2</sub> values, and the range of SiO<sub>2</sub> values is decreased. Most geochemical trends were similar for the hand-picked and non-hand picked ignimbrites. The ferromagnesian components were most affected by contamination due to mafic lithic fragments, and these trends are shown to represent mixing lines between felsic melt and the lithic contaminant, or to scatter within a triangular area (Fig. 7.7). This scatter reflects the dual control of the trends by lithic contamination, and by magmatic differentiation processes. Although the depletion of ferromagnesian elements with increasing SiO<sub>2</sub> is much reduced when samples handpicked to remove lithic contaminants are plotted (indicating these trends are largely controlled by mafic clast contamination), some fractionation of ferromagnesian minerals (magnetite and possibly titanomagnetite and/or ilmenite, and perhaps biotite) is also likely to have occurred.

Linear variation trends such as those of the Gimbat Ignimbrite Member can be explained by fractional crystallisation processes (Whalen et al 1982), or by the mixing of a melt end-member and refractory source residue, 'restite' (Chappell et al, 1987). There are several lines of evidence to indicate the compositional variation observed is mainly attributed to restite unmixing.

(1) The K/Rb ratio of the samples remains constant towards high silica values (Fig 7.8), implying that little or no fractional crystallisation has occurred (Collins et al, 1982).

(2) Trace element values and in particular incompatible elements have constant values throughout the range of SiO<sub>2</sub>. That is, they are not concentrated by fractional crystallisation processes at higher silica levels.

(3) Chemical variation within the ignimbrite suite is not systematic with respect to stratigraphic position in the sequence, indicating that the ignimbrites are not zoned. One chemically distinct ignimbrite unit I<sub>C</sub> (discussed below), occurs in the middle of the succession, but is overlain and underlain by higher silica ignimbrites which are chemically identical to each other. This suggests that fractional crystallisation did not play a significant role in magma chamber dynamics and was insufficient or did not have sufficient time to produce a compositionally stratified magma chamber, which would be reflected by a regular chemical zoning in the ignimbrites.

(4) Finally, a restite component to the melt is implied by the LREE enrichment of the ignimbrites. Miller & Mittlefehldt (1982) state that LREE enriched felsic igneous rocks which were derived by crustal anatexis, as proposed for the Gimbat Ignimbrite Member ignimbrites (Section 7.9), must contain a significant restite component. This is because the extremely LREE-rich accessory phases allanite and monazite, form residual phases in partial melting of crustal material. They do not breakdown and release LREE into the melt, and therefore must exist as a restite phase if the magma is LREE enriched.

In summary, geochemical trends are controlled by three processes. Firstly, most trends reflect magmatic differentiation by restite unmixing resulting in flat or constant trends. These straight-line trends are explained by progressive separation of restite and melt. They are two-component systems with residuum as one end-member and melt as the other. Secondly, for some trends (involving the ferromagnesian minerals) a third component (mafic lithic contaminants) is introduced resulting in a scatter of points above magmatic trends. These trends no longer represent a single line of liquid descent, but plot within a triangular area representing a three component

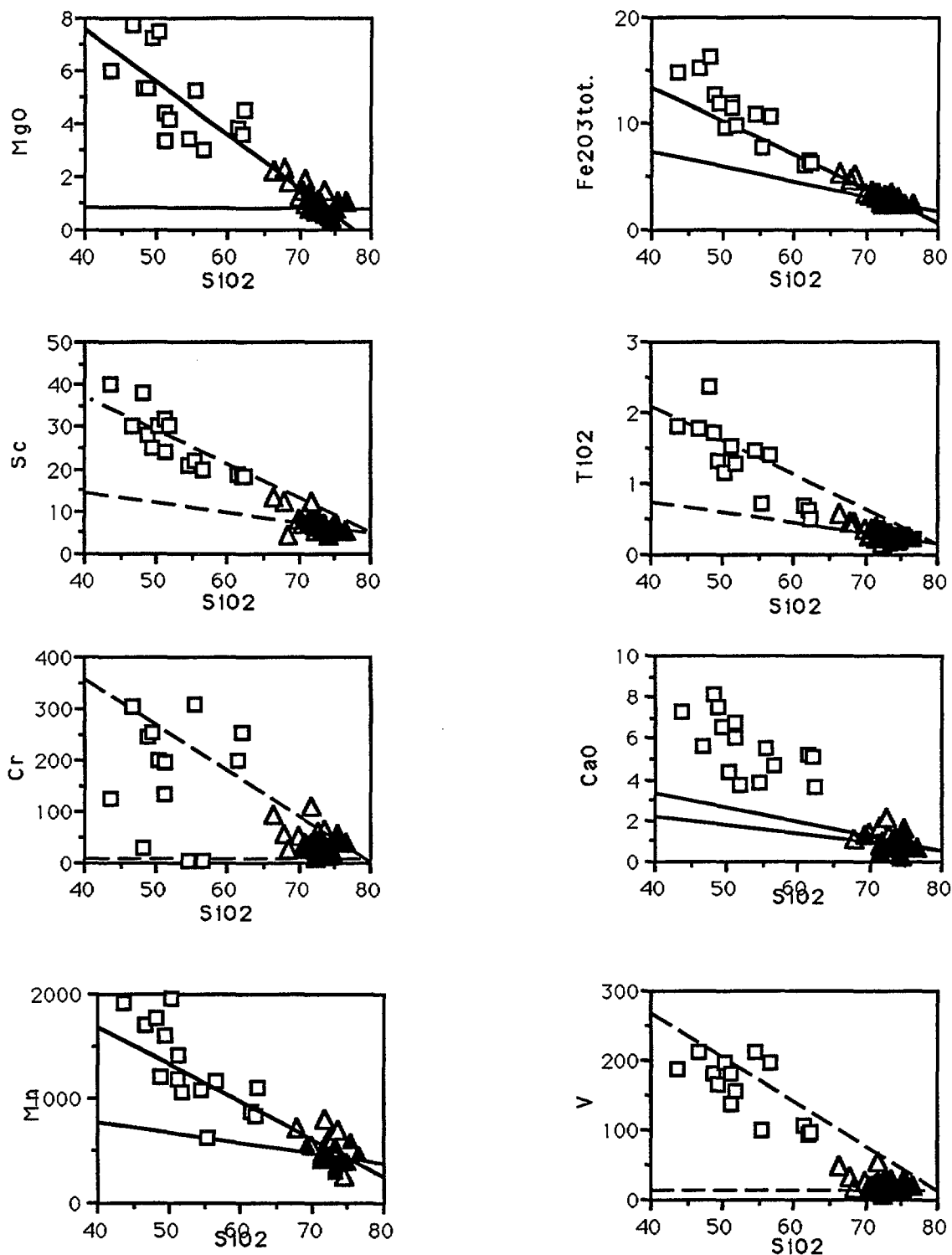


**Figure 7.7:** Variation diagrams showing the effect of dolerite lithic contamination on ignimbrite trends. Solid lines are trends through ignimbrites samples handpicked to remove lithic contaminants, and represent primary magmatic differentiation (restite unmixing) trends, and through bulk-rock ignimbrite samples. Trends through bulk-rock samples are clearly mixing lines between dolerite contaminant and felsic melt. Dashed lines on other plots define the area of scatter of data points which are affected by both processes.  
 ▲ handpicked ignimbrites    △ bulk-rock ignimbrites    □ representative analyses of mafic rocks which outcrop in the vicinity of the ignimbrites and probably source the dolerite lithic component in the ignimbrites.

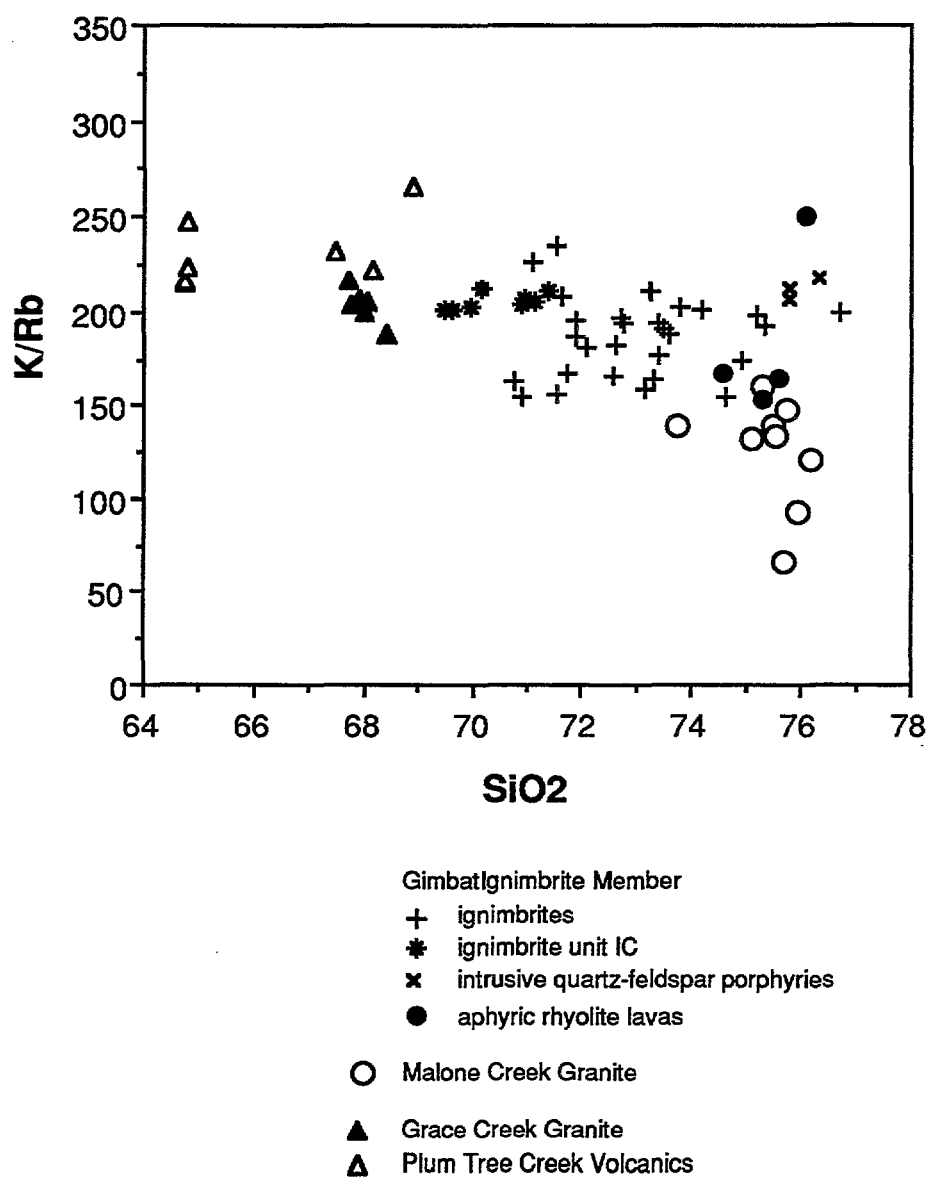


**Figure 7.8:** K/Rb vs silica plot showing non-fractionating trends for the Gimbat Ignimbrite Member, Plum Tree Creek Volcanics and Grace Creek Granite, and fractionation in the Malone Creek Granite.

system (Fig. 7.7). A third process affecting trends may be ash-loss during eruption and deposition of the ignimbrites, but this appears to be insignificant.

#### 7.4.1 Geochemistry of unit I<sub>C</sub>, and implications for magma chamber dynamics

Geochemical data for one ignimbrite unit (the densely welded ignimbrite, unit I<sub>C</sub>) define separate linear arrays to the rest of the ignimbrites on several variation diagrams (Fig. 7.4). Specifically, this unit contains less MgO (and Sc and Cr), and Ga/Al ratios are lower. On a primordial mantle-normalised, extended trace element diagram, unit I<sub>C</sub> has the least fractionated trace element pattern (Fig. 7.9). Zr, La and Ce are relatively enriched and show trends of progressive depletion with increasing silica. The Eu anomaly is smaller, and the unit has a higher proportion of trace elements such as Ba and Sr than the other ignimbrite units, which is consistent with petrographic observations that it contains more plagioclase and K-feldspar as phenocryst phases than the other ignimbrites, which contain more quartz. In addition, it must contain more accessory phases to explain the higher Zr and LREE contents.

Usually with restite-controlled melts, crystallisation is dominated by freezing of the interstitial liquid, and the large amounts of solid residual material in the melt would inhibit fractionating processes within the magma chamber. In contrast, granites that intrude as liquids can differentiate by convective fractional crystallisation (Sparks et al, 1984). As the ignimbrites are relatively crystal-poor (10-20% crystals) it is likely that the amount of restite in the melt was small, and not enough inhibit convection in the magma chamber. Thus some crystal-liquid

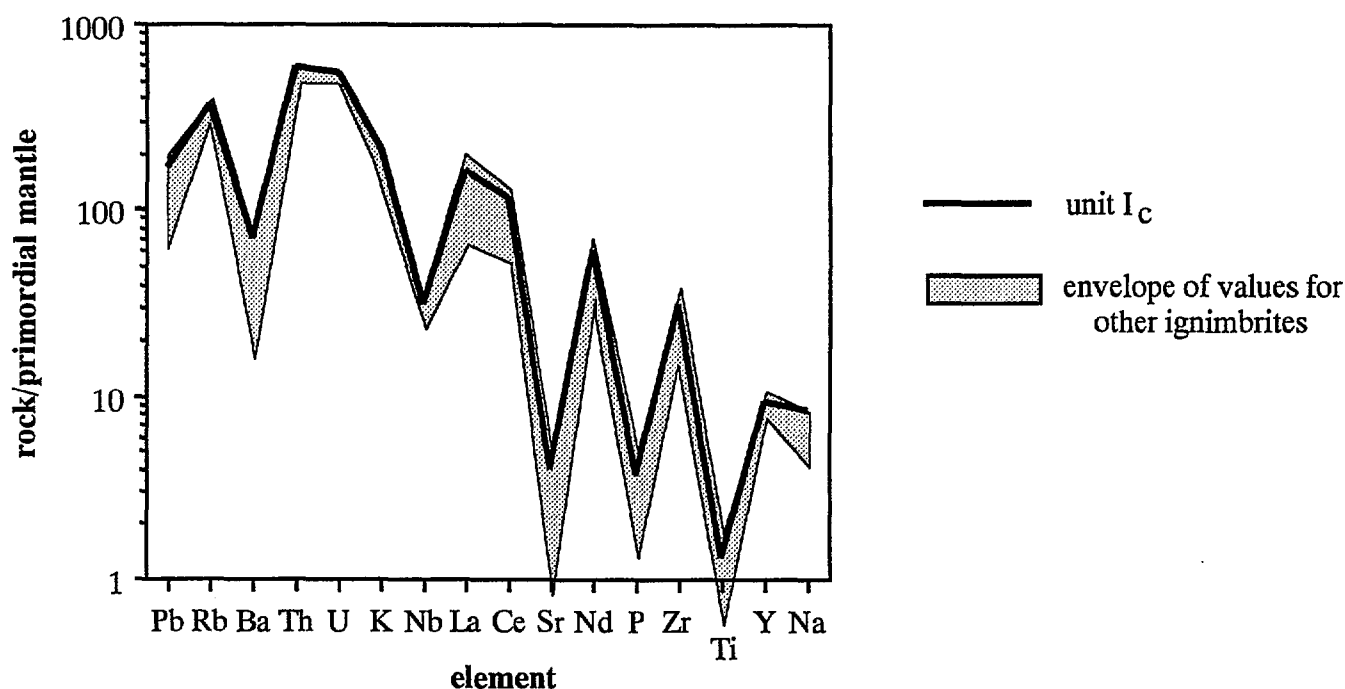


**Figure 7.9:** Extended trace element diagram comparing unit I<sub>C</sub> with other ignimbrites of the Gimbat Ignimbrite Member. Note that unit I<sub>C</sub> plots as the least evolved end-member of the ignimbrite sequence.

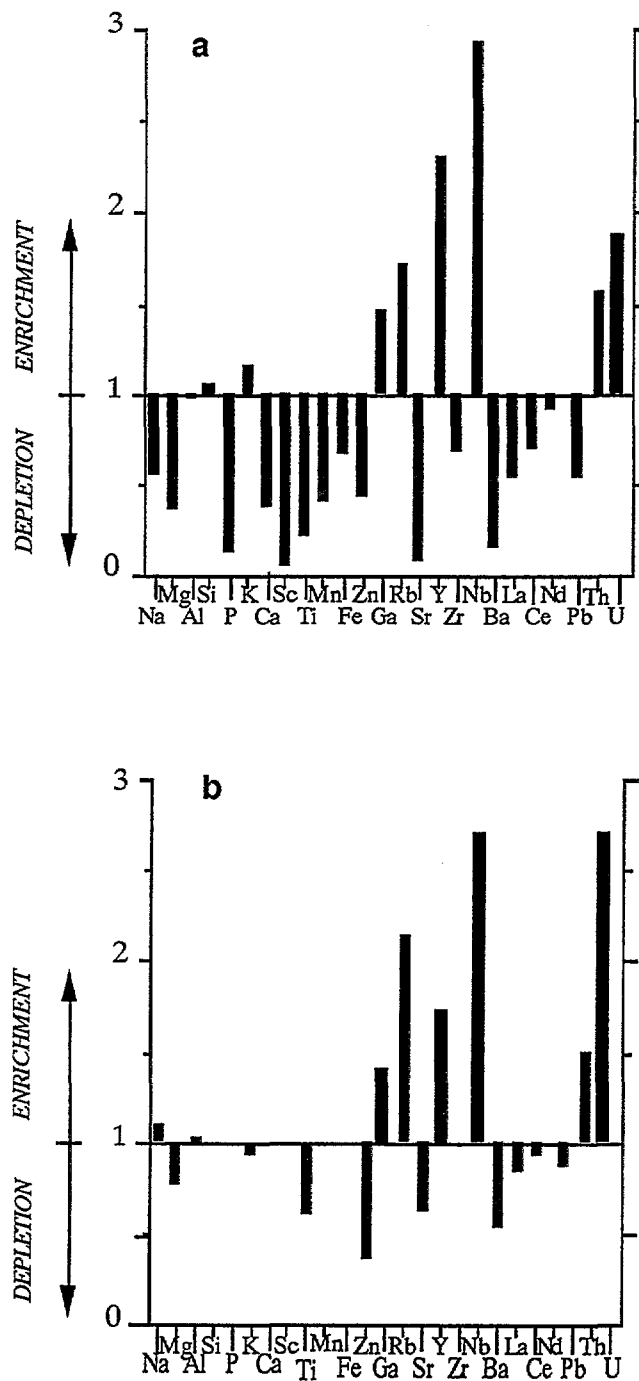


**Figure 7.10:** Enrichment/depletion diagrams (Hildreth 1981) showing (a) average major and trace element abundances for the Malone Creek Granite normalised to average composition of the Gimbat Ignimbrite Member and (b) the most fractionated (89126047) normalised to the least fractionated (81120019) sample of the Malone Creek Granite. This summarises the major and trace element variations that occur in the granite, which can be explained by fractional crystallisation.

fractionation may have occurred by crystal settling (Martin & Noakes, 1988), or by convective accretion of residual plagioclase and accessory phases, and early-formed phenocrysts to chamber walls so that these phases were locally concentrated within the magma chamber. The pyroclastic eruption resulting in the deposition of unit I<sub>C</sub>, would then have randomly tapped the section of the magma chamber where the less evolved phases concentrated, explaining the differences in composition and mineralogy.

A problem with this model is the depletion of MgO and elements compatible with MgO such as V, Sc and Cr in unit I<sub>C</sub>. If unit I<sub>C</sub> was tapping a concentration of early-formed crystals, the ferromagnesian mineral phases should also be concentrated, so that these values would be higher than in the 'normal' ignimbrites. These trends are largely controlled by dolerite lithic contamination, so depletion of these ferromagnesian elements in unit I<sub>C</sub> can be explained due to the much lower percentage of dolerite lithic contaminants in this unit.

### 7.5 COMPARISON WITH THE MALONE CREEK GRANITE

The Malone Creek Granite is a circular pluton which intrudes the Gimbat Ignimbrite Member, and the spatial relationship between the granite and ignimbrites is highly suggestive of a resurgent caldera complex. This section considers whether the Malone Creek Granite and Gimbat Ignimbrite Member could be genetically related, based on geochemical, isotopic and geochronological evidence.

Wyborn et al (1992) classify the Malone Creek Granite as a Proterozoic Anorogenic (Atype) granite of the type that is unrelated to earlier I-type granites, and its chemistry is similar to other granites of this category distributed throughout Australia, and shows the same enrichment of incompatible elements relative to earlier I-type granites (in this case, the Gimbat Ignimbrite Member).

The Malone Creek Granite plots as a high silica end member to the Gimbat Ignimbrite Member and has a very narrow range of SiO<sub>2</sub> values (1%). The granite has a high F content and contains visible fluorite. Relative to the Gimbat Ignimbrite Member it is enriched in incompatible elements such as Nb, Th, U, Y, Ga, and Rb. It is markedly depleted in Ba, Sr, Fe<sub>2</sub>O<sub>3</sub>TOT, V, Sc, Cr and P<sub>2</sub>O<sub>5</sub>, and less depleted in La, Ce, Pb, Zr, Zn, MgO and TiO<sub>2</sub> (Figs 7.4; 7.10a). Plotting all samples of the Malone Creek Granite, it also appears at first to be strongly enriched in K<sub>2</sub>O, but upon removal of samples affected by alteration (those with < 2% Na<sub>2</sub>O), this is seen to be an alteration effect, and K<sub>2</sub>O is only slightly enriched.

The Malone Creek Granite is not chemically zoned. Stuart-Smith et al (1988) mapped a concentric textural zoning within the pluton, but as these boundaries were probably photo-interpreted, the existence of this zoning is questionable. Certainly there is no difference in chemistry between the concentric zones. However, there is evidence that the granite has fractionated. K/Rb decreases with increasing SiO<sub>2</sub> and Fig. 7.10b summarises the chemical variations that occur as the granite evolves. Depletion in Ba, Sr and Pb may be explained by fractionation of plagioclase and K-feldspar, and enrichment of Ga, by fractionation of feldspars and quartz. Also, in high fluorine granites, Ga is concentrated in the melt by forming GaF<sup>3-6</sup> complexes (Collins et al, 1982). Depletion of Zr and LREE's is consistent with fractionation of zircon and monazite and allanite. Nb, F, Rb and the incompatible elements are strongly partitioned into the melt of felsic magmas, explaining their enrichment in the more differentiated samples.

Thus the geochemical data are consistent with the Malone Creek Granite having evolved by fractional crystallisation by the removal of K-feldspar, albite, some quartz, and accessory

phases from the melt. MgO and TiO<sub>2</sub> depletion suggest biotite and ilmenite may also control the fractionation trends. This interpretation is consistent with the mineral assemblage observed in the granite.

#### 7.6 ORIGIN OF THE MALONE CREEK GRANITE

Two possibilities are considered for the origin of the Malone Creek Granite. It may be the product of extreme fractional crystallisation of the ignimbrites, intruding as a discrete body of magma probably at depth, and probably after crystallisation of the Gimbat Ignimbrite Member was complete. The second possibility is that the granite and the ignimbrites represent separate batches of melt from different source compositions.

The Malone Creek Granite has a highly evolved composition relative to the Gimbat Ignimbrite Member, suggesting that if the granite and ignimbrites are related, the granite must have had considerable time to differentiate, and undergo extreme fractional crystallisation prior to emplacement. The K/Rb vs silica trends for granite and ignimbrite are continuous and may suggest a single melt which evolved firstly by restite separation and later by fractional crystallisation (Fig. 7.8). The continuous trends on a spider diagram also suggest the granite may be the product of extreme fractionation of the ignimbrites and major and trace element variations between the facies (Fig. 7.11) are consistent with fractionation by crystallisation of feldspars, quartz, zircon, apatite and other accessory phases, and a mafic phase. However, although most elemental abundances are compatible with plagioclase, mafic and minor phase fractionation to generate the granite from the ignimbrites, the REE data preclude such a simple origin. Relative to the Gimbat Ignimbrite Member, the Malone Creek Granite has a flatter REE pattern. It is depleted in LREE, but enriched in HREE and Y; a reversal of the ignimbrite trend. The LREE depletion could be the result of allanite and monazite fractionation (Miller & Mittlefehldt, 1982). Y and HREE enrichment could only be due to zircon accumulation, but this explanation conflicts with the lower Zr content of the Malone Creek Granite relative to the Gimbat Ignimbrite Member. In addition, trends of Y vs Ga/Al are the reverse for both suites. The ignimbrites become progressively depleted in Y and Ga/Al with differentiation, whereas values for the granite dramatically increase (Fig. 7.12). These features suggest that the Malone Creek Granite was not derived from the ignimbrites by simple fractional crystallisation. Finally, the best age constraint on the Malone Creek Granite is a maximum age of ~ 1820. (unpublished ion microprobe data) which makes it at least 10 Ma younger than the Gimbat Ignimbrite Member. The 10 Ma age difference between them, suggests that the Malone Creek Granite intruded the ignimbrites as a discrete body of magma, long after the ignimbrites has crystallised, and given the coarse, crystalline texture of the granite, at considerable depth.

The best explanation for the REE and incompatible element trends, is that the granite was derived from a source richer in HREE and Y and other incompatible elements, and more depleted in LREE, than the Gimbat Ignimbrite Member. Based on current models put forward to explain the origin of A-type granites, it may have been the refractory residue from which a previous melt phase (possibly represented by the ignimbrites) had been extracted, or a separate, enriched mantle-derived mafic source.

The first model is that of Collins et al, 1982 and Clemens et al 1986, and involves partial melting of a felsic granulitic source which is the residue remaining in the lower crust after production of a previous felsic melt. The first melt to be extracted would be a minimum or near-minimum melt, formed under hydrous conditions, at relatively low temperatures (<850°C). The release of volatiles by the breakdown of biotite and amphibole initiates partial melting, of quartz+K-feldspar+plagioclase, which according to the restite model of White & Chappell (1977), produces an I-type magma consisting of unmelted residual material and felsic melt. The residue remaining in the lower crust after production of a minimum melt magma is a

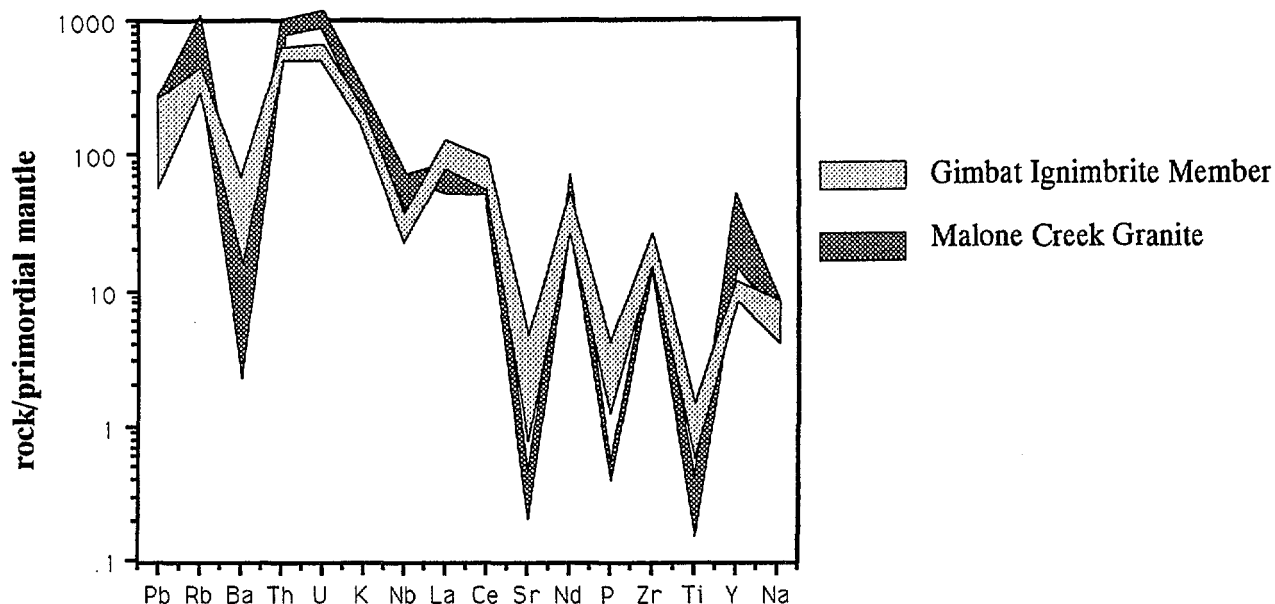


**Figure 7.11:** Extended trace element diagram comparing the Malone Creek Granite and the Gimbat Ignimbrite Member. Note the Malone Creek Granite has a more evolved composition.

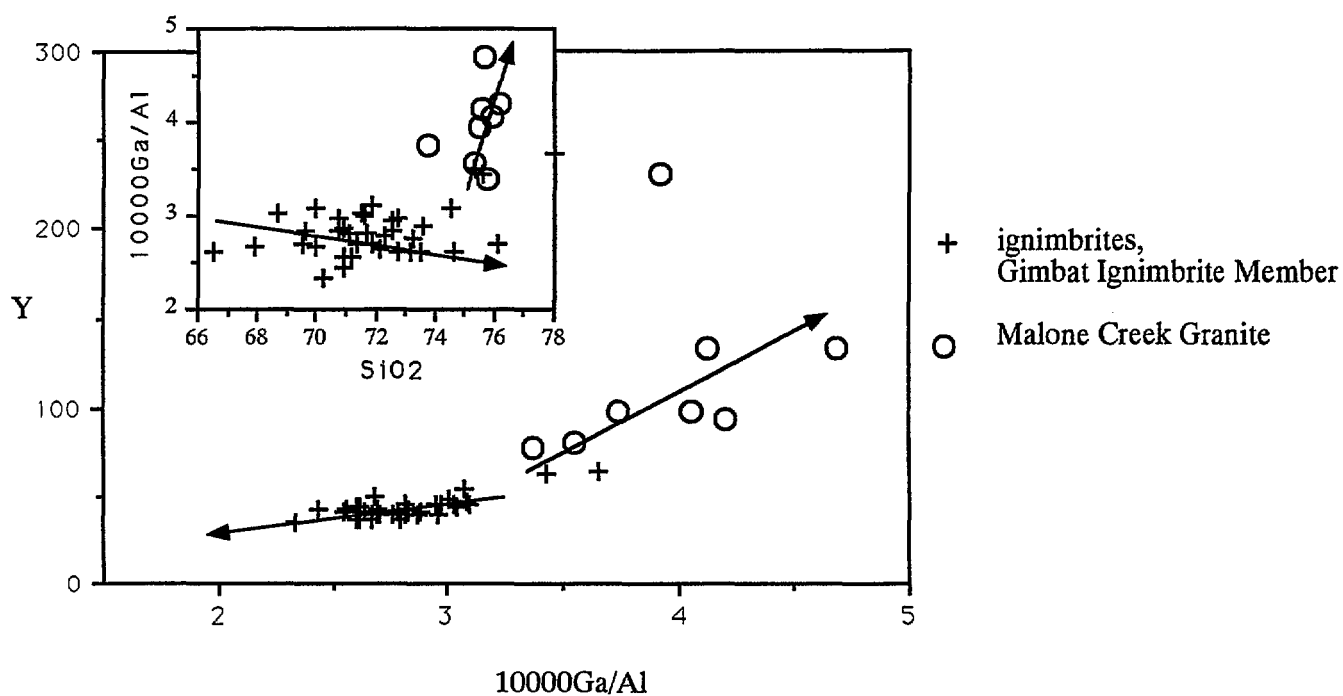


**Figure 7.12:** Ga/Al vs Y, showing the different differentiation trends for the Gimbat Ignimbrite Member and Malone Creek Granite.

granulite, consisting of quartz+K-feldspar+plagioclase+orthopyroxene±clinopyroxene. If amphibole±biotite remain, they are F-rich (Munoz & Ludington 1974). Other residuals include zircon±sphene±apatite (Collins et al 1982) and monazite±allanite (Miller & Mittlefehldt, 1982). Due to removal of H<sub>2</sub>O by the minimum melt, the residue would be anhydrous. Formation of a second melt from this residue must occur at higher temperatures, and the main volatile components would be F and Cl rather than H<sub>2</sub>O.

The chemistry of the two suites is compatible with this model. LREE enrichment in the ignimbrites suggests that the first melt extracted contained monazite±allanite as restite phases (Miller & Mittlefehldt, 1982). The residue would then be LREE depleted, explaining the flat REE pattern of the Malone Creek Granite, although this is in part due to fractionation of allanite and monazite in the late stages of crystallisation of the granite. F and Cl complexing in the melt produces a melt framework which favours the retention of high field strength cations and incompatible elements, explaining their strong enrichment in the Malone Creek Granite. The high Ga/Al ratio of the Malone Creek Granite is a diagnostic feature of A-type granites, and reflects preferential retention of anorthite in the in the source region, because Ga is excluded from the anorthite structure relative to Al (Goodman, 1972). Also, Ga is partitioned into the melt more readily than Al by forming GaF<sup>3</sup>-<sub>6</sub> complexes (Collins et al, 1982).

The second possibility is that the Malone Creek Granite was derived from high temperature melting of a source more mafic, (i.e. less fractionated) in composition than the ignimbrite source rock. A source with a higher mafic component would not yield a melt under minimum melt conditions. At higher temperatures, the hydrous minerals (F-rich amphibole and biotite) and trigger partial melting, to produce a melt with A-type affinities. Wyborn et al (1988) suggested the source may derived from a mantle region enriched in incompatible elements; that is, a fractionated mantle source. As discussed in more detail in Section, 7.9, this source may have been emplaced in the lower crust during a crustal underplating event between 2400 and 2000 Ma. Most of the source melted during the Australia-wide Barramundi Orogeny, between 1870-1830 Ma. Some, less fractionated parts did not melt until later extensional events (Wyborn et al, 1988).

## 7.7 COMPARISON WITH OTHER GRANITES

The only other felsic suites in the near vicinity of the Gimbat Ignimbrite Member are the type volcanics of the Pul Pul Rhyolite which outcrop in the South Alligator Valley to the northwest, and the Plum Tree Creek Volcanics and consanguinous Grace Creek Granite, which outcrop ~ 15 km to the south.

The geochemistry of the Gimbat Ignimbrite Member could not be compared with the lavas and ignimbrites in the type section of the Pul Pul Rhyolite, because all samples of the Pul Pul Rhyolite collected in the South Alligator Valley have been subjected to extreme alteration.

The Plum Tree Creek Volcanics and Grace Creek Granite have a less evolved composition than the Gimbat Ignimbrite Member, and differs petrographically in that the main phenocryst phases are plagioclase and K-feldspar, with mainly interstitial quartz. This contrasts with the Gimbat Ignimbrite Member, where quartz is a major phenocryst phase. A relationship between the Gimbat Ignimbrite Member and this suite is considered, because they may be derived from the same magma chamber, with the rhyolitic ignimbrites representing a crystal-poor silicic upper layer developed from the phenocryst-rich dacites of the Grace Creek Granite and Plum Tree Creek Volcanics. The segregation of silicic caps from magmas of dominantly intermediate compositions is a well-recognised style of compositional gradation (zonation) in magma chambers (Hildreth, 1981; eg Valley of Ten Thousand Smokes, Hildreth & Gruner, 1980;

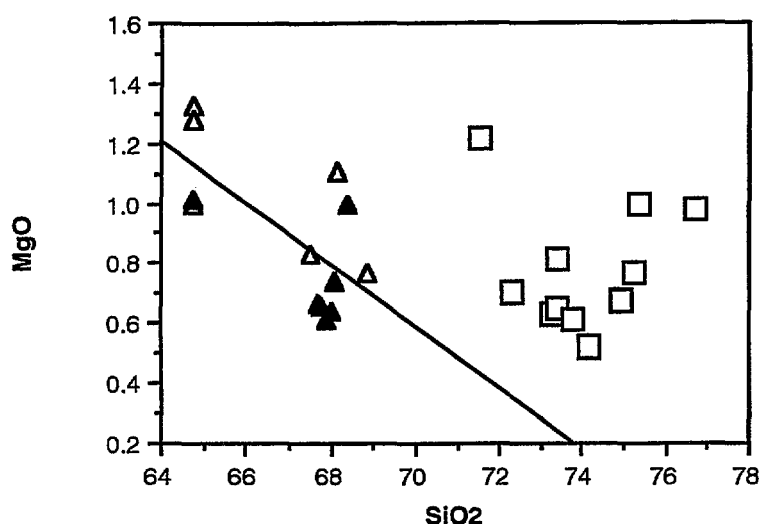


**Figure 7.13:** SiO<sub>2</sub> vs MgO plot comparing the MgO content of hand-picked ignimbrites of the Gimbat Ignimbrite Member, believed to represent original magmatic concentrations, with that of the Grace Creek Granite and Plum Tree Creek Volcanics. The plot shows a distinct enrichment of MgO in the ignimbrites compared with the dacitic suite.

Carpenter Ridge Tuff, Lipman 1975; Ammonia Tanks member of the Timber Mountain Tuff, Quinlivan and Byers, 1977).

The suite is metaluminous dacitic in composition, with SiO<sub>2</sub> values ranging between 65 and 70 %, and becomes progressively more evolved with increasing SiO<sub>2</sub> (lower total iron, MgO, CaO, TiO<sub>2</sub> and P<sub>2</sub>O<sub>5</sub>). The near constant K/Rb ratios of the Plum Tree Creek Volcanics and the Grace Creek Granite with increasing SiO<sub>2</sub>, and the fact that the volcanics have an identical composition to the co-magmatic granites, suggests they are derived from a restite-dominated pluton (Wyborn & Chappell, 1986), with the granite intruding its own volcanic ejecta.

The Plum Tree Creek Volcanics/Grace Creek Granite dacite suite and the rhyolitic ignimbrites of the Gimbat Ignimbrite Member are separated by a significant composition gap in silica, total iron and TiO<sub>2</sub> abundances (Fig. 7.4). Trends for MgO and elements whose behaviour is compatible with Mg such as Sc, Cr and Mn form separate trends that are at large angles to each other. These trends indicate distinct sources for the two suites, as it is impossible for the high MgO rhyolite to be derived by fractional crystallisation of a magma containing lower MgO contents. The higher MgO contents in the rhyolitic ignimbrites are not attributed in this case to contamination of the magma with doleritic lithic clasts, because the hand-picked ignimbrites are also enriched in MgO relative to the dacite suite (Fig. 7.13). Thus the Grace Creek Granite and Plum Tree Creek Volcanics must have evolved from a more iron-rich and MgO depleted source. The dacitic composition, high Ba and Sr contents in the dacites, and strong depletion of these elements with increasing SiO<sub>2</sub> are consistent with plagioclase-controlled fractionation, and the fact that feldspars are the main phenocryst phase, with quartz only forming interstitially. High P<sub>2</sub>O<sub>5</sub> and CaO contents relative to the Gimbat Ignimbrite Member suggest apatite is an accessory mineral in the dacites.

### 7.8 RB-SR AND SM-ND ISOTOPIC DATA

The isotopic characteristics of selected samples from the Gimbat Ignimbrite Member are presented in Table 7.1.  $\epsilon_{\text{Nd}}$  values are all negative and range from -3.1 to -4.9. These correspond with model source ages ( $T_{\text{Nd}}^{\text{CHUR}}$ ) between 2080 and 2365 Ma. Model ages based on depleted mantle values of DePaolo (1981), have slightly older values between 2328 and 2635 Ma. It is interesting to note that the quartz-feldspar porphyry chosen for isotopic analysis has  $\epsilon_{\text{Nd}}$  and  $T_{\text{Nd}}^{\text{CHUR}}$  values (-1.4 & 1949 Ma respectively) which fall well out of the ignimbrite's range. This suggests at least some of the quartz-feldspar porphyries are unrelated to the ignimbrites.

Isotopic analysis of a representative sample from the Malone Creek Granite yielded an initial  $\epsilon_{\text{Nd}}$  value of -5.93 (assuming it is the same age as the ignimbrites), which is similar to the ignimbrite values. However, the corresponding  $T_{\text{Nd}}^{\text{CHUR}}$  model age for the Malone Creek Granite is much older than model ages obtained for the ignimbrites (3693 Ma c.f. 2300-2600 Ga). It is likely however, that this older intersection with the depleted mantle curve is an aberration caused by the high Sm-Nd ratio of the Malone Creek Granite, and is geologically meaningless. Extreme fractionation and subsequent LREE depletion in the Malone Creek Granite has resulted in low LREE abundances and flat REE patterns. Miller & Mittlefehldt (1982) showed that this is the result of LREE partitioning into the accessory phases allanite and monazite in felsic magmas. When this occurs, the magma fractionates to form Sm/Nd ratios considerably higher than those of their source materials, which precludes calculation of meaningful source model ages. Thus the different  $T_{\text{Nd}}^{\text{CHUR}}$  model ages for the Malone Creek Granite and the Gimbat Ignimbrite Member do not preclude the possibility that the two units are derived from the same source region.

Representative analyses of the mafic volcanics that underlie the Gimbat Ignimbrite Member (Coronation Sandstone basalts) and dolerites which intrude the ignimbrites are LREE enriched and also have negative  $\epsilon_{\text{Nd}}$  values (similar in range to the ignimbrites) and older  $T_{\text{Nd}}^{\text{CHUR}}$  model ages. Sun (1985) recognised two types of trace element abundance patterns in Precambrian mafic volcanics of Australia. One type has flat patterns (LREE depleted), positive initial  $\epsilon_{\text{Nd}}$  values, and fall near the depleted mantle evolution curve. The second type is LREE enriched with depletions of Nb and Ti and commonly have negative  $\epsilon_{\text{Nd}}$  values (eg Middle Proterozoic Eastern Creek Volcanics, Qld; Hart Dolerites, N.T). The mafic volcanics in the study area fall into the second category. Sun (1985) suggests the negative  $\epsilon_{\text{Nd}}$  values and LREE enrichments may be a result of contamination of magmas derived from depleted convecting mantle with Archaean crust and/or lithosphere.

### 7.9 ORIGIN OF THE GIMBAT IGNIMBRITE MEMBER

As is the case for the majority of Proterozoic granites (Wyborn et al, 1988), the felsic rocks of the Gimbat Ignimbrite Member are characterised by a Sr-depleted, Y-undepleted trace element pattern (Fig. 7.11). This suggests that plagioclase was a stable phase in the source region, and that garnet was absent or only present in minor amounts (Tarney et al, 1987;

## 7. GEOCHEMISTRY AND MAGMA PETROGENESIS

sample no.	lithology	Sm	Nd	$^{143}\text{Sm}/^{144}\text{Nd}$	$^{143}/^{144}\text{m}$	$^{143}/^{144}\text{i}$	$\text{epsNd}(T)$	$T_{\text{nd}}(\text{chur})$	$T_{\text{nd}}(\text{dep})^*$
89123062	ignimbrite	13.8	90.9	0.0922	0.511207	0.510091	-3.2	2080	2328
89123063	ignimbrite	12.2	71.3	0.1039	0.511353	0.510096	-3.1	2103	2372
89123104	ignimbrite	8.6	42	0.1244	0.511511	0.510005	-4.9	2365	2635
89123153	ignimbrite	9.3	51.7	0.1098	0.511362	0.510033	-4.4	2229	2490
89123123	tz-fspar porph.	18.5	115.1	0.0973	0.511363	0.510185	-1.4	1949	2230
89123136	dolerite clast	11.4	58.4	0.1185	0.511456	0.510022	-4.6	2294	2564
89123001	basalt	6	31	0.1177	0.511368	0.509943	-6.1	2439	2677
89123014	basalt	9.3	54.7	0.1028	0.511277	0.510033	-4.4	2200	2450
89123038	dolerite	11.9	63.3	0.114	0.511412	0.510032	-4.4	2250	2517
89123105	dolerite	8.9	44.4	0.1212	0.511514	0.510046	-4.1	2260	2545
89126048#	granite	21.64	76.17	0.0733	0.512036	0.509978	-5.9	3659	3693

N.B: T is taken to be 1831 Ma

\* DePaolo 1981

# Malone Creek Granite

**Table 7.1:** Isotope data for the Gimbat Ignimbrite Member, Malone Creek Granite and local mafic volcanics and intrusives.

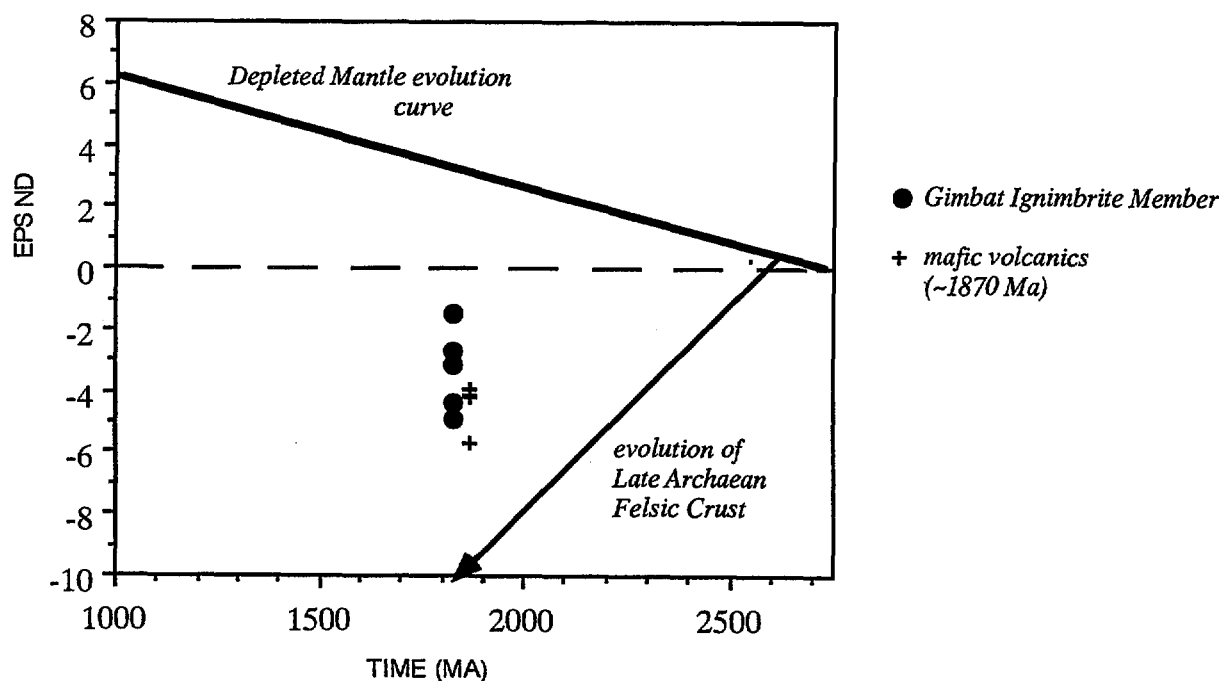


**Figure 7.14:**  $\epsilon_{\text{Nd}}$  vs crystallisation age of samples, showing negative  $\epsilon_{\text{Nd}}$  values for the Gimbat Ignimbrite Member with respect to depleted mantle at 1831 Ma.

Wyborn et al, 1988). This is supported by the REE patterns of the samples analysed. All samples have negative Eu anomalies, confirming the presence of plagioclase in the source region. The flat HREE patterns indicate that phases which strongly fractionate the heavy REE's with respect to the light REE's such as garnet and hornblende were absent from the source rock.

Melting in the plagioclase stability field suggests a lower crustal source region for the suite. In contrast, a garnet-rich source may suggest a deeper, high-pressure source region such as the upper mantle, and a Sr-undepleted, Y-depleted signature is typical of modern subduction settings (Wyborn et al, 1992), where melts are derived from the upper mantle region above the subducting slab.

Other geochemical and petrographic evidence also precludes a direct mantle origin for the Gimbat Ignimbrite Member. If the ignimbrites represent highly fractionated melts from mantle-derived basalts, a large volume of basaltic parent magma is required. However, basalts are volumetrically minor in the sequence, and in the Pine Creek Inlier as a whole. The ~ 1870 Ma Zamu Dolerite is a possible basaltic parent, but Sm-Nd model source ages of 2328-2635 Ma for the felsic volcanics are incompatible with derivation from this unit. The absence of rocks of intermediate composition (andesites and dacites) between the basaltic and rhyolitic end members of the suite also makes fractionation from a basaltic parent unlikely.

$\epsilon_{\text{Nd}}$  values for the Gimbat Ignimbrite Member are all negative and range from -3.1 to -4.9, corresponding with model source ages (based on depleted mantle values of McCulloch, 1987) between 2080 and 2365 Ma. These Sm-Nd model ages are 400-600 Ma older than the crystallisation age of the Gimbat Ignimbrite Member, as defined by U-Pb zircon ages ( $1831 \pm 11$  Ma; Section 2).

Based on a model of McCulloch (1987) in which the depleted mantle reservoir evolves to increasingly more positive  $\epsilon_{\text{Nd}}$  values with time, at 1830 Ma the mantle source reservoir should have an  $\epsilon_{\text{Nd}}$  value of ~ +3.5. In contrast  $\epsilon_{\text{Nd}}$  values for the Gimbat Ignimbrite Member and Malone Creek Granite are all negative and range between -3.1 and -5.9 (Table 7.1; Fig. 7.14). There are two ways of interpreting these results, and the discrepancy between  $T^{\text{Nd}}$  model ages and the crystallisation age of the samples. (1) That the older  $T^{\text{Nd}}$  model ages and negative  $\epsilon_{\text{Nd}}$  values reflect a source derived from the mixing of Archaean crustal material with a juvenile Proterozoic (1830 Ma) mantle-derived melt. (2) That the source had an extended crustal prehistory. i.e. the material was originally derived from the mantle at the time specified by the  $T^{\text{Nd}}$  ages but then resided in the lower crust for a short period prior to remelting to form the volcanics at 1830 Ma.

#### (1) Crustal contamination

A common explanation for the occurrence of  $\epsilon_{\text{Nd}}$  values which fall below the model mantle curve is contamination by Archaean crust (Nelson & DePaolo, 1985; Patchett & Arndt, 1986), and the assimilation of Archaean crustal components into Proterozoic orogenic terrains has been well illustrated near the margins of Archaean blocks (eg Fletcher et al, 1983). In this case however, large-scale assimilation of Archaean crust is not strongly supported by any other evidence. The range of  $\epsilon_{\text{Nd}}$  values implies assimilation of up to 30-60% of Archaean crust (of age 2500 Ma). However, U-Pb zircon studies have not revealed the presence of such a dominant Archaean component in the zircon population, which contains only rare inherited

Archaean zircons (section 2). In addition, it can be shown that mixing of Early Proterozoic sediments and contemporaneous mantle-derived mafic igneous rocks is unlikely to produce chemical compositions similar to the ignimbrite suite. Wyborn (1988) showed that the 1860 Ma I-type felsic volcanics (Nimbuwah Complex) of the Pine Creek Inlier could not be derived by mixing of Archaean crust and a contemporary Proterozoic mantle-derived source (represented by the Zamu Dolerite). This is also the case for the Gimbat Ignimbrite Member.

## (2) A Proterozoic underplating event

The isotopic data can be explained by an alternative model for Proterozoic crustal development, which has been developed by several workers for the Early Proterozoic of Northern Australia (Etheridge et al, 1987; McCulloch 1987; Wyborn, 1988). This evokes a two-stage model of origin, in which mantle-derived material is introduced into the lower crust at around 2400 Ma (McCulloch, 1987), and is later remelted and introduced into the upper crust at 1830 Ma. If the protolith is LREE enriched relative to the mantle source reservoir it will evolve to produce negative  $\epsilon_{Nd}$  values at the time of crystallisation. Wyborn et al, (1988) state that the source regions for Proterozoic granites are fractionated mafics, and enriched in incompatible elements (such as the LREE), indicating the source has evolved or fractionated relative to the mantle reservoir. The mantle-derived source was also enriched in  $K_2O$  and the incompatible elements Th, U, La Ce and Rb; a composition characteristic of this specific period in the evolution of the Australian crust (Wyborn, 1988; Wyborn et al, 1992).

Etheridge et al (1987) propose that the source material was emplaced in the lower crust during a major mantle underplating event in the Early Proterozoic, in which large volumes of incompatible element enriched mantle accreted to the base of the lower crust and then fractionated significantly. Underplating occurred as a result of small-scale convection of the upper mantle in the Early Proterozoic triggered mantle melting, underplating and continental extension above a polygonal array of upwelling zones (Etheridge et al, 1987). The more felsic or fractionated part of the underplate was then remelted during orogenesis (1880-1830 Ma) to produce felsic volcanic and granitic suites.

Isotopic analysis of a representative sample from the Malone Creek Granite yielded an initial  $\epsilon_{Nd}$  value of -5.9 which is close to the range of those for the Gimbat Ignimbrite Member. Thus it is likely that the granite was sourced from the same fractionated mantle-derived underplate.

The underplating model has significant implications for Proterozoic tectonics, and ties in well with the three tectonic stages recognised in the Pine Creek Inlier and most other Proterozoic basins in Australia; a lower rift phase (continental sediments and rift-related basalts), overlain by a shallow water thermal subsidence phase, followed by the onset of orogeny, which began with local increases in subsidence rates and deposition of a thick turbidite sequence (Needham et al, 1988).

The onset of mantle melting is considered to have occurred between 2400 and 2000 Ma, and continental rifting began between 1950 and 1900 Ma. Rift basins developed during continental extension which resulted from gravitational spreading of the areas that had been significantly thickened by underplating (Houseman & England, 1986). With time, the upper mantle cooled and mantle convection and continental extension terminated. Thermal relaxation allowed continued subsidence of continental crust for a few tens of million years, forming thick, intracratonic Early Proterozoic sedimentary basins such as the Pine Creek Geosyncline, across northern Australia (sag phase). It is possible that cooling of the lithosphere and enriched mantle underplate, and sediment loading during thermal subsidence triggered crustal-mantle delamination (Bird, 1978; 1979), and that lithospheric delamination then provided the driving

force for a compressional orogenic event (recorded throughout Northern Australia and termed the Barramundi Orogeny; Etheridge et al, 1987). This model explains the initial rapid subsidence and flyschoid sedimentation, and the intense thermal anomaly that accompanied the Barramundi orogeny. According to Bird and Baumgardner (1981), the asthenosphere above the delaminating plate convects, giving rise to steep thermal gradients in the lower crust, leading to a widespread melting event with partial melting of the accreted or underplated material forming I-type felsic magmas, emplaced during the 1880-1840 Ma volcano-plutonic event recorded in all the early sedimentary Proterozoic basins of Northern Australia.

This model is illustrated in Fig. 7.15. It is similar to models proposed by Kroner (1977; 1983; 1984), and differs from the conventional actualistic Wilson-cycle model in two ways. (1) Continental extension ceased prior to the formation of oceanic crust, so that the Proterozoic belts are ensialic. (2) Subduction of the lithospheric plate did not occur. Only the delaminated mantle underplate is subducted back into the mantle. Lithospheric delamination is considered to be a likely mechanism in the Proterozoic, because at this time, a higher heat-flow gradient and thinner lithosphere meant that the lithosphere was not as rigid as it is today. As the dense subcrustal lithosphere subsided into the mantle, the upper crust remained positively buoyant, resulting in delamination. Continued cooling of the earth accompanied by thickening and increased rigidity of the lithosphere lead to the present tectonic regime, with the onset of Wilson-cycle tectonics at about 1.0 Ga. At this time the upper and subcrustal lithosphere remained coupled, and upper crustal material began to subduct back into the mantle. Thus this model can be readily interpreted within a modern plate-tectonics framework, with some differences resulting from the higher heat-flow, and less rigid lithosphere present in Proterozoic and early Phanerozoic times.

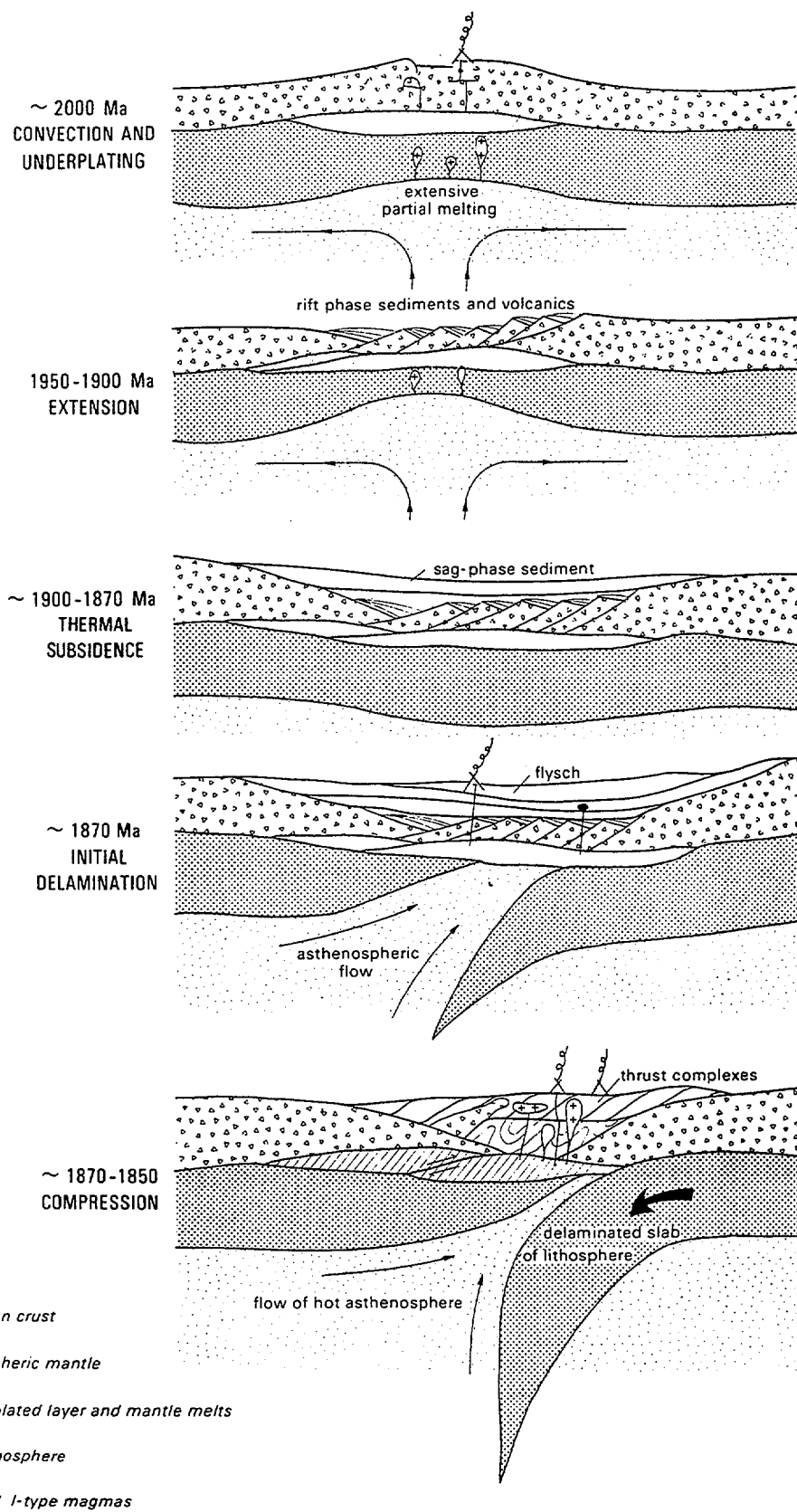


**Figure 7.15** Summary of working hypothesis for intracratonic basin development and orogeny in the early Proterozoic of northern Australia. Continental extension is driven by small-scale convection, and the subsequent orogeny by crust-mantle delamination.

(from Etheridge et al 1987)

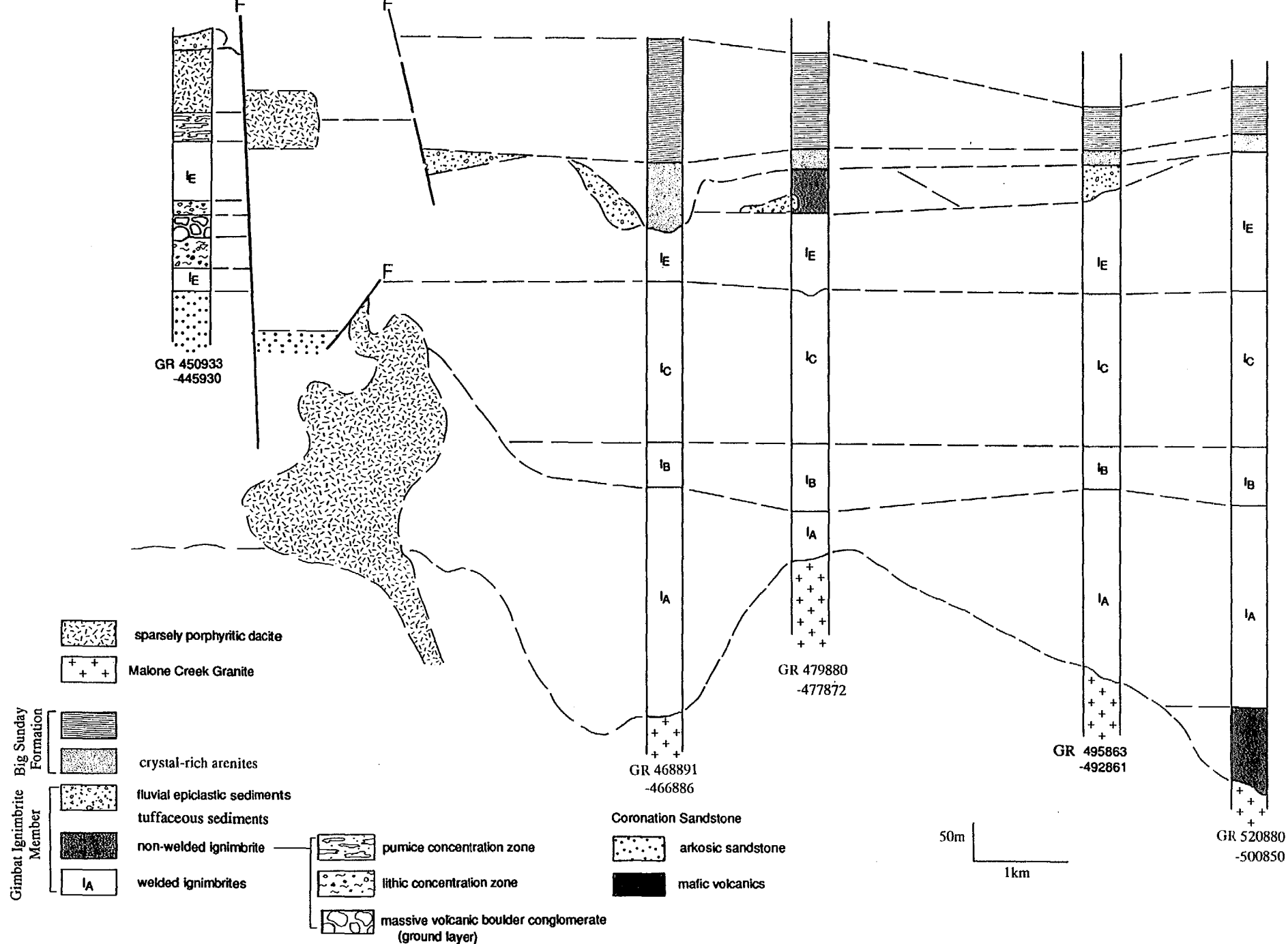


Figure 8.1: Stratigraphic profile showing correlations between measured sections through the Gimbat Ignimbrite Member.

## 8. PALAEOVOLCANOLOGY AND PALAEOENVIRONMENT

### 8.1 PALAEOENVIRONMENT OF THE GIMBAT IGNIMBRITE MEMBER AND BIG SUNDAY FORMATION

The abundance of welded ignimbrite and restricted fluvial deposits in the Gimbat Ignimbrite Member, indicates that volcanic activity took place in a palaeoenvironment that was dominantly subaerial. Unconformable stratigraphic relationships at the base of the Gimbat Ignimbrite Member suggest the ignimbrites infilled a palaeotopography or land-surface developed on fluvial sediments and basalts of the Coronation Sandstone (Figs 1.2: 1.3: 8.1: 8.2). Sedimentary facies of the Coronation Sandstone are consistent with those of braided river systems (Friedmann & Grotzinger, 1991), and they are interpreted to have partly filled a wide shallow graben, within which a strike-ridge topography developed in the area of the present South Alligator Valley (Needham & Stuart-Smith, 1985b). The graben is either a rift valley or extensional basin, genetically related to an extensional tectonic system which was also active during deposition of the Pine Creek Geosyncline sequence (Needham & Stuart-Smith, 1985b; Friedmann & Grotzinger, 1991), or a strike-slip pull-apart basin (Friedmann & Grotzinger, 1991). The volcanics of the Gimbat Ignimbrite Member extruded to infill this previously existing subaerial basin or valley.

By the time the sediments of the Big Sunday Formation were deposited the host environment was subaqueous, as indicated by the deposition of a relatively deep-water turbiditic sequence. This setting appears to have been geographically restricted however, suggesting a local lacustrine setting probably developed in a dominantly subaerial volcanic terrain. As discussed in detail in Section 5, the crystal-rich arenite facies underlying the turbidite sequence is interpreted to have resulted from subaerially-erupted pyroclastic flows entering the lake, suggesting subaerial volcanism was still ongoing in the near vicinity at the time this area was under subaqueous conditions. Palaeocurrent and petrologic data indicate that sediments of the Big Sunday Formation were largely sourced from the northwest end of the South Alligator Valley west of Saddle Ridge, where the Coronation Sandstone and Pine Creek Geosyncline Sequence were uplifted and denuded relative to the southeast (Friedmann & Grotzinger, 1991). This indicates that only 15 kms to the northwest of the subaqueous basin, subaerial conditions prevailed.

### 8.2 PALAEOGEOGRAPHY

In the previous sections, the Gimbat Ignimbrite Member was subdivided into facies, and facies characteristics were documented in detail. The mode of emplacement for each facies was determined, and genetic origins of each facies were deduced from their facies characteristics and relationships with other facies. In brief summary, the succession is the erosional relict of a small volcano-plutonic centre comprised mainly of pyroclastic flow deposits, which form a very thick volcanic sequence. The pyroclastic flow deposits are mainly densely-welded ignimbrites or ash-flow tuffs (based on the criteria of Ross & Smith 1961). A finer-grained, non-welded ignimbrite ~ 60m thick is preserved at the top of the thick ignimbrite sequence. Included in the pyroclastic flow deposits are Layer 2B lithic and pumice concentration zones which are vertically and laterally gradational with welded ignimbrite units, and one coarse lithic-boulder conglomerate interpreted to be a co-ignimbrite breccia, probably a ground layer. The thick sequence was rapidly deposited without welding or erosional breaks between successive depositional units to form a sequence at least 830 m thick. The geochemical and petrographic homogeneity of the ignimbrite units suggests they accumulated in a very short time period and are the product of a single eruption cycle. Intrusive and extrusive coherent rhyolite bodies also occur throughout the Gimbat Ignimbrite Member, but these are volumetrically subordinate to the welded ignimbrites. A small mafic component is represented by intrusive dolerites, and doleritic lithic fragments in the ignimbrites. Epiclastic deposits include intraformational fluvial facies associations in the Gimbat Ignimbrite Member, and

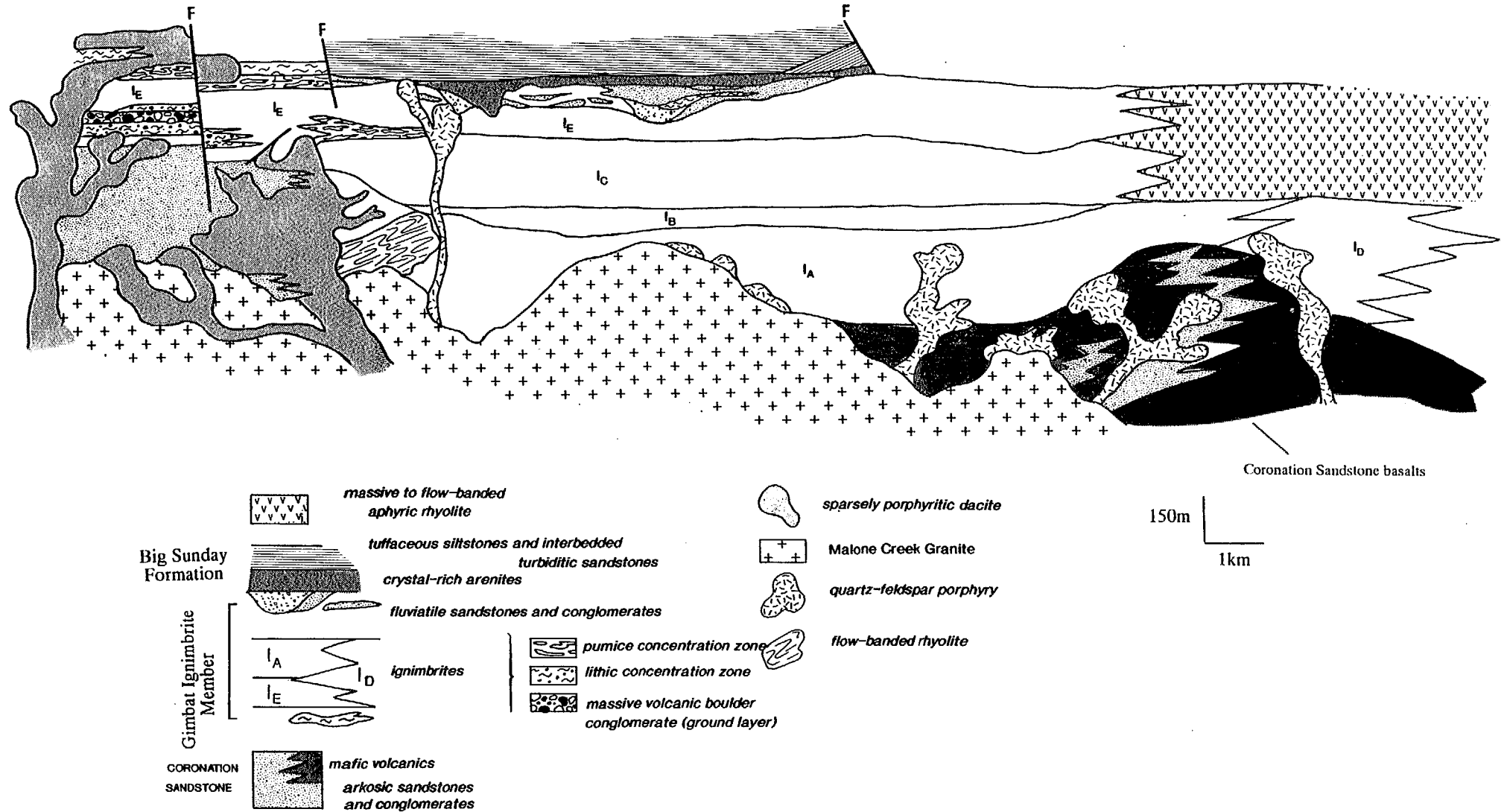


**Figure 8.2:** Schematic interactive stratigraphic column showing the distribution of facies and facies relationships for the Gimbat Ignimbrite Member.

the subaqueously deposited pyroclastic flows and lacustrine-deltaic facies associations in the overlying Big Sunday Formation.

To determine the palaeogeographic-palaeovolcanological setting of the Gimbat Ignimbrite Member, the possible situations in which such a thick, densely welded sequence of ignimbrite could be deposited are considered. Two possible host settings exist. The first possibility is that the ignimbrites are an intracaldera accumulation, as the thickness of the ignimbrite sequence is comparable to the intracaldera ignimbrites in modern silicic volcanic centres. The second is that they are a proximal outflow sequence deposited on the flanks of the eruptive centre to build up a low-angle volcanic/pyroclastic shield or cone, which ponded within a depression in the pre-existing topography to form a sequence much thicker than is typical of outflow ignimbrite sheets.

### 8.2.1 Proximity to Vent

In order to constrain the depositional environment of the sequence, its proximity to the eruption centre must be determined. To do this, the sequence is compared with a facies model for silicic volcanic centres devised by Cas & Wright (1987) and Orth et al (1989). The model recognises two broad associations of facies related to the distance from source vent, designated the proximal and distal facies. It is based on studies of modern silicic volcanic centres, in which the proximal facies usually corresponds to the intracaldera sequence, while the extra-caldera or outflow deposits are termed the distal facies. The facies characteristics and facies associations that are typical of each region are outlined in Table 8.1 and Fig. 8.3.

The facies associations of the Gimbat Ignimbrite Member would be classified as proximal in terms of this facies model (Table 8.1; Fig. 8.3). The ignimbrite sequence has many of the attributes of proximal facies such as extreme thickness, dense welding, coarse-grained lithic and pumice clasts, and the sequence contains proximal facies such as co-ignimbrite breccias and layer 2B concentration zones containing coarse lithic fragments. The ignimbrites are also associated with other facies that usually occur in a proximal setting, such as coherent rhyolite lava domes and intrusives, and high-energy fluvial deposits.

The pyroclastic flow deposits are high-grade ignimbrites which indicates they were emplaced at relatively high temperatures (Smith, 1960). This is consistent with deposition in a proximal setting, as pyroclastic flow deposits in the distal regions are thinner than their proximal counterparts and are emplaced at lower temperatures. They are subsequently less strongly welded, and non-welded ignimbrites are common.

Pyroclastic flows display a rapid decrease in clast size away from the vent (Sparks, 1976), and the high concentrations of coarse lithic and pumice fractions (averaging 5-30 cm in diameter) in the ignimbrites of the Gimbat Ignimbrite Member suggest the ignimbrites were deposited near vent. The homogeneous Layer 2B deposits have lithic concentrations of ~ 8-25%, and lithic clasts range in diameter from 0.5 to 25 cm. Lithic concentrations increase further to 20-25% in basal lithic concentration zones, and grainsizes of 50 cm are recorded. Pumice fragments vary considerably in size throughout the sequence, up to extremely coarse dimensions of 100 x 40 cm. In addition, the ignimbrite succession contains an extremely thick ground layer ~ 30 m thick, containing accessory lithic fragments ranging from 10-50 cm in diameter, and lithic boulders up to 2 m in diameter. A pyroclastic flow can segregate to form a well-developed flow head within a few kilometres of the vent (Druitt & Sparks, 1982; Suzuki-Kamata & Kamata, 1990) and the resultant ground layer can extend to nearly the distal limits of the ignimbrite (Walker et al, 1981; Suzuki-Kamata & Kamata, 1990). However, the ground layer systematically decreases in size and lithic content with distance from vent (Walker et al, 1981), and such a coarse-grained deposit as found in the Gimbat Ignimbrite Member, is likely to be located near vent. It would have thinned out considerably in the distal regions of the flow.

Proximal Facies Characteristics	Distal Facies
<ol style="list-style-type: none"> <li>1. Pyroclastic flows contain coarser lithic and pumice fragments near vent (Sparks 1976), and vents are often marked by coarse co-ignimbrite lag-breccias (Druitt &amp; Sparks 1982; Walker 1985). They thin towards the distal margins and the degree of welding becomes less. Intracaldera deposits can be densely welded, crystal-rich, voluminous outpourings of a single eruptive event (eg Fish Canyon Tuff; Self &amp; Wright 1983), forming deposits 200m to &gt; 2 km thick (Busby-Spera 1984; Lipman 1984), or a thick pile accumulated from a number of successive eruptions (eg Rio Caliente Ignimbrite; Wright 1981).</li> <li>2. Extrusive and intrusive lava domes can mark the vent site, and are generally present within, on the margin or just outside calderas (Walker 1984).</li> <li>3. Pyroclastic fall deposits contain coarse pumice and lithic fragments, and may be thick and welded (Cas &amp; Wright 1987).</li> <li>4. Pyroclastic surge deposits and associated airfall material can form at phreatomagmatic vents.</li> <li>5. Caldera margins are marked by strong relief, dykes, faults, unconformities and disconformities. Collapse breccias are present at some margins, formed by rock fall, slide or avalanche as the caldera collapses. Deposits include megabreccias, mudflows, debris flows and lahars (Walker 1985). They may interleave with the eruption-forming ignimbrites (Lipman 1976).</li> <li>6. Epiclastic deposits are commonly rich in texturally and compositionally immature volcanoclastic detritus. Environments range from short-lived erosional gullies containing fluvial deposits formed under high-energy conditions, to alluvial fan, deltaic and lacustrine systems.</li> <li>7. Hydrothermal systems may develop due to the high geothermal gradient in the caldera region. Features include hydrothermal alteration zones, hydraulic breccias, mineralisation (Henley &amp; Ellis 1983), and sinter deposits, sulphurous lakes and mudpools.</li> </ol>	<ol style="list-style-type: none"> <li>1. Pyroclastic flows are topographically controlled, contain smaller lithic and pumice clasts than proximal deposits, and are thinner and commonly non-welded.</li> <li>2. Pyroclastic fall deposits are more common and contain smaller and fewer lithic and pumice fragments than their proximal equivalents.</li> <li>3. Lenses of ground-surge and ash-cloud surge may be present above and below ignimbrite units (Fisher 1979; Wilson &amp; Walker 1982).</li> <li>4. There is a complex interplay between epiclastic sedimentation and ignimbrite deposition. Mature drainage patterns (fluvial and lacustrine systems) may be established in the low-slope distal environments. Palaeovalleys will be periodically choked with ignimbrite, then cleared by fluvial erosion to re-establish the pre-existing drainage pattern (McPhie 1983). This leads to repeated infilling and excavation of the same valley (Smith &amp; Bailey 1966).</li> </ol>

Table 8.1: A facies model comparing features characteristic of proximal and distal environments (based on Orth 1989)

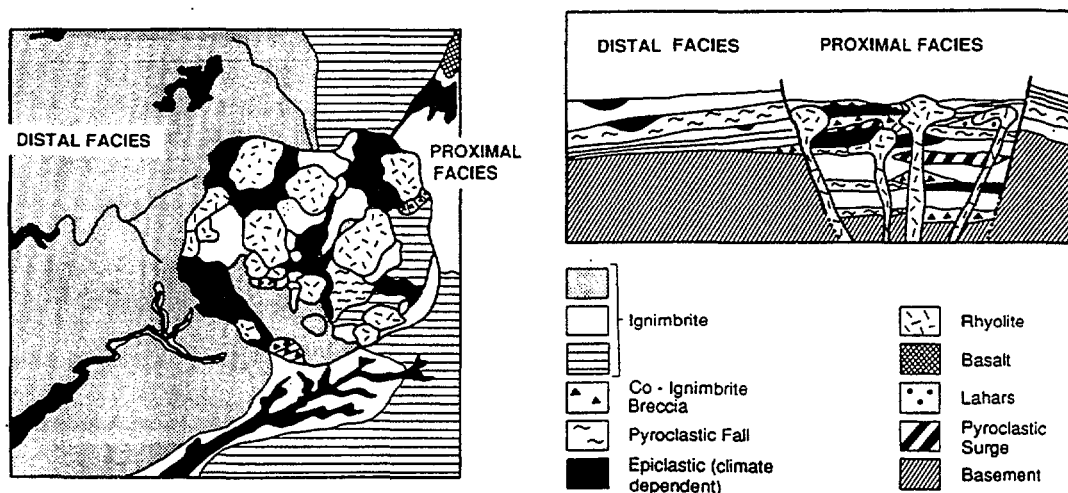


Figure 8.3: Schematic diagram of a modern terrestrial volcanic terrain showing distal and proximal facies associations (from Orth, 1989)

The composition of lithic fragments in the ignimbrite facies also suggest the volcanic vent was situated locally. Accessory lithic fragments include dolerite of Zamu Dolerite generation, metasediments derived from the Burrell Creek Formation and sandstone and basalt derived from the Coronation Sandstone. These lithologies outcrop locally, to the north and west of the ignimbrites, and undoubtedly underlie the ignimbrite succession (Fig. 4.7). If the vent had been situated further northwest for example, sediments of the Burrell Creek Formation would be absent from the lithic population and quartzites, banded ironstones and cherts of the Masson Formation, Mundogie Sandstone and Koolpin Formation would have comprised much of the lithic population.

The presence of coherent rhyolite lava flows and intrusive domes in the sequence is also consistent with deposition near the volcanic vent system, as rhyolite lavas and domes usually mark vent positions. Since rhyolite lavas generally only flow up to a few kilometres from their source vents, their position generally marks the position of eruption points. Even low viscosity silicic aphyric lavas generally only flow up to 6 km in distance (Bailey et al, 1976).

The epiclastic units associated with the ignimbrite sequence were deposited in high energy fluvial environments such as fluvial gullies formed between ignimbrite eruptions. On the distal flanks of a volcanic shield, lower slope angles would promote the development of more mature fluvial and lacustrine systems and well established drainage patterns. In distal settings there is a complex interplay between epiclastic sedimentation, volcanic eruption and contemporaneous erosion, which is not observed in the Gimbat Ignimbrite Member. The volume of epiclastic material is likely to be much greater in the distal setting. In the proximal environment, epiclastic processes are dominantly erosional, whereas in the distal setting they are depositional and ignimbrites are commonly intercalated with a sedimentary sequence flanking the volcanic shield (McPhie, 1983).

Caldera	Ignimbrite	Thickness of intracaldera sequence	Thickness of outflow sequence
<i>San Juan Mountains</i>			
La Garita	Fish Canyon Tuff	1.4 km	30-200 m <sup>†</sup>
Platoro	La Jara Canyon Member	> 800 m	50-100 m
"	Ojito Creek Member	180 m	15-30 m
Uncomphrage & San Juan	Sapinero Mesa Tuff	700 m	< 100 m
Bachelor	Carpenter Ridge Tuff	1.5 km	< 400 m
Bonanza	Bonanza Tuff	300 m	150 m
San Luis	Rat Creek Tuff	> 350 m	150-200 m
"	Nelson Mountain Tuff	> 1.5 km	300 m
Creede	Snowshoe Mountain Tuff	> 1.4 km	thin
<i>California</i>			
Long Valley	Bishop Tuff	1-1.5 km	200 m
<i>New Mexico</i>			
Valles	Bandalier Tuff	1.5 km	≤ 250 m
Mogollon	Cooney Tuff	700 m	30-60 m
<i>Western Mexico</i>			
Nuevo	Nuevo Tuff	> 800 m	20-200 m
Chupaderos	Aguila Fm	> 250 m	75 m
"	Santa Maria Fm	> 60 m	15 m
<i>Nevada</i>			
Claim Canyon	Paintbrush Tuff	> 2 km	420 m
Washburn	tuff of Oregon Canyon	400 m	≤ 100 m
Calavera	tuff of Double H	> 300 m	≤ 220 m
Long Ridge		> 300 m	150 m
Hoppins Peak	tuff of Hoppins Peak	> 350 m	≤ 90 m
<i>Trans-Pecos Texas</i>			
Infiernito	Buckshot Ignimbrite	800 m	< 20 m
<i>Utah</i>			
Three Creeks	Three Creeks Tuff (1)	> 200 m	100 m
"	Three Creeks Tuff (2)	> 500 m	200-250 m
Monroe Peak	Osiris Tuff	550 m	< 60 m
<i>NW Canadian Shield</i>			
Cornwall	Cornwall Tuff	> 1 km	< 60 m
<i>Arizona</i>			
Turkey Creek	Rhyolite Canyon Tuff	1.2 km	400 m
<i>Currabubula Formation (Late Carboniferous) NSW</i>			
	Cana Creek Tuff Member		50-100 m
	Iventure Ignimbrite Member		60 m
	Taggarts Mountain Ignimbrite Member		200 m
	Piallaway Trig Ignimbrite Member		180 m
	Plagyan Rhyolite		180 m
	Others		< 5 m

<sup>†</sup> locally up to 1.1 km

Table 8.2: A comparison of intracaldera and outflow ignimbrite thicknesses for several silicic volcanic centres. Also thicknesses for the outflow facies of the Currabubula Formation NSW (McPhie, 1983).

### 8.2.2 Interpretation as an Intracaldera setting

Given that the sequence is a proximal facies association, the possibility that it represents a caldera setting must be examined. The Gimbat Ignimbrite Member (850m) is comparable in thickness to intracaldera ignimbrites of modern silicic volcanic provinces (such as the San Juan volcanic field of the Western United States; Table 8.2), and it contains some features found in intracaldera ignimbrites (dense welding, well developed columnar joints, lithic-rich horizons, and an association with co-ignimbrite lag breccias).

A comparison of the sequence with the facies model of Orth et al (1989), shows that the combination of facies associations preserved in the Gimbat Ignimbrite Member is consistent with an intracaldera setting (Table 8.1; Fig. 8.3). In addition, the spatial relationship between the Gimbat Ignimbrite Member and the Malone Creek Granite is highly suggestive of a resurgent dome structure. Resurgent domes are characterised by radially outward-dipping ignimbrites and fill (Lipman, 1984) and in this case the ignimbrites strike around, and dip away from a circular pluton, which appears to have been the cause of domal uplift.

Although the facies associations of the Gimbat Ignimbrite Member are consistent with intracaldera facies associations, none of the features that would be conclusive proof of an intracaldera setting are present. There is no evidence that the ignimbrites infilled a steep-walled structural or topographic depression, such as strongly unconformable relationships between the ignimbrites and older units, or within the ignimbrite sequence, or marked thickness variations between intra- and extra-caldera ignimbrite units. Nor are collapse breccias intercalated with normal ignimbrite facies (Lipman, 1976;1984), which would infer the existence of a steep-walled, unstable caldera rim at the time of ignimbrite emplacement. Other margin facies such as ring-dyke or ring-fracture systems are also absent. Finally although the spatial relationship between the Gimbat Ignimbrite Member and the Malone Creek Granite is suggestive of resurgent doming, the geochemical and age discrepancy between the Malone Creek Granite and the ignimbrites of the Gimbat Ignimbrite Member (Section 7.6) suggest the granite is unrelated to the main ignimbrite-forming magmatic event, and intruded much later. This implies that the volcano-plutonic structure is not a resurgent caldera complex. In the absence of critical evidence that a caldera structure existed, it can only remain a possibility that the Gimbat Ignimbrite Member represents an intracaldera setting. An alternative model is therefore proposed.

### 8.2.3 Interpretation as a Proximal Shield Setting

An alternative to the model proposed in Section 8.2.2 is that the Gimbat Ignimbrite Member is a thick, proximal outflow sequence forming a low-angle shield to the volcanic centre.

Studies of Cainozoic silicic volcanic provinces in western North America and Mexico have shown that the most common vent-type is the caldera-style volcano. In the San Juan volcanic field, there is almost a 1:1 ratio of calderas to large-volume ignimbrites. This suggests that most ignimbrite eruptions are accompanied or closely followed by caldera collapse into the evacuated magma chamber (Smith & Bailey, 1968; Lipman, 1984). Lipman (1984) claims to know of no carefully studied caldera associated with large volume ignimbrites, that lacks a thick intracaldera ignimbrite, which implies that caldera collapse generally accompanies rather than follows the main phase of pyroclastic eruption. This also means that typically, intracaldera accumulations are an order of magnitude thicker than outflow sheets, and total thicknesses of greater than 1 km of intracaldera fill are not uncommon (Busby-Spera, 1984; Lipman, 1984). In contrast, outflow sheets are thin and widespread, averaging 10-100m and rarely exceeding 250 m in thickness (Table 8.2).

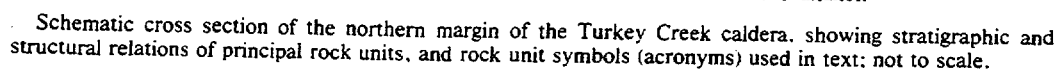
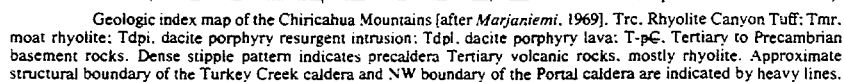


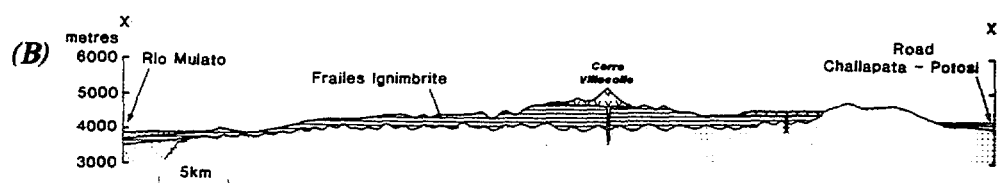
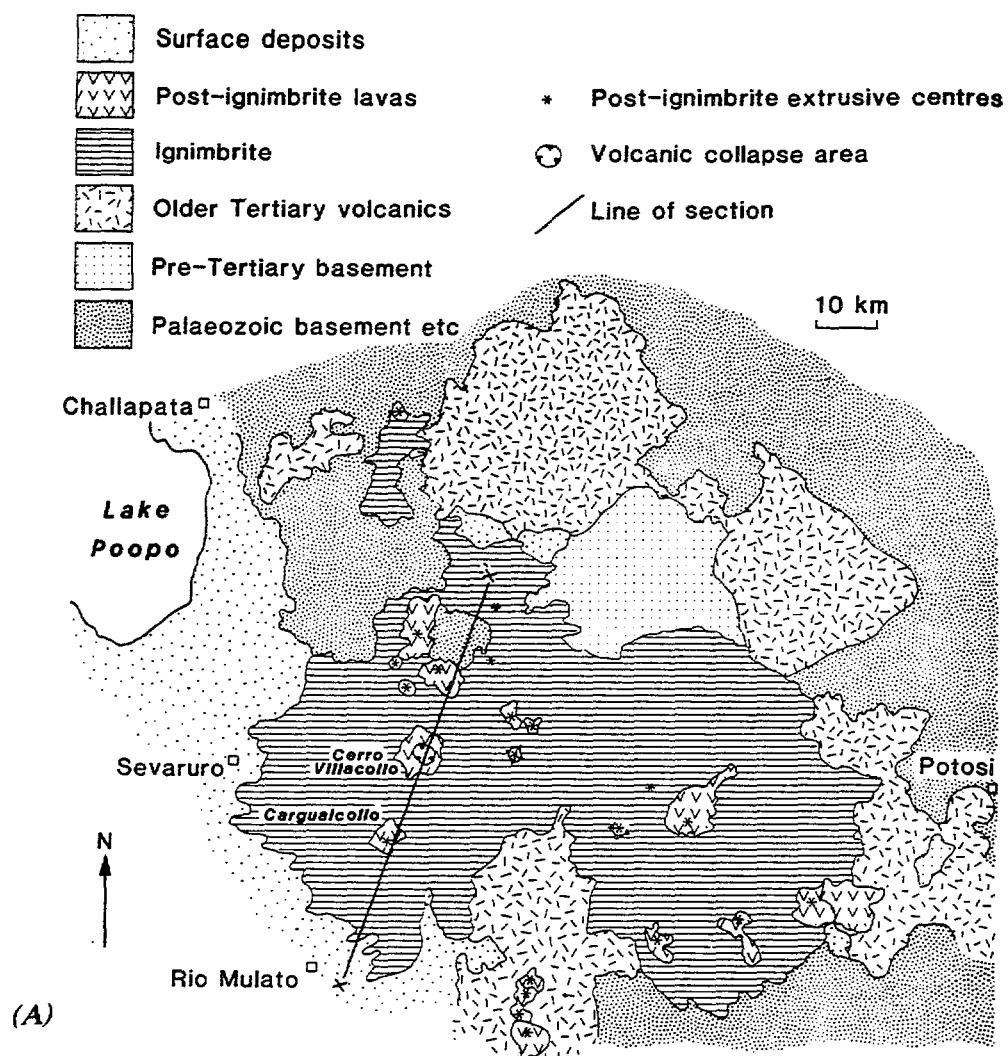
**Figure 8.4: Cross section through the Turkey Creek caldera (from DuBray & Pallister 1991).**

The preserved thickness of the Gimbat Ignimbrite Member is comparable to intracaldera thicknesses in modern silicic centres. Outflow sheets would rarely attain a thickness in the order of 830 m. This is not always the case however, and some situations may arise in the distal environment which complicate the assumption that a thick ignimbrite sequence is always a proximal facies. In large silicic volcanic fields comprised of several silicic centres such as the San Juan Volcanic Field of the western United States and the Taupo Volcanic Zone of New Zealand, the shield areas of several volcanic centres can overlap, accumulating thick outflow successions comprised of the distal products of several eruptive centres. Another possibility is that ignimbrites from one centre may fill in older calderas of another centre. For example the outflow sheet of the Fish Canyon Tuff generally ranges between 30-200 m, but reaches local thicknesses of 1100 m where it infills a pre-existing caldera and 500 m in a localised downfaulted block (Lipman, 1975; 1984). Neither scenario is likely in the case of the Gimbat Ignimbrite Member, because there is no evidence that the sequence forms part of a larger volcanic field. Volcanic activity appears to be restricted to an isolated volcanic centre which erupted in a relatively small sedimentary basin. It is possible however, that the outflow ignimbrite accumulated in a palaeovalley or topographic depression in the pre-existing land surface, and this is suggested by the unconformable relationship between the ignimbrites and the underlying Coronation Sandstone. This situation has an analogy in the outflow facies of the Rhyolite Canyon Tuff of the Turkey Creek Caldera, which accumulated in palaeobasins to the north and south of the caldera, reaching a maximum thickness of 400 m at Sugarloaf Mountain to the North (DuBray & Pallister, 1991; Fig. 8.4).

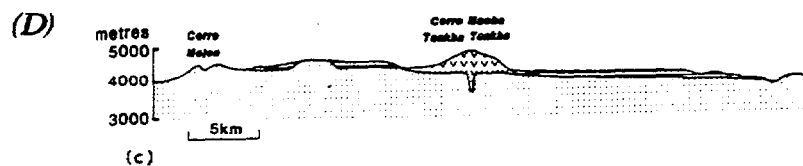
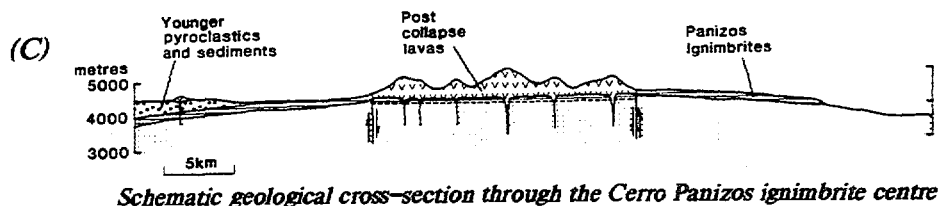
The assumption that outflow sequences are relatively thin, is based on studies of the large silicic centres of the San Juan Volcanic Field, where the great differences in thickness between the outflow sheets and intracaldera accumulations is due to ponding of much of the volcanic ejecta within the concurrently-forming caldera depression. It is conceivable however, that not all ignimbrite eruptions culminate in subsidence and the formation of a caldera structure, or that caldera collapse may follow rather than accompany major pyroclastic eruptions. In these cases, a more even distribution of pyroclastic material in the proximal and distal regions would be expected, as more material is released into the outflow region, and the intracaldera ignimbrite pile will show no thickening relative to the outflow sheet (eg Cochetopa Park Caldera, Steven & Lipman 1976).

Baker (1981) identified a wide variety of Cainozoic ignimbrite centres in the Central Andes, and found that not all ignimbrite centres have well-defined calderas. Silicic centres include partial or total caldera structures, some of which have resurgent centres, low angle shield structures which may have a central intrusive dome, and more widely dispersed ignimbrite sheets. In silicic centres where caldera collapse did not occur, a thick, even distribution of ignimbrite infilled pre-existing topography to build up a shield structure with slope angles of approximately  $1-3^{\circ}$ , surrounding the eruption centre (Baker, 1981; Fig. 8.5). The thickness profiles of the ignimbrite sheets depend on the yield strength or aspect ratio (Walker, 1973) of the pyroclastic flow, and the effects of pre-existing topography. The thickness of the Frailles Ignimbrite (Baker, 1981; Fig. 8.5a) varies from < 100 m over buried hills to over 900 m in buried valleys, indicating that ignimbrite successions can attain thicknesses comparable to the Gimbat Ignimbrite Member.

It is difficult to propose a model for a proximal shield setting, because few outflow regions have been studied in detail for comparison. Studies of Cainozoic silicic centres tend to focus on the intracaldera-fill sequences and their implications for caldera formation. This is partly due to the poor preservation of outflow sheets, which are typically non-welded and less resistant to erosion. Outflow sheets are rarely preserved in ancient successions. McPhie (1983) however, interpreted the Late Carboniferous Currabubula Formation as an outflow succession. The



(a) Geological sketch map of the Frailes Ignimbrite Plateau. (b) Schematic geological cross-section through the western half of the plateau.



Schematic geological cross-section through the Morococala Ignimbrite Plateau

Figure 8.5: Cross section through shield volcanoes of the central Andes (from Baker 1981).

Currabubula Formation is a moderately thick accumulation of ignimbrites (minimum thickness = 630 m; Table 8.2) which is comparable in thickness to the Gimbat Ignimbrite Member. McPhie (1983) interpreted the palaeoenvironment to be a distal ring-plain setting. The absence of coherent rhyolite facies and of proximal facies indicators, and the intercalation of ignimbrites within a sedimentary sequence implied a setting distal from the source vent. This distal setting is characterised by a complex interplay between sedimentation and volcanism and contemporaneous erosion. Palaeovalleys are repeatedly infilled by ignimbrites and excavated by fluvial processes as drainage systems are disturbed by eruptions then re-establish themselves (eg Valles Caldera, Smith & Bailey 1966; Vulsini Volcano, Sparks 1975).

By comparison, the Gimbat Ignimbrite Member is more proximal in character and consistent with a setting in the more proximal regions of a shield or ring-plain. Ignimbrites have well developed welding and coarse lithic fragments, and are associated with other proximal facies such as co-ignimbrite breccias and coherent rhyolite flows and domes. The pattern of sedimentation is markedly different to that of the Currabubula Formation, with volcanic sediments deposited in short-lived erosional gullies, rather than a well-developed drainage system being evident.

#### *A Proximal Shield Model*

It is plausible that the Gimbat Ignimbrite Member represents a proximal shield facies association flanking the summit of a volcano, which may have been a small caldera. A central vent-type eruption is favoured for the ignimbrite, and caldera collapse may have post-dated ignimbrite eruption, forming a small caldera at the summit of the volcanic shield. However, the volcanic centre is not presently exposed, but must have been in the near vicinity of the currently preserved sequence. The caldera or volcanic centre may have been eroded away, or still be buried beneath the present land surface. Another possibility is that the centre was engulfed by the Malone Creek Granite as it intruded the structural weakness supplied by the volcanic edifice. This would imply that the volcanic centre was positioned where the Malone Creek Granite presently outcrops, an interpretation which is compatible with the proximal nature of the facies, and the composition of accessory lithic clasts within the ignimbrite units. These include Burrell Creek Formation, Zamu Dolerite and basalts and sandstones of the Coronation Sandstone, which all outcrop around the margins of the Malone Creek Granite.

Facies associated with the ignimbrite sequence can easily be accommodated by a proximal shield model, as illustrated in Fig. 8.6. Lava flows and domes often extrude on the flanks of a volcano just outside the caldera margins (Walker, 1984). The lake-deposited sediments of the Big Sunday Formation could have formed a palaeobasin marginal to the volcanic shield. Locally-derived volcanoclastic sediments would have accumulated in the basin as fluvial systems drained into the locally developed lake, which represented a local base level in the area.

#### **8.2.4 Conclusions**

The outcropping remnants of the Gimbat Ignimbrite Member have been identified as a proximal facies association and two models have been considered for its palaeovolcanological setting. The first interprets the Gimbat Ignimbrite Member as an intracaldera sequence. The second as a proximal shield sequence. There is an absence of facies that would positively identify the sequence as an intracaldera sequence, such as collapse breccias and ring intrusions. The stratigraphic relationships are highly suggestive of resurgent doming which would be strong evidence for an intracaldera setting if the situation was that of a subvolcanic pluton intruding its own volcanic ejecta. This is not the case however, and the Malone Creek Granite intruded the ignimbrites ~ 10 Ma after their deposition. It is unlikely that the Malone Creek Granite is part of the same magmatic event as the ignimbrites and even if it was, it would have

.....



.....

## 9. IMPLICATIONS FOR MINERALISATION

The new stratigraphic interpretations presented in this report have significant implications for the evaluation of mineral prospectivity in the region surrounding the Coronation Hill deposit. The original discovery announcement of the Au-Pt-Pd at Coronation Hill suggested that there were "clear inferences that the Au is related to subaerial acid volcanism and is of epithermal type" (Noranda, 1984). It was also inferred that the uranium mineralisation, although having the same focus and structural control, was as a result of a later uranium mineralising event (Noranda, 1984). As a result of this first description of the Coronation Hill deposit, felsic volcanics in the region were considered potential hosts for additional Au deposits in the region and the felsic volcanic succession to the southeast of Coronation Hill were considered highly prospective.

Subsequent, more detailed studies on the Coronation Hill deposit have shown that the Au-Pd-Pt and U mineralisation were all part of the one event, which is a variant on the unconformity-style of mineralisation typical of the Alligator Rivers region to the north (Carville et al, 1990; Carville et al, 1991; Wyborn, 1990; Wyborn et al, 1990). In addition, fluid inclusion studies have shown that the fluids associated with both the U and the Au-Pt-Pd mineralisation at Coronation Hill have  $\delta^{18}\text{O}$  values which are incompatible with a magmatic origin for these fluids. The age determinations on the Gimbat Ignimbrite Member also show that they are younger than the main felsic volcanic event at the Coronation Hill deposit, which is now interpreted to be older than the 1870 Ma unconformity (Carville et al, 1991).

The recognition that the crystallisation of these volcanics has been dominated by restite-separation also downgrades their potential for hosting mineralisation. As pointed out by Whalen et al (1982) restite-rich systems cannot give a greater concentration of any element than that concentrated in the initial melt or the restite component. In contrast, convective fractionation provides a better mechanism whereby elements, particularly those of economic importance can be concentrated. Thus the Gimbat Ignimbrite Member is considered unlikely to host any epithermal mineralisation related to the time of emplacement. There are also no alteration zones apart from those related to the Palette Fault system which imply that the volcanics have not been affected by fluids associated with younger mineralising events. This has also been verified by stream sediment surveys which showed no significant anomalies for Au, Pt and Pd over the distribution of the volcanics of the Gimbat Ignimbrite Member: in contrast significant Au, Pd, Pt anomalies were always located in the vicinity of the unconformity (Cruikshank et al, 1992; Leckie, 1988; Leaman & Jurica, 1987).

## REFERENCES

---

- Allen, J.R.L. 1970. *Physical processes of sedimentation: - an introduction*. London: Allen and Unwin. 248 p.
- Bailes, A.H. 1980. Origin of Early Proterozoic volcanoclastic turbidites, south margin of the Kiseeynew sedimentary gneiss belt, File Lake Manitoba. *Precambrian Res.* 12: 197-225.
- Bailey, R.A., Dalrymple, G.B., and Lanphere, M.A. 1976. Volcanism, structure and geochronology of Long Valley Caldera, Mono County, California. *J. Geophys. Res.* 81: 725-744.
- Baker, M.C.W. 1981. The nature and distribution of Upper Cenozoic ignimbrite centres in the central Andes. *J. Volcanol. Geotherm. Res.* 11: 293-315.
- Bird, P. 1978. Initiation of intracontinental subduction in the Himalaya. *J. Geophys. Res.* 83: 4975-4987.
- Bird, P. 1979. Continental delamination and the Colorado Plateau. *J. Geophys. Res.* 84: 7561-7571.
- Bird, P., and Baumgardner, J. 1981. Steady propagation of delamination events. *J. Geophys. Res.* 86: 4891-4903.
- Blake, D.H. 1966. The net-veined complex of the Austurhorn intrusion, southeastern Iceland. *J. Geol.* 74: 891-907.
- Blake, D.H. 1981. Intrusive felsic-mafic net-veined complexes in north Queensland. *BMR Journal of Australian Geology and Geophysics.* 6: 95-99.
- Blake, D.H., Elwell, R.W.D., Gibson, I.L., Skelhorn, R.R., and Walker, G.P.L. 1965. Some relationships resulting from the intimate association of acid and basic magmas. *Quarterly Journal of the Geological Society of London.* 121: 31-49.
- Bouma, A.H. 1962. *Sedimentology of some flysch deposits*. Amsterdam: Elsevier.
- Brenchley, P.J. and Pickerell R.K. 1980. Shallow subtidal sediments of Soudleyan (Caradoc) age in Berwyn Hills, North Wales, and their palaeogeographic context. *Proc. Geol. Assoc.* 91: 177-197.
- Bryan, R. 1962. Lower Proterozoic basic intrusive rocks of the Katherine-Darwin area, Northern Territory. *Bureau of Mineral Resources, Australia. Record* 1962/7.
- Busby-Spera, C. 1984. Large-volume rhyolite ash-flow eruptions and submarine caldera collapse in the lower Mesozoic Sierra Nevada, California. *J. Geophys. Res.* 89: 8417-8427.
- Byers, F.M. Jr, Carr, W.J., Orkitt, P.P., Quinlivan, W.D., and Sargent, K.A. 1976. Volcanic suites and related cauldrons of Timber Mountain - Oasis Valley Caldera Complex, southern Nevada. *US Geol Surv. Prof. Pap.* no. 919.
- Carey, S.N., and Sigurdsson, H. 1980. The Roseau Ash: deep-sea tephra deposits from a major eruption on Dominica, Lesser Antilles arc. *J. Volcanol. Geotherm. Res.* 7: 67-86.
- Carville, D.P., Leckie, J.F., Moorhead, C.F., and Rayner, J.G. 1991. Coronation Hill Unconformity-related Gold-Platinum-Palladium Prospect, Northern Territory. *World Gold '91*.
- Carville, D.P., Leckie, J.F., Moorhead, C.F., Rayner, J.G., and Durbin, A.A. 1990. Coronation Hill Gold-Platinum-Palladium Deposit. In: *Geology of Mineral Deposits of Australia and Papua New Guinea*. Hughes, F.E. (Ed.) Monograph No. 14.
- Cas, R.A.F. 1979. Mass-flow arenites from a Palaeozoic interarc basin, New South Wales, Australia: mode and environment of emplacement. *J. Sed. Petrol.* 49: 29-44.

## REFERENCES

---

- Cas, R.A.F. 1983. Submarine 'crystal-tuffs': their origin using a Lower Devonian example from southeastern Australia. *Geol. Mag.* 120: 471-486.
- Cas, R.A.F., and Wright, J.V. 1987. *Volcanic succesions: modern and ancient. A geological approach to processes, products and successions*. London: Allen and Unwin.
- Cas, R.A.F., and Wright, J.V. 1991. Subaqueous pyroclastic flows and ignimbrites: an assessment. *Bull. Volcanol.* 53: 357-380.
- Chapin, C.E., and Elston, W.E. (eds) 1979. *Ash flow tuffs*. Geol. Soc. Am. Spec. Pap., no. 180.
- Chapin, C.E., and Lowell, G.R. 1979. Primary and secondary flow structures in ash-flow tuffs of the Gribbles run palaeovalley, Central Colorado. In Chapin and Elston (1979), 137-154.
- Chappell, B.W. 1984. Source rocks of I- and S-type granites in the Lachlan Fold Belt, southeastern Australia. *Philos. Trans. R. Soc. Lond.* A310: 693-707.
- Chappell, B.W., and White, A.J.R. 1974. Two contrasting granite types. *Pac. Geol.* 8:173-174.
- Chappell, B.W., and White, A.J.R. 1984. I-type and S-type granites in the Lachlan Fold Belt, southeastern Australia. In *Geology of granites and their Metallogenic relations. Proceedings of the International Symposium, Nanjing University, Nanjing, China*. Xu Kequin & Tu Guangchi (eds). 87-101. Beijing: Science Press.
- Chappell, B.W., White, A.J.R., and Wyborn, D. 1987. The importance of residual source material (restite) in granite petrogenesis. *J.Petrol.* 28: 1111-1138.
- Christiansen, R.L. 1979. Cooling units and composite sheets in relation to caldera structure. In Chapin and Elston (1979), 29-42.
- Clemens, J.D., Holloway, J.R., and White, A.J.R. 1986. Origin of A-type granites: experimental constraints. *Am.Mineral.* 71: 317-324.
- Coates, R.R., Hay, R.L., and Anderson, C.A. (eds) 1968. *Studies in volcanology (Howell Williams volume)*. *Geol Soc. Am. Mem.* no. 116.
- Cole, R.B., and DeCelles, P.G. 1991. Subaerial to submarine transitions in early Miocene pyroclastic flow deposits, southern San Joaquin basin, California. *Geol. Soc. Am. Bull.* 103: 221-235.
- Collins, W.J., Beams, S.D., White, A.J.R., and Chappell, B.W. 1982. Nature and origin of A-type granites with particular reference to southeastern Australia. *Contrib. Mineral. Petrol.* 80: 189-200.
- Compston, W., Williams, I.S., and Meyer, C. 1984. U-Pb geochronology of zircons from Lunar breccia 73217 using a sensitive high mass-resolution ion microprobe. *Proceedings of the 14th Lunar and Planet. Sci. Conference, Part 2, J.Geophys. Res. Supp.* 89: B525-B534.
- Cruikshank, B., Jagodzinski, E.A., and Pyke, J.G. 1992.
- Cumming, G.L., and Richards, J.R. 1975. Ore lead isotopes in a continuously changing earth. *Earth. Planet. Sci. Lett.* 28: 155-171.
- DePaolo, D.J. 1981. Neodymium isotopes in the Colorado Front Range and crust-mantle evolution in the Proterozoic. *Nature.* 291: 193-196.

## REFERENCES

---

- Dewey, J.F. 1963. The lower Palaeozoic stratigraphy of central Murrisk, County Mayo, Ireland, and the evolution of the South Mayo Trough. *Q. J. Geol. Soc. Lond.* 119: 313-343.
- Druitt, T.H., and Sparks, R.S.J. 1982. A proximal breccia facies on Santorini volcano, Greece. *J. Volcanol. Geotherm. Res.* 13: 147-171.
- Druitt, T.H., and Sparks, R.S.J. 1984. On the formation of calderas during ignimbrite eruptions. *Nature.* 310: 679-681.
- DuBray, E.A., and Pallister, J.S. 1991. An Ash-flow caldera in cross-section: Ongoing field and geochemical studies of the mid-Tertiary Turkey Creek Caldera, Chiricahau Mountains, SE Arizona. *J. Geophys. Res.* 96: 13435-13457.
- Eichelberger, J.C., and Koch, F.G. 1979. Lithic fragments in the Bandalier Tuff, Jemez Mountains, New Mexico. *J. Volcanol. Geotherm. Res.* 5: 115-134.
- Elston, W.E. 1984. Mid-Tertiary ash flow tuff cauldrons, southwestern New Mexico. *J. Geophys. Res.* 89: 8733-8750.
- Etheridge, M.A., Rutland, R.W.R., and Wyborn, L.A.I. 1987. Orogenesis and tectonic processes in the early to middle Proterozoic of Northern Australia. *Geodynamic Series, 17, Am. Geophys. Union, Washington DC*, 131-147.
- Ewart, A. 1979. A review of the mineralogy and geochemistry of Tertiary-Recent dacitic, latitic, rhyolitic and related salic volcanic rocks. In *Tronhjemitic, Dacites and related rocks*, F. Baker (ed.), 113-221. The Hague: Elsevier.
- Fisher, R.V. 1979. Models for pyroclastic surges and pyroclastic flows. *J. Volcanol. Geotherm. Res.* 6: 305-318.
- Fisher, R.V. 1989. Large volume, hot pyroclastic flows: If they can weld, how can they flow? *IAVCEI Continental Magmatism Abstracts* p 91.
- Fiske, R.S. 1963. Sibaqueous pyroclastic flows in the Ohanapecosh Formation, Washington. *Geol. Soc. Am. Bull.* 74: 391-406.
- Fiske, R.S., and Matsuda, T. 1964. Submarine equivalents of ash flows in the Tokiwa Formation, Japan. *Am. J. Sci.* 262: 76-106.
- Fletcher, I.R., Williams, S.J., Gee, R.D., and Rosman, K.J.R. 1983. Sm-Nd model ages across the margins of the Archaean Yilgarn Block, Western Australia; northwest transect into the Proterozoic Gascoyne Province. *J. Geol. Soc. Aust.* 30: 167-174.
- Folk, R.L. 1980. *Petrology of Sedimentary Rocks*. Austin: Hemphills.
- Francis, E.H., and Howells, M.F. 1973. Transgressive welded ash-flow tuffs among Ordovician sediments of N.E. Snowdonia. *J. Geol. Soc. Lond.* 140: 165-183.
- Friedmann, S.J., and Grotzinger, J.P. 1991. Stratigraphy, Sedimentology and Tectonic Evolution El Sherana and Edith River Groups, Northern Territory, Australia. *Bureau of Mineral Resources, Geology and Geophysics, Record* 1991/108.
- Glikson, A.Y. 1983. Precambrian Sial-Sima relations: Evidence for earth expansion. *Tectonophysics.* 63: 193-234.

## REFERENCES

---

- Goodman, R.J. 1972. The distribution of Ga and Rb in co-existing groundmass and phenocryst phases of some basic volcanic rocks. *Geochim. Cosmochim. Acta*. 36: 303-317.
- Henley, R.W., and Ellis, A.J. 1983. Geothermal systems ancient and modern: a geochemical review. *Earth Sci. Rev.* 19: 1-50.
- Henry, C.D., and Price, J.G. 1984. Variations in caldera development in the Tertiary volcanic field of Trand-Pecos Texas. *J. Geophys. Res.* 89: 8765-786.
- Hildebrand, R.S. 1984. Folded cauldrons of the Early Proterozoic Labine Group, northwestern Canadian Shield. *J. Geophys. Res.* 89: 8429-8440.
- Hildreth, E.W. 1981. Gradients in silicic magma chambers: Implications for lithospheric magmatism. *J. Geophys. Res.* 86: 10153-10192.
- Hildreth, W., and Grunder, A.L. 1980. The Valley-of-Ten-Thousand-Smokes Tuff, II, Compositional and isotopic variability of the ejecta. *Geol. Soc. Am. Abstr. Programs*. 12: 111.
- Houseman, G.A., and England, P.C. 1986. A dynamical model of lithosphere extension and sedimentary basin formation. *J. Geophys. Res.* 91: 719-729.
- Howells, M.F., Campbell, S.D.G., and Reedman, A.J. 1985. Isolated pods of subaqueous welded ash-flow tuff: a distal facies of the Capel Curig Volcanic Formation (Ordovician), North Wales. *Geol. Mag.* 122: 175-180.
- Howells, M.F., Leveridge, B.E., Addison, R., Evans, C.D.R., and Nutt, M.J.C. 1979. The Capel Curig Volcanic Formation Snowdonia, North Wales; variations in ash-flow tuffs related to emplacement environment. In *Caledonides of the British Isles - reviewed*, A.L. Harris, C.H. Holland and B.E. Leake (eds), 611-618. *Geol. Soc. Lond. Spec. Publ.*, no. 8.
- Howells, M.F., Leveridge, R., and Evans, C.D.R. 1973. Ordovician ash-flow tuffs in eastern Snowdonia. *Inst. Geol. Sci. Rep.* No. 73/3.
- Johnson, A.M. 1970. *Physical processes in geology*. San Francisco: Freeman, Cooper.
- Kano, K. 1990. An ash-flow tuff emplaced in shallow water, Early Miocene Koura Formation southwest Japan. *J. Volcanol. Geotherm. Res.* 40: 1-9.
- Kroner, A. 1977. Precambrian mobile belts of southern and eastern Africa - ancient sutures or sites of ensialic mobility? A case for crustal evolution towards plate tectonics. *Tectonophysics*. 40: 101-135.
- Kroner, A. 1983. Proterozoic mobile belts compatible with the plate tectonics concept. In: *Proterozoic Geology: selected Papers from an International Proterozoic Symposium*. G.M. Medaris, C.W. Byers and W.G. Shanks (eds). *Geol. Soc. Am. Mem.* 161: 59-74.
- Kroner, A. 1984. Evolution, growth and stabilization of the Precambrian lithosphere. In: *Structure and Evolution of the Continental Lithosphere*. Pollack, H.N., and Murthy, U.R. (eds). *Physics and Chemistry of the Earth*. 15: 69-106.
- Leaman, P., and Jurica, A. 1987. Reconnaissance stream sediment sampling for diamonds and metalliferous mineralisation, north Katherine River. *BHP Minerals confidential Company Report*. CR 5421.
- Leckie, J.F. 1988. Regional geochemical sampling programme within the proposed Conservation Zone, Kakadu Stage III, Northern Territory. *BHP Minerals confidential Company Report*. CR 5840.
-

## REFERENCES

---

- Lipman, P.W. 1975. Evolution of the Platoro caldera complex and related volcanic rocks, southeastern San Juan Mountains, Colorado. *US Geol Surv. Prof. Pap.* no. 852.
- Lipman, P.W. 1976. Caldera-collapse breccias in the western San Juan Mountains, Colorado. *Geol. Soc. Am. Bull.* 87: 1397-1410.
- Lipman, P.W., 1984. The roots of ash flow calderas in western North America: windows into the tops of granitic batholiths. *J. Geophys. Res.* 89: 8801-8841.
- Lipman, P.W., and Mullineaux (eds) 1981. The 1980 eruption of Mount St. Helens, Washington. *US Geol Surv. Prof. Pap.* no. 1250.
- Lipman, P.W., Self, S., and Heiken, G., (eds) 1984. Calderas and associated igneous rocks. *J. Geophys. Res.* 89 B10: 8219-8841.
- Lowe, D.R. 1982. Sediment gravity flows: II, depositional models with special reference to the deposits of high density turbidity currents. *J. Sed. Petrol.* 52: 279-297.
- Lowman, R.D.W., and Bloxam, T.W. 1981. The petrology of the Lower Palaeozoic Fishguard Volcanic Group and associated rocks E. of Fishguard, N. Pembrokeshire (Dyfed), South Wales. *J. Geol. Soc. Lond.* 138: 47-68.
- Martin, D., and Noakes, R. 1988. Crystal settling in a vigorously convecting magma chamber. *Nature.* 332: 534-536.
- McBirney, 1963. Factors governing the nature of submarine volcanism. *Bull. Volcanol.* 26: 455-469.
- McCulloch, M.T. 1987. Sm-Nd isotopic constraints on the evolution of Precambrian crust in the Australian continent. In: *Proterozoic Lithospheric Evolution*. Kroner (ed). *Geodynamic Series, 17, Am. Geophys. Union, Washington, DC.* pp 115-130.
- McPhie, J. 1983. Outflow ignimbrite sheets from Late Carboniferous calderas, Currabubula Formation, New South Wales, Australia. *Geol. Mag.* 120: 487-503.
- Mernagh, T.P., Leckie, J.F., Carville, D.P., Valenta, R.K., and Wyborn, L.A.I. 1992. A fluid inclusion study of mineralisation at Coronation Hill, Northern Territory, Australia. *11th Geol. Soc. Aust. Abstr.* 32: Ballarat 1992.
- Middleton, G.V., and Hampton, M.A. 1976. Subaqueous sediment transport and deposition by sediment gravity flows. In *Marine sediment transport and environmental management*, D.J. Stanley and D.J.P. Swift (eds), 197-218. New York: Wiley.
- Miller, C.F., and Mittlefehldt, D.W. 1982. Depletion of light rare-earth elements in felsic magmas. *Geology.* 10: 129-133.
- Munoz, and Ludington, S.D. 1974. Fluoride-hydroxyl exchange in biotite. *Am. J. Sci.* 274: 396-413.
- Needham, R.S., and Stuart-Smith, P.G. 1985a. Revised stratigraphic nomenclature and correlation of Early Proterozoic rocks of the Darwin-Katherine region, Northern Territory. *BMR Journal of Australian Geology and Geophysics.* 10: 121-131.
- Needham, R.S., and Stuart-Smith, P.G. 1985b. Stratigraphy and tectonics of the Early to Middle Proterozoic transition, Katherine-El Sherana area, Northern Territory. *Aust. Journal of Earth Sci.* 32: 219-230.
-

## REFERENCES

---

- Needham, R.S., and Stuart-Smith, P.G. 1987. Coronation Hill U-Au mine, South Alligator Valley, Northern Territory: an epigenetic sandstone-type deposit hosted by debris-flow conglomerate. *BMR Journal of Australian Geology and Geophysics*. 10: 121-131.
- Needham, R.S., Stuart-Smith, P.G., and Page, R.W. 1988. Tectonic evolution of the Pine Creek Inlier, Northern Territory. *Precambrian Res.* 40/41: 543-564.
- Nelson, B.K., and dePaolo, D.J. 1985. Rapid production of continental crust 1.7 to 1.9 b.y. ago: Nd isotopic evidence from the basement of the North America midcontinent. *Geol. Soc. Am. Bull.* 96:746-754.
- Noranda Pacific Limited Prospectus, 1984.
- Norrish, K., and Chappell, B.W. 1977. X-ray fluorescence spectrometry. In *Physical methods in determinative mineralogy*. Zussman, J (ed). 201-272. Academic Press, London.
- O'Connor, J.T. 1965. A classification of quartz rich igneous rocks based of feldspar ratios. *U.S. Geol. Surv. Prof. Pap.* 525B: 79-84.
- Oftedahl, C. 1978. Cauldrons of the Permian Oslo rift. *J. Volcanol. Geotherm. Res.* 3, 343-371.
- Orth, K., Cas, R.A.F., and Wright, J.V. 1989. Facies analysis and facies associations in the recognition of volcanic centres in silicic terranes: An example from the Early Devonian of Australia. *Aust. J. Earth. Sci.* 36: 167-188.
- Orton, G.J. 1988. Volcaniclastic sedimentation in a Caradocian marginal basin. *Unpub PhD thesis, Oxford*: 252 pp.
- Orton, G.J. 1989. Misbehavior of pyroclastic flows at the land-sea interface: a tale from Wales. *10th Geol. Soc. Aust. Abstract*, Hobart 1989.
- Page, R.W., and Williams, I.S. 1988. Age of the Barramundi Orogeny in Northern Australia by means of ion microprobe and conventional U-Pb zircon studies. *Precambrian Res.* 40/41: 21-36.
- Page, R.W., Compston, W., and Needham, R.S. 1980. Geochronology and evolution of the late-Archaeon basement and Proterozoic rocks in the Alligator Rivers Uranium Fields, Northern Territory, Australia. In: *Uranium in the Pine Creek Geosyncline*. Ferguson, J. & Golby, A.B. (eds). *International Atomic Energy Agency, Vienna* 39-68.
- Patchett, P.J., and Arndt, N. 1986. Continental crust genesis on earth: need for systematic Nd isotopic study of terrains 3.8 Ga to present. *Lunar Planet. Sci. (abstr.) XVII*. 650-651.
- Pickerell, R.K. and Brenchley P.J. 1979. Caradoc marine benthic communities in the South Berwyn Hills, North Wales. *Palaeontology*. 22: 229-264.
- Pudsey, C.J. 1984. Fluvial to marine transition in the Ordovician of Ireland - a humid-region fandelta? *J.Geol.* 19: 143-172.
- Quinlivan, W.D., and Byers, F.M. 1977. Chemical data and variation diagrams of igneous rocks from the Timber Mountain-Oasis Valley caldera complex, southern Nevada. *U.S.G.eol. Surv. Open-file Rep.* 77-724:9 pp.
- Rattigan, J.H., and Clark, A.B. 1955. The geology of the Katherine, Mt. Todd and Lewin Springs sheets, Northern Territory. *Bureau of Mineral Resources, Geology and Geophysics, Record* 1955/54.
-

## REFERENCES

---

- Reading, H.G. (ed.) 1986. *Sedimentary environments and facies*. Oxford: Blackwell Scientific.
- Reedman, A.J., Howells, M.F., Orton, G., Campbell, S.D.G. 1987. The Pitts Head Tuff Formation : a subaerial to submarine welded ash-flow tuff of Ordovician age, North Wales. *Geol. Mag.* 124: 427- 439.
- Ross, G.S., and Smith, R.L. 1961. Ash-flow tuffs, their origin, geological relations and identification. *US Geol. Surv. Prof. Pap.* no. 366.
- Schmincke, H.-U. and Swanson, D.A. 1967. Laminar viscous flowage structures in ash-flow tuffs from Gran Canaria, Canary Islands. *J. Geol.* 75: 641-664.
- Self, S., and Wright, J.V. 1983. Large wave-forms from the Fish Canyon Tuff, Colorado. *Geology*. 11: 443-446.
- Smith, R.L. 1960. *Zones and zonal variations in welded ash-flows*, 149-159. *US Geol. Surv. Prof. Pap.*, no. 354-F.
- Smith, R.L., 1979. Ash-flow magmatism. In *Chapin and Elston (1979)*, 5-27.
- Smith, R.L., and Bailey, R.A. 1966. The Bandalier Tuff, a study of ash-flow eruption cycles from zoned magma chambers. *Bull. Volcanol.* 29: 83-104.
- Smith, R.L., and Bailey, R.A. 1968. Resurgent cauldrons. In Coates *et al.* (1968). 153-210.
- Sparks, R.S.J. 1975. Stratigraphy and geology of the ignimbrites of Vulsini volcano, Central Italy. *Geol. Rundsch.* 64: 497-523.
- Sparks, R.S.J. 1976. Grain size variations in ignimbrites and implications for the transport of pyroclastic flows. *Sedimentology*. 23: 147-188.
- Sparks, R.S.J., and Walker, G.P.L. 1977. The significance of vitric-enriched air-fall ashes associated with crystal-enriched ignimbrites. *Journal of Volcanology and Geothermal Research*. 2: 329-341.
- Sparks, R.S.J., Huppert, H.E., and Turner, J.S. 1984. The fluid dynamics of evolving magma chambers. *Phil. Trans. Roy. Soc. Lond.* A310: 511-534.
- Sparks, R.S.J., Self, S., and Walker, G.P.L. 1973. Products of ignimbrite eruptions. *Geology*. 1: 115-118.
- Sparks, R.S.J., Sigurdsson, H., and Carey, S.N. 1980a. The entrance of pyroclastic flows into the sea. I. Oceanographic and geological evidence from Dominica, Lesser Antilles. *J. Volcanol. Geotherm. Res.* 7: 87-96.
- Sparks, R.S.J., Sigurdsson, H., and Carey, S.N. 1980b. The entrance of pyroclastic flows into the sea. II. Theoretical considerations on subaqueous emplacement and welding. *J. Volcanol. Geotherm. Res.* 7: 97-105.
- Sparks, S.J.R., Sigurdsson, H., and Wilson, L. 1977. Magma mixing; a mechanism for triggering acid explosive eruptions. *Nature*. 267: 315-318.
- Stanton, W.I. 1960. The lower Palaeozoic rocks of southwest Murrisk, Ireland. *J. Geol. Soc. Lond.* 116, 269-296.
- Steiger, R.H., and Jager, E. 1977. Subcommission of geochronology: Convention on the use of decay constants in geo- and cosmochronology. *Earth. Planet. Sci. Lett.* 36: 359-362.
- Steven, T.A., and Lipman, P.W. 1976. Calderas of the San Juan volcanic field, south-western Colorado. *US Geol. Surv. Prof. Pap.* no. 958.
- Stewart, J.R. 1965. Middle Proterozoic Volcanic Rocks in the Katherine-Darwin Area, Northern Territory. *Bureau of Mineral Resources, Geology and Geophysics, Report No.* 90.

## REFERENCES

---

- Streckeisen, A.L. 1973. Plutonic rocks. Classification and nomenclature recommended by the IUGS Subcommission on the systematics of igneous rocks. *Geotimes*. 18: 26-30.
- Stuart-Smith, P.G., Needham, R.S., & Bagas, L. 1988. Stow, Northern Territory (Sheet 5470). *Bureau of Mineral Resources, Australia, 1:100 000 Geological Map and Commentary*.
- Stuart-Smith, P.G., Wills, K., Crick, I.H., and Needham, R.S. 1980. Evolution of the Pine Creek Geosyncline. In *Uranium in the Pine Creek Geosyncline*. Ferguson, J., and Goleby, A.B. (eds), 273-285. Vienna: International Atomic Energy Agency.
- Sun, S-S. 1985. Chemical and Nd isotope study of late Archaean to Middle Proterozoic mafic volcanic rocks in northern Australia. In *Tectonics and Geochemistry of early to middle Proterozoic fold belts* Program & Abstracts, Darwin, Australia.
- Suzuki-Kamata, K., and Kamata, H. 1990. The proximal facies of the Tosu pyroclastic-flow deposit erupted from Aso caldera, Japan. *Bull. Volcanol.* 52: 325-333.
- Swanson, E.R., and McDowell, F.W. 1984. Calderas of the Sierra Madre Occidental volcanic field Western Mexico. *J. Geophys. Res.* 89: 8787-8799.
- Tarney, J. Wyborn, L.A.I., Sheraton, J.W., and Wyborn, D. 1987. Trace element differences between Archaean, Proterozoic and Phanerozoic crustal components - implications for crustal growth processes. In: *Workshop on the growth of continental crust*. Ashwal, L.D. (ed). *Lunar Planet. Inst. Tech. Report*. 88.02: 139-140.
- Taylor, S.R., and Gorton, M.P. 1977. Geochemical applications of spark source mass spectrometry. III. Element sensitivity, precision and accuracy. *Geochim. Cosmochim. Acta*. 41: 1375-1380.
- Taylor, S.R., and McLennan, S.M. 1981. The composition and evolution of the continental crust: rare earth element evidence from sedimentary rocks. *Phil. Trans. R. Soc. Lond.* A301: 381-399.
- Taylor, T.R., Vogel, T.A., and Wilband, J.T. 1980. The composite dikes at Mount Desert Island, Maine: an example of co-existing acidic and basic magmas. *J. Geol.* 88: 433-444.
- Walker, G.P.L. 1972. Crystal Concentration in ignimbrites. *Contrib. Mineral. Petrol.* 36: 135-146.
- Walker, G.P.L. 1973. Lengths of lava flows. *Philos Trans Roy. Soc. Lond. Ser. A*. 274: 107-118.
- Walker, G.P.L. 1974. Eruptive mechanisms in Iceland. In *Geodynamics of Iceland and the North Atlantic Area*, N.N. Kristjansson (ed.), 189-201. Reidel, Dordrecht, Holland.
- Walker, G.P.L. 1979. A volcanic ash generated explosions where ignimbrite entered the sea. *Nature*, 281: 642-646.
- Walker, G.P.L. 1983 Ignimbrite types and ignimbrite problems. *J. Volcanol. Geotherm. Res.* 17:65-88.
- Walker, G.P.L. 1985. Origin of Coarse lithic breccias near ignimbrite source vents. *J. Volcanol. Geotherm. Res.* 25: 157-171.
- Walker, G.P.L., and Skelhorn, R.R. 1966. Some association of acid and basic igneous rocks. *Earth-Science Reviews*. 2: 93-109.
- Walker, G.P.L., Self, S., and Froggatt, P.C. 1981. The ground layer of the Taupo Ignimbrite: a striking example of sedimentation from a pyroclastic flow. *J. Volcanol. Geotherm. Res.* 10: 1-11.

## REFERENCES

---

- Walker, G.P.L., Wilson, C.J.N., and Froggatt, P.C. 1980. Fines-depleted ignimbrite in New Zealand - the product of a turbulent pyroclastic flow. *Geology*. 8: 245-249.
- Walker, R.G. (ed.) 1984. *Facies Models*, 2nd edition. Geol. Assoc. Can., Repr. Ser. 1.
- Walker, R.G. 1978. Deep-water sandstone facies and ancient submarine fans: models for exploration for stratigraphic traps. *Am. Assoc. Petrol. Geol. Bull.* 62: 932-966.
- Walker, G.P.L. 1973. Length of Lava Flows. *Phil Trans R. Soc. Lond.* 274: 107-118.
- Walpole, B.P., Crohn, P.W., Dunn, P.R. and Randal, M.A. 1968. Geology of the Katherine-Darwin region, Northern Territory. *Bulletin of the Bureau of Mineral Resources, Australia*. 82.
- Warren, R.G., and Kamprad, J.L. 1990. Mineralogical, petrographic and geochemical studies in the South Alligator Region, Pine Creek Inlier, N.T. *Bureau of Mineral Resources, Geology and Geophysics, Record* 1990/54.
- Whalen, J.B., Currie, K.L., and Chappell, B.W. 1987. A-type granites: Geochemical characteristics, discrimination and petrogenesis. *Contrib. Mineral. Petrol.* 95: 407-419.
- White, A.J.R., and Chappell, B.W. 1977. Ultrametamorphism and granitoid genesis. *Tectonophysics*. 43: 7-22.
- Whitham, A.G. 1989. The behavior of subaerially produced pyroclastic flows in a subaqueous environment: evidence from the Roseau eruption, Dominica, West Indies. *Marine Geol.* 86: 27-40.
- Wiebe, R.A. 1980. Comingling of contrasted magmas in the plutonic environment: examples from the Nain anorthositic complex. *J. Geol.* 88: 197-209.
- Wilson, C.J.N. 1985. The Taupo eruption, New Zealand II. The Taupo Ignimbrite. *Phil. Trans. R. Soc. Lond.* A314: 229-310.
- Wilson, C.J.N., and Walker, G.P.L. 1982. Ignimbrite depositional facies: the anatomy of a pyroclastic flow. *J. Geol. Soc. Lond.* A314: 199-228.
- Wilson, I.H. 1978. Volcanism on a Proterozoic continental margin in northwestern Queensland. *BMR J. Aust. Geol. Geophys.* 8: 109-117.
- Wright, J.V. 1981. The Rio-Caliente ignimbrite: analysis of a compound intraplinian ignimbrite from a major late Quaternary Mexican eruption. *Bull. Volcanol.* 44: 189-212.
- Wright, J.V. and Coward, M.P. 1977. Rootless Vents in welded ash-flow tuffs from Northern Snowdonia, North Wales. *Geol. Mag.* 114: 133-140.
- Wright, J.V. and Mutti, E. 1981. The Dali Ash, Island of Rhodes, Greece: a problem in interpreting submarine volcanogenic sediments. *Bull. Volcanol.* 44: 153-167.
- Wyborn, D. 1983. Fractionation processes in the Boggy Plain Zoned Pluton. Unpublished PhD thesis submitted to Australian National University.
- Wyborn, D., and Chappell, B.W. 1986. The petrogenetic significance of chemically related plutonic and volcanic rock units. *Geol. Mag.* 123: 619-628.
- Wyborn, L.A.I. 1988. Petrology, geochemistry and age of a major Australian 1880-1840 Ma felsic volcano-plutonic suite: a model for intracontinental felsic magma generation. In: *The early to middle Proterozoic of Australia*. Wyborn, L.A.I. and Etheridge, M.A. (eds). *Precambrian Res.* 40/41: 37-60.
-

## REFERENCES

---

- Wyborn, L.A.I., 1990. Localisation of mineralisation in the Coronation Hill and related deposits, South Alligator Valley Mineral Field, N.T. *BMR Research Newsletter*. April 1990.
- Wyborn, L.A.I., and Chappell, B.W. 1983. Chemistry of the Ordovician and Silurian greywackes of the Snowy Mountains, southeastern Australia: an example of chemical evolution of sediments with time. *Chem. Geol.* 39: 81-92.
- Wyborn, L.A.I., and Page, R.W. 1983. The Proterozoic Kalkadoon and Ewen Batholiths, Mount Isa Inlier, Queensland: source, chemistry, age, and metamorphism. *BMR J. Aust. Geol. Geophys.* 8: 53-69.
- Wyborn, L.A.I., Page, R.W., and McCulloch, M.T. 1988. Petrology, geochronology and isotope geochemistry of the post-1820 Ma granites of the Mount Isa Inlier: mechanisms for the generation of Proterozoic anorogenic granites. *Precambrian Res.* 40/41: 509-541.
- Wyborn, L.A.I., Valenta, R.K., Needham R.S., Jagodzinski, E.A., Whittaker, A., and Moerse, M.P. 1990. A review of the geological, geophysical and geochemical data of the Kakadu Conservation Zone as a basis for assessing the resource potential. *Report by the BMR to the Resource Assessment Commission inquiry on the Kakadu Conservation Zone*.
- Wyborn, L.A.I., Warren, R.G., and Drummond, B.J. 1992. Proterozoic granitic types in Australia: implications for lower crustal structure and evolution. *Trans Roy. Soc. Lond.* in press.
- Yoder, H.S. Jr. 1973. Contemporaneous basaltic and rhyolitic magmas. *Am. Mineral.* 58: 153-171.

## ACKNOWLEDGEMENTS

Logistical support for this study was provided by the BMR Kakadu Conservation Zone Project during 1989-1991, which was led by Dr Lesley Wyborn.

Major and trace elements were obtained from the BMR laboratories (John Pyke, Bill Pappas) and XRD data were collected by Julie Kamprad.

Bob Skinner, Richard Morse and Matt Noakes provided assistance in the field.

This project benefitted from discussions with Ray Cas, Lesley Wyborn, Doone Wyborn, John Sheraton, Shen-Su Sun, Marc Norman, Stewart Needham, Peter Stuart-Smith, Gladys Warren, Rod Page, Jeremy Richards, Julio Friedmann and Rick Valenta.

The report was comprehensively reviewed by Ray Cas, Lesley Wyborn and Jon Claoue-Long and rigorously edited by Stewart Needham, and was much improved by their efforts.

The summary of implications for mineralisation was written by Dr Lesley Wyborn.

**APPENDIX A**  
**POINT COUNT DATA**

Appendix A - point counts for samples of the crystal-rich arenite facies  
(Big Sunday Formation, El Sherana Group)

sample†	3194	3154	3156	3158	3079	3195a	3195b	3077	3192a	3192b	3035	3068
n	1000	500	1000	1400	1000	1000	1026	1000	700	1506	1000	1000
matrix	502	108	286	1014	548	385	589	595	240	1074	324	325
Q	282	194	344	142	182	321	229	185	201	120	315	305
F	115	122	156	54	120	170	117	123	97	95	86	164
L	99	75	205	188	150	97	88	97	161	217	274	205
Qv	163	105	241	102	112		137	128	131	90	126	189
Qu	119	89	103	40	70		92	57	70	30	189	116
Fv	86	87	135	34	76	138	94	68	68	63	66	117
perth	29	35	15	19	42	29	23	52	28	31	20	43
plag	0	0	3	1	2	3	0	3	1	1	0	4
Qplut	38	26	77	45	37	36	18	35	29	38	88	46
Qmm	41	39	65	52	69	32	47	48	76	59	100	68
ch	12	8	14	17	7	21	12	2	8	7	21	12
dol	8	2	49	73	11	6	10	6	27	103	58	16
gn	0	0	0	0	0	2	1	0	0	0	4	0
sst	0	0	0	0	0	0	0	0	0	0	0	1
silt	0	0	0	1	0	0	0	0	0	0	2	0
Fcomp	0	0	3	0	9	0	0	6	7	2	1	7
vitri	2	0	7	0	17	27	0	0	14	8	0	55
opaq	0	0	0	0	0	0	3	0	0	0	1	1
zir	0	1	2	1	0	0	0	0	1	0	0	0

†sample numbers are prefixed by 8912-

• see Figure A1

n= number of counts per slide

Qv= volcanic quartz: angular to rounded (resorbed) grains

Qu = quartz exhibiting undulose extinction, probably basement-derived

Fv= undifferentiated K-feldspar & plagioclase (K-spar predominant)

perth = perthite: includes plutonic feldspar and diagenetically altered feldspar

plag= plagioclase, where positively identified by multiple twinning

mcline = microcline

Lplut= plutonic quartz and granite fragments

Lm= polycrystalline metamorphic basement

gn= gneiss, containing phyllosilicates or mylonite

Fcomp= composite aggregates of plagioclase or K-feldspar

vitri = fragments of volcanic matrix (possibly some are pumice)

qfp = quartz-feldspar porphyry

ig = fragments of welded ignimbrite

Q= Qv + Qu

F= Fv+Fper+plag+ mcline

L= Lplut+Lm+ch+dol+gn+myl+sst+silt+Fcomp  
+ vitri+qfp+ig

ch= chert

dol= dolerite

sst= sandstone

silt= siltstone

opaq= opaques

zir = zircon

chl = chlorite

epid = epidote

calc = calcite

fluor = fluorite

## Appendix A - point counts for ignimbrites of the Gimbat Ignimbrite Member

[illegible]

.....

[illegible]

*Appendix A - point counts for fluvial epiclastic sediments of the Gimbat Ignimbrite Member*

<i>sample†</i>	<i>3028</i>	<i>3029a</i>	<i>3036</i>	<i>3056</i>	<i>3080</i>	<i>3081</i>	<i>3178a</i>	<i>3178b</i>
n	500	800	700	500	700	800	800	800
matrix	273	184	111	191	131	156	352	273
Q	69	190	128	136	58	179	133	218
F	41	64	23	67	10	87	69	97
L	116	361	430	105	494	77	233	203
Qv	28	54	40	65	27	87	77	130
Qu	41	136	88	71	31	92	56	88
Fv	39	56	18	60	8	62	53	73
perth	1	4	5	6	1	25	14	19
plag	1	4	0	1	1	0	2	5
mcline	0	0	0	0	0	0	0	0
Qplut	28	139	75	36	66	128	81	105
Qmm	23	101	101	36	44	127	47	38
ch	4	4	5	3	6	6	5	1
dol	31	97	220	10	348	98	52	23
gn	2	0	0	2	0	0	0	0
sst	0	0	13	0	17	0	0	0
silt	12	1	1	0	8	3	17	5
Fcomp	12	4	0	8	0	1	7	9
qfp	0	7	7	5	0	3	4	0
vitri	5	6	8	5	5	11	5	22
ig	0	2	0	0	0	0	15	0
opaq	1		3	1	0	0	13	8
zir	0		0	0	0	0	0	1
chl	0		0	0	0	0	0	0
epid	0		5	0	7	1	0	0
calc	0		0	0	0	0	0	0
seric	0		0	0	0	0	0	0

[illegible]

*Appendix A - point counts for samples of  
quartz-feldspar porphyry*

<i>sample†</i>	3002	3102	3123	3155
<i>n</i>	900	875	900	820
<i>matrix</i>	663	479	446	580
<i>Q</i>	101	105	215	90
<i>F</i>	43	195	206	54
<i>Qcomp</i>	5	73	3	8
<i>perth</i>	60	3	9	0
<i>Fcomp</i>	19	15	11	66
<i>opaq</i>	0	4	10	5
<i>plag</i>	9	0	0	14

*† sample numbers are prefixed by 8912-  
n= number of counts per slide*

*Qcomp = composite quartz grains*

*Fcomp = composite grains of feldspar*

*perth= perthite: includes plutonic feldspar and diagenetically altered feldspar*

*plag= plagioclase, where positively identified by multiple twinning*

*opaq = opaques*

Appendix A - point counts for samples of Coronation  
Sandstone and Big Sunday Formation

<i>sample†</i>	<i>3208</i>	<i>3188</i>	<i>3189</i>
n	510	600	800
matrix	0	115	260
Q	251	231	221
F	128	143	228
L	131	49	13
Fv	112	116	179
perth	16	21	6
plag	0	6	7
mcline	0	36	4
Qplut	69	30	6
Qmm	46	0	0
ch	15	6	4
dol	0	1	2
gn	0	7	1
sst	1	0	0
silt	0	0	0
Fcomp	0	0	0
qfp	0	0	0
vitri	0	1	0
ig	0	0	0
opaq	0	0	1
zir	0	2	0
chl	0	4	13
epid	0	27	7
calc	0	23	38
seric	0	6	18

3208 = Coronation Sandstone  
3188 = Big Sunday Formation  
3189 = Big Sunday Formation

**APPENDIX B**  
**GEOCHEMICAL DATA TABLES**

## GEOCHEMICAL SAMPLE LOCALITIES

Sample#	Lithology	Strat. Unit	Gridref	Sample#	Lithology	Strat. Unit	Gridref
89123001	basalt	Coronation Sst	541874	89123025	tuffaceous siltst.	Big Sunday Fm	486488
89123004	basalt	Coronation Sst	543870	89123022A	fluvial epiclastic	Gimbat Ig. Mem.	479879
89123009	basalt+rhyolite	Coronation Sst	534871	89123022B	fluvial epiclastic	Gimbat Ig. Mem.	479879
89123014	basalt+rhyolite	Coronation Sst	525875	89123028	fluvial epiclastic	Gimbat Ig. Mem.	482876
89123017A	basalt+rhyolite	Coronation Sst	525873	89123029	fluvial epiclastic	Gimbat Ig. Mem.	483877
89123018	basalt+rhyolite	Coronation Sst	524875	89123045	fluvial epiclastic	Gimbat Ig. Mem.	482876
89123117	basalt	Coronation Sst	556873	89123081	fluvial epiclastic	Gimbat Ig. Mem.	467889
89123026	dolerite		480884	89123142	fluvial epiclastic	Gimbat Ig. Mem.	500860
89123027	dolerite		478871	89123143	fluvial epiclastic	Gimbat Ig. Mem.	500861
89123038	dolerite		477872	89123144	fluvial epiclastic	Gimbat Ig. Mem.	499860
89123057	dolerite		451935	89123035	xal-rich arenite	Big Sunday Fm	479876
89123072	dolerite		498864	89123077	xal-rich arenite	Big Sunday Fm	467887
89123103	dolerite		645911	89123079	xal-rich arenite	Big Sunday Fm	467889
89123105	dolerite		579869	89123145	xal-rich arenite	Big Sunday Fm	499860
89123115	dolerite		568861	89123154	xal-rich arenite	Big Sunday Fm	468890
89123136b	dolerite xenolith		500876	89123156	xal-rich arenite	Big Sunday Fm	468890
89123021A	non-welded IG	Gimbat Ig. Mem.	478879	89123101	flow bded rhyol	Gimbat Ig. Mem.	635869
89123021B*	non-welded IG	Gimbat Ig. Mem.	478879	89123108	flow bded rhyol	Gimbat Ig. Mem.	598844
89123055	IG unit IC	Gimbat Ig. Mem.	464903	89123109	aphyrice rhyolite	Gimbat Ig. Mem.	583849
89123058A	IG unit IE	Gimbat Ig. Mem.	452934	89123111	aphyrice rhyolite	Gimbat Ig. Mem.	578847
89123058B*	IG unit IE	Gimbat Ig. Mem.	452934	89123114	aphyrice rhyolite	Gimbat Ig. Mem.	567844
89123058C*	IG unit IE	Gimbat Ig. Mem.	452934	89123090A	flow bded rhyol	Gimbat Ig. Mem.	470905
89123062A	IG unit IC	Gimbat Ig. Mem.	491873	89123090B	flow bded rhyol	Gimbat Ig. Mem.	470905
89123062B*	IG unit IC	Gimbat Ig. Mem.	491873	89123002	qtz-fspar porph		532874
89123062C*	IG unit IC	Gimbat Ig. Mem.	491873	89123102	qtz-fspar porph		643912
89123063	non-welded IG	Gimbat Ig. Mem.	478879	89123123	qtz-fspar porph		554872
89123083	IG unit IE	Gimbat Ig. Mem.	455915	89123133	qtz-fspar porph		526860
89123087	IG unit IE	Gimbat Ig. Mem.	450914	89123155	qtz-fspar porph		468890
89123097	IG unit IA	Gimbat Ig. Mem.	481896	89123202	Q-F porph clast	Gimbat Ig. Mem.	451935
89123104A	IG unit ID	Gimbat Ig. Mem.	582878	89123059	spars. porph. dacite		
89123104B*	IG unit ID	Gimbat Ig. Mem.	582878	89123084	spars. porph. dacite		463921
89123106	IG unit ID	Gimbat Ig. Mem.	579869	89123086	spars. porph. dacite		459922
89123106A*	IG unit ID	Gimbat Ig. Mem.	579869	89123088	spars. porph. dacite		444938
89123106B*	IG unit ID	Gimbat Ig. Mem.	579869	89123073	spars. porph. dacite		449931
89123107	IG unit ID	Gimbat Ig. Mem.	587869	89123149	felsic sill		498860
89123129	IG unit IE	Gimbat Ig. Mem.	512850				
89123132A	IG unit IA	Gimbat Ig. Mem.	525858				
89123132B*	IG unit IA	Gimbat Ig. Mem.	525858				
89123134	IG unit IA	Gimbat Ig. Mem.	527861				
89123136A	IG unit IA	Gimbat Ig. Mem.	500876				
89123137A	IG unit IA	Gimbat Ig. Mem.	500876				
89123137B*	IG unit IA	Gimbat Ig. Mem.	500876				
89123138A	IG unit IB	Gimbat Ig. Mem.	499870				
89123138B*	IG unit IB	Gimbat Ig. Mem.	499870				
89123139A	IG unit IC	Gimbat Ig. Mem.	499869				
89123139B*	IG unit IC	Gimbat Ig. Mem.	499869				
89123139C*	IG unit IC	Gimbat Ig. Mem.	499869				
89123146	IG unit IE	Gimbat Ig. Mem.	502843				
89123147A	IG unit IE	Gimbat Ig. Mem.	499844				
89123147B*	IG unit IE	Gimbat Ig. Mem.	499844				
89123148	IG unit IE	Gimbat Ig. Mem.	496845				
89123152A	IG unit IE	Gimbat Ig. Mem.	468890				
89123152B*	IG unit IE	Gimbat Ig. Mem.	468890				
89123153	IG unit IE	Gimbat Ig. Mem.	468491				
89123157	ig clast	Big Sunday Fm	468890				
89123172	IG unit IE	Gimbat Ig. Mem.	463898				
89123173	IG unit IE	Gimbat Ig. Mem.	463897				
89123174	IG unit IE	Gimbat Ig. Mem.	454915				

\* denotes samples handpicked to remove  
lithic fragments

Appendix B - major element data for subaerial ignimbrites of the Gimbat Ignimbrite Member

Sample#	3021A	3021B	3055	3058a	3058b	3058c	3062a	3062b	3062C	3063	3082	3083	3087	3089	3097	3104a
Lithology	ig	hp ig	cj ig	ig IEli	hp ig	hp ig	cj ig	cj ig	cj ig	ig.	cj ig	ig	ig	ig	ig	ig
Unit	non-weld	non-weld	IC	IE lith	IE lith	IE lith	IC	IC	IC	non weld	IC	IE	IE	Ie	IA	ID
SiO <sub>2</sub>	72.71	75.23	71.37	73.57	75.37	76.71	69.61	69.5	69.99	70.74	70.19	71.09	66.56	72.03	74.44	72.55
TiO <sub>2</sub>	0.28	0.28	0.28	0.29	0.26	0.22	0.35	0.34	0.35	0.34	0.34	0.34	0.55	0.28	0.15	0.25
Al <sub>2</sub> O <sub>3</sub>	12.13	11.85	13.34	11.79	11.74	11.08	13.4	13.35	13.45	13.39	12.92	12.85	12.99	11.86	12.57	11.34
Fe <sub>2</sub> O <sub>3</sub> tot	3.12	2.35	2.82	3.24	2.36	2.25	3.48	3.49	3.59	3.25	3.23	3.61	5.25	1.3	2.48	2.88
Fe <sub>2</sub> O <sub>3</sub>	1.56	1.11	1.24	1.14	0.88	0.85	1.97	2.09	1.89	1.22	1.64	1.98	2.06	1.35	0.76	1.55
FeO	1.4	1.12	1.42	1.89	1.33	1.26	1.36	1.26	1.53	1.83	1.43	1.47	2.87	0.05	1.55	1.2
MnO		0.04	0.03	0.08	0.07	0.05	0.06	0.06	0.06	0.06	0.05	0.05	0.1	0.88		0.06
MgO	1.04	0.77	0.78	1.38	1	0.98	0.63	0.6	0.66	1.05	0.59	0.92	2.17	1.99	1.04	0.84
CaO	1.3	0.78	0.7	1.11	0.84	0.61	1.26	1.23	1.32	1.45	1.75	0.96	2.83	3.46	0.11	2.08
Na <sub>2</sub> O	2.84	2.97	3.2	2.52	2.42	2.43	3.16	3.14	3.13	2.43	2.89	3.23	2.58	3.59	2.52	2.04
K <sub>2</sub> O	4.67	4.6	5.85	4.07	4.41	4.47	5.71	5.73	5.71	5.4	5.41	5.27	4.59	0.08	5.44	4.52
P <sub>2</sub> O <sub>5</sub>	0.07	0.08	0.08	0.08	0.07	0.06	0.1	0.1	0.1	0.09	0.1	0.1	0.17	0.2	0.03	0.06
rest	1.77	1.17	1.44	1.66	1.27	1.13	1.88	1.94	1.79	1.78	2.49	1.77	2.07	2.79	1.38	3.4
L.O.I.	0.23	0.25	0.28	0.21	0.27	0.24	0.3	0.29	0.28	0.28	0.27	0.26	0.32	99.86	0.21	0.21
TOTAL	100.06	100.25	100.01	99.79	99.93	100.09	99.79	99.63	100.26	100.06	100.07	100.29	99.86	317	100.24	100.1

# all samples are prefixed by 8912-

'hp' denotes samples that were hand picked to remove lithic fragments

† relic ignimbrite clasts in crystal rich arenites

\* acid volcanic intruding dolerite in net veined complex

*Appendix B - major element data for subaerial ignimbrites of the Gimbat Ignimbrite Member*

Sample#	3104b	3106	3106a	3106b	3107	3129	3132A	3132b	3134	3136a	3137a	3137b	3138a	3138b	3139A	3139B
Lithology	hp ig	ig	ig	hp ig	ig	ig	ig	hp ig	ig	ig	ig	hp ig	ig	hp ig	cj ig	cj ig
Unit	ID	ID	ID	ID	ID	IE	IA	IA	IA	IA	IA	IA	IB	IB	IC	IC
SiO2	74.9	74.64	73.5	74.18	71.88	72.6	71.89	73.39	71.64	68.66	71.73	73.42	67.91	71.55	71.15	70.94
TiO2	0.18	0.2	0.24	0.2	0.28	0.17	0.29	0.19	0.37	0.45	0.28	0.2	0.44	0.38	0.32	0.29
Al2O3	10.91	12.26	12.32	12.5	11.9	12.82	12.81	12.61	12.57	12.44	12.77	12.48	12.72	12.64	13.32	13.21
Fe2O3tot	2.5	2.89	3.02	2.74	3.12	2.24	3.06	2.35	3.23	4.98	3.27	2.37	4.57	3.29	3.08	3.11
Fe2O3	1.46	2.53	1.93	1.9	1.6	1.46	1.63	1.44	1.8	1.5	0.9	0.98	2.15	1.78	1.98	2.15
FeO	0.94	0.32	0.98	0.76	1.37	0.7	1.29	0.82	1.29	3.13	2.13	1.25	2.18	1.36	0.99	0.86
MnO	0.05	0.03	0.06	0.05	0.05	0.06	0.05	0.04	0.05	0.09	0.06	0.04	0.08	0.04	0.05	0.04
MgO	0.68	0.43	0.7	0.52	0.95	0.77	1.11	0.65	1.37	1.73	1.17	0.81	2.22	1.22	0.61	0.61
CaO	1.6	0.17	0.86	0.33	1.59	0.71	0.96	0.72	0.79	2.35	0.91	0.63	1.02	0.42	0.81	0.79
Na2O	1.99	1.99	3.2	3.4	2.87	2.6	3.15	2.96	3.49	3.78	3.21	3.16	2.82	2.81	3.51	3.52
K2O	4.64	5.31	4.62	5.07	4.77	5.36	5.07	5.62	4.3	3.56	4.83	5.31	4.95	5.87	5.67	5.71
P2O5	0.04	0.04	0.06	0.04	0.08	0.03	0.07	0.04	0.08	0.13	0.07	0.05	0.14	0.11	0.09	0.09
rest	2.66	2.03	1.74	1.11	2.48	2.67	1.49	1.3	1.95	1.97	1.56	1.35	3.1	1.67	1.37	1.47
L.O.I.	0.24	0.2	0.21	0.26	0.24	0.19	0.24	0.26	0.23	0.21	0.23	0.27	0.28	0.3	0.29	0.28
TOTAL	100.29	100.15	100.42	100.32	100.06	100.14	100.05	100.04	99.93	100	99.85	99.95	100.01	100.15	100.16	99.99

Appendix B - major element data for subaerial ignimbrites of the Gimbat Ignimbrite Member

Sample#	3139C	3146	3147a	3147b	3148	3152a	3152b	3153	3157	3172	3173	3174	3182
Lithology	cj ig	ig	ig	hp ig	ig	ig	hp ig	ig	igt	ig	ig	ig	ig*
Unit	IC	IE	IE	IE	IE	IE	IE	IE		IE	IE	IE	
SiO <sub>2</sub>	70.91	70.74	71.53	73.3	69.95	73.27	73.81	73.16	71.35	70.91	72.09	72.77	74.22
TiO <sub>2</sub>	0.31	0.26	0.22	0.16	0.33	0.29	0.29	0.29	0.42	0.28	0.31	0.31	0.13
Al <sub>2</sub> O <sub>3</sub>	13.28	12.69	12.49	12.28	12.87	12.31	12.16	12.36	12.08	11.84	12.18	12.32	12.17
Fe <sub>2</sub> O <sub>3</sub> tot	3.15	3.15	2.88	2.42	3.41	3.07	2.52	2.82	3.76	3.08	2.49	3.12	2.19
Fe <sub>2</sub> O <sub>3</sub>	1.99	1.19	1.22	1.21	0.98	1.55	1.63	0.95	1.65	1.28	1.12	1.25	1.3
FeO	1.04	1.76	1.49	1.09	2.19	1.37	0.8	1.68	1.9	1.62	1.23	1.68	0.8
MnO	0.05	0.06	0.05	0.03	0.06	0.06	0.05	0.06			0.05	0.06	0.05
MgO	0.67	1.44	0.79	0.63	1.2	0.76	0.61	0.98	1.45	1.82	0.79	1.11	0.94
CaO	0.9	1.09	1.69	1.08	1.8	0.97	0.7	0.63	0.89	1.41	1.63	1.14	0.67
Na <sub>2</sub> O	3.59	2.56	2.71	2.7	2.71	3.27	3.15	2.38	1.49	1.65	2.52	2.81	1.88
K <sub>2</sub> O	5.56	4.96	4.68	4.92	4.51	4.84	4.94	5.16	6.52	4.84	5.13	4.59	5
P <sub>2</sub> O <sub>5</sub>	0.09	0.08	0.05	0.04	0.08	0.08	0.07	0.08	0.12	0.07	0.08	0.1	0.03
rest	1.5	2.9	2.82	2.15	3.06	1.11	1.24	2.1	1.92	4.08	2.56	1.7	2.7
L.O.I.	0.26	0.2	0.2	0.2	0.22	0.25	0.28	0.24	0.31	0.26	0.24	0.26	0.23
TOTAL	100.15	99.93	99.94	99.79	99.96	100.13	99.73	100.07	100.16	100.17	99.93	100.1	100.12

Appendix B - trace element data for ignimbrites of the Gimbat Ignimbrite Member

Sample#	3021A	3021B	3055	3058a	3058b	3058c	3062a	3062b	3062C	3063	3082	3083	3087	3089	3097	3104a
Lithology	ig	hp ig	cj ig	ig IEli	hp ig	hp ig	cj ig	cj ig	cj ig	ig	cj ig	ig	ig	ig	ig	ig
Unit	non-weld	non-weld	IC	IE lith	IE lith	IE lith	IC	IC	IC	non weld	IC	IE	IE	IE	IA	ID
Ba	330	333	482	340	378	361	461	458	445	394	472	490	652	11	195	246
Li	16	14	6	24	20	17	7	3	7	29	10	14	22	150	16	11
Rb	197	192	230	180	190	186	236	236	234	239	212	193	154	50	249	226
Sr	64	61	84	92	87	86	71	71	69	103	59	74	177	20	45	53
Pb	29	30	34	77	66	51	35	36	35	63	19	29	32	47	28	22
Th	50	48	54	48	50	50	53	52	52	52	50	47	39	12	57	45
U	12	12	12	12	13	12	11	11	12	13	11	10	9	242	14	11
Zr	236	233	349	186	190	181	417	423	413	305	389	354	314	19	203	210
Nb	20	20	22	20	19	17	20	20	20	21	19	18	17	41	24	19
Y	40	38	42	41	39	38	40	40	40	43	35	36	37	67	51	42
La	69	56	114	47	49	46	138	139	127	91	129	126	87	129	63	65
Ce	130	111	206	100	96	92	241	242	225	170	223	217	159	57	124	119
Nd	52	46	81	47	44	39	91	91	86	69	84	84	63	16	56	53
Sc	8	6	7	7	6	5	10	10	10	9	10	9	13	8	3	7
V	21	16	13	29	28	19	10	10	13	26	11	14	47	20	9	21
Cr	41	38	28	63	55	37	15	15	16	34	21	24	91	44	12	24
Mn	563	381	269	686	579	467	550	538	547	498	410	437	923	427	315	604
Co	6	5	3	8	9	7	4	4	3	6	3	5	13	5	4	8
Ni	10	9	7	17	14	12	5	4	5	10	6	8	26	10	4	6
Cu	-1	-1	1	17	15	5	-1	-1	-1	7	-1	-1	7	1	7	-1
Zn	104	77	40	111	93	85	106	104	105	80	39	61	127	69	46	49
Sn	3	-2	-2	-2	-2	4	4	3	4	8	-2	4	2	2	4	-2
W	375	602	411	203	696	582	394	312	344	404	307	232	459	294	455	398
Mo	-2	-2	-2	-2	-2	-2	-2	-2	-2	-2	-2	-2	-2	<2	6	-2
Ga	19	14	19	18	16	13	20	19	19	20	16	19	18	17	20	17
Ar	5	4	2	4	4	4	3	2	2	5	2	3	5	2.5	3	
S	-100	-100	-100	-100	-100	-100	-100	-100	-100	-100	-100	-100	-100	<100	-100	-100
Ag	2	2	2	2	2	2	2	2	2	2	2	2	2	2	2	3
Ge	3	4	3	3	3	3	3	3	4	4	3	4	4	3	4	2.5

Appendix B - trace element data for ignimbrites of the Gimbat Ignimbrite Member

Sample#	3104b	3106	3106a	3106b	3107	3129	3132A	3132b	3134	3136a	3137a	3137b	3138a	3138b	3139A	3139B
Lithology	hp ig	ig	ig	hp ig	ig	ig	ig	hp ig	ig	ig	ig	hp ig	ig	hp ig	cj ig	cj ig
Unit	ID	ID	ID	ID	ID	IE	IA	IA	IA	IA	IA	IA	IB	IB	IC	IC
Ba	252	320	295	313	347	114	271	285	244	280	275	274	613	737	447	442
Li	9	9	12	12	12	6	15	10	13	16	11	9	15	10	7	7
Rb	221	285	200	210	212	243	216	240	172	192	240	249	178	207	230	230
Sr	50	41	51	51	58	23	62	57	54	118	89	85	65	73	65	63
Pb	21	21	18	18	21	17	26	28	22	23	39	32	25	30	23	24
Th	46	56	52	55	47	57	50	55	50	35	48	52	42	47	54	53
U	12	9	6	6	12	14	11	12	13	10	11	12	9	10	12	11.5
Zr	203	259	243	253	246	279	253	249	243	230	221	224	342	385	360	361
Nb	17	22	21	21	19	23	22	22	24	22	19	24	17	17	21	20
Y	38	44	44	44	40	46	45	49	49	44	46	42	36	37	41	42
La	69	63	76	70	66	84	74	74	70	71	61	63	104	107	112	111
Ce	131	109	144	128	135	158	146	142	130	129	119	123	197	202	198	204
Nd	56	51	61	56	54	67	61	59	57	56	49	50	76	77	74	80
Sc	6	5	6	4	7	5	8	6	8	4	12	7	12	7	7	8
V	16	13	14	11	17	6	25	13	23	17	53	25	31	19	10	11
Cr	16	15	21	11	39	8	37	14	35	25	107	41	54	24	16	14
Mn	405	244	521	391	464	507	478	323	493	390	785	535	703	387	432	433
Co	5	5	5	5	5	2	6	5	6	13	6	6	9	7	5	5
Ni	6	4	7	4	10	2	11	7	10	24	23	10	15	11	5	6
Cu	-1	-1	-1	2	-1	2	6	6	1	8	8	12	-1	-1	-1	-1
Zn	41	53	70	54	68	17	80	53	90	91	90	140	174	114	84	85
Sn	3	4	-2	-2	-2	-2	2	-2	9	3	4	6	-2	-2	-2	-2
W	687	167	310	709	500	337	413	638	426	234	279	639	233	324	507	447
Mo	-2	-2	-2	-2	-2	-2	-2	-2	-2	-2	-2	-2	-2	-2	-2	-2
Ga	15	17	17	16	17	20	21	17	20	20	19	18	18	13	18	17
Ar	3	3	2	3	3	5	4	4	3	7	3	3	2	2		
S	-100	-100	-100	-100	-100	100	-100	-100	-100	-100	-100	-100	-100	-100	-100	-100
Ag	2	3	3	1	1	2	2	2	2	2	2	2	2	2	2	2
Ge	3	3	3	3	3	3	4	4	4	4	4	4	3	3	4	4

Appendix B - trace element data for ignimbrites of the Gumbat Ignimbrite Member

Sample#	3139C	3146	3147a	3147b	3148	3152a	3152b	3153	3157	3172	3173	3174	3182
Lithology	cj ig	ig	ig	hp ig	ig	ig	hp ig	ig	igt	ig	ig	ig	ig*
Unit	IC	IE	IE	IE	IE	IE	IE	IE		IE	IE	IE	
Ba	429	187	198	206	249	335	353	356	977	433	458	414	393
Li	8	15	16	13	17	15	15	18	31	35	22	22	17
Rb	227	252	250	249	276	190	203	269	243	260	234	196	225
Sr	64	32	47	44	58	64	63	65	83	42	69	83	18
Pb	22	13	21	18	18	36	36	20	31	80	24	38	12
Th	54	51	53	54	48	48	50	49	42	47	49	48	51
U	12	12	11	12	11	13	13	11	10	12	12	13	12
Zr	356	253	260	257	242	286	299	275	300	256	257	256	238
Nb	20	22	23	22	23	20	21	20	18	19	20	20	22
Y	42	46	46	44	47	40	41	37	36	40	41	41	49
La	112	73	79	80	73	87	80	90	89	76	71	75	88
Ce	202	140	154	155	138	165	149	166	155	145	134	139	166
Nd	78	57	66	65	58	66	58	66	62	57	56	56	69
Sc	7	7	7	5	8	7	5	7	9	9	7	7	4
V	14	20	17	12	25	16	11	18	31	18	21	27	6
Cr	19	31	24	16	50	28	27	43	61	36	43	59	7
Mn	492	529	450	289	515	470	370	497	569	905	424	573	492
Co	5	6	7	5	8	6	4	6	11	9	4	6	3
Ni	6	9	10	7	13	9	8	10	16	13	12	14	4
Cu	-1	1	7	8	6	47	2	5	2	23	-1	-1	-1
Zn	93	69	62	51	72	93	83	80	84	123	59	129	119
Sn	-2	6	3	3	5	3	-2	5	-2	8	2	3	3
W	281	209	187	274	260	406	731	249	206	325	317	408	315
Mo	-2	-2	-2	-2	-2	-2	-2	-2	-2	-2	-2	-2	-2
Ga	18	20	20	18	21	18	16	17	15	18	17	17	18
Ar		4	4	4	4	3	4	3	3	10	5	3	3
S	-100	-100	-100	-100	-100	-100	-100	-100	-100	-100	-100	-100	-100
Ag	2	2	2	2	1	2	1	2	2	2	2	2	2
Ge	4	3	3	4	3	3	4	3	3	3	3	4	3

Appendix B - CIPW Norms for the subaerial ignimbrites of the Gimbat Ignimbrite Member

Sample#	3021A	3021B	3055	3058a	3058b	3058c	3062a	3062b	3062C	3063	3082	3083	3087	3089	3097	3104a
Lithology	ig	hp ig	cj ig	ig IEli	hp ig	hp ig	cj ig	cj ig	cj ig	ig	cj ig	ig	ig	ig	ig	ig
Unit	non-weld	non-weld	IC	IE lith	IE lith	IE lith	IC	IC	IC	non weld	IC	IE	IE	Ie	IA	ID
Quartz	32.58	36.58	26.5	37.44	40.09	41.69	24.32	24.33	24.65	29.85	27.11	27.16	23.19	32.11	35.92	36.71
Corundum	0.15	0.71	0.6	1.35	1.56	1.22				1.05		0.26			2.36	
Zircon	0.05	0.05	0.07	0.04	0.04	0.04	0.08	0.09	0.08	0.06	0.08	0.07	0.06	0.05	0.04	0.04
Orthoclase	27.67	27.26	34.66	24.12	26.13	26.49	33.83	33.95	33.83	32	32.05	31.22	27.18	21.27	32.24	26.8
Albite	24.03	25.13	27.08	21.32	20.48	20.56	26.74	26.57	26.49	20.56	24.45	27.33	21.83	29.28	21.32	17.26
Anorthite	6.1	3.46	3.11	5.11	3.84	2.76	5.49	5.39	5.76	6.75	6.27	4.27	10.28	6.2	0.41	8.39
Diopside							0.21	0.18	0.23		1.62		2.39	2.72		1.36
Di(CaMg)							0.07	0.06	0.08		0.55		1.29	1.27		0.6
Hedenbergite							0.14	0.12	0.15		1.07		1.11	1.45		0.76
Hypersthene	5.84	4.25	4.79	6.85	4.91	4.77	5.02	4.99	5.21	5.92	3.91	6	9.56	3.7	5.29	4.44
Enstatite	2.59	1.92	1.94	3.44	2.49	2.44	1.54	1.47	1.61	2.62	1.22	2.29	4.81	1.6	2.59	1.81
Ferrosilite	3.25	2.33	2.85	3.41	2.42	2.33	3.48	3.52	3.6	3.31	2.7	3.71	4.75	2.1	2.7	2.63
Magnetite	0.91	0.69	0.82	0.95	0.69	0.66	1.01	1.01	1.04	0.95	0.94	1.05	1.53	0.82	0.72	0.84
Chromite	0.01	0.01	0.01	0.01	0.01	0.01				0.01		0.01	0.02	0.01		0.01
Ilmenite	0.53	0.53	0.53	0.55	0.49	0.42	0.66	0.65	0.66	0.65	0.65	0.65	1.04	0.53	0.28	0.47
Apatite	0.17	0.19	0.2	0.19	0.17	0.15	0.24	0.24	0.24	0.22	0.24	0.24	0.41	0.19	0.08	0.14
Diff. Index	84.28	88.97	88.24	82.88	86.7	88.74	84.89	84.86	84.97	82.41	83.62	85.71	72.2	82.66	89.49	80.77
Colour Index	7.29	5.47	6.15	8.36	6.11	5.85	6.91	6.83	7.15	7.52	7.12	7.7	14.55	7.78	6.3	7.12
Pl	30.14	28.59	30.18	26.43	24.32	23.32	32.23	31.96	32.25	27.31	30.73	31.6	32.11	35.47	21.74	25.66
Norm Plag	20.26	12.09	10.29	19.33	15.8	11.84	17.04	16.87	17.87	24.71	20.42	13.5	32.01	17.47	1.91	32.72
100An/(An+A	20.26	12.09	10.29	19.33	15.8	11.84	17.04	16.87	17.87	24.71	20.42	13.5	32.01	17.47	1.91	32.72
Ab	24.03	25.13	27.08	21.32	20.48	20.56	26.74	26.57	26.49	20.56	24.45	27.33	21.83	29.28	21.32	17.26
Q	34.09	37.68	27.73	39.24	41.39	42.95	25.57	25.58	25.95	31.38	28.09	28.69	25.71	33.07	37.31	37.85
Ol	4.32	3.14	3.56	5.04	3.61	3.51	3.77	3.75	3.91	4.39	2.94	4.47	7.04	2.74	3.9	3.3
Ne	13.02	13.62	14.68	11.56	11.1	11.14	14.49	14.4	14.35	11.14	13.25	14.81	11.83	15.87	11.56	9.36
Q	45.1	49.19	40.13	49.01	50.76	52.36	37.81	37.74	38.08	40.8	39.29	41.21	35.71	46.48	47.07	45.75
mg number	45.24	44.74	40.66	51.32	51.21	51.88	30.94	29.85	31.27	44.41	31.14	38.66	50.57	43.75	50.91	41.9

*Appendix B - CIPW Norms for the subaerial ignimbrites of the Gimbat Ignimbrite Member*

Sample#	3104b	3106	3106a	3106b	3107	3129	3132A	3132b	3134	3136a	3137a	3137b	3138a	3138b	3139A	3139B
Lithology	hp ig	ig	ig	hp ig	ig	ig	ig	hp ig	ig	ig	ig	hp ig	ig	hp ig	cj ig	cj ig
Unit	ID	ID	ID	ID	ID	IE	IA	IA	IA	IA	IA	IA	IB	IB	IC	IC
Quartz	40.05	40.33	32.92	32.18	31.17	33.2	29.1	31.02	29.81	24.29	29.4	31.06	25.17	28.69	25.09	24.69
Corundum		2.97	0.59	0.86		1.49	0.51	0.39	0.89		0.72	0.46	1.13	1.08	0.09	
Zircon	0.04	0.05	0.05	0.05	0.05	0.06	0.05	0.05	0.05	0.05	0.04	0.05	0.07	0.08	0.07	0.07
Orthoclase	27.51	31.49	27.38	30.04	28.27	31.77	30.04	33.3	25.48	21.11	28.64	31.48	29.32	34.77	33.6	33.83
Albite	16.84	16.84	27.08	28.77	24.29	22	26.65	25.05	29.53	31.99	27.16	26.74	23.86	23.78	29.7	29.79
Anorthite	7.1	0.68	3.97	1.48	5.46	3.37	4.4	3.41	3.48	6.41	4.16	2.9	4.33	1.58	3.57	3.44
Diopside	0.56				1.69					3.76						0.03
Di(CaMg)	0.23				0.77					1.84						0.01
Hedenbergite	0.33				0.92					1.92						0.02
Hypersthene	4.1	4.13	4.95	4.23	4.76	4.31	5.92	4.1	6.63	7.62	6.33	4.5	10.23	6.29	4.64	4.69
Enstatite	1.59	1.07	1.74	1.3	2.01	1.92	2.76	1.62	3.41	3.46	2.91	2.02	5.53	3.04	1.52	1.52
Ferrosilite	2.52	3.06	3.2	2.93	2.75	2.4	3.15	2.48	3.22	4.16	3.41	2.48	4.7	3.25	3.12	3.18
Magnetite	0.73	0.84	0.88	0.8	0.91	0.65	0.89	0.68	0.94	1.45	0.96	0.69	1.33	0.96	0.9	0.9
Chromite					0.01		0.01		0.01	0.01	0.02	0.01	0.01	0.01		
Ilmenite	0.34	0.38	0.46	0.38	0.53	0.32	0.55	0.36	0.7	0.85	0.53	0.38	0.84	0.72	0.61	0.55
Apatite	0.1	0.1	0.14	0.1	0.19	0.07	0.17	0.1	0.19	0.31	0.17	0.12	0.34	0.28	0.22	0.22
Diff. Index	84.4	88.66	87.38	90.99	83.73	86.96	85.79	89.37	84.82	77.39	85.2	89.27	78.36	87.24	88.38	88.31
Colour Index	5.74	5.35	6.29	5.41	7.9	5.31	7.37	5.15	8.28	13.69	7.84	5.58	12.41	7.97	6.15	6.17
Pl	23.94	17.52	31.05	30.25	29.74	25.37	31.05	28.45	33.01	38.4	31.33	29.64	28.19	25.35	33.27	33.23
Norm Plag	29.65	3.87	12.79	4.88	18.35	13.27	14.17	11.98	10.54	16.7	13.29	9.79	15.36	6.22	10.73	10.36
100An/(An+A	29.65	3.87	12.79	4.88	18.35	13.27	14.17	11.98	10.54	16.7	13.29	9.79	15.36	6.22	10.73	10.36
Ab	16.84	16.84	27.08	28.77	24.29	22	26.65	25.05	29.53	31.99	27.16	26.74	23.86	23.78	29.7	29.79
Q	41.1	41.35	34.17	33.24	32.4	34.31	30.64	32.07	31.56	26.27	31.05	32.22	27.9	30.34	26.26	25.87
Ol	3.05	3.11	3.7	3.17	3.53	3.19	4.37	3.05	4.87	5.64	4.68	3.33	7.51	4.64	3.48	3.51
Ne	9.13	9.13	14.68	15.59	13.16	11.92	14.45	13.58	16.01	17.34	14.72	14.49	12.93	12.89	16.1	16.14
Q	48.81	49.06	46.57	46.41	43.52	44.39	42.85	43.54	45.09	40.92	43.49	44.47	38.83	41.23	39.86	39.51
mg number	40.19	26.95	36.47	31.93	42.96	46	47.28	40.63	51.19	46.24	46.99	45.84	54.58	47.85	32.9	32.71

Appendix B - CIPW Norms for the subaerial ignimbrites of the Gimbat Ignimbrite Member

Sample#	3139C	3146	3147a	3147b	3148	3152a	3152b	3153	3157	3172	3173	3174	3182
Lithology	cj ig	ig	ig	hp ig	ig	ig	hp ig	ig	igt	ig	ig	ig	ig*
Unit	IC	IE	IE	IE	IE	IE	IE	IE		IE	IE	IE	
Quartz	24.55	30.98	31.71	34.33	29.78	31.17	33.09	35.52	32.07	35.58	32.3	33.44	40.17
Corundum		1.28		0.6	0.4	0.07	0.47	1.84	1.12	1.41		0.83	2.46
Zircon	0.07	0.05	0.05	0.05	0.05	0.06	0.06	0.06	0.06	0.05	0.05	0.05	0.05
Orthoclase	32.94	29.41	27.75	29.17	26.76	28.68	29.27	30.6	38.62	28.7	30.41	27.2	29.63
Albite	30.38	21.66	22.93	22.85	22.93	27.67	26.65	20.14	12.61	13.96	21.32	23.78	15.91
Anorthite	3.67	4.95	8.04	5.17	8.5	4.4	3.13	2.72	3.92	6.67	6.72	5.14	3.24
Diopside	0.29		0.08								0.83		
Di(CaMg)	0.11			0.03								0.4	
Jedenbergite	0.18			0.04							0.43		
Hypersthene	4.74	6.9	4.98	4.16	6.5	5.08	4.04	5.33	7.37	7.81	4.01	5.96	4.75
Enstatite	1.62	3.59	1.95	1.57	2.99	1.89	1.52	2.44	3.61	4.53	1.78	2.76	2.34
Ferrosilite	3.12	3.32	3.03	2.59	3.51	3.18	2.52	2.88	3.76	3.28	2.22	3.2	2.41
Magnetite	0.92	0.92	0.84	0.7	1	0.89	0.73	0.82	1.1	0.9	0.73	0.91	0.64
Chromite		0.01	0.01		0.01	0.01	0.01	0.01	0.01	0.1	0.01	0.01	
Ilmenite	0.59	0.49	0.42	0.3	0.63	0.55	0.55	0.55	0.8	0.53	0.59	0.59	0.25
Apatite	0.22	0.19	0.12	0.1	0.19	0.19	0.17	0.19	0.3	0.17	0.19	0.24	0.07
Diff. Index	87.88	82.06	82.39	86.35	79.47	87.51	89.02	86.26	83.3	78.25	84.03	84.42	85.71
Colour Index	6.54	8.32	6.32	5.17	8.13	6.53	5.33	6.71	9.28	9.25	6.16	7.47	5.63
Pl	34.05	26.61	30.97	28.02	31.43	32.07	29.79	22.86	16.52	20.63	28.04	28.92	19.15
Norm Plag	10.79	18.59	25.95	18.45	27.03	13.73	10.51	11.9	23.7	32.33	23.96	17.78	16.92
100An/(An+	10.79	18.59	25.95	18.45	27.03	13.73	10.51	11.9	23.7	32.33	23.96	17.78	16.92
Ab	30.38	21.66	22.93	22.85	22.93	27.67	26.65	20.14	12.61	13.96	21.32	23.78	15.91
Q	25.75	32.81	32.98	35.39	31.47	32.46	34.12	36.91	34	37.69	33.34	35	41.42
Ol	3.54	5.07	3.71	3.1	4.8	3.78	3.01	3.94	5.43	5.71	2.97	4.41	3.5
Ne	16.46	11.74	12.43	12.38	12.43	15	14.45	10.92	6.83	7.57	11.56	12.89	8.62
Q	39.66	42.73	43.48	45.85	41.97	45.13	46.33	46.14	39.78	44.08	43.1	45.89	48.71
mg number	34.52	53.12	40.48	39.18	46.53	37.98	37.48	46.27	48.83	59.39	44.02	46.85	51.53

*Appendix B - major element data for fluvial epiclastic sediments (Gimbat Ignimbrite Member)  
and crystal-rich arenite facies (Big Sunday Formation)*

Sample#	3025	3022a	3022b	3028	3029	3045	3081	3142	3143	3144	3035	3077	3079	3145	3154	3156
Lithology	tuff silt	epiclastic	epiclastic	epiclastic	epiclastic	epiclastic	epiclastic	epiclastic	epiclastic	epiclastic	xtal rich	xtal rich	xtal rich	xtal rich	xtal rich	xtal rich†
SiO <sub>2</sub>	74.6	75.38	76.1	74.16	72.8	70.42	76.85	80.29	71.8	69.83	72.95	72.82	73.16	82.09	76.17	76.63
TiO <sub>2</sub>	0.17	0.27	0.3	0.31	0.4	0.53	0.42	0.29	0.5	0.47	0.61	0.32	0.34	0.41	0.53	0.58
Al <sub>2</sub> O <sub>3</sub>	12.28	10.4	10.63	9.98	10.55	12.81	7.73	7.02	9.13	11.85	8.89	11.64	10.98	6.35	8.51	8.53
Fe <sub>2</sub> O <sub>3</sub> tot	2.07	2.62	2.82	3.17	3056	4.28	3.58	2.92	4.79	4.14	6.23	3.1	3.09	3.24	4.14	4.67
Fe <sub>2</sub> O <sub>3</sub>	1.03	1.13	1.02	1.18	1.95	3.02	0.48	1.06	1.6		1.34	0.92	1.04	0.87	1.31	1.43
FeO	0.94	1.34	1.62	1.79	1.45	2.53	2.29	2.2	3.36	2.29	4.4	1.96	1.98	2.13	2.55	2.92
MnO	0.05	0.05	0.05	0.07	0.06	0.08	0.1	0.07	0.1	0.08	0.09	0.12	0.1	0.06		0.08
MgO	0.36	1.39	1.32	1.91	1.63	1.21	2.61	1.83	3.47	1.35	2.06	1.5	1.06	1.25	2.07	2.05
CaO	1.22	0.92	0.26	1.28	2.48	1.44	1.25	0.95	1.58	2.38	2.46	0.97	1.87	1.18	0.98	1.1
Na <sub>2</sub> O	2.73	2.08	2.06	1.96	1.71	2.54	1	0.9	1.26	1.93	1.48	2.01	2.18	0.59	1.1	1.03
K <sub>2</sub> O	3.51	3.82	4.39	3.63	3.89	4.33	2.72	3.06	2.91	4.51	1.81	4.51	4.17	2.83	3.83	3.45
P <sub>2</sub> O <sub>5</sub>	0.03	0.07	0.09	0.09	0.14	0.11	0.16	0.1	0.18	0.12	0.12	0.09	0.11	0.1	0.12	0.13
rest	2.67	2.7	1.76	3.01	2.73	2.27	3.64	2.53	4.4	3.59	3.57	2.86	2.9	2.36	2.71	2.18
L.O.I.	0.18	0.23	0.31	0.23	0.31	0.24	0.25	0.22	0.25	0.23	0.2	0.26	0.24	0.2	0.27	0.26
TOTAL	99.77	99.78	99.91	99.6	100.1	99.98	100.06	99.94	100	100.23	99.98	99.98	99.98	100.42	100.22	100.37

# all samples are prefixed by 8912-

† crystal-rich matrix hosting relic ignimbrite clasts

epiclastics = fluvial epiclastic sediments

xtal rich = crystal-rich arenite facies

tuff silt = tuffaceous siltstone of the Nilyanjurrung Member

*Appendix B - trace element data for fluvial epiclastic sediments (Gimbat Ignimbrite Member)  
and crystal-rich arenite facies (Big Sunday Formation)*

Sample#	3025	3022a	3022b	3028	3029	3045	3081	3142	3143	3144	3035	3077	3079	3145	3154	3156
Lithology	tuff silt	epiclastic	epiclastic	epiclastic	epiclastic	epiclastic	epiclastic	epiclastic	epiclastic	epiclastic	xtal rich	xtal rich	xtal rich	xtal rich	xtal rich	xtal rich†
Ba	119	383	478	523	1063	474	654	584	668	540	490	564	627	598	798	643
Li	9	11	23	21	24	23	50	16	29	16	26	20	23	16	27	39
Rb	210	187	200	197	169	211	115	110	103	215	87	242	203	100	153	119
Sr	31	53	61	55	116	98	48	58	64	90	55	66	87	59	61	81
Pb	26	19	26	17	28	38	15	14	13	47	177	21	27	15	16	28
Th	53	38	38	33	33	39	15	19	21	38	16	41	39	14	18	20
U	12	10	9	9	9	10	5	6	7	11	5	10	10	4	5	5
Zr	195	191	203	196	196	220	143	144	162	217	157	246	221	167	191	205
Nb	22	15	16	13	14	17	7	8	10	17	8	17	17	6	9	9
Y	44	32	33	31	34	37	20	17	31	36	24	35	34	17	23	22
La	54	50	54	53	50	57	36	25	38	50	33	60	50	32	34	32
Ce	111	96	97	97	102	112	70	51	71	104	53	113	104	54	61	64
Nd	50	41	42	43	43	48	30	19	33	45	24	49	43	24	26	29
Sc	4	6	6	8	9	10	10	7	12	10	15	8	9	8	8	10
V	7	22	23	30	51	49	50	29	63	43	72	24	28	36	52	50
Cr	12	47	53	60	103	62	119	65	141	88	67	56	67	57	73	85
Mn	428	475	458	612	523	727	915	579	973	703	813	1161	955	491	699	696
Co	11	6	6	6	10	9	14	9	15	12	14	7	8	10	14	14
Ni	4	14	14	17	27	20	31	19	40	25	21	16	18	18	24	26
Cu	4	-1	6	-1	3	2	8	2	1	17	40	4	4	2	2	8
Zn	44	80	91	121	136	128	73	70	136	101	87	68	68	55	97	115
Sn	-2	3	-2	3	-2	-2	-2	5	-2	-2	-2	-2	3	-2	-2	-2
W	349	526	1007	277	313	194	403	514	295	121	239	426	253	348	442	437
Mo	-2	-2	-2	-2	-2	-2	-2	-2	-2	-2	-2	-2	-2	-2	-2	-2
Ga	18	15	16	14	14	17	10	10	14	17	12	16	15	7	10	13
Ar	3	3	2	3	5	4	2	2	2	5	6	4	5	2	2	2
S	-100	-100	-100	-100	-100	-100	-100	-100	-100	-100	500	100	100	-100	-100	-100
Ag	2	2	2	2	2	2	2	2	2	2	2	2	2	1	2	2
Ge	3	3	3	3	3	3	3	3	4	3	3	2	2	3	3	3

*Appendix B - CIPW Norms for fluvial epiclastic sediments (Gimbat Ignimbrite Member)  
and crystal-rich arenite facies (Big Sunday Formation)*

Sample#	3025	3022a	3022b	3028	3029	3045	3081	3142	3143	3144	3035	3077	3079	3145	3154	3156
Lithology	tuff silt	epiclastic	epiclastic	epiclastic	epiclastic	epiclastic	epiclastic	epiclastic	epiclastic	epiclastic	xtal rich	xtal rich	xtal rich	xtal rich	xtal rich	xtal rich†
Quartz	41.13	43.49	43.16	41.9	39.25	32.42	52.67	57.37	42.91	32.72	46.44	38.17	37.84	62.15	48.26	50.13
Corundum	1.81	1.28	2.16	0.64		1.51	1.15	0.67	1.38		0.24	1.83		0.34	0.97	1.32
Zircon	0.04	0.04	0.04	0.04	0.04	0.04	0.03	0.03	0.03	0.04	0.03	0.05	0.04	0.03	0.04	0.04
Orthoclase	20.82	22.65	26.02	21.53	23.05	25.67	16.12	18.13	17.24	26.74	10.73	26.75	24.72	16.76	22.69	20.43
Albite	23.1	17.6	17.43	16.58	14.47	21.49	8.46	7.62	10.66	16.33	12.52	17.01	18.45	4.99	9.31	8.72
Anorthite	5.9	4.23	0.84	5.92	9.61	6.59	5.34	4.23	6.86	10.32	11.57	4.4	7.82	5.38	4.31	4.81
Diopside					1.74					0.73			0.78			
Di(CaMg)					0.99					0.35			0.38			
Hedenbergite					0.75					0.38			0.4			
Hypersthene	3.11	6.13	6.14	8.03	6.77	7.23	10.12	7.58	13.53	7.15	11.38	6.99	5.42	6.28	6.28	9.69
Enstatite	0.9	3.46	3.29	4.76	3.61	3.01	6.5	4.56	8.64	3.2	5.13	3.74	2.46	3.11	3.11	5.11
Ferrosilite	2.21	2.67	2.85	3.28	3.16	4.22	3.62	3.03	4.89	3.95	6.25	3.25	2.96	3.17	3.17	4.59
Magnetite	0.6	0.76	0.82	0.93	1.04	1.25	1.05	0.85	1.4	1.21	1.82	0.9	0.9	0.95	0.95	1.37
Chromite		0.01	0.01	0.01	0.02	0.01	0.03	0.01	0.03	0.02	0.01	0.01	0.01	0.01	0.01	0.02
Ilmenite	0.32	0.51	0.57	0.59	0.76	1.01	0.8	0.55	0.95	0.89	1.16	0.61	0.65	0.78	0.78	1.1
Apatite	0.07	0.17	0.23	0.22	0.34	0.26	0.39	0.24	0.43	0.29	0.29	0.22	0.26	0.24	0.24	0.32
Diff. Index	85.05	83.74	87.05	80.01	76.77	79.59	77.25	83.11	70.81	75.79	69.69	81.92	81.01	83.91	83.91	79.28
Colour Ind	4.03	7.42		9.56	10.33	9.5	12	9	15.91	10.01	14.47	8.53	7.78	8.02	8.02	12.18
Pl	29	21.83		22.51	24.08	28.08	13.81	11.85	17.52	26.65	24.1	21.41	26.27	10.37	10.37	13.52
norm plag	20.34	19.37		26.31	39.91	23.46	38.71	35.74	39.16	38.73	48.03	20.54	29.77	51.87	51.87	35.54
Ab	23.1	17.6		16.58	14.47	21.49	8.46	7.62	10.66	16.33	12.52	17.01	18.45	4.99	4.99	8.72
Q	41.9	45.13		44.06	41.05	34.28	55.44	59.42	46.61	34.58	49.4	40.03	39.25	63.81	63.81	52.7
Ol	2.33	4.49		5.86	4.97	5.37	7.35	5.53	9.83	5.29	8.42	5.13	4.01	4.63	4.63	7.12
Ne	12.52	9.54		8.99	7.84	11.65	4.59	4.13	5.78	8.85	6.79	9.22	10	2.71	2.71	4.72
Q	52.48	53.19		51.66	47.68	44.13	59.32	62.91	51.49	42.06	55.14	47.82	47.7	66.09	66.09	56.69
mg no.	30.05	56.78		59.87	53.12	41.16	64.31	60.76	64.18	44.64	45.01	54.51	45.92	48.87	48.87	52.05

*Appendix B - major element data for coherent rhyolite lavas of the Gimbat Ignimbrite Member*

<i>Sample#</i>	<i>3101</i>	<i>3108</i>	<i>3109</i>	<i>3111</i>	<i>3114</i>	<i>3090A</i>	<i>3090b</i>
<i>Lithology</i>	<i>flow bded</i>	<i>flow bded</i>	<i>aphanitic</i>	<i>aphanitic</i>	<i>aphanitic</i>	<i>bded rhy</i>	<i>bded rhy</i>
<i>Unit</i>							
SiO <sub>2</sub>	75.58	74.55	77.99	75.29	76.08	71.55	72.34
TiO <sub>2</sub>	0.09	0.09	0.08	0.1	0.08	0.28	0.24
Al <sub>2</sub> O <sub>3</sub>	12.12	12.29	11.87	11.86	11.97	12.99	12.91
Fe <sub>2</sub> O <sub>3</sub> tot	1.7	1.64		2.49	1.78	3.08	2.7
Fe <sub>2</sub> O <sub>3</sub>	0.84	0.76	1.02	0.89	1.29	1.37	1.22
FeO	0.77	0.79	0.38	1.44	0.44	1.54	1.33
MnO	0.02	0.04	0.02	0.07	0.02	0.06	0.05
MgO	0.23	0.21	0.16	0.13	0.27	0.86	0.7
CaO	0.52	1.24	0.03	0.45	0.01	0.71	0.63
Na <sub>2</sub> O	2.59	2.6	1.43	2.45	2.22	3.11	3.09
K <sub>2</sub> O	5.96	5.27	4.91	4.82	6.36	5.64	5.86
P <sub>2</sub> O <sub>5</sub>	0.01	0.01	0	0.01	0.01	0.07	0.07
rest	1.14	2.2	1.88	2.22	1.28	1.46	1.24
L.O.I.	0.22	0.17		0.12	0.22	0.23	0.3
<b>TOTAL</b>	<b>100.09</b>	<b>100.22</b>	<b>99.79</b>	<b>99.85</b>	<b>100.25</b>	<b>99.87</b>	<b>99.98</b>

*Appendix B - trace element data for coherent rhyolite lavas of the Gimbat Ignimbrite Member*

<i>Sample#</i>	<i>3101</i>	<i>3108</i>	<i>3109</i>	<i>3111</i>	<i>3114</i>	<i>3090A</i>	<i>3090b</i>
<i>Lithology</i>	<i>flow bded</i>	<i>flow bded</i>	<i>aphanitic</i>	<i>aphanitic</i>	<i>aphanitic</i>	<i>oded rhy</i>	<i>oded rhy</i>
<i>Unit</i>							
Ba	62	73	142	73	161	317	387
Li	9	9	9	3	12	11	6
Rb	300	261	264	261	211	150	237
Sr	13	15	12	7	10	50	67
Pb	23	11	54	52	8	20	30
Th	56	49	52	52	51	47	55
U	14	10	13	13	12	12	13
Zr	215	185	225	234	220	242	304
Nb	30	23	28	64	27	19	20
Y	63	54	64	64	50	41	41
La	65	77	233	81	100	67	95
Ce	129	147	434	151	195	129	173
Nd	61	65	185	67	80	57	71
Pr	13	16	47	14	19		
Sc	2	5	-1	2	1	8	6
V	-2	-2	-2	-2	-2	20	9
Cr	-1	-1	-1	1	1	44	11
Mn	151	376	193	540	157	427	450
Co	2	0	2	2	5	5	4
Ni	-1	-1	-1	-1	-1	10	5
Cu	3	1	3	-1	-1	1	15
Zn	35	50	31	29	50	69	49
Sn	6	3	-2	0	5	294	761
Mo	-2	-2	-2		14	-2	-2
Ga	22	20	23	22	17	17	19
Ar	3	3	3	2	3	3	4
S	-100	-100	200	-100	-100	-100	-100
Ag	2	1	1	2	1	2	2
Ge	3	3	3	3	3	3	3

*Appendix B - CIPW Norms for coherent rhyolite lavas of the Gimbat Ignimbrite Member*

<i>Sample#</i>	<i>3101</i>	<i>3108</i>	<i>3109</i>	<i>3111</i>	<i>3114</i>	<i>3090A</i>	<i>3090b</i>
<i>Lithology</i>	<i>flow bded</i>	<i>flow bded</i>	<i>aphanitic</i>	<i>aphanitic</i>	<i>aphanitic</i>	<i>bded rhy</i>	<i>bded rhy</i>
<i>Unit</i>							
Quartz	35.33	35.4	49.78	40.11	37.44	27.68	28.34
Corundum	0.46	0.05	4.11	1.8	1.41	0.59	0.45
Zircon	0.04	0.04	0.05	—	0.04	0.06	0.06
Orthoclase	35.34	31.24	29.12	28.58	37.67	33.42	34.72
Albite	21.92	22	12.1	20.73	18.79	26.32	26.15
Anorthite	2.54	6.11	0.19	2.17	0.02	3.19	2.79
Hypersthene	2.43	4.31	1.93	3.17	2.63	5.35	4.56
Enstatite	0.57	1.92	0.4	0.32	0.67	2.14	1.74
Ferrosilite	1.85	2.4	1.53	2.84	1.96	3.21	2.82
Magnetite	0.49	0.65	0.42	0.72	0.52	0.9	0.78
Chromite							
Ilmenite	0.17	0.32	0.15	0.19	0.15	0.53	0.46
Apatite	0.02	0.07		0.02	0.03	0.17	0.17
Diff. Index	92.59	86	91	89.42	93.89	87.42	89.21
Colour Index	3.09	5.31	2.54	4.08	3.3	6.78	5.8
Pl	24.45	25.37	12.29	22.9	18.81	29.51	28.94
Norm Plag	10.37	13.27	1.56	9.47	0.12	10.82	9.66
100An/(An+A	10.37	13.27	1.56	9.47	0.12	10.82	9.66
Ab	21.92	22	12.1	20.73	18.79	26.32	26.15
Q	35.93	34.31	50.25	40.85	38.09	29.06	29.5
Ol	1.83	3.19	1.46	2.42	1.99	3.98	3.4
Ne	11.88	11.92	6.56	11.24	10.18	14.26	14.17
Q	45.97	44.39	55.79	50.35	46.7	41.11	41.48
mg number	25.14	46	21.54	11.44	27.31	40.86	39.11

Appendix B - major element data for rocks of acidic composition that intrude the Gimbat Ignimbrite Member

Sample#	3002	3102	3123	3133	3155	3059	3084	3086	3088	3073	3149	8112- O139	8812- 6006	8812- 6007
Lithology	q/f porph	q/f porph	q/f porph	q/f porph	q/f porph	dacite	dacite	dacite	dacite	dacite	elsic dyke	syenite	syenite	syenite
SiO <sub>2</sub>	75.93	75.37	75.78	76.35	75.78	66.32	64.19	63.61	63.71	63.55	76.77	53.51	64.25	64.09
TiO <sub>2</sub>	0.11	0.05	0.1	0.1	0.11	0.51	0.64	0.69	0.57	0.58	0.09	1.19	0.5	0.5
Al <sub>2</sub> O <sub>3</sub>	12.02	11.93	11.51	11.43	11.81	14.72	12.17	12.82	15.31	15.14	11.25	13.97	15.86	15.61
Fe <sub>2</sub> O <sub>3</sub> tot	1.69	1.77	2.07	2.57	1.37	4.75	5.25	4.89	5.24	5.2	1.02			
Fe <sub>2</sub> O <sub>3</sub>	0.65	0.68	1.04	1.41	0.79	1.22	2.69	2.15	1.84	1.09	0.32	7.99	1.14	1.52
FeO	0.94	0.98	0.93	1.04	0.52	3.18	2.3	2.47	3.06	3.7	0.63	2.06	3.06	2.68
MnO	0.03	0.02	0.03	0.02	0.04		0.08	0.1	0.13	0.08	0.05	0.14	0.09	0.09
MgO	0.39	0.41	0.72	0.49	0.38	0.66	3.35	3.95	0.93	1.42	0.32	5.43	1.17	0.95
CaO	0.21	0.75	0.04	0.03	0.69	1.08	3.01	2.59	1.39	1.16	1.33	5.96	0.7	1.24
Na <sub>2</sub> O	2.16	1.41	1.1	2.77	2.44	2.89	1.48	1.98	3.28	2.55	4.53	0.95	3	3.2
K <sub>2</sub> O	5.69	6.8	7.51	5.39	5.8	6.66	7.29	5.88	6.68	6.83	2.81	5.89	7.57	7.18
P <sub>2</sub> O <sub>5</sub>	0.01	0.01	0.01	0.01	0.01	0.14	0.62	0.58	0.17	0.17	0.01	0.16	0.12	0.12
rest	1.31	1.44	1.31	0.8	1.56	2.02	1.68	3.03	2.61	3.15	1.61	0.45	0.5	0.45
L.O.I.	0.26	0.26	0.27	0.22	0.21	0.35	0.43	0.41	0.37	0.29	0.27	2.38	2.12	2.52
TOTAL	99.71	100.11	100.35	100.06	100.14	99.81	99.93	100.26	100.05	99.71	99.99	100.08	100.08	100.15

# all samples are prefixed by 8912- unless otherwise stated

Appendix B - trace element data for rocks of acidic composition that intrude the Gimbat Ignimbrite Member

Sample#	3002	3102	3123	3133	3155	3059	3084	3086	3088	3073	3149	8112- O139	8812- 6006	8812- 6007
Lithology	q/f porph	q/f porph	q/f porph	q/f porph	q/f porph	dacite	dacite	dacite	dacite	dacite	elsic dyke	syenite	syenite	syenite
Ba	1363	247	411	386	329	703	1564	1400	674	625	151	1179	1947	1314
Li	40	21	21	8	7	15	18	30	7	16	8	20	16	13
Rb	110	582	293	206	233	144	280	253	168	172	104	176	183	194
Sr	256	21	60	47	28	100	267	307	95	78	13	98	165	109
Pb	19	9	16	10	15	26	20	40	18	20	474	34	57	18
Th	3	85	38	40	49	52	40	37	46	46	53	47	34	39
U	2	23	4	5	10	10	12	12	8	8	12	7	5.5	6
Zr	137	193	179	185	195	688	316	303	793	785	197	709	614	708
Nb	7	49	20	17	23	19	14	13	17	17	27	20	17	19
Y	26	94	57	35	53	37	29	26	33	33	55	37	28	32
La	32	52	74	22	67	233	83	70	241	226	75	342	201	236
Ce	57	120	144	57	134	399	156	136	410	385	151	614	342	398
Nd	29	62	61	23	63	139	70	62	144	133	68	190	121	138
Pr	15	15	15	8								53	36	38
Sc	25	-1	3	2	3	16	16	15	18	18	2	16	13	14
V	165	-2	7	7	-2	9	82	100	6	5	-2	8	5	9
Cr	253	-1	-1	2	-1	10	129	110	8	9	-1	23	96	10
Mn	1609	150	278	152	258	507	737	883	1189	734	406	-	752	766
Co	42	3	2	2	3	3	15	14	4	3	4	-	-	-
Ni	66	-1	1	-1	1	3	30	29	3	3	1	7	27	5
Cu	20	-1	1	-1	3	8	-1	2	33	7	6	5	7	4
Zn	218	31	40	32	16	23	177	236	73	22	18	127	108	84
Sn	-2	8	-2	-2	-2	-2	3	-2	-2	2	-2	2	<2	<2
W	168	494	764	665	433	272	175	130	126	137	827	-	165	282
Mo	-2	-2	-2	-2	3	-2	-2	-2	-2	-2	7	3	<2	<2
Ga	19	25	17	17	17	18	14	15	18	17	15	20	18	19
As	4	8	3	2	3	4	11	4	2	15	13	4	2	6.5
S	-100	-100	-100	-100	-100	600	-100	-100	-100	2200	100	-	<100	<100
Ag	3	2	2	1	2	2	3	2	3	3	2	1	2	2
Ge	2	3	4	3	3	3	3	3	3	2	3	-	1.5	1.5

Appendix B - CIPW Norms for rocks of acidic composition that intrude the Gimbat Ignimbrite Member

Sample#	3002	3102	3123	3133	3155	3059	3084	3086	3088	3073	3149	8112- O139	8812- 6006	8812- 6007
Lithology	q/f porph	q/f porph	q/f porph	q/f porph	q/f porph	dacite	dacite	dacite	dacite	dacite	felsic dyke	syenite	syenite	syenite
Quartz	39.61	37.85	38.31	37.44	36.6	18.83	16.73	17.54	12.57	16.11	36.78	2.84	12.54	11.96
Corundum	9.93	0.84	1.45	0.96	0.24	1.05			0.49	1.77			1.56	0.48
Zircon	0.04	0.04	0.04	0.04	0.04	0.14	0.06	0.06	0.16	0.16	0.04	0.14	0.12	0.14
Orthoclase	33.75	40.41	44.49	31.93	34.37	39.41	43.19	34.85	39.54	40.43	16.65	34.87	44.8	42.5
Albite	18.28	11.93	9.31	23.44	20.65	24.45	12.52	16.75	27.75	21.58	38.33	8.04	25.39	27.08
Anorthite	1.09	3.73	0.26	0.2	3.46	4.66	4.99	8.7	6	4.83	2.03	16.44	3.25	5.76
Diopside							5.21	0.67			3.8	10.2		
Di(CaMg)							3.39	0.47			1.72	6.16		
Hedenbergite							1.82	0.2			2.08	4.04		
Hypersthene	2.81	3.02	4.08	4.06	2.42	6.29	10.97	14.21	7.68	8.29		18.72	7.5	6.91
Enstatite	0.97	1.02	1.79	1.22	0.95	1.64	6.79	9.62	2.32	3.54		10.68	2.91	2.37
Ferrosilite	1.83	2	2.29	2.84	1.47	4.64	4.18	4.58	5.36	4.75		8.04	4.59	4.54
Magnetite	0.49	0.51	0.6	0.75	0.4	1.38	1.54	1.44	1.52	1.51	0.3	2.98	1.32	1.31
Chromite							0.03	0.02					0.02	
Ilmenite	0.21	0.09	0.19	0.19	0.21	0.97	1.22	1.31	1.08	1.1	0.17	2.26	0.95	0.95
Apatite	0.03	0.02	0.03	0.03	0.02	0.34	1.5	1.41	0.41	0.41	0.02	0.38	0.31	0.3
Diff. Index	91.63	90.19	92.12	92.81	91.61	82.69	72.44	69.14	79.86	78.12	91.76	45.75	82.73	81.54
Colour Index	3.51	3.63	4.87	4.99	3.03	8.75	18.96	17.65	10.28	11.31	4.29	34.17	9.79	9.17
Pl	19.37	15.66	9.57	23.64	24.1	29.12	17.52	25.46	33.75	26.41	40.37	24.48	28.64	32.83
Norm Plag	5.63	23.82	2.73	0.84	14.34	16.02	28.5	34.18	17.77	18.31	5.04	67.16	11.36	17.53
100An/(An+A	5.63	23.82	2.73	0.84	14.34	16.02	28.5	34.18	17.77	18.31	5.04	67.16	11.36	17.53
Ab	18.28	11.93	9.31	23.44	20.65	24.45	12.52	16.75	27.75	21.58	38.33	8.04	25.39	27.08
Q	40.32	38.61	39.37	38.45	37.22	20.38	19.71	21.46	14.48	18.25	36.78	7.86	14.45	13.7
Ol	2.1	2.26	3.02	3.05	1.8	4.74	7.99	10.28	5.76	6.15		13.69	5.58	5.17
Ne	9.91	6.47	5.04	12.7	11.19	13.25	6.79	9.08	15.04	11.69	20.78	4.36	13.76	14.68
Q	48.69	44.07	43.64	49.19	46.67	31.58	25.45	29.14	27.2	28.13	54.34	11.54	26.08	26.1
mg number	36.29	36.46	46.22	32.1	40.75	25.58	61.25	66.64	30.52	40.32	43.71	56.67	38.94	34.33

Appendix B - major element data for mafic volcanics of the Coronation Sandstone  
and dolerites intrusive into the Gimbat Ignimbrite Member

Sample#	3001	3004	3009	3014	3017a	3018	3117	3026	3027	3038	3057	3072	3103	3105	3115	3136b
Lithology	basalt	basalt	basalt, mix	basalt, mix	basalt, mix	basalt, mix	basalt	dolerite	dolerite	dolerite	dolerite	dolerite	dolerite	dolerite	dolerite	xenolith
Unit	Coro Sst	Coro Sst	Coro Sst	Coro Sst	Coro Sst	Coro Sst	Coro Sst									
SiO <sub>2</sub>	49.44	56.46	62.15	61.38	55.45	61.86	54.35	48.04	48.84	51.24	46.55	50.95	50.28	51.23	43.7	51.81
TiO <sub>2</sub>	1.32	1.41	0.5	0.68	0.71	0.62	1.46	2.38	1.72	1.54	1.77	0.96	1.16	1.49	1.82	1.28
Al <sub>2</sub> O <sub>3</sub>	14.85	14.68	13.21	14.46	16.6	14.16	15.06	12.97	14.32	14.99	14.63	14.71	12.73	13.3	13.84	17.38
Fe <sub>2</sub> O <sub>3</sub> tot	11.9	10.66	6.21	6.14	7.65	6.49	10.81	16.26	12.81	11.37	15.17	9.95	9.49	11.89	14.74	9.87
Fe <sub>2</sub> O <sub>3</sub>	3.89	4.91	1.42	3.05	4.04	3.7	6.55	4.85	4.01	3.47	5	0.89	3.22	4.02	3.43	2.32
FeO	7.21	5.17	4.31	2.78	3.25	2.51	3.83	10.27	7.92	7.11	9.15	6.24	5.64	7.08	10.18	6.79
MnO	0.19	0.14	0.12	0.1	0.07	0.09	0.12	0.22	0.13	0.15	0.21	0.15	7.48	0.16	0.21	0.12
MgO	7.21	3.01	4.51	3.84	5.27	3.59	3.41	5.34	5.36	4.45	7.76	8.04	7.48	3.33	5.96	4.16
CaO	6.52	4.71	3.63	5.17	5.49	5.1	3.86	8.08	7.45	6.8	5.66	6.6	4.4	6.03	7.29	3.8
Na <sub>2</sub> O	2.42	2.78	2.64	2.77	2.91	2.75	2.84	2.27	1.96	3.05	2.21	1.63	2.44	3.97	2.34	5.13
K <sub>2</sub> O	2.44	3.13	4.63	4.11	2.23	3.96	4.18	1.82	1.64	2.35	1.71	2.39	2.4	1.38	0.68	3.64
P <sub>2</sub> O <sub>5</sub>	0.42	0.84	0.28	0.36	0.32	0.3	0.88	0.21	0.58	0.68	0.51	0.49	0.41	0.21	0.22	0.47
rest	3.79	2.45	2.04	1.05	3.23	1.1	3.19	3.05	5.69	3.71	4.21	4.23	9.02	7.75	10.08	2.61
L.O.I.	0.38	2.46	0.57	0.43	0.37	0.41	0.4	0.23	0.35	0.39	0.34	0.43	0.33	0.26	0.21	0.35
TOTAL	100.08	100.17	100.01	100.18	99.94	100.15	100.13	99.73	99.97	99.93	99.71	99.84	99.72	100.21	99.96	99.86

# all sample numbers are prefixed by 8912-

*Appendix B - trace element data for mafic volcanics of the Coronation Sandstone  
and dolerites intrusive into the Gimbat Ignimbrite Member*

<i>Sample#</i>	<i>3001</i>	<i>3004</i>	<i>3009</i>	<i>3014</i>	<i>3017a</i>	<i>3018</i>	<i>3117</i>	<i>3026</i>	<i>3027</i>	<i>3038</i>	<i>3057</i>	<i>3072</i>	<i>3103</i>	<i>3105</i>	<i>3115</i>	<i>3136b</i>
<i>Lithology</i>	<i>basalt</i>	<i>basalt</i>	<i>basalt, mix</i>	<i>basalt, mix</i>	<i>basalt, mix</i>	<i>basalt, mix</i>	<i>basalt</i>	<i>dolerite</i>	<i>dolerite</i>	<i>dolerite</i>	<i>dolerite</i>	<i>dolerite</i>	<i>dolerite</i>	<i>dolerite</i>	<i>dolerite</i>	<i>xenolith</i>
<i>Unit</i>	<i>Coro Sst</i>	<i>Coro Sst</i>	<i>Coro Sst</i>	<i>Coro Sst</i>	<i>Coro Sst</i>	<i>Coro Sst</i>	<i>Coro Sst</i>									
Ba	1363	2086	2291	1499	917	1382	1575	323	1019	1271	786	1120	610	392	169	225
Li	40	32	21	12	32	11	27	38	47	38	37	26	193	19	11	44
Rb	110	88	210	142	99	134	168	78	51	81	110	98	87	45	133	482
Sr	256	355	320	430	405	409	281	224	329	520	284	307	320	93	49	125
Pb	19	28	58	41	24	33	17	18	16	12	17	16	20	18	8	9
Th	3	16	47	30	34	31	17	2	7	10	4	13	8	9	28	10
U	2	5	11	7	8	8	4	1	2	2	1	2	2	2	4	5
Zr	137	246	198	220	238	206	255	125	171	227	190	180	145	341	127	171
Nb	7	13	11	13	13	12	13	12	10	12	8	9	11	15	6	16
Y	26	32	24	28	31	26	35	29	36	36	36	23	29	52	29	45
La	32	64	98	73	59	67	66	17	43	59	27	58	48	45	10	65
Ce	57	129	162	134	125	132	136	42	94	121	63	123	93	87	26	129
Nd	29	59	64	57	56	54	64	20	49	57	35	56	44	46	16	57
Pr	7	14	14	16	15	12		5	15	13	9	14	9	13	4	12
Sc	25	20	18	19	22	18	21	38	28	24	30	29	30	32	40	30
V	165	198	97	107	99	94	211	442	181	182	213	173	196	136	187	156
Cr	253	6	417	200	310	255	4	29	244	194	305	626	199	135	126	511
Mn	1609	1162	1110	878	630	828	1091	1775	1217	1182	1712	1310	1965	1419	1918	1071
Co	42	24	20	20	27	21	24	51	39	36	49	34	31	31	4	29
Ni	66	4	57	32	61	49	5	36	58	37	124	114	56	14	59	76
Cu	20	15	3	33	-1	13	1	72	29	21	37	12	37	115	59	-1
Zn	218	205	275	85	141	99	194	194	137	126	214	199	412	276	255	199
Sn	-2	-2	3	-2	2	-2	-2	-2	-2	-2	-2	-2	-2	-2	-2	-2
W	168	227	288	291	154	296	104	149	91	148	38	135	90	59	488	160
Mo	-2	-2	-2	-2	-2	-2	-2	-2	-2	-2	-2	-2	-2	-2	-2	-2
Ga	19	20	15	18	22	17	21	23	20	20	23	18	16	23	12	31
Ar	4	4	3	4	9	4	5	4	3	4	4	3	3	4	1	4
S	-100	-100	-100	-100	-100	-100	-100	1500	-100	500	-100	-100	1100	-100	1300	-100
Ag	3	3	2	2	3	2	3	4	3	3	3	4	3	4	1	3
Ge	2	2	2	2	3	1	4	4	3	3	4	3	4	4	3	5

Appendix B - CIPW Norms for mafic volcanics of the Coronation Sandstone  
and dolerites intrusive into the Gimbat Ignimbrite Member

Sample#	3001	3004	3009	3014	3017a	3018	3117	3026	3027	3038	3057	3072	3103	3105	3115	3136b
Lithology	basalt	basalt	basalt, mix	basalt, mix	basalt, mix	basalt, mix	basalt	dolerite	dolerite	dolerite	dolerite	dolerite	dolerite	dolerite	dolerite	xenolith
Unit	Coro Sst	Coro Sst	Coro Sst	Coro Sst	Coro Sst	Coro Sst	Coro Sst									
Quartz	—	11.16	13.41	12.63	7.51	14.01	6	0.37	4.82	2.11	—	3.65	3.51	3.28	—	—
Zircon	0.03	0.05	0.04	0.04	0.05	0.04	0.05	0.03	0.03	0.05	0.04	0.04	0.03	0.07	0.03	0.03
Orthoclase	14.46	18.53	27.44	24.34	13.22	23.45	24.77	10.79	9.71	13.92	10.15	14.16	14.22	8.17	4.07	21.7
Albite	20.48	23.52	22.34	23.44	24.62	23.27	24.03	19.21	16.58	25.81	18.7	13.79	20.65	33.59	19.8	34.69
Anorthite	22.43	18.38	10.55	14.91	25.54	14.62	13.9	19.75	25.39	20.25	24.92	25.77	16.34	14.36	25.22	13.5
Diopside	6.24	0.13	5.18	7.3	—	7.58		15.89	6.74	7.91	0.12	3.39	2.5	11.98	7.91	1.97
Di(CaMg)	3.95	0.06	3.44	4.69	—	4.61		8.03	3.76	4.29	0.07	2.35	1.75	5.41	4.32	1.1
edenbergite	2.28	0.07	1.74	2.62	—	2.97		7.86	2.99	3.62	0.05	1.04	0.75	6.57	3.59	0.87
Hypersther	21.13	17.66	15.27	12.15	20.89	11.86	18.78	20.33	22.21	17.93	26.4	28.52	26.6	13.85	21.87	
Enstatite	12.71	7.47	9.66	7.41	13.13	6.82	8.49	9.58	11.61	9.1	14.88	18.94	17.82	5.79	11.2	
Ferrosilite	8.42	10.19	5.61	4.75	7.77	5.04	10.28	10.75	10.59	8.83	11.53		8.78	8.06	10.67	
Olivine	4.15										5.74				2.36	13.84
Forsterite	2.4											3.1			1.15	6.9
Fayalite	1.75										2.64	9.58			1.21	6.94
Magnetite	3.49	3.13	1.82	1.8	2.24	1.9	3.18	4.81	3.75	3.34	4.44	2.92	2.79	3.48	4.32	2.89
Chromite	0.05	—	0.09	0.04	0.07	0.05		0.01	0.05	0.04	0.07	0.13	0.04	0.03	0.03	0.11
Ilmenite	2.51	2.68	0.95	1.29	1.35	1.18	2.77	4.52	3.27	2.92	3.36	1.82	2.2	2.83	3.46	2.43
Apatite	1	2.03	0.68	0.86	0.76	0.72	2.12	0.5	1.38	1.63	1.22	1.17	0.98	0.5	0.52	1.12
Diff. Index	34.94	53.21	63.2	60.41	45.35	60.74	54.8	30.36	31.12	41.83	28.85	31.6	38.37	45.04	23.87	56.38
Colour Ind.	37.57	23.61	23.31	22.59	24.55	22.57	24.73	45.84	36.02	32.24	40.13		34.35	32.17	40.18	21.26
PI	42.91	41.91	32.88	38.35	50.16	37.89	37.93	38.96	41.98	46.06	43.62		36.98	47.96	45.02	48.18
Norm Plag	52.27	43.87	32.07	38.88	50.19	38.59	36.64	50.7	60.49	43.97	57.13		44.18	29.95	56.02	28.01
100An/(An	52.27	43.87	32.07	38.88	50.19	38.59	36.64	50.7	60.49	43.97	57.13		44.18	29.95	56.02	23.72
Ab	20.48	23.52	22.34	23.44	24.62	23.27	24.03	19.21	16.58	25.81	18.7		20.65	33.59	19.8	43.41
Q	5.72	15.71	17.58	15.92	13.2	17.2	10.89	5.69	10.71	6.84	7.08		10.84	6.85	5.78	—
Ol	19.56	13.1	11.1	8.86	15.2	8.67	13.89	15.02	16.32	13.19	25.07		19.27	10.28	18.45	13.84
Ne	11.1	12.75	12.11	12.7	13.35	12.61	13.02	10.41	8.99	13.99	10.14		11.19	18.21	10.73	23.53
Q	15.1	26.49	27.81	26.66	24.48	27.86	21.89	14.48	18.31	18.66	15.64		20.29	22.23	14.85	15.89
mg number	59.99	41.15	64.26	60.76	63.03	57.8	43.86	44.84	50.87	49.2	55.88		66.12	40.95	50.02	51.07

*Appendix B - Rare Earth Element Data for selected samples of the Gimbat Ignimbrite Member, Coronation Sandstone, and intrusive units*

<i>Sample#</i>	<i>89123001</i>	<i>89123014</i>	<i>89123038</i>	<i>89123062</i>	<i>89123063</i>	<i>89123092</i>	<i>89123104</i>	<i>89123111</i>	<i>89123123</i>	<i>89123136</i>	<i>89123153</i>
<i>Lithology</i>	<i>basalt</i>	<i>basalt</i>	<i>dolerite</i>	<i>cj ig</i>	<i>ignim</i>	<i>dolerite</i>	<i>ignim</i>	<i>aph rhy</i>	<i>qlf porph</i>	<i>xenolith</i>	<i>ignim</i>
<i>Unit</i>	<i>Coro Sst</i>	<i>Coro Sst</i>		<i>IC</i>	<i>non weld</i>		<i>ID</i>				<i>IE</i>
La	32.2	109.18	75.58	151.72	98.56	35.45	53.23	77.88	58.6	57.08	64.03
Ce	64.25	217.86	151.33	299.43	188.33	67.74	115.18	160.02	133.83	127.27	125.21
Pr	7.97	17.26	17.26	30.98	20.89	8.95	14.21	17.1	13.37	13.43	14.66
Nd	33.5	63.53	70.96	108.42	75.88	37.02	48.39	64.49	48.05	56.44	52.13
Sm	6.76	10.34	12.16	16.59	12.64	7.65	9.69	14.92	10.02	11.66	9.27
Eu	2.1	2.18	3.47	1.52	1.05	2.72	0.5	0.2	0.58	1.2	0.825
Gd	5.56	7.47	5.72	10.84	10.09	6.82	6.94	13.45	7.44	12.76	6.84
Tb	0.92	0.82	1.21	1.453	1.35	1	1.13	2.02	1.06	1.42	0.91
Dy	5.52	3.61	8.9	7.357	7.31	5.72	6.84	10.21	6.74	5.66	5.68
Ho	1.01	0.71	0.97	1.27	1.29	1.025	1.42	2.07	1.42	1.24	1.04
Er	2.8	1.41	2.05	3.56	3.55	2.75	4.09	5.99	4.48	3.11	3.05
Yb	2.35	0.777	1.36	3.1	3.24	2.87	4.07	5.08	4.76	2.75	3.47

**APPENDIX C**  
**DEFINITION OF A NEW**  
**STRATIGRAPHIC UNIT:**  
**THE GIMBAT IGNIMBRITE MEMBER**

## DEFINITION OF A NEW STRATIGRAPHIC UNIT: THE GIMBAT IGIMBRITE MEMBER

**Name:** Gimbat Ignimbrite Member (Pul Pul Rhyolite; El Sherana Group).

**Rank:** Member

**Derivation:** Gimbat Homestead, STOW 1:100 000 Sheet area, grid reference 414981.

**Synonymy:** Previously mapped as undivided Pul Pul Rhyolite of the El Sherana Group.

**Distribution:** The Gimbat Ignimbrite Member extends around the southern margin of the Malone Creek Granite, approximately 10 km southeast of Coronation Hill, on the STOW 1:100 000 Sheet area. It encompasses the volcanics, which outcrop east of the Palette Fault in this area. Total outcrop area is ~ 40km<sup>2</sup>. These are mainly ignimbrites, related volcanoclastic sediments, aphyric rhyolite lava and subvolcanic intrusives

**Type Section:** A type section is proposed for the Gimbat Ignimbrite Member along a tributary side creek to the South Alligator River 2.5 km ESE of Big Sunday (grid reference 485890-476877). Along rock pavements in the creek bed, and upon the low ridges to either side, the main rock types of the Gimbat Ignimbrite Member are well exposed. The dominant rock type is rhyolitic ignimbrite, and most of the subfacies of the ignimbrites of the Gimbat Ignimbrite Member outcrop at this locality. Fluvial epiclastic sediments outcrop in low ridges surrounding the creek. The ignimbrites are intruded by the Malone Creek Granite at the base of the sequence, a felsic sill at the top of the sequence, and a late-stage vertical dolerite dyke. Crystal-rich arenites of the Big Sunday Formation overlie the Gimbat Ignimbrite Member where the tributary meets the South Alligator River.

**Lithology:** The Gimbat Ignimbrite Member consists mainly of quartz-feldspar-lithic bearing rhyolitic welded ignimbrites. The welded ignimbrites are subdivided into 5 sub-units on the basis of main lithic contaminant, degree of welding, and stratigraphic position (Units IA - IE). They are conformably overlain by a non-welded ignimbrite which hosts discontinuous lenses of volcanic sandstone and pebble conglomerate. In the southeast of the outcrop area, the ignimbrites are overlain by a massive to flow banded, aphyric to sparsely porphyritic, quartz-feldspar bearing rhyolite lava. Comagmatic quartz-feldspar porphyry intrusives, and felsic sills and dykes have also been included in the Gimbat Ignimbrite Member.

**Thickness:** The exposed thickness of the Gimbat Ignimbrite Member is approximately 830 m.

**Relationships:** The Gimbat Ignimbrite Member overlies the Coronation Sandstone of the El Sherana Group. The nature of the contact can not be directly discerned, but appears to be unconformable, as the ignimbrites infill a palaeotopography formed on Coronation Sandstone. The Gimbat Ignimbrite Member is unconformably overlain by the Big Sunday Formation. The top of the sequence is locally truncated by the main Palette Fault System, isolating it from units of the El Sherana Group and Edith River Group to the west of the fault. To the south and east it is overlain by Quaternary soils and sandplains. It is intruded by the Malone Creek Granite, unnamed quartz-feldspar porphyries and syenite porphyries, felsic sills and dykes, large dolerite bodies and late-stage vertical dolerite dykes.

**Distinguishing Features:** Rhyolitic in composition, contains large red fiamme and lithic fragments. Red to dark brown in colour.

**Depositional Environment:** The Gimbat Ignimbrite Member is a subaerially erupted and deposited volcanic sequence. The palaeoenvironment is interpreted to be a proximal shield setting.

**Correlation with other units:** The Gimbat Ignimbrite Member may correlate with ignimbrite and rhyolite lava of the Pul Pul Rhyolite type section, but evidence of this is inconclusive.

**Age:** Early Proterozoic. Zircon U-Pb age determination by SHRIMP (ion-microprobe) gave an age of  $1831 \pm 12$  Ma on a sample of quartz-feldspar porphyry intruding the Gimbat Ignimbrite Member, and on a porphyry lithic fragment within the ignimbrites, suggesting this is the crystallisation age of the sequence. A sample of ignimbrite yielded an age of  $1844 \pm 12$  Ma. The older age is attributed to inheritance from older zircon xenocrysts in the sample.

**References:** Jagodzinski, E.A. 1992. A study of the felsic volcanic succession southeast of Coronation Hill. Palaeovolcanology-Geochemistry-Geochronology. *BMR Record* 1992/9.  
Needham, R.S., and Stuart-Smith, P.G. 1985a. Revised stratigraphic nomenclature and correlation of Early Proterozoic rocks of the Darwin-Katherine region, Northern Territory. *BMR Journal of Australian Geology and Geophysics* . 10: 121-131.  
Needham, R.S., and Stuart-Smith, P.G. 1985b. Stratigraphy and tectonics of the Early to Middle Proterozoic transition, Katherine-El Sherana area, Northern Territory. *Aust. Journal of Earth Sci.* 32: 219-230.  
Stewart, J.R. 1965. Middle Proterozoic Volcanic Rocks in the Katherine-Darwin Area, Northern Territory. *Bureau of Mineral Resources, Geology and Geophysics, Report No. 90.*  
Stuart-Smith, P.G., Needham, R.S., & Bagas, L. 1988. Stow, Northern Territory (Sheet 5470). *Bureau of Mineral Resources, Australia, 1:100 000 Geological Map and Commentary.*

**APPENDIX D**  
**XRD DATA**

## XRD ANALYSIS OF THE CLAY FRACTION OF Gimbat Formation MATERIAL

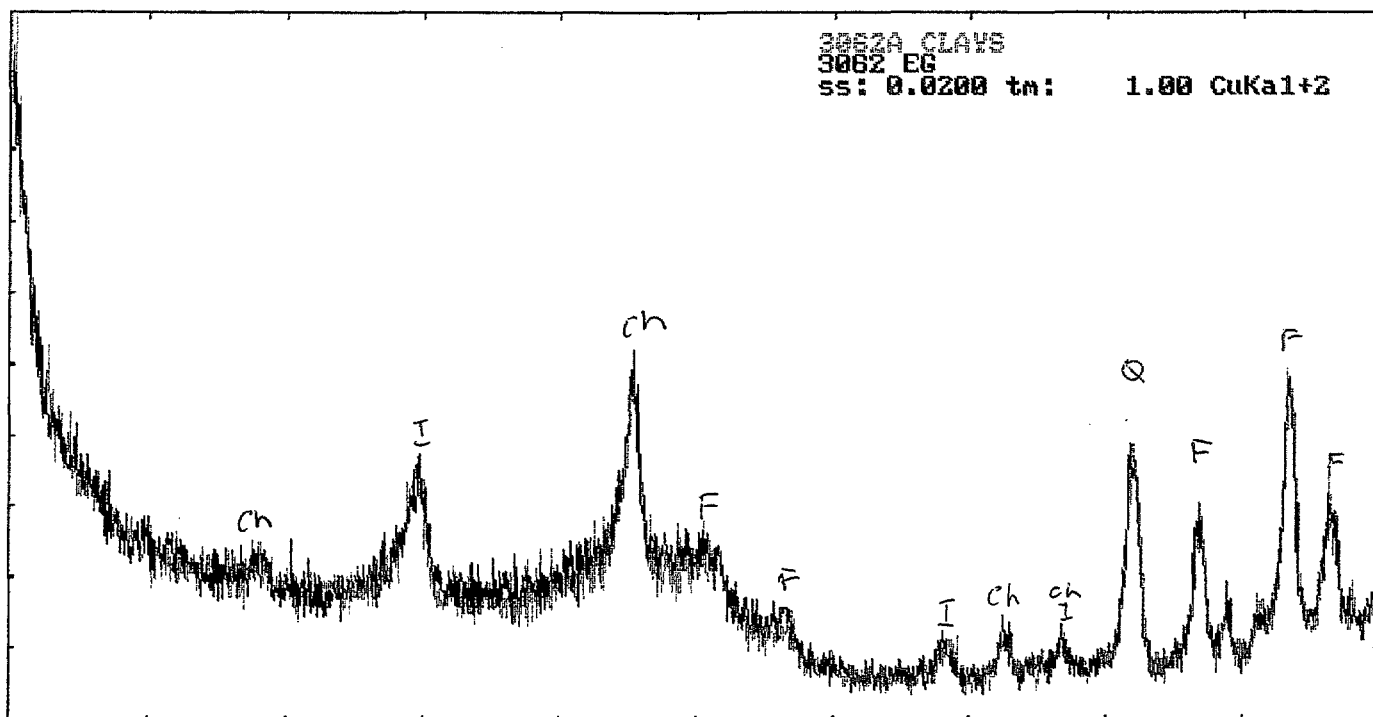
As a follow up on preliminary work carried out, earlier this year, on Kakadu Gimbat Formation samples, the clay fractions of the remaining samples were separated and analysed as natural and glycolated material. The results of the analysis show, as with the previously tested material, the presence of chlorite and mica (illite) in all samples with the addition of montmorillonite in sample number '3142. The traces of two samples are provided.

### RESULTS

Sample	Description	Clays
8912 31062A	ignimbrite	chlorite, mica(illite)
8912 3079	epiclastic	chlorite, mica (illite)
8912 3081	epiclastic	chlorite, mica (illite)
8912 3082	ignimbrite	chlorite, mica (illite)
8912 3104C	ignimbrite	chlorite, mica (illite)
8912 3137A	ignimbrite	chlorite, mica (illite) ?
8912 3142	epiclastic	chlorite, montmorillonite, mica (illite)
8912 3143	epiclastic	chlorite, mica (illite) ?
8912 3145		chlorite, mica(illite)
8912 3147A		chlorite, mica(illite)
8912 3152A		chlorite, mica(illite)
8912 3153		chlorite, mica(illite)
8912 3154		chlorite, mica(illite)
8912 3156		chlorite, mica(illite)
8912 3172		chlorite, mica(illite)
8912 3173		chlorite, mica(illite)

*Julienne Kamprad*

Julienne Kamprad  
28/11/91

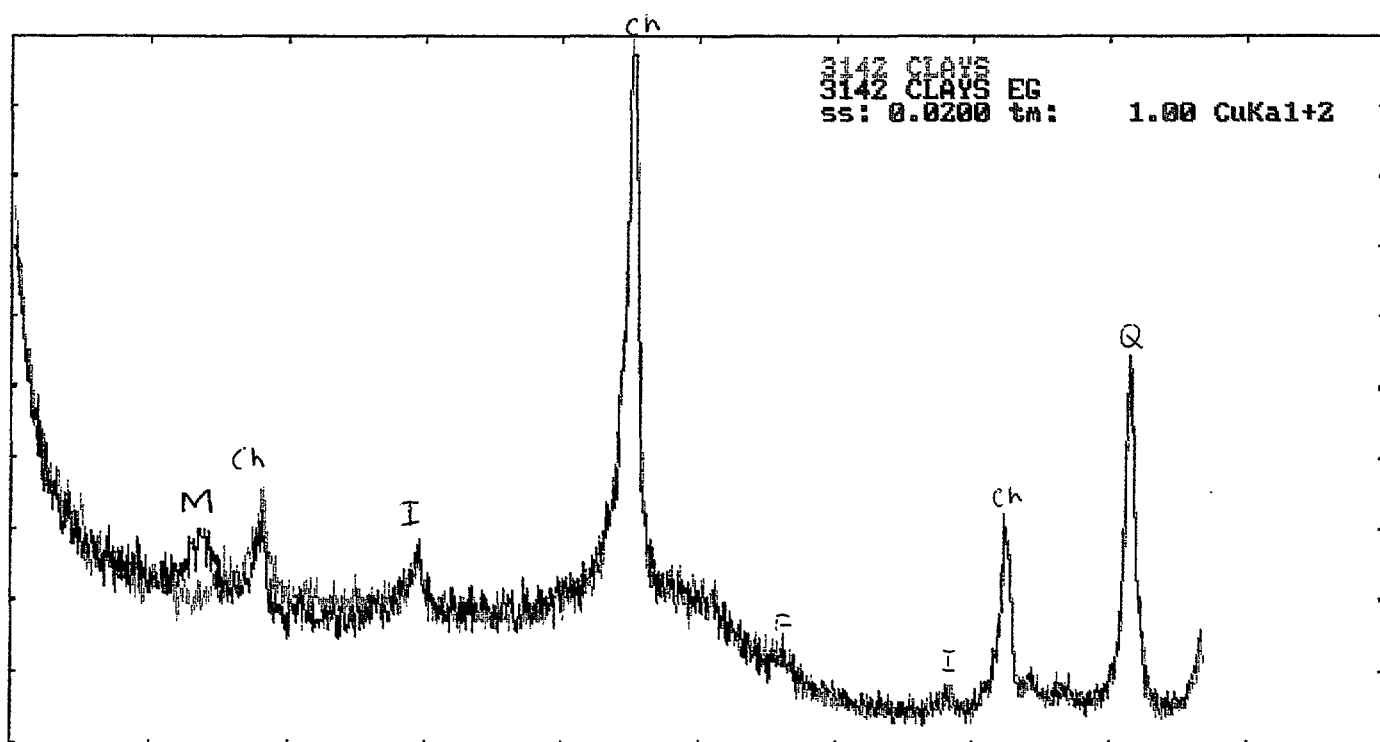


< 2.000 Overline x : 2theta y : 628. Linear 25.000 >

ch - chlorite  
I - mica(illite)  
M - montmorillonite  
F - ferrospar

Test rm\_Ab tgl\_0 Quant Imm\_Q subtr Retrn -> R

Q - QUARTZ



< 2.000 Overline x : 2theta y : 737. Linear 25.000 >

**APPENDIX E**  
**CONTRACTOR'S REPORT:**  
**PROFESSOR R.A.F. CAS**  
**MONASH UNIVERSITY**  
**1990**

THE PROTEROZOIC PUL PUL RHYOLITE FORMATION,  
SOUTH ALLIGATOR RIVER REGION, KAKADU NATIONAL PARK, STAGE 3

INTRODUCTION

This report is a summary of observations made during a field trip to the above area from the 17th - 22nd June, 1990 inclusive to advise on the detailed mapping of the Pul Pul Rhyolite by Ms. Elizabeth Jagodzinski, contract geologist employed by the B.M.R. during 1990. The area examined was the area defined as Pul Pul Rhyolite in the belt from southeast of Coronation Hill, and lying along the southwestern margin of the Malone Creek Granite, northeast of the Palette Fault (Stow Region 1:100,00 Geological Map, Stuart-Smith et al. 1988, Bureau of Mineral Resources).

THE PUL PUL RHYOLITE

In the area examined, the Pul Pul Rhyolite is dominated by quartz-feldspar bearing rhyolitic ignimbrites. The basal contact with the underlying (?) fluvial arkosic sedimentary rocks and basalts/dolerites of the Coronation Sandstone appeared to be complicated by faulting, and the nature of the relationship between this basal section and the Malone Creek Granite was not resolved.

The ignimbrites of the Pul Pul Rhyolite are variably welded, as defined by a clear eutaxitic texture of flattened pumice clasts in weather-etched, largely bouldery outcrop. Variation in the degree of welding is defined by variable degrees of attenuation of pumice clasts and the variable development of columnar jointing. The ignimbrite succession is massive and generally structureless, but it may be possible to subdivide the ignimbrite succession on the basis of variable degrees of welding as defined by pumice attenuation and columnar jointing, and of horizons of lithics, which almost certainly represent the bases of separate pyroclastic flow units. Lithics include dolerite, (?Zamu Dolerite derived?) which is very common, quartz feldspar porphyry, quartz sandstone (?Coronation Sandstone derived) and cleaved and crenulated metapelite/metapsamnite (?basement derived).

2

In general the lithic horizons contain low to moderate lithic clast concentrations (up to 20%), and are consistent with basal lithic concentration zones of layer 2b of ignimbrite depositional facies models (see Cas & Wright 1988). However, one horizon of lithics noted in ridge exposure to the southeast of Dinner Creek is many metres thick, is clast-supported with lithics up to 2m in maximum dimension. The nature of the matrix is not clear from outcrop. If it is ignimbrite as proposed by Ms. Jagodzinski (pers.comm), then it likely to be a ground layer (the deposit of the highly fluidised head of the extremely "violent" or high velocity pyroclastic flow, or a lag fall breccia, the result of collapse and deflation of an eruption column. The former could form any distance from vent, the latter no more than 3-4km from vent. If the matrix is volcanic sediment, a thought supported by rounding of many lithics, then the lithic horizon could simply be an incised, high relief fluvial conglomerate.

Lenses of pebble conglomerate and volcanic sandstone occur as discontinuous bodies within the ignimbrite succession and appear to represent local sediment filled fluvial gullies formed during a short break between emplacement of ignimbrite flow units. Clasts include large vein quartz as well as volcanic pebbles in the conglomerate, and angular quartz, feldspar and lithic fragments in the sandstones, indicating mixed basement derived, and contemporaneous pyroclastic deposit (almost certainly the subjacent ignimbrites) detritus. One such epiclastic horizon examined was upward fining from pebble conglomerate to fine volcanic sandstone and varied from being massive to diffusely planar stratified to cross-bedded.

The upper part of the Pul Pul Rhyolite is characterised by thick (up to tens of metres thick) crystal-lithic rich volcanic sandstone beds. Although there appears to be a laterally extensive horizon of this facies below the overlying Big Sunday Formation, in a superb stretch of across strike exposure in the South Alligator River (G.R. 468 887-892, Stow Region 1:100,000 Geological Sheet), there appears to be a somewhat thicker succession of this facies, suggesting a possible palaeovalley or canyon infill.

This crystal rich facies is dimensionally comparable with subaerial ignimbrites in terms of thickness, but it is anomalous in being so clast/grain rich and ash-matrix poor. Such thick, massive crystal rich units are only known from subaqueous successions of juvenile volcanoclastics (e.g. Cas 1979, 1983). Ignimbrites are never wholly crystal or grain rich, closed framework grain aggregates. Only certain

subfacies such as groundlayers are fines depleted, but these are only a matter of a few metres thick.

The identification of this crystal rich facies at the top of the Pul Pul Rhyolite is significant because the conformably overlying Big Sunday Formation is a subaqueous succession of tuffaceous sedimentary rocks, many beds being clearly turbidites. Other facies in the Big Sunday Formation include laminated to cross-laminated tuffaceous siltstones in intervals tens of metres thick. The cross-laminae indicate lateral current transport, and the huge thickness of this facies, without intervening normal mudstones, indicates a continuous supply process, probably as an underflow from the mouth of a river draining into the basin.

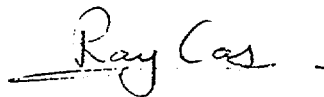
The occurrence of the crystal rich, massive facies at the transition from the clearly subaerial welded ignimbrite succession of the Pul Pul Rhyolite to the subaqueous succession of the Big Sunday Formation, therefore probably indicates the response of pyroclastic flows entering water. Preliminary interpretation would involve a model of pyroclastic flows entering the shoreline zones, and probably triggering phreatic explosions. Loss of fine ash through such explosions, as well as transformation of the gas-supported pyroclastic flows into water supported mass-flows (c.f. turbidity currents), and winnowing of fines out of the body of such flows may explain the crystal rich nature.

This model of pyroclastic flows entering water and disintegrating and transforming into water supported mass-flows is supported by what appear to be very irregular clasts of ignimbrite at several horizons as well as very diffusely bounded pods of ignimbrite occurring randomly throughout the crystal rich facies. Similarly enclaves of crystal rich facies occur within ignimbrite pods.

#### RECOMMENDATIONS

- (1) If this interpretation is correct and it seems the most likely, then the South Alligator River exposure cited herein, is unique, not only in Australia, but internationally. The only other location where such features and processes may be preserved is the Ordovician of the Welsh Basin, United Kingdom. This marvellously exposed section is not only a beautiful scenic location, but is also geologically unique and should be declared a geological and scenic monument.

- 4
- (2) It is not yet clear what the nature of the eruptive centre for the Pul Pul Rhyolite volcanics was or where it was located. The spatial relationship between the Malone Creek Granite and the Pul Pul Rhyolite is suggestive of a resurgent intrusion of the comagmatic volcanic pile of a caldera volcano, but such a model would have to be verified by a combination of mapping field relationships, investigating the geochemical compatibility of the volcanics and the granite, and if possible detailed geochronology.
- (3) Further detailed documentation is required of the volcanic succession to investigate the eruptive history and the depositional context. To this end Ms. Jagodzinski's work should produce a definitive interpretation of the volcanological history of this part of the South Alligator River Succession for the consumption of the scientific community and the general public visiting the Kakadu National Park. Such detailed geological research should be encouraged and supported in the public interest.



Dr. Ray Cas,  
Senior Lecturer,  
Department of Earth Sciences  
Monash University.  
3rd July, 1990.

**APPENDIX F**  
**ELECTRON MICROPROBE DATA**

## 3001 probe data

	A	B	C	D	E	F	G	H	I	J	K	L	M	N
1		cpx	cpx rim	cpx core	cpx	cpx	cpx core	cpx rim	cpx core	cpx rim	cpx core	cpx rim	cpx	cpx
2	SiO <sub>2</sub>	49.08	50.41	50.39	50.41	52.52	50.74	50.86	50.61	51.86	50.72	50.55	51	50.95
3	TiO <sub>2</sub>	0.96	1.06	1.16	1.16	0.39	1.08	1.04	1.29	0.81	0.95	0.91	0.99	0.96
4	Al <sub>2</sub> O <sub>3</sub>	2.56	2.38	2.63	2.11	1.01	2.52	2.17	2.11	0.98	2.09	2.37	1.95	2.5
5	Cr <sub>2</sub> O <sub>3</sub>	0.5	0.32	0.71	<.1	0.37	0.31	0.26	0.14	0.16	0.22	0.32	0.34	0.51
6	FeO	10.9	11.51	10.28	11.84	8.09	10.67	11.11	11.21	12.69	11.82	10.52	10.48	9.57
7	MnO	<.1	0.11	0.13	<.1	0.15	0.17	0.11	<.11	0.17	0.13	0.19	<.11	<.1
8	MgO	14.86	15.36	15.12	13.87	14.42	14.55	14.45	13.61	15.12	15.53	15.69	15.07	15.33
9	CaO	17.48	18.06	19.01	19.57	23.36	20.13	19.47	20.34	18.21	17.82	18.23	19.49	19.84
10	Na <sub>2</sub> O	<.15	0.15	0.19	<.15	<.15	0.24	0.17	0.16	<.15	<.15	<.15	<.15	<.15
11	K <sub>2</sub> O	<.06	<.06	<.06	<.06	<.06	<.06	<.06	<.06	<.06	<.06	<.06	<.06	<.06
12	Total	96.35	99.36	99.62	98.97	100.32	100.41	99.66	99.47	100	99.28	98.78	99.32	99.66
13														
14	Si	1.9034	1.9009	1.8918	1.916	1.954	1.897	1.9146	1.9138	1.9489	1.9133	1.9084	1.9192	1.9051
15	Ti	0.028	0.03	0.0328	0.0322	0.011	0.0303	0.0294	0.0368	0.0228	0.0269	0.026	0.028	0.027
16	Al <sub>6</sub>	0.1171	0.1059	0.1162	0.0945	0.0441	0.111	0.0964	0.0939	0.0434	0.0066	0.1054	0.0863	0.1101
17	Cr	0.0154	0.0096	0.0211	0.0109	0.011	0.0092	0.0077	0.0043	0.0047	0.373	0.0096	0.0102	0.0151
18	Fe <sub>3+</sub>	0.3536	0.3629	0.3227	0.3765	0.2518	0.3337	0.3499	0.3544	0.3989	0.0041	0.3321	0.3297	0.2993
19	Mn		0.0036	0.0043	0.0044	0.0048	0.0053	0.0035		0.0053	0.8732	0.0061		
20	Mg	0.8588	0.8631	0.8463	0.786	0.7997	0.811	0.811	0.767	0.8471	0.7204	0.8831	0.8455	0.8541
21	Ca	0.7263	0.7298	0.7645	0.7972	0.931	0.8065	0.7851	0.8243	0.7331		0.7374	0.7857	0.7947
22	Na		0.0113	0.0139			0.0172	0.0127	0.0116					
23	K													
24	MG													

3001 probe data

	O	P	Q	R	S
1	opaque	opaque	opaque	opaque	opaque
2	0.52	10.56	35.66	<.09	2.44
3	74.26	51.31	0.2	1.54	0.15
4	0.32	0.56	9.53	24.23	0.82
5	<.11	<.11	<.11	30.58	<.11
6	21.36	21.67	16.65	36.94	90.45
7	<.11	4.99	<.11	<.19	<.11
8	<.11	0.33	<.11	6.31	0.57
9	0.13	9.43	34.95	<.07	<.07
10	<.17	<.17	<.16	<.19	<.2
11	<.06	<.06	<.06	<.06	<.06
12	96.59	99.87	97	99.6	94.42
13					
14	0.0157	0.3159	1.02		0.1174
15	1.7015	1.1765	0.0042	0.0381	0.0055
16	0.0115	0.0199	0.3214	0.9384	0.0466
17				0.7944	
18	0.5441	0.542	0.3983	1.0153	3.6437
19		0.1265			
20		0.0147		0.3092	0.0406
21	0.0044	0.3022	1.0712		
22					
23					
24					

## 3018 probe data

	A	B	C	D	E	F	G	H	I	J	K
1		cpx	cpx	cpx	cpx	plag	plag	plag	plag	opaque	epidote
2	SiO <sub>2</sub>	52.54	53.04	52.78	51.08	59.63	59.53	57.96	58.41	2.49	37.94
3	TiO <sub>2</sub>	0.35	0.18	0.31	0.46	<.09	<.09	<.09	<.09	0.6	<.09
4	Al <sub>2</sub> O <sub>3</sub>	1.78	2.15	2.14	2.73	24.39	24.44	26	25.48	0.62	22.89
5	Cr <sub>2</sub> O <sub>3</sub>	0.28	0.69	0.25	0.37	<.1	<.1	<.1	<.1	<.11	<.1
6	FeO	8.03	5.84	7.91	9.39	0.14	0.14	0.19	<.11	90.84	12.36
7	MnO	<.1	<.1	<.1	0.14	<.1	<.1	<.1	<.1	<.11	0.7
8	MgO	17.37	18.32	16.99	16.86	<.1	<.1	<.1	<.1	0.18	<.11
9	CaO	19.6	19.68	19.72	17.71	6.6	6.66	8.15	7.86	<.07	22.22
10	Na <sub>2</sub> O	<.15	<.15	<.15	0.39	7.63	7.35	6.68	6.84	<.2	<.15
11	K <sub>2</sub> O	<.06	<.06	<.06	<.06	0.44	0.49	0.29	0.35	<.06	<.06
12	Total	99.97	99.92	100.09	99.13	98.84	98.61	99.28	98.95	94.72	96.11
13											
14	Si	1.9375	1.9375	1.941	1.9087	10.7654	10.765	10.4531	10.5509	0.1196	6.2784
15	Ti	0.0098	0.005	0.0086	0.013					0.0218	
16	Al <sub>6</sub>	0.0774	0.0926	0.0927	0.1202	5.1891	5.2094	5.5253	5.425	0.0352	4.4633
17	Cr	0.0082	0.0199	0.0072	0.0109			0.029			
18	Fe <sub>3+</sub>	0.2477	0.1785	0.2432	0.2934	0.0218	0.0212			3.6519	1.71
19	Mn	0.9548	0.9975		0.0044						0.0984
20	Mg	0.7745	0.7702	0.9311	0.939					0.0126	
21	Ca			0.7768	0.7089	1.2768	1.29	1.575	1.5219		3.9398
22	Na				0.0283	2.6713	2.577	2.3364	2.3957		
23	K					0.1023	0.1124	0.0675	0.0818		
24	Mg										

## 3019 probe data

	A	B	C	D	E	F	G	H	I	J	K
1		cpx core	cpx rim	cpx core	cpx rim	cpx core	cpx core	cpx rim	cpx	plag	plag
2	SiO2	52.72	53.03	53.12	53.03	53.41	53.62	53.58	53.2	59.65	60
3	TiO2	0.14	0.31	0.16	0.22	<.09	<.09	0.16	0.1	<.09	<.08
4	Al2O3	1.7	1.83	1.29	1.63	0.94	1.19	1.19	1.2	24.79	24.95
5	Cr2O3	0.88	0.16	0.66	0.47	0.91	0.99	1.13	0.86	<.1	<.1
6	FeO	4.94	7.37	4.85	6.02	3.94	4.06	4.28	4.78	<.11	<.11
7	MnO	<.1	0.13	<.1	<.1	<.1	<.1	<.1	<.1	<.1	<.1
8	MgO	17.89	18.37	18.5	18.5	18.3	18.33	18.63	18.55	<.1	<.1
9	CaO	20.79	18.85	20.73	19.47	21.08	21.1	21.09	20.25	7.06	6.72
10	Na2O	<.15	<.15	<.15	<.15	<.15	<.15	<.15	<.15	7.31	7.17
11	K2O	<.06	<.06	<.06	<.06	<.06	<.06	<.06	<.06	0.25	0.52
12	Total	99.07	100.06	99.32	99.35	98.58	99.3	100.06	98.95	99.06	99.35
13											
14	Si	1.9432	1.9424	1.9507	1.9483	1.9695	1.9636	1.9509	1.9579	10.7272	10.7514
15	Ti	0.004	0.0086	0.0044	0.0062			0.0043	0.0027		
16	Al6	0.0739	0.0792	0.0558	0.0707	0.0408	0.0514	0.0511	0.0521	5.2544	5.2685
17	Cr	0.0257	0.0046	0.0192	0.0136	0.0264	0.0287	0.0325	0.0251		
18	Fe3+	0.1524	0.2258	0.149	0.185	0.1216	0.1244	0.1301	0.1472		
19	Mn		0.0041								
20	Mg	0.9827	1.003	1.0124	1.0133	1.0056	1.0003	1.0111	1.0174		
21	Ca	0.8211	0.7396	0.8158	0.7664	0.8329	0.828	0.8227	0.7985	1.3596	1.2904
22	Na									2.5504	2.49
23	K									0.0584	0.1182
24	MG										

## 3026 probe data

	A	B	C	D	E	F	G	H	I	J	K	L	M
1		cpx	CPX	zoned cpx	zoned cpx	zoned cpx	zoned cpx	zoned cpx	cpx	twinned cpx	twinned cpx	opaque	opaque
2	SiO <sub>2</sub>	50.58	50.26	49.65	49.75	50.05	50.52	50.67	50.35	50.63	51.64	14.07	0.47
3	TiO <sub>2</sub>	0.96	0.96	1.05	1.12	1.02	0.81	0.73	0.75	0.94	0.47	27.51	31.14
4	Al <sub>2</sub> O <sub>3</sub>	2.24	2.87	3.12	3.11	3.01	2.41	2.15	2.65	2.56	1.27	1.8	1.09
5	Cr <sub>2</sub> O <sub>3</sub>	<.1	<.1	<.1	<.1	<.1	<.1	<.1	0.12	<.1	<.1	<.11	<.11
6	FeO	13.1	11.4	11.28	13.14	13.03	11.98	12.47	11.79	13.17	14.32	42.8	59.86
7	MnO	0.19	0.1	0.18	<.1	0.12	<.1	<.1	0.14	0.12	0.17	1.02	2.33
8	MgO	14.55	15.24	15.1	15.42	14.9	15.5	15.7	15.5	14.75	16.12	<.11	<.12
9	CaO	18.41	18.37	18.49	17.02	17.1	17.82	17.26	18.37	17.83	15.5	12.35	0.22
10	Na <sub>2</sub> O	0.27	<.15	<.15	<.15	<.15	<.15	<.15	<.15	<.15	<.15	0.24	0.77
11	K <sub>2</sub> O	<.06	<.06	<.06	<.06	<.06	<.06	<.06	<.06	<.06	<.06	<.06	<.06
12	Total	100.31	99.2	98.87	99.56	98.22	99.04	98.98	99.66	99.99	99.49	99.8	95.87
13													
14	Si	1.9044	1.8959	1.8819	1.8786	1.8948	1.9097	1.9173	1.8951	1.9058	1.949	0.3436	0.0136
15	Ti	0.0271	0.0273	0.0301	0.0319	0.0289	0.0231	0.0207	0.0212	0.0267	0.0134	0.5053	0.6839
16	Al <sub>6</sub>	0.0993	0.1274	0.1393	0.1384	0.1345	0.1074	0.096	0.1174	0.1134	0.0563	0.0518	0.0377
17	Cr								0.0036				
18	Fe <sub>3+</sub>	0.4126	0.3595	0.3575	0.415	0.4125	0.3787	0.3945	0.371	0.4145	0.4519	0.8743	1.4622
19	Mn	0.006	0.0033	0.0059		0.0039			0.0043	0.0039	0.0054	0.0211	0.0576
20	Mg	0.8166	0.8571	0.8529	0.8677	0.8407	0.8731	0.8855	0.8696	0.8274	0.9069		
21	Ca	0.7428	0.7426	0.7508	0.6888	0.6937	0.7215	0.6999	0.741	0.7191	0.6266	0.3233	0.0068
22	Na	0.0198										0.0115	0.0434
23	K												
24	MG												

## 3028 probe data

	A	B	C	D	E	F
1		K-feldspar	albite	albitised K	plag	plag
2	SiO <sub>2</sub>	65.27	69.05	66.68	69.53	69.55
3	Al <sub>2</sub> O <sub>3</sub>	18.57	19.51	18.88	19.89	19.79
4	FeO	<.1	0.12	0.11	0.12	<.1
5	CaO	<.09	<.06	<.08	0.2	0.21
6	BaO	<.11	<.1	<.1		
7	Na <sub>2</sub> O	0.35	10.75	3.17	12.78	11.98
8	K <sub>2</sub> O	16.14	0.31	13.31	0.12	0.09
9	Total	100.32	99.74	102.16	102.64	101.62
10			12.0539	11.961		
11	Si	12.0037	4.0134	3.9915		
12	Al	4.0243	0.0174	0.0166		
13	Fe					
14	Ca					
15	Ba					
16	Na	0.1262	3.6403	1.1031		
17	K	3.7862	0.0691	20.1173		
18	Ca:Na:k	0:3.2:96.8	0:98.1:1.9	0:26.6:73.4		

## 3038 probe data

	A	B	C	D	E	F	G	H	I	J	K	L	M	N
1		cpx	cpx	cpx core	cpx rim	cpx core	cpx rim	cpx core	cpx rim	cpx	plag	plag	plag	chlorite
2	SiO2	52.38	51.06	51.75	51.42	52.39	51.88	51.75	51.68	51.29	68.2	68.27	68.16	26.73
3	TiO2	0.94	0.64	0.81	0.75	0.62	0.8	0.83	0.72	0.93	<.08	<.08	<.08	<.09
4	Al2O3	2.03	1.94	1.38	1.15	1.52	1.27	1.82	1.23	1.58	20.2	19.7	19.66	15.87
5	Cr2O3	0.41	0.36	<.1	<.1	0.19	<.1	0.22	<.1	0.14	<.09	<.09	<.09	<.1
6	FeO	10.18	9.86	11.37	15.11	10.46	13.24	10.92	14.05	11.35	<.1	<.1	<.11	31.43
7	MnO	0.19	<.1	0.11	0.26	<.1	0.16	0.11	0.21	<.1	<.09	<.09	<.09	0.19
8	MgO	15.3	14.96	14.5	12.71	15.35	13.93	14.83	13.6	14.38	<.1	<.1	<.1	11.61
9	CaO	20.74	19.97	20.14	19.53	20.44	19.86	20.68	19.95	19.95	0.6	0.24	0.27	<.06
10	Na2O	0.25	<.17	<.17	<.17	<.17	<.17	<.17	0.23	<.17	12.77	12.18	12.72	<.18
11	K2O	<.06	<.06	<.06	<.06	<.06	<.06	<.06	<.06	<.06	0.08	<.05	0.16	<.06
12	Total	102.43	98.79	100.05	100.92	100.97	101.15	101.17	101.67	99.61	101.86	100.39	100.97	85.83
13														
14	Si	1.9141	1.9283	1.9413	1.9438	1.9383	1.9398	1.9199	1.9332	1.9327	11.7849	11.9095	11.8674	3.8416
15	Ti	0.0258	0.0183	0.0229	0.0212	0.0174	0.0226	0.0231	0.0202	0.0262				
16	Al6	0.0874	0.0863	0.0609	0.0512	0.0664	0.0561	0.0797	0.0544	0.0701	4.114	4.0507	4.0338	2.687
17	Cr	0.012	0.0107			0.0057		0.0063		0.0041				
18	Fe3+	0.311	0.3114	0.3567	0.4777	0.3236	0.4139	0.3389	0.4395	0.3577				3.7773
19	Mn	0.0058	0.0033	0.0034	0.0084		0.0052	0.0035	0.0067					0.0234
20	Mg	0.8332	0.8419	0.8106	0.7161	0.8465	0.7764	0.8202	0.7579	0.8076				2.4857
21	Ca	0.812	0.8081	0.8094	0.7909	0.8105	0.7955	0.8222	0.7996	0.8055	0.1117	0.0442	0.0503	
22	Na	0.0177							0.0163			4.1213	4.2928	
23	K												0.0358	
24	MG													

## 3076 probe data

	A	B	C	D	E	F	G	H	I	J	K
1	ig matrix										dolerite
2		plag	plag	matrix	plag	plag	matrix	epidote	epidote	epidote	plag
3	SiO2	68.61	67.44	65.75	66.98	68.55	66.94	37.55	37.34	37.34	68.65
4	TiO2	<.09	<.08	<.09	0.32	<.08	<.09	<.09	0.52	<.09	<.09
5	Al2O3	19.48	19.37	20.12	19.43	19.53	18	23.72	22.24	23.33	19.43
6	Cr2O3	<.1	<.09	<.1	<.1	<.09	<.1	<.1	<.1	<.1	<.1
7	FeO	0.27	0.37	0.58	<.11	0.12	0.86	12.09	12.47	12.29	0.22
8	MnO	<.1	<.09	<.1	<.1	<.09	<.1	0.32	<.1	<.1	<.09
9	MgO	<.1	<.1	<.1	<.1	<.1	<.1	<.11	<.11	<.11	<.1
10	CaO	0.08	0.28	1.08	1.15	0.21	0.62	23.12	23.64	23.74	<.06
11	Na2O	12.19	12.09	11.36	12.23	12.29	6.34	<.17	<.17	<.17	13.18
12	K2O	0.11	0.43	0.51	0.28	0.5	6.78	<.06	<.06	<.06	0.18
13	Total	100.74	99.97	99.4	100.39	101.19	99.54	96.8	96.22	96.71	101.67
14											
15	Si	11.9413	11.8757	11.6856	11.7732	11.91	12.0645	3.2074	3.2245	3.2012	11.8917
16	Ti				0.042				0.0341		
17	Al6	3.9964	4.0193	4.2144	4.0257	3.9993	3.823	2.3879	2.2638	2.3573	3.9675
18	Cr										
19	Fe3+	0.0389	0.0552	0.0859		0.0172	0.1293	0.8637	0.9003	0.8811	0.0316
20	Mn							0.0234			
21	Mg										
22	Ca	0.0149	0.052	0.2057	0.2161	0.0387	0.1199	2.1163	2.1869	2.1805	4.4267
23	Na	4.1128	4.1278	3.9159	4.1683	4.1397	2.2156				0.0406
24	K	0.0254	0.0971	0.1157	0.0618	0.1107	1.5592				
25	MG										

	L	M	N	O	P
1	clast				
2	plag	plag	plag	epidote	epidote
3	68.07	67.94	68.36	37.49	50.07
4	<.08	<.08	<.09	0.14	<.09
5	19.47	19.11	18.98	21.32	2.8
6	<.09	<.09	<.1	<.1	<.1
7	<.11	0.22	<.11	14.58	20.89
8	<.09	<.09	<.09	<.1	0.26
9	<.1	<.1	<.1	<.11	10.82
10	0.15	0.09	<.06	23.2	11.38
11	12.19	12.64	11.92	<.17	0.23
12	0.41	0.21	0.25	<.06	<.06
13	100.29	100.2	99.51	96.73	96.45
14					
15	11.9162	11.9242	12.0197	3.2506	4.3018
16				0.0089	
17	4.0167	3.9532	3.9337	2.1791	0.2833
18					
19		0.0321		1.0574	1.5009
20					0.0191
21	0.0282				1.385
22	4.1374	0.0167	4.0633	2.1551	1.0471
23	0.0911	4.2995	0.0566		0.0387
24		0.0453			
25					

## 3105 probe data

	A	B	C	D	E	F
1		plag	plag	plag	plag	plag
2	SiO2	72.01	69.93	69.12	69.53	69.55
3	TiO2	<.08	<.08	<.08	<.08	<.08
4	Al2O3	20.19	19.77	20.08	19.89	19.79
5	Cr2O3	<.09	<.09	<.09	<.09	<.09
6	FeO	<.1	<.1	<.1	0.12	<.1
7	MnO	<.09	<.09	<.09	<.09	<.09
8	MgO	<.1	<.1	<.1	<.1	<.1
9	CaO	<.06	<.06	0.3	0.2	0.21
10	Na2O	12.05	12.81	11.9	12.78	11.98
11	K2O	0.09	0.17	0.16	0.12	0.09
12	Total	104.35	102.68	101.57	102.64	101.62
13						
14	Si	12.0356	11.9444	11.9105	11.8982	11.9669
15	Ti					
16	Al6	3.9774	3.9804	4.0785	4.0108	4.0127
17	Cr					0.0172
18	Fe3+				0.0172	
19	Mn					
20	Mg					
21	Ca			0.0549	0.0372	0.039
22	Na	3.9057	4.2436	3.9769	4.2395	3.9965
23	K	0.0199	0.0378	0.0359	0.0265	0.0198
24	MG					

	A	B	C	D	E	F
1		K-feldspar	K-feldspar	albitised K	K-feldspar	K-feldspar
2	SiO <sub>2</sub>	65.75	69.05	66.68	69.53	69.55
3	Al <sub>2</sub> O <sub>3</sub>	18.46	19.51	18.88	19.89	19.79
4	FeO	0.16	0.12	0.11	0.12	<.1
5	CaO	<.09	<.06	<.08	0.2	0.21
6	BaO	<.1	<.1	<.1		
7	Na <sub>2</sub> O	<.12	10.75	3.17	12.78	11.98
8	K <sub>2</sub> O	16.74	0.31	13.31	0.12	0.09
9	Total	101.11	99.74	102.16	102.64	101.62
10			12.0539	11.961		
11	Si	12.0037	4.0134	3.9915		
12	Al	4.0243	0.0174	0.0166		
13	Fe					
14	Ca					
15	Ba					
16	Na	0.1262	3.6403	1.1031		
17	K	3.7862	0.0691	20.1173		
18	Ca:Na:k	0:3.2:96.8	0:98.1:1.9	0:26.6:73.4		